

# **Improving the aircraft safety by advanced structures and protecting nanofillers**

**Marialuigia Raimondo**





Unione Europea



*Ministero dell'Istruzione,  
dell'Università e della Ricerca*



UNIVERSITA' DEGLI  
STUDI DI SALERNO

***Department of Industrial Engineering***

***Ph.D. Course in Chemical Engineering  
(XII Cycle-New Series)***

**Improving the aircraft safety  
by advanced structures and  
protecting nanofillers**

**Supervisor**

*Prof. Liberata Guadagno*

**Ph.D. student**

*Marialuigia Raimondo*

**Scientific Referees**

*Prof. Vittoria Vittoria*

*Dr. Carlo Naddeo*

*Prof. Vincenzo Tucci*

*Prof. Pasquale Longo*

**Ph.D. Course Coordinator**

*Prof. Paolo Ciambelli*



*First and foremost I would like to express my sincere gratitude to my supervisor Liberata (Tina) Guadagno. She taught me how it is important to believe in themselves and how the will and tenacity may allow to reach all the goals, even the most ambitious and difficult.*

*She is a role model to me, able to transmit the joy and enthusiasm she has for her research: an excellent example of a successful woman, scientist and professor.*

*I would like to acknowledge my scientific referees for their valuable suggestions and helpful discussions.*

*Kind thanks to Prof. Khalid Lafdi (University of Dayton-USA) and Prof. Maria Rossella Nobile (University of Salerno), who through a friendly and fruitful collaboration and their specialist skills have contributed to the success of my PhD.*

*I am very grateful to the IASS project (Seventh Framework Programme, FP7/2007-2013, under Grant Agreement No.313978) not only for the financial support but also for giving me the opportunity to carry out a high quality research in a very professional and exciting environment.*

*This work has been partly supported by POR CAMPANIA FSE 2007/2013, Asse IV e V, Reti di eccellenza tra Università -Centri di ricerca-Imprese (linea di azione 1), MASTRI.*

*I would like to extend my particular thanks to all my colleagues from the laboratory of chemistry I4.*

*Thanks again to all those who have supported me during these three exciting years.*

*Last but not least, I would like to thank my family for all their love and encouragement. I am especially grateful to my husband Carmine whose unconditional love and patience are my true strength.*

*Thank you  
Marialuigia Raimondo  
University of Salerno  
January 2014*



# Publications list related to the Ph.D. research activity

## International research papers

- [1] **M. Raimondo** and L. Guadagno. Effect of incorporation of carbon nanotubes on the mechanical properties of epoxy-amine composites. *AIP Conferences Proceedings*, 1459 (1), 226-228 (2012)
- [2] B. De Vivo, L. Guadagno, P. Lamberti, **M. Raimondo**, G. Spinelli, V. Tucci, L. Vertuccio, V. Vittoria. Electrical properties of multi-walled carbon nanotube/tetrafunctional epoxy-amine composites. *AIP Conference Proceedings*, 1459 (1), 199-201 (2012)
- [3] L. Guadagno, **M. Raimondo**, V. Vittoria, L. Vertuccio, K. Lafdi, B. De Vivo, P. Lamberti, G. Spinelli, V. Tucci. The role of carbon nanofiber defects on the electrical and mechanical properties of CNF-based resins. *Nanotechnology*, 24 (30), 305704 (10pp) (2013) art. no. 305704
- [4] U. Vietri, L. Guadagno, **M. Raimondo**, L. Vertuccio, K. Lafdi. Nanofilled epoxy adhesive for structural aeronautic materials. *Composites Part B : Engineering*, 61, 73-83 (2014)
- [5] L. Guadagno, **M. Raimondo**, V. Vittoria, L. Vertuccio, C. Naddeo, S. Russo, B. De Vivo, P. Lamberti, G. Spinelli, V. Tucci. Development of epoxy mixtures for application in aeronautics and aerospace. *RCS Advances* (under review)

## International conferences

- [1] L. Guadagno, **M. Raimondo**, L. Vertuccio, C. Naddeo, V. Vittoria, B. De Vivo, P. Lamberti, G. Spinelli, V. Tucci. Investigation of electrical, and dynamic mechanical properties of multi-walled carbon nanotube/epoxy composite. **11<sup>th</sup> International Workshop Nanoscience & Nanotechnology 2011** September, 19<sup>th</sup> – 23<sup>rd</sup>, 2011, Frascati (Italy) (book of abstracts: p. 94-99)
- [2] L. Guadagno, **M. Raimondo**, V. Vittoria, K. Lafdi, B. De Vivo, P. Lamberti, G. Spinelli, V. Tucci. Role of The Carbon Nanotube Defects On The Electrical Properties of *CNT-Based* Composites. **ACMA 2012, International Symposium on Aircraft Materials**. May 09-12, 2012 Fez, Morocco (book of abstracts (pag.55-56) + full paper electronic format on CD, Editors: A. Menou, M. Karama, A. Moudden, A. Benejedou, A. Saouab, El Ham; ISBN:9782953480429)

- [3] B. De Vivo, L. Guadagno, P. Lamberti, **M. Raimondo**, G. Spinelli, V. Tucci, L. Vertuccio, V. Vittoria. Electrical Properties of Multi-Walled Carbon Nanotube/Tetrafunctional Epoxy-Amine Composites. **6<sup>th</sup> International Conference on Times of Polymers (TOP) and composites**. June 10-14, 2012, Ischia (Italy)
- [4] **M. Raimondo**, L. Guadagno. Effect of incorporation of carbon nanotubes on the mechanical properties of epoxy-amine composites. **6<sup>th</sup> International Conference on Times of Polymers (TOP) and composites**. June 10-14, 2012, Ischia (Italy)
- [5] L. Guadagno, **M. Raimondo**, L. Vertuccio, C. Naddeo, V. Vittoria, B. De Vivo, P. Lamberti, G. Spinelli, V. Tucci. Electrical, and dynamic mechanical properties of MWCNTs/epoxy composite for high performance aerospace applications. **ECCM 15 – 15<sup>th</sup> European Conference on Composite Materials**. June 24-28, 2012 Venice-Italy ISBN:9788888785332
- [6] L. Guadagno, **M. Raimondo**, V. Vittoria, L. Vertuccio, K. Lafdi, B. De Vivo, P. Lamberti, G. Spinelli, V. Tucci . Effect of conductive nanofiller structures on electrical properties of epoxy composite for aeronautic applications. **ICEAF III 3rd International Conference of Engineering Against Failure**. 26-28 June, 2013 - Kos island, Greece, Patras Spiros Pantelakis Vol.III, Pag. 527-533 ISBN:9789608810433
- [7] L. Guadagno, **M. Raimondo**, V. Vittoria, L. Vertuccio, K. Lafdi, B. De Vivo, P. Lamberti, G. Spinelli , V. Tucci. Electrical properties of CNFs/Epoxy-Amine Resin for aeronautic and aerospace applications. **ICEAF III 3rd International Conference of Engineering Against Failure**. 26-28 June, 2013 - Kos island, Greece, Patras Spiros Pantelakis Vol.III, Pag.534-541 ISBN:9789608810433
- [8] **M. Raimondo**, L. Guadagno, L. Bonnaud, O. Murariu, Ph. Dubois. Effect of Incorporation of POSS Compounds on Thermal and Fire Resistance of Aeronautic Resins. **ICEAF III 3rd International Conference of Engineering Against Failure**. 26-28 June, 2013 - Kos island, Greece, Patras Spiros Pantelakis Vol.III, Pag.542-550 ISBN:9789608810433
- [9] **M. Raimondo**, L. Vertuccio, G. Barra, L. Bonnaud, O. Murariu, Ph. Dubois, S. Russo, L. Guadagno. Thermal Degradation and fire properties of epoxy modified resins. **3rd EASN Association International Workshop on AeroStructures Proc.** 9th-11th October 2013, Milan, Italy (ISSN 2309-7213)
- [10] **M. Raimondo**, S. Chirico, L. Guadagno, P. Longo, A. Mariconda, L. Bonnaud, O. Murariu, Ph. Dubois, L. Dumas. Fire properties of TGMDA resins for aeronautic applications. **3rd EASN Association International Workshop on AeroStructures Proc.** 9th-11th October 2013, Milan, Italy (ISSN 2309-7213)
- [11] L. Guadagno, **M. Raimondo**, V. Vittoria, L. Vertuccio, K. Lafdi, B. De Vivo, P. Lamberti, G. Spinelli, V. Tucci. Exfoliated graphite as conductive filler in aeronautic epoxy mixtures. **3rd EASN Association International**

**Workshop on AeroStructures Proc.**, 9th-11th October 2013, Milan, Italy (ISSN 2309-7213)

[12] M.R. Nobile, A. Fierro, S. Rosolia, L. Guadagno, **M. Raimondo**. Viscoelastic Properties of CNT/Epoxy-Amine Resins for Structural Applications. **NanotechITALY 2013 – 6<sup>TH</sup> edition** Key Enabling Technologies for Responsible Innovation Proc., 27th – 29th November 2013, Venice, Italy.

[13] K.I. Tserpes, L. Guadagno, I. Floros, **M. Raimondo** and U. Vietri. Numerical modelling of nanoparticle-reinforced adhesively bonded joints. **11th World Congress on Computational Mechanics (WCCM2014)**, Barcelona, Spain, 20-25 July 2014 (accepted)

[14] L. Guadagno, **M. Raimondo**, K. Lafdi, A. Fierro, S. Rosolia, M.R. Nobile. Influence of Nanofiller Morphology on the Viscoelastic Properties of CNF/Epoxy Resins. **7<sup>th</sup> International Conference on Times of Polymers (TOP) and composites**. June 22-26, 2014, Ischia (Italy) (accepted)

[15] L. Guadagno, U. Vietri, **M. Raimondo**, L. Vertuccio. Nanofilled Epoxy Adhesive for Metal Adherends. **7th International Conference on Times of Polymers (TOP) and composites**. June 22-26, 2014, Ischia (Italy) (accepted)

[16] L. Guadagno, U. Vietri, M. Sarno, **M. Raimondo**, C. Cirillo, P. Ciambelli. Nanofilled epoxy adhesives for structural applications. **7th International Conference on Times of Polymers (TOP) and composites**. June 22-26, 2014, Ischia (Italy) (accepted)

[17] L. Guadagno, **M. Raimondo**, U. Vietri, G. Barra, L. Vertuccio, R. Volponi, G. Cosentino, F. De Nicola, A. Grilli, P. Spina. Development of Multifunctional Carbon Fiber Reinforced Composites (CFRCs) - Manufacturing Process. **7th International Conference on Times of Polymers (TOP) and composites**. June 22-26, 2014, Ischia (Italy) (accepted)

## **Italian Patents**

[1] L. Guadagno, **M. Raimondo**, V. Vittoria, L. Vertuccio, C. Naddeo, P. Lamberti, V. Tucci. **Resina epossidica con basso tenore di umidità.**

*Filing number: TO2013A000926 Filing date: 15.11.2013*

[2] L. Guadagno, **M. Raimondo**, P. Longo, L. Bonnaud, O. Murariu, Ph. Dubois. **Resina epossidica multifunzionale con accresciuta resistenza alla fiamma.**

*Filing number: TO2013A001021 Filing date: 13.12.2013*

# Other publications during Ph.D. course

## International research papers

- [1] L. Guadagno, P. Longo, **M. Raimondo**, C. Naddeo, A. Mariconda, V. Vittoria, G. Iannuzzo, S. Russo. Use of Hoveyda-Grubbs' 2<sup>nd</sup> Generation Catalyst in Self-Healing Epoxy Mixtures. *Composites Part B : Engineering*, 42(2), 296-301 (2011)
- [2] L. Guadagno, **M. Raimondo**, C. Naddeo, G. Russo, V. Vittoria, S. Russo, G. Iannuzzo. Dynamic Mechanical Properties of Structural Self-healing Epoxy Resins. *Applied Mechanics and Materials*, 62, 95-105 (2011)
- [3] L. Guadagno, **M. Raimondo**, C. Naddeo, A. Di Bartolomeo, K. Lafdi. Influence of multi-wall carbon nanotubes on morphological and structural changes during UV irradiation of syndiotactic polypropylene films. *J. Polym. Sci.-Part B: Polymer Physics*, 50(14), 963-965 (2012)
- [4] B. De Vivo, P. Lamberti, G. Spinelli, V. Tucci, L. Guadagno, **M. Raimondo**, L. Vertuccio, V. Vittoria, E. Caponetti. Impact of the inclusion of hydrotalcite on the morphological and electrical characteristics of an epoxy-based CNT nanocomposites. *IEEE International Symposium on Electromagnetic Compatibility*, art. no. 6396851 (2012)
- [5] B. De Vivo, P. Lamberti, R. Raimo, G. Spinelli, V. Tucci, L. Guadagno, **M. Raimondo**, L. Vertuccio, V. Vittoria, M.S. Sarto, A. Tamburrano. Electromagnetic and Mechanical Properties of a multiphase Carbon NanoTube/Clay/Epoxy Nanocomposite. *IEEE International Symposium on Electromagnetic Compatibility*, art. no. 6396809 (2012)
- [6] L. Guadagno, **M. Raimondo**, C. Naddeo, P. Longo, A. Mariconda. Self-healing Materials for Structural Applications. *Polymer Engineering and Science* Online ISSN: 1548-2634 pp 1-8 DOI: 10.1002/pen.23621 Article first published online: 7 JUN 2013
- [7] **M. Raimondo** and L. Guadagno. Healing efficiency of epoxy-based materials for structural application. *AIP Conferences Proceedings*, 1459 (1), 223-225 (2012)
- [8] B. De Vivo, G. Spinelli, V. Tucci, L. Guadagno, **M. Raimondo**, L. Vertuccio, V. Vittoria, P. Lamberti. Improvement of the electrical conductivity in multiphase epoxy-based MWCNT nanocomposites by means of an optimized clay content. *Composites Science and Technology*, 89, 69-76 (2013)

- [9] L. Vertuccio, A. Sorrentino, L. Guadagno, V. Bugatti, **M. Raimondo**, C. Naddeo, V. Vittoria. Behavior of epoxy composite resins in environments at high moisture content. *Journal of Polymer Research*, 20(6), 1-13 (2013) art. no. 178
- [10] **M. Raimondo** and L. Guadagno. Healing efficiency of epoxy-based materials for structural applications. *Polymer Composites*, 34(9), 1525-1532 (2013)
- [11] **M. Raimondo**, L. Guadagno, C. Naddeo, P. Longo, A. Mariconda. Efficient self-healing resins. *Plastics Engineering*. Pag.1-3 ISSN:0091-9578 (2013) DOI: 10.2417/spepro.004911 (web site: <http://www.4spepro.org/view.php?source=004911-2013-06-06>)
- [12] L. Guadagno, **M. Raimondo**, C. Naddeo, P. Longo, A. Mariconda, W.H. Binder. Healing efficiency and dynamic mechanical properties of self-healing epoxy systems. *Smart Mater. Struct.*, 23(4), 045001 (11pp) (2014)
- [13] **M. Raimondo**, P. Longo, A. Mariconda, L. Guadagno. Healing Agent for the Activation of Self-Healing Function at Low Temperature. *Advanced Composites Materials* (under review)

### International conferences

- [1] **M. Raimondo**, L. Guadagno, C. Naddeo. Effect of multiwall carbon nanotubes on the morphology of irradiated syndiotactic polypropylene. Workshop “**Advances in Polymer based Materials and Related Technologies**”. May 29<sup>th</sup> – June 1<sup>st</sup>, 2011, Capri (Italy) (book of abstracts: p. 121)
- [2] L. Guadagno, **M. Raimondo**, C. Naddeo, R. Corvino, V. Vittoria, G. Russo, S. Russo, K. Lafdi. Composites for Self-healing Structural Materials. Workshop “**Advances in Polymer based Materials and Related Technologies**”. May 29<sup>th</sup> – June 1<sup>st</sup>, 2011, Capri (Italy) (book of abstracts: p. 122)
- [3] G. Russo, L. Guadagno, G. W. M. Peters, **M. Raimondo**, R. H. M. Solberg. Electrospinning of drug-loaded mesh samples: Morphological analysis (AFM) and drug release. Workshop “**Advances in Polymer based Materials and Related Technologies**”. May 29<sup>th</sup> – June 1<sup>st</sup>, 2011, Capri (Italy) (book of abstracts: p. 125)
- [4] **M. Raimondo**, R. Corvino, L. Guadagno, P. Longo, C. Naddeo, A. Mariconda. Advanced Polymeric Composites for Self-healing Structural Materials. **European Polymer Congress 2011 (XII Congress of the Specialized Group of Polymers (GEP))**, 26<sup>th</sup> June-1<sup>st</sup> July 2011, Granada, Spain. (Book of abstracts: p. 749, ISBN: 978-84-694-3124-5)
- [5] L. Guadagno, **M. Raimondo**. Development of self-healing epoxy nanocomposites for structural applications. **11<sup>th</sup> International Workshop**

**Nanoscience & Nanotechnology 2011** September, 19<sup>th</sup> – 23<sup>rd</sup>, 2011, Frascati (Italy) (book of abstracts: p. 103-108)

[6] G. Russo, L. Guadagno, G. W. M. Peters, **M. Raimondo**, R.H.M. Solberg, V. Vittoria. Preparation and morphological characterization of Mesh Membranes obtained using Electrospinning technique. **11<sup>th</sup> International Workshop Nanoscience & Nanotechnology 2011** September, 19<sup>th</sup> – 23<sup>rd</sup>, 2011, Frascati (Italy) (book of abstracts: p. 84-88)

[7] **M. Raimondo**, L. Guadagno. Healing efficiency of epoxy-based materials for structural applications. **6<sup>th</sup> International Conference on Times of Polymers (TOP) and composites**. June 10-14, 2012, Ischia (Italy)

[8] B. De Vivo, P. Lamberti, R. Raimo, G. Spinelli, V. Tucci, L. Guadagno, **M. Raimondo**, L. Vertuccio, V. Vittoria, M. S. Sarto, A. Tamburrano. Electromagnetic and Mechanical Properties of a multiphase Carbon NanoTube/Clay/Epoxy Nanocomposite. **EMC Europe 2012. Rome**. September 17-21, 2012 Rome, Italy, pp. 1-6 ISBN:9781467307178

[9] B. De Vivo, P. Lamberti, G. Spinelli, V. Tucci, L. Guadagno, **M. Raimondo**, L. Vertuccio, V. Vittoria, E. Caponetti. Impact of the inclusion of hydrotalcite on the morphological and electrical characteristics of an epoxy-based CNT nanocomposite. **EMC Europe 2012. Rome**. September 17-21, 2012 Rome, Italy, pp.1-4 ISBN:9781467307185

[10] **M. Raimondo**, P. Longo, A. Mariconda, L. Guadagno. Healing Agent for the Activation of Self-Healing Function at Low Temperature. **ICEAF III 3rd International Conference of Engineering Against Failure**. 26-28 June, 2013 - Kos island, Greece, Patras Spiros Pantelakis Vol.III, Pag.519-526 ISBN:9789608810433

[11] L. Guadagno, **M. Raimondo**, C. Naddeo, P. Longo, A. Mariconda, W. H. Binder. Healing Efficiency and Dynamic Mechanical Properties of self-healing epoxy systems. **3rd EASN Association International Workshop on AeroStructures Proc.**. 9th-11th October 2013, Milan, Italy (ISSN 2309-7213)

[12] B. De Vivo, L. Guadagno, P. Lamberti, **M. Raimondo**, G. Spinelli, V. Tucci, L. Vertuccio and V. Vittoria. Temperature Effects on the Electrical Properties of Multiphase Polymer Composites. **7th International Conference on Times of Polymers (TOP) and composites**. June 22-26, 2014, Ischia (Italy) (accepted)

### **Book chapters**

[1] L. Guadagno and **M. Raimondo**. Use of FT/IR analysis to control the self-healing functionality of epoxy resins. In "*Infrared Spectroscopy – Materials Science, Engineering and Technology / Book I*", Prof. Theophile Theophanides (Editor) ISBN: 978-953-51-0537-4 chapter 14 pp 286-300 DOI: 10.5772/36029 Published Online: April 25, 2012 **Publisher: InTech**.

[2] L. Guadagno, **M. Raimondo**, C. Naddeo, P. Longo. Application of Self-Healing Materials in Aerospace Engineering. In Wolfgang H. Binder **Self-Healing Polymers: From Principles to Applications** (book) Wolfgang H. Binder (Editor) ISBN: 9783527334391 chapter 17 pp 401-412 DOI: 10.1002/9783527670185.ch17 Published Online: 24 JUN 2013 **Publisher: Wiley-VCH Books**

### US Patent Publications

[1] L. Guadagno, **M. Raimondo**, C. Naddeo, A. Mariconda, R. Corvino, P. Longo, V. Vittoria, S. Russo, G. Iannuzzo. **Process for preparing self-healing composite materials of high efficiency for structural applications.**

*Patent No.:* **US 8481615 B2** *Date of Patent:* **July 9, 2013**

*Assignee:* Alenia Aeronautica S.p.A

*Prior Publication Date* US 2011118385 (A1) May. 19, 2011

*Also published as:*

EP 2325254 (A1) Publication date: November 11, 2010

IT TO20090870 (A1) Filing date: 13 novembre 2009

[2] L. Guadagno, P. Longo, **M. Raimondo**, A. Mariconda, C. Naddeo, A. Sorrentino, V. Vittoria, G. Iannuzzo, S. Russo, E. Calvi. **Process for preparing a self-healing composite material.**

*Patent No.:* **US 8273806 B2** *Date of Patent:* **Sep. 25, 2012**

*Assignee:* Alenia Aeronautica S.p.A

*Prior Publication Date* US 2010168280 (A1) Jul. 1, 2010

*Also published as:*

EP 2172518 (A1) Publication date: 07.04.2010

IT TO20080723 (A1) Filing date: 02 ottobre 2008

[3] L. Tamaro, L. Guadagno, **M. Raimondo**, O. Petillo, S. Margarucci, A. Calarco, V. Vittoria, G. Peluso. **Composite material with properties of self-healing and release of active ingredients, for biomedical applications.**

*Publication number:* **US 20120208895 (A1)** *Publication date:* **August 16, 2012**

*Also published as:*

EP 2379045 (A1) Publication date: 26.10.2011

WO 2010072347 (A1) Publication date: 01 July 2010

IT MI20082284 (A1) Filing date: 22 dicembre 2008

## **EP Patent Publications**

- [1] L. Guadagno, P. Longo, **M. Raimondo**, A. Mariconda, C. Naddeo, A. Sorrentino, V. Vittoria, G. Iannuzzo, S. Russo, E. Calvi. **A composite material which is self-repairing even at low temperature.**

*Patent No.: EP2257422 B1 Date of Publication: 10.07.2013*

*Also published as:*

EP 2257422 (A1) Publication date: 08.12.2010.

WO 2009113025 (A1) Publication date: 17.09.2009

IT TO20080194 (A1) Filing date: 13 marzo 2008

- [2] V. Vittoria, L. Guadagno, A. Sorrentino, **M. Raimondo**, C. Naddeo, L. Vertuccio, G. Iannuzzo, S. Russo, E. Calvi. **Epoxy resin based composition and method for the curing thereof.**

*Publication number: EP 2271706 (A1) Publication date: 12.01.2011*

*Also published as:*

WO 2009113027 (A1) Publication date: 17.09.2009

IT TO20080191 (A1) Filing date: 13 marzo 2008

## **PhD School Partecipation**

- [1] **PhD Forum– GRICU PhD National School Mathematical**

Methods for Chemical Engineering/Nanotechnologies

Santa Margherita di Pula (CA), 26th September – 1st October 2011

- [2] **GRICU PhD NATIONAL SCHOOL 2012**

Transport phenomena Separation processes

Montesilvano (PE) September 20th – 23rd 2012

- [3] **GRICU PhD NATIONAL SCHOOL 2013**

Free radical polymerization: kinetics, statistical thermodynamics and engineering aspects

Advanced topics in sustainable chemical engineering

Salice Terme (PV) September 15th – 21th 2013

# Index

<b>CHAPTER I.....</b>	<b>1</b>
<b>INTRODUCTION .....</b>	<b>1</b>
<b>I.1 Preface.....</b>	<b>1</b>
<b>I.2 State of the art and progress beyond the state of the art:     Multifunctional concept .....</b>	<b>6</b>
<b>I.3 Research strategies.....</b>	<b>7</b>
<b>I.3.1 Reduced electrical conductivity: Current technology .....</b>	<b>8</b>
I.3.1.1 Research activity.....	8
<b>I.3.2 Poor flame resistance: Current Technology.....</b>	<b>12</b>
I.3.2.1 Research strategy .....	12
I.3.2.2 Motivation of the chosen work strategies .....	13
<b>CHAPTER II .....</b>	<b>19</b>
<b>DEVELOPMENT OF EPOXY MIXTURES FOR APPLICATION IN AERONAUTICS AND AEROSPACE.....</b>	<b>19</b>
<b>II.1 Preface .....</b>	<b>19</b>
<b>II.2 General remarks .....</b>	<b>19</b>
<b>II.3 Experimental section .....</b>	<b>22</b>
<b>II.3.1 Materials and sample preparation .....</b>	<b>22</b>
<b>II.3.2 Methods.....</b>	<b>23</b>
<b>II.3.3 Results and discussions.....</b>	<b>25</b>
II.3.3.1 Choice of the curing cycle: Thermal analysis .....	25
II.3.3.2 Dynamic Mechanical Results .....	27
II.3.3.3 Water Transport Properties.....	30
II.3.3.4 Thermogravimetric analysis .....	33
II.3.3.5 Morphological investigation.....	35
II.3.3.6 Electrical Behavior.....	39
II.3.3.6.1 Dielectric properties of the resin .....	39
II.3.3.6.2 DC conductivity of nanofilled resins .....	41
II.3.3.7 Impedance spectroscopy of nanocomposites.....	44
<b>II.4 Conclusions.....</b>	<b>48</b>
<b>CHAPTER III.....</b>	<b>51</b>
<b>ROLE OF THE CNF DEFECTS ON THE ELECTRICAL AND MECHANICAL PROPERTIES OF CNF-BASED RESINS.....</b>	<b>51</b>
<b>III.1 Preface.....</b>	<b>51</b>

<b>III.2 General remarks .....</b>	<b>52</b>
<b>III.3 Experimental section .....</b>	<b>53</b>
<b>III.3.1 Materials.....</b>	<b>53</b>
III.3.1.1 Carbon nanofibers .....	53
III.3.1.2 Nanofilled Epoxy Resins.....	54
<b>III.3.2 Characterizations.....</b>	<b>54</b>
<b>III.3.3 Results and discussion .....</b>	<b>55</b>
III.3.3.1 Carbon nanofibers characterization .....	55
<i>III.3.3.1.1 Morphological and structural investigation .....</i>	<i>55</i>
<i>III.3.3.1.2 Structural investigation.....</i>	<i>58</i>
<i>III.3.3.1.3 Raman and FT/IR spectroscopy .....</i>	<i>59</i>
<i>III.3.3.1.4 Thermogravimetric analysis .....</i>	<i>61</i>
III.3.3.2 CNF/epoxy resin characterization .....	62
<i>III.3.3.2.1 Thermogravimetric analysis .....</i>	<i>62</i>
<i>III.3.3.2.2 Morphological analysis .....</i>	<i>63</i>
<i>III.3.3.2.3 Electrical behavior.....</i>	<i>64</i>
<i>III.3.3.2.4 Dynamic mechanical properties .....</i>	<i>67</i>
<b>III.4 Conclusions.....</b>	<b>68</b>
<b>CHAPTER IV .....</b>	<b>71</b>
<b>VISCOELASTIC PROPERTIES OF CNT/EPOXY-AMINE RESINS FOR STRUCTURAL APPLICATIONS .....</b>	<b>71</b>
<b>IV.1 General remarks .....</b>	<b>71</b>
<b>IV.2 Materials and Methods.....</b>	<b>72</b>
<b>IV.3 Results and discussion .....</b>	<b>72</b>
<b>IV.3.1 Rheological, dynamic mechanical and morphological properties .....</b>	<b>72</b>
<b>IV.4 Conclusions .....</b>	<b>76</b>
<b>CHAPTER V .....</b>	<b>77</b>
<b>INFLUENCE OF NANOFILLER MORPHOLOGY ON THE VISCOELASTIC PROPERTIES OF CNF/EPOXY RESINS .....</b>	<b>77</b>
<b>V.1 General remarks.....</b>	<b>77</b>
<b>V.2 Materials.....</b>	<b>78</b>
<b>V.3 Morphological analysis .....</b>	<b>79</b>
<b>V.4 Rheological analysis.....</b>	<b>79</b>
<b>V.5 Conclusions .....</b>	<b>81</b>
<b>CHAPTER VI .....</b>	<b>83</b>

<b>EXFOLIATED GRAPHITE AS CONDUCTIVE FILLER IN AERONAUTIC EPOXY MIXTURES .....</b>	<b>83</b>
<b>VI.1 Preface .....</b>	<b>83</b>
<b>VI.2 General Remarks.....</b>	<b>83</b>
<b>VI.3 Material and Experimental Part.....</b>	<b>85</b>
<b>VI.4 Methods .....</b>	<b>86</b>
<b>VI.5 Results .....</b>	<b>87</b>
<b>VI.5.1 Carbon nanofiller characterization (Raman Spectroscopy) .</b>	<b>87</b>
<b>VI.5.2 Exfoliated graphite and epoxy/exfoliated graphite nanocomposites: X-Ray Diffraction Analysis .....</b>	<b>88</b>
<b>VI.5.3 Epoxy/exfoliated graphite nanocomposites: Dynamic Mechanical Analysis .....</b>	<b>89</b>
<b>VI.5.4 Epoxy/exfoliated graphite nanocomposites: Electrical Characterization.....</b>	<b>90</b>
<b>VI.5.5 Exfoliated graphite and epoxy/ exfoliated graphite nanocomposites: Morphological investigation .....</b>	<b>92</b>
<b>VI.6 Conclusions .....</b>	<b>95</b>
<b>CHAPTER VII .....</b>	<b>97</b>
<b>FIRE RETARDANCY CONCEPTS.....</b>	<b>97</b>
<b>VII.1 Preface .....</b>	<b>97</b>
<b>VII.2 Polymer combustion .....</b>	<b>97</b>
<b>VII.2.1 Mechanism of action .....</b>	<b>99</b>
<b>VII.2.1.1.Chemical Effect Condensed Phase .....</b>	<b>101</b>
<b>VII.2.1.2 Intumescence .....</b>	<b>102</b>
<b>VII.2.1.3 Chemical Effect Gas Phase.....</b>	<b>103</b>
<b>VII.2.1.4 Synergism with Antimony trioxide (Sb<sub>2</sub>O<sub>3</sub>) .....</b>	<b>104</b>
<b>VII.2.1.5 Physical Effect.....</b>	<b>105</b>
<b>VII.2.1.5.1 Formation of a protective layer .....</b>	<b>105</b>
<b>VII.2.1.6 Cooling effect .....</b>	<b>105</b>
<b>VII.2.1.7 Dilution .....</b>	<b>105</b>
<b>CHAPTER VIII.....</b>	<b>107</b>
<b>EFFECT OF INCORPORATION OF POSS COMPOUNDS ON THERMAL AND FIRE RESISTANCE OF AERONAUTIC RESINS.....</b>	<b>107</b>
<b>VIII.1 Preface .....</b>	<b>107</b>
<b>VIII.2 General remarks.....</b>	<b>107</b>
<b>VIII.3 Experimental .....</b>	<b>112</b>

<b>VIII.3.1 Materials</b> .....	112
<b>VIII.3.2 Characterizations and Experimental procedure</b> .....	112
<b>VIII.4 Results and discussion</b> .....	114
<b>VIII.4.1 Dispersion of POSS inside the epoxy mixture</b> .....	114
VIII.4.1.1 Results on the dispersion of DPHPOSS in the epoxy mixture.	115
VIII.4.1.2 Results on the dispersion of ECPOSS in the epoxy mixture ....	116
VIII.4.1.3 Results on the dispersion of GPOSS in the epoxy mixture .....	117
VIII.4.1.4 Results on the dispersion of TCPOSS in the epoxy mixture ....	118
<b>VIII.4.2 Thermogravimetric analysis</b> .....	119
<b>VIII.4.3 Fire behavior of POSS/EPM</b> .....	120
<b>VIII.5 Conclusions</b> .....	121
<b>CHAPTER IX</b> .....	123
<b>MULTIFUNCTIONAL EPOXY RESIN WITH ENHANCED FLAME RESISTANCE</b> .....	123
<b>IX.1 General remarks</b> .....	123
<b>IX.2 Synthesis of new hardener agents</b> .....	127
<b>IX.2.1 Materials</b> .....	127
<b>IX.2.2 Characterization</b> .....	127
<b>IX.2.3 Synthesis procedure of BAPPO</b> .....	128
<b>IX.2.4 Synthesis procedure of BAMPO</b> .....	131
<b>IX.3 Thermal and oxidative degradation of BAPPO and BAMPO</b> .....	138
<b>IX.4 Dissolution of BAMPO and BAPPO in epoxy matrix</b> ....	141
<b>IX.5 Evaluation of the BAPPO and BAMPO as hardeners for improving fire properties</b> .....	145
<b>IX.5.1 Materials</b> .....	145
<b>IX.5.2 Sample preparation</b> .....	145
<b>IX.5.3 Characterizations</b> .....	146
<b>IX.6 Conclusions</b> .....	152
<b>CHAPTER X</b> .....	153
<b>DEVELOPMENT OF MULTIFUNCTIONAL CARBON FIBER REINFORCED COMPOSITES (CFRCs) - MANUFACTURING PROCESS</b> .....	153
<b>X.1 Preface</b> .....	153
<b>X.2 General remarks</b> .....	153
<b>X.3 Materials</b> .....	154

<b>X.4 CFRCs –Manufacturing Process .....</b>	<b>154</b>
<b>X.5 Results and discussion .....</b>	<b>156</b>
<b>X.6 Morphological investigation.....</b>	<b>157</b>
<b>X.7 Conclusions.....</b>	<b>158</b>
<b>GENERAL CONCLUSIONS .....</b>	<b>159</b>
<b>REFERENCES .....</b>	<b>161</b>



# List of figures

Figure I.1 Catastrophic damage from a lightning strike on an airliner.....	1
Figure I.2 Growth of Composites in Commercial Jets .....	2
Figure I.3 China Airlines jet exploded in flames.....	3
Figure I.4 Schematic of multiscale concept: from nanomaterials to new-concept aircrafts .....	5
Figure I.5 Top-down methods for production of graphene and modified graphene starting from graphene or via graphene oxide (GO).....	11
Figure I.6 Synthesis scheme of chemically reduced graphite oxide .....	12
Figure I.7 Scheme of research strategies .....	13
Figure I.8 Structural formula of bis(3-aminophenyl)methylphosphine oxide and bis(3 aminophenyl)phenylphosphine oxide.....	14
Figure I.9 Generalized structure of a POSS material .....	16
Figure I.10 4,4'-Diaminodiphenyl sulfone (DDS) and bis(3-aminophenyl)phenylphosphine oxide (BAPPO) .....	16
Figure II.1 Chemical structures of compounds used for the epoxy matrix composite .....	22
Figure II.2 DSC curves of: a) the uncured and cured epoxy resin TGMDA+DDS (without reactive diluent) on the left side, and b) the uncured and cured epoxy mixture TGMDA+DDS+BDE(20%)(TGMDA with reactive diluent/DDS) on the right side.....	26
Figure II.3 DSC curves of: the uncured epoxy mixture TGMDA+DDS+BDE(20%)+CNT(0.32%), and the same epoxy mixture cured by two different curing cycles.....	27
Figure II.4 Storage modulus (MPa) (at the top), and Loss factor ( $\tan\delta$ ) (at the bottom) of the pure epoxy and the composites 0.32 wt% MWCNTs solidified up to 180 and 200°C respectively.....	29
Figure II.5 The concentration at time ( $C_t$ ) as a function of the time (hours) of the epoxy resin (without BDE), and the epoxy mixture containing the diluent .....	31
Figure II.6 $C_t/C_{eq}$ against the square root of time of unfilled and nanofilled mixtures .....	32
Figure II.7 Thermogravimetric curves in air of: a) the uncured and cured unfilled epoxy resin TGMDA/DDS (without reactive diluent) on the left side, and b) the reactive diluent BDE on the right side .....	34
Figure II.8 Thermogravimetric curves in air of : a) the uncured and cured unfilled epoxy mixture TGMDA+DDS+BDE(20%) (TGMDA with reactive diluent/DDS) on the left side, and b) the same epoxy formulation nanofilled with a percentage of 0.32% of MWCNTs on the right .....	34
Figure II.9 Fracture surface SEM images of the nanofilled epoxy composites at loading rate of A) 0.64, B) 0.32 and C) 0.05 per cent by weight of CNTs.....	36
Figure II.10 TEM image of sample B (epoxy resin at loading rate of 0.32 per cent by weight of CNTs).....	36
Figure II.11 Fracture surface SEM images of the nanofilled epoxy composites at loading rate of 0.64 per cent by weight: as received CNFs filled resin is on the top, heat-treated CNFs filled resin is on the bottom.....	37

Figure II.12 Fracture surface SEM images of the nanofilled epoxy resins at loading rate of 1.0 per cent by weight: as received CNFs filled resin is on the top, heat-treated CNFs filled resin is on the bottom.....	38
Figure II.13 Fracture surface SEM images (enlargement) of the nanofilled epoxy resins at loading rate of 1.0 per cent by weight: as received CNFs filled resin is on the top, heat-treated CNFs filled resin is on the bottom.....	38
Figure II.14 AC behaviour of the relative electric permittivity for the TGMDA epoxy formulations (with and without diluent) compared with the formulation based on DGEBA at T=30°C.....	40
Figure II.15 AC behaviour of the electrical conductivity for the TGMDA epoxy formulations (with and without diluent) compared with the formulation based on DGEBA at T=30°C.....	41
Figure II.16 DC volume conductivity of the nanofilled composites as a function of the nanofiller concentration .....	42
Figure II.17 Plot of the log of conductivity against $\phi^{-1/3}$ .....	43
Figure II.18 Normalized impedance a) and phase angle b) vs frequency .....	46
Figure II.19 $ Z_{norm} $ and $\phi$ vs frequency for composites at filler loadings beyond percolation threshold.....	47
Figure III.1(a) An SEM image of as-received CNFs (PR25XTPS1100); (b) SEM images of as-received CNFs (PR25XTPS1100) and CNFs heat treated at 2500°C (PR25XTPS2500); the inset shows higher magnifications for each sample .....	56
Figure III.2 Bright field micrograph of the 'Dixie cup' carbon nanofiber structure on the left side and a cross-sectional view of the CNF.....	57
Figure III.3 High-resolution imaging of the localized area of the coalesced Dixie cup structure.....	58
Figure III.4 X-ray diffraction patterns of pristine and annealed nanofibers.....	59
Figure III.5 Raman spectra of samples PR25XTPS1100 and PR25XTPS2500.....	59
Figure III.6 FTIR spectra of the samples PR25XTPS1100 (thick line) and PR25XTPS2500 (thin line) .....	61
Figure III.7 TGA of samples PR25XTPS1100 and PR25XTPS2500 .....	62
Figure III.8 TGA curves of the unfilled and PR25XTPS2500 filled epoxy resins.....	63
Figure III.9 Fracture surface SEM images of the nanofilled epoxy resins at a loading rate of 0.64% by weight: as-received CNF filled resins are on the left side, heat-treated CNFs filled resins are on the right side.....	64
Figure III.10 DC volume conductivity of the samples versus CNF weight percentage .....	65
Figure III.11 Storage modulus of the epoxy resin filled with untreated and heat-treated CNFs.....	67
Figure III.12 Loss factor ( $\tan\delta$ ) of the unfilled epoxy mixture and its resins filled with 1% (weight percentage) of untreated and heat-treated CNFs .....	68
Figure IV.1 Complex viscosity vs frequency for TGMDA epoxy resin at different temperatures.....	73
Figure IV.2 Complex viscosity vs frequency for the 0.5 wt% MWCNT-TBD nanocomposite at different temperatures.....	74
Figure IV.3 Storage ( $G'$ ) and Loss ( $G''$ ) moduli vs. frequency for the 0.5 wt% MWCNT-TBD composite at T= 75°C.....	75
Figure V.1 Complex viscosity ( $\eta^*$ ) vs frequency ( $\omega$ ) for the TGMDA epoxy precursor and for the TGMDA-BDE blend (TB); T= 75°C.....	79

Figure V.2 Complex viscosity ( $\eta^*$ ), storage ( $G'$ ) and loss ( $G''$ ) moduli vs frequency ( $\omega$ ) for the 0.5 wt% PR25XTPS2500-TBD nanocomposite; $T = 75^\circ\text{C}$ .....	80
Figure V.3 Storage ( $G'$ ) and loss ( $G''$ ) moduli vs frequency ( $\omega$ ) for the 0.5 wt% PR25XTPS2500-TBD nanocomposite (filled symbols) and for the 0.5 wt% PR25XTPS1100-TBD nanocomposite (empty symbols); $T = 75^\circ\text{C}$ .....	81
Figure VI.1 Schematic of the intercalation/exfoliation process (2006 Princeton University, Ceramic Materials Laboratory).....	85
Figure VI.2 Raman spectrum of exfoliated graphite (EG) sample .....	87
Figure VI.3 XRD plots of EG and HEG samples.....	88
Figure VI.4 XRD patterns of: A) EG, B) TBD, C) TBD_EG 1%wt, D)TBD_EG 2%wt, E) TBD_EG 4%wt, F) TBD_EG 6.5%wt.....	89
Figure VI.5 Storage modulus (see graphic on the left) and loss factor ( $\tan\delta$ ) (see graphic on the right) of the sample T20BD+2% EG (AP 56%), and sample T20BD+1.8 % HEG (AP 60%) .....	90
Figure VI.6 Electrical conductivity of two nanocomposites as a function of nanofiller percentage: EG (filled circles) - nanocomposite filled with exfoliated graphite (AP 56%); HEG (square dots) - nanocomposite filled with exfoliated graphite (AP 60%).....	91
Figure VI.7 Electrical conductivity of nanofilled resins at different nanofiller percentage .....	91
Figure VI.8 SEM images of EG (on the left) and HEG (on the right) samples .....	93
Figure VI.9 Fracture surface SEM images of the nanofilled epoxy composites at two different loading rates:0.64% by weight (see images on the top) and 5% by weight (see images on the bottom) of exfoliated graphite EG.....	93
Figure VI.10 Fracture surface FESEM images of the epoxy composites nanofilled with EG and HEG at different loading rates: 3% by weight of EG (see image on the right), and the sample loaded at 0.5% (see image on the left) and 1.8% (see image in the middle) by weight of HEG respectively .....	94
Figure VI.11 Fracture surface AFM images of the nanofilled epoxy composite at loading concentration of 3% by weight of EG.....	94
Figure VI.12 TEM images of the nanofilled epoxy composite at 1.8 wt% of HEG ..	95
Figure VI.13 TEM images of the nanofilled epoxy composite at 2 wt% of EG.....	95
Figure VII.1 The fire triangle.....	100
Figure VII.2 Combustion cycle.....	100
Figure VII.3 Char and intumescence formation.....	101
Figure VII.4 Mechanism of action of halogenated flame retardants.....	103
Figure VII.5 Formation of protective layer inhibiting, combustion and volatiles..	105
Figure VIII.1 Experimental set-up for LOI measurement (see image on the left) and Mass loss calorimeter measurement (see image on the right).....	113
Figure VIII.2 Optical image of T20BD+5%DPHPOSS sample (before ultrasonication). .....	115
Figure VIII.3 Optical image of T20BD+5%DPHPOSS sample (after ultrasonication) .....	115
Figure VIII.4 Optical image of T20BD+5%DPHPOSS sample (after ultrasonication and magnetic stirring in oil bath at $120^\circ\text{C}$ for 1h).....	116
Figure VIII.5 Photos of T20BD+5%ECPOSS mixture after ultrasonication (on the left) and after 1h in a stirred oil bath at $120^\circ\text{C}$ (on the right).....	116

Figure VIII.6 Optical image of T20BD+5%ECPOSS sample after ultrasonication (on the left) and magnetic stirring in oil bath at 120°C for 1h (on the right).....	117
Figure VIII.7 Photos of T20BD+5%GPOSS mixture after ultrasonication (on the left) and after 1h in a stirred oil bath at 120°C (on the right).....	117
Figure VIII.8 Optical image of T20BD+5%GPOSS sample after ultrasonication and magnetic stirring in oil bath at 120°C for 1h .....	118
Figure VIII.9 Optical image of T20BD+5%TCPOSS sample after ultrasonication and magnetic stirring in oil bath at 120°C for 1h .....	118
Figure VIII.10 TG profiles for POSS (on the left side), EPM and POSS/EPM (on the right side).....	119
Figure VIII.11 HRR of T20BD and POSS/EPM formulations.....	120
Figure VIII.12 Photographs of residues from left to right (neat T20BD, T20BD+5%DPHPOSS, T20BD+5%ECPOSS, T20BD+5%GPOSS, T20BD+5%TCPOSS).....	121
Figure IX.1 Hardening agents.....	125
Figure IX.2 Scheme of synthesis of bis(3-aminophenyl) phenyl phosphine oxide (BAPPO) 3.....	125
Figure IX.3 Scheme of synthesis of bis(3-aminophenyl) methyl phosphine oxide (BAMPO) 4.....	126
Figure IX.4 Scheme of synthesis of bis (3-nitro phenyl) phenyl phosphine oxide 2.....	128
Figure IX.5 <sup>1</sup> H spectrum of bis(3-nitrophenyl) phenyl phosphine oxide 2 in DMSO-d <sub>6</sub> .....	129
Figure IX.6 <sup>31</sup> P spectrum of bis(3-nitrophenyl) phenyl phosphine oxide 2 in DMSO-d <sub>6</sub> .....	129
Figure IX.7 <sup>13</sup> C spectrum of bis(3-nitrophenyl) phenyl phosphine oxide 2 in DMSO-d <sub>6</sub> .....	129
Figure IX.8 Scheme of synthesis bis(3-aminophenyl)phenyl phosphine oxide 3 (BAPPO).....	129
Figure IX.9 <sup>1</sup> H spectrum of bis(3-aminophenyl)phenyl phosphine oxide 3 (BAPPO) in DMSO-d <sub>6</sub> .....	130
Figure IX.10 <sup>31</sup> P spectrum of bis(3-aminophenyl)phenyl phosphine oxide 3 (BAPPO) in DMSO-d <sub>6</sub> .....	131
Figure IX.11 <sup>13</sup> C spectrum of bis(3-aminophenyl)phenyl phosphine oxide 3 (BAPPO) in DMSO-d <sub>6</sub> .....	131
Figure IX.12 Scheme of synthesis of biphenyl methyl phosphine oxide (2).....	133
Figure IX.13 <sup>1</sup> H spectrum of biphenyl methyl phosphine oxide (2) in DMSO-d <sub>6</sub> ....	134
Figure IX.14 <sup>31</sup> P spectrum of biphenyl methyl phosphine oxide (2) in DMSO-d <sub>6</sub> ....	134
Figure IX.15 <sup>13</sup> C spectrum of biphenyl methyl phosphine oxide (2) in DMSO-d <sub>6</sub> ....	134
Figure IX.16 Scheme of synthesis of binitro phenyl methyl phosphine oxide (3) .....	134
Figure IX.17 <sup>1</sup> H spectrum of binitro phenyl methyl phosphine oxide (3) in DMSO-d <sub>6</sub> .....	135
Figure IX.18 <sup>31</sup> P spectrum of binitro phenyl methyl phosphine oxide (3) in DMSO-d <sub>6</sub> .....	136
Figure IX.19 <sup>13</sup> C spectrum of binitro phenyl methyl phosphine oxide (3) in DMSO-d <sub>6</sub> .....	136
Figure IX.20 Scheme of synthesis of bis(3-aminophenyl)methyl phosphine oxide ...	136
Figure IX.21 <sup>1</sup> H spectrum of bis(3-aminophenyl)methyl phosphine oxide (4)BAMPO in DMSO-d <sub>6</sub> .....	138

Figure IX.22 $^{31}\text{P}$ spectrum of bis(3-aminophenyl)methyl phosphine oxide (4) BAMPO in DMSO- $d_6$ .....	138
Figure IX.23 $^{13}\text{C}$ spectrum of bis(3-aminophenyl)methyl phosphine oxide (4) BAMPO .....	138
Figure IX.24 TGA curves of BAMPO and BAPPO .....	139
Figure IX.25 First derivative TGA curves (in air and nitrogen) of BAMPO and BAPPO .....	140
Figure IX.26 FTIR spectra of BAMPO and BAPPO .....	141
Figure IX.27 Thermogravimetric analysis of TGMDA.....	142
Figure IX.28 Finely pulverized BAMPO .....	142
Figure IX.29 BAMPO based uncured epoxy mixture poured into molds used for fire testing .....	143
Figure IX.30 Tested BAMPO based epoxy samples after the curing process, before (see image on the left) and after (see image on the right) extraction from the molds .....	143
Figure IX.31 Cross-linked BAMPO based epoxy sample at 120°C.....	144
Figure IX.32 Tested epoxy samples containing BAPPO particle aggregates and lumps .....	144
Figure IX.33 Tested epoxy sample containing BAPPO particles homogeneously dispersed.....	145
Figure IX.34 TGA curves of BAMPO and BAPPO based composites.....	146
Figure IX.35 Char aspect of T20B systems with different hardeners.....	147
Figure IX.36 Char aspect of T20BD+CNTs composites .....	148
Figure IX.37 Photo of multifunctional tested samples .....	150
Figure IX.38 Loss factor ( $\tan\delta$ ) and storage modulus (Mpa) of the unfilled epoxy mixture and its multifunctional resins .....	151
Figure IX.39 TGA curves of multifunctional composites .....	152
Figure X.1 Scheme of Liquid resin infusion technique .....	155
Figure X.2 Steps of laminate preparation .....	155
Figure X.3 Impregnation and curing cycle.....	156
Figure X.4 Manufactured panel .....	157
Figure X.5 Sections of the manufactured panels .....	157
Figure X.6 Optical images of the section of the manufactured panels .....	158

# List of tables

<i>Table II.1 Diffusion parameters (D) and Sorption values at equilibrium of liquid water (<math>C_{eq}</math>) of the epoxy resin (without BDE), the epoxy mixture containing the diluent and the nanofilled mixtures .....</i>	<i>31</i>
<i>Table V.1 Morphological parameters of PR25XTPS1100 CNFs.....</i>	<i>78</i>
<i>Table VI.1 Physical properties of the EG and HEG for a filler amount of 1.8%wt..</i>	<i>92</i>
<i>Table VII.1 Main components of intumescent systems .....</i>	<i>103</i>
<i>Table VIII.1 POSS compounds investigated in this chapter .....</i>	<i>114</i>
<i>Table VIII.2 LOI and PHRR of the POSS/EPM samples.....</i>	<i>121</i>
<i>Table IX.1 LOI and PHRR of the T20B formulation cured with BAMPO and BAPPO .....</i>	<i>147</i>
<i>Table IX.2 LOI and PHRR values of the epoxy samples.....</i>	<i>148</i>
<i>Table IX.3 LOI and PHRR values of the epoxy samples.....</i>	<i>149</i>
<i>Table IX.4 Maximum of temperature of the main mechanical transition <math>T_m</math> associated to the glass transition temperature of the epoxy systems .....</i>	<i>149</i>
<i>Table IX.5 DC conductivities data of nanofilled epoxy resin samples.....</i>	<i>150</i>
<i>Table IX.6 LOI and PHRR values of the multifunctional composites.....</i>	<i>151</i>
<i>Table X.1 Values of the viscosity <math>\eta^*</math> (Pa s) at three different temperatures.....</i>	<i>156</i>

# Abstract

Inspection and Maintenance are important aspects when considering the availability of aircraft for revenue flights. Modern airframe design is exploiting new exciting developments in materials and structures to construct ever more efficient air vehicle able to enable efficient maintenance. The improvement in the aircraft safety by advanced structures and protecting nanofillers is a revolutionary approach that should lead to the creation of novel generation of multifunctional aircraft materials with strongly desired properties and design flexibilities. In recent years, the development of new nanostructured materials has enabled an evolving shift from single purpose materials to multifunctional systems that can provide greater value than the base materials alone; these materials possess attributes beyond the basic strength and stiffness that typically drive the science and engineering of the material for structural systems. Structural materials can be designed to have integrated electrical, electromagnetic, flame resistance, and possibly other functionalities that work in synergy to provide advantages that reach beyond that of the sum of the individual capabilities. Materials of this kind have tremendous potential to impact future structural performance by reducing size, weight, cost, power consumption and complexity while improving efficiency, safety and versatility. It is a well-known fact that, actually, also a very advanced design of an aircraft has to take required inspection intervals into account. An aircraft with inherent protective abilities could help to significantly extend the inspection intervals, thereby increasing aircraft availability. The challenge in this research is to develop and apply a multifunctional composite for structural applications.

The aim of this project is the formulation, preparation and characterization of structural thermosetting composites containing dispersed protective nanofillers. This project specifically targets composites tailored for multifunctional applications such as lightning strike protection, and flame resistance. These composites were designed to enable their application on next generation aircrafts. With regard to the objectives of this PhD project the multifunctional composite systems were developed with the aim of overcoming the following drawbacks of the composite materials:

- reduced electrical conductivity;
- poor flame resistance

The thermosetting material was projected considering compatibility criteria so that to integrate different functions into a material that is capable of bearing mechanical loads and serves as a structural material element.



---

# Chapter I

---

## Introduction

### I.1 Preface

The use of composite materials for aeronautic primary structures was driven by performance gains (better fatigue performance, no corrosion, better design flexibility, etc.) and most of all by weight reduction. However, composites also possess some properties which reduce their advantage with respect to traditional metal alloys. One inherent shortcoming is the reduced electrical conductivity of the composites. This fact has raised concern over the performance of the composite structure during a lightning strike event due to the remarkable risk that a puncture of the structural part would cause a catastrophic failure of the aircraft. Figure I.1 shows an airplane struck by lightning.



**Figure I.1** Catastrophic damage from a lightning strike on an airliner

In a traditional aircraft structure, the aluminium skin of the aircraft provides highly conductive paths for the lightning to flow around the structure without causing damage. Without a conductive path on the skin of a composite aircraft the lightning may pass through the airframe which could vaporize metal control cables, weld hinges on control surfaces and explode fuel vapours within fuel tanks. These *direct effects* also typically include vaporization of resin in the immediate strike area, with possible burn-through of the laminate. *Indirect effects* occur due to electromagnetic

phenomena: high and steep-fronted transient over-voltages can damage and even destroy onboard electronics or ignite potentially dangerous sparks. In addition electromagnetic interference may affect the proper functioning of the different on board electrical and electronic systems. Airplanes get struck by lightning frequently; obviously and fortunately, they're built to handle it. Some modern aircrafts are made of advanced composites, reinforced with conductive metal fibres or metal screen in order to dissipate lightning currents, which are significantly less conductive than aluminium. But many of these solutions add additional weight and partially reduce the advantage of the composite applications.

In the last decades the use of composite in the primary structures in the Aeronautics is rapidly increased (see Figure I.2). The new Airbus A380 is expected to have about 22% of the structural weight in composites. About 50% of the structural weight of the new Boeing 787 (which represents the next generation of airplanes for the 21st Century), is proposed to be composites, including for the first time a composite fuselage and wings in a large commercial airliner. Advanced composites are attractive to airplane manufacturers for a variety of reasons: being lighter, composite-based aircraft consume less fuel. Meanwhile, composite parts are usually easier to mould and assemble than metal airframes, and require no rivets. Up to 20-30% in operating costs per seat can be saved by airlines flying higher composite-content aircraft.

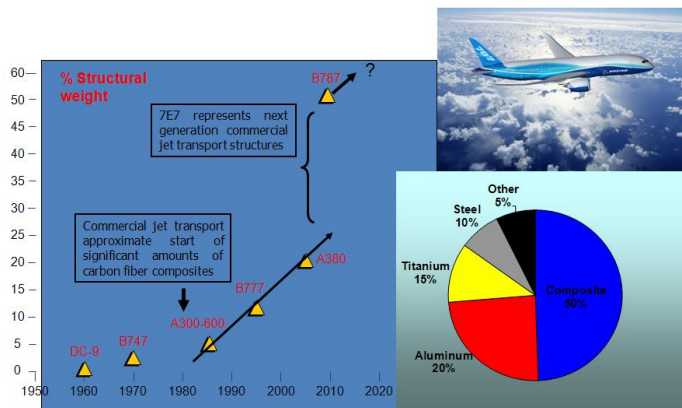


**Figure I.2** Growth of Composites in Commercial Jets

The aircraft manufacturer will be required to demonstrate that polymer structural composites provide equivalent safety to the current material system (aluminum alloy).

However, in the last decade, the availability of different nanofiller or nanostructured conductive materials has sensibly contributed to the

continuous improvement of the engineering properties or abilities of the composites for aeronautic or automotive industries.

By choosing the appropriate control of the matter structure as well as the specific fillers, researchers with appropriate expertise can work to overcome this critical point.

Another critical point related to the composite materials for aeronautic and aerospace applications is due to the fact that currently, no fire resistance requirements exist for exterior polymer composite structures on airplanes. Consequential damages from poor flame resistance are rare but possible (see Figure I.3).

However, the aircraft manufacturer will be required to demonstrate that polymer structural composites provide equivalent safety to the traditional material systems (aluminium alloy). The primary hazards during aircraft fires are heat, smoke, and toxic gas. In a severe aircraft fire, life threatening levels of these hazards are produced by cabin flashover, the time to which is largely governed by the rate of heat release of the materials in the fire.



**Figure I.3** *China Airlines jet exploded in flames*

Other concerns in a carbon fiber composite fire include the potential release of electrically conductive small carbon fibers that can cause damage to electrical equipment and health problems (from inhalation).

Fire contributes to aircraft accidents and many fatalities. The growing use of polymer composite materials in aircraft has the potential to increase the fire hazard due to the flammable nature of the organic matrix. The polymer composite most often used in the external structures of aircraft is carbon/epoxy, which is a flammable material that easily ignites and burns when exposed to fire. A large percentage of the cabin interior of wide-bodied passenger aircraft is made using composite materials, mostly glass/phenolic. Phenolic composites have good flammability, but newer materials are being developed that offer the promise of increasing the fire safety of aircraft cabins. In fact, a large number of new composite materials are being

developed for cabins and external structures that have the potential to increase the fire safety of aircraft, but a detailed analysis of the fire performance of these materials against conventional materials now used in aircraft has not been performed. Such an evaluation will provide a clear indication of the potential improvements in fire safety by using new fire resistant composites in aircraft.

The composite of the new Boeing 787 consists of multiple, alternately directed layers of epoxy-impregnated continuous graphite fibers (Carbon fiber reinforced composites–CFRCs). Unfortunately, the epoxy resin between the carbon fiber layers can burn under accidental aircraft fire conditions; for this reason FAA certification for Boeing 787 required to demonstrate that the level of fire safety in the B-787 was equivalent to a conventional transport (aluminum) aircraft. This regulation has been extended to any other structural aeronautic materials. It is evident that no new material can be developed in this field without considering its behavior in the flame condition. To design a material able to resist under fire conditions, new research strategies can be developed.

Currently, the material scientists have the possibility "to use" the advantages of the nanotechnologies in addition to the classical methods to protect the materials. In this thesis a similar approach was applied.

The materials here described were designed using current discoveries in the nanotechnology field. In particular, a big effort was directed toward the development of light-weight multifunctional materials, capable of bearing mechanical loads and then suitable as structural material.

The next revolution in air travel and space exploration is in fact, contingent upon our ability to dramatically reduce mass, size, and power consumption while increasing reliability. The key actually seems to be the integration of intelligence and multifunctionality into the varied components of aerospace systems and vehicles. The fundamental challenges are to develop new multifunctional materials through nano- and micro-technology and to devise strategies for exploiting these enhanced properties to enable revolutionary structural concepts (see Figure I.4). Multifunctional materials are typically a composite or hybrid of several distinct material phases in which each phase performs a different but necessary function. Because each phase of the material is used to perform an essential function so there is little or no parasitic weight or volume, multifunctional materials promise to achieve performance flexibility but with lower weight and volume efficiency and potentially less maintenance than the traditional multicomponent, brassboard system solutions. In addition, as the integration scale in the material becomes finer and more distributed, reaction times may become faster and more autonomous. Multifunctionality within a material can be integrated on several dimensional scales with increasing interconnectivity between phases and engineering difficulty as the scale decreases.

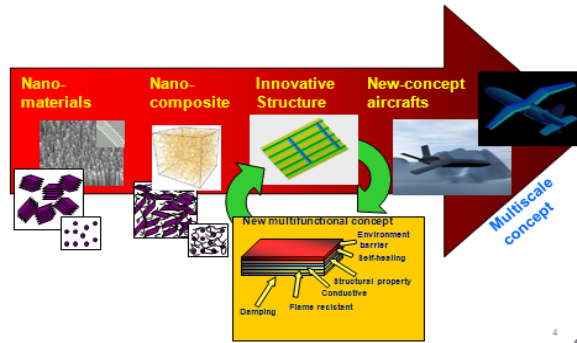


**Figure I.4** Schematic of multiscale concept: from nanomaterials to new-concept aircrafts

### *Outline of thesis*

This thesis has been divided into ten chapters.

Chapter I presents an overview on the composite materials for aeronautic and aerospace applications. Particular attention has been given to the multifunctional concept and to the research strategies proposed to overcome drawbacks related to technical targets required for aeronautical composite: reduced electrical conductivity and poor flame resistance.

Chapter II describes a successful attempt toward the development of aeronautic materials based on nanofilled epoxy resins. As nanofiller, different carbon nanostructured fiber-shaped fillers were embedded in the epoxy matrix with the aim of improving the electrical properties of the formulated resin.

Chapter III highlights the role of the CNF defects on the electrical and mechanical properties of CNF-based resins. Nanofilled resins made of heat-treated CNF show significant increase in the electrical conductivity even at low concentration.

Chapter IV describes the viscoelastic properties of CNT/epoxy-amine resins for structural applications.

Chapter V describes the influence of nanofiller morphology on the viscoelastic properties of CNF/epoxy resins.

Chapter VI focuses on the use of the exfoliated graphite as conductive filler in aeronautic epoxy mixtures.

Chapter VII presents fire retardancy concepts.

Chapter VIII focuses on the effect of incorporation of POSS compounds on the thermal and fire resistance of aeronautic resins.

Chapter IX describes multifunctional epoxy resin with enhanced flame resistance. In this chapter experimental results related to the synthesis

procedure of fire-resistant curing agents (BAMPO and BAPPO) together with the description of sample preparation are reported.

Chapter X describes a successful attempt toward the development of multifunctional carbon fiber reinforced composites (CFRCs) based on nanofilled epoxy resins.

General conclusions are drawn from all these results in the last part of this thesis.

## **I.2 State of the art and progress beyond the state of the art: Multifunctional concept**

The increased interest in multifunctional materials and structures is driven by the need for the development of new materials and structures that simultaneously perform multiple structural functions, combined non-structural and structural functions, or both. As previously said, multifunctional materials are necessarily composite materials, and the strong growth in the use of composites has been greatly influenced by multifunctional design requirements. Up to now, the traditional approach to the development of structures is to address the load-carrying function and other functional requirements separately, resulting in a suboptimal load-bearing structure with add-on attachments which perform the non-structural functions with the penalty of added weight. Recently, however, there has been increased interest in the development of load-bearing materials and structures which have integral non-load-bearing functions, guided by recent discoveries about nanofillers and nanotechnology that can help to project materials working as multifunctional systems.

Due to the interdisciplinary nature of multifunctional materials and structures, it is appropriate to cite several relevant review articles. For example, “Baur and Silverman (2007)” reviewed the challenges and opportunities in multifunctional nanocomposite aerospace structures. They reported that one important application of nanocomposites is their use in engineered structural composites. Among the wide variety of structural applications, fiber-reinforced composites for aerospace structures have some of the most demanding physical, chemical, electrical, thermal, and mechanical property requirements. Nanocomposites offer tremendous potential to improve the properties of advanced engineered composites with modest or without additional weight and easy integration into current processing schemes. In particular, nanocomposites have been applied at numerous locations within hierarchical composites to improve specific properties and optimize the multifunctional properties of the overall structure. “Ye *et al.*(2005)” reviewed developments in the application of artificial intelligence to functionalize composite airframes. It is becoming increasingly apparent that nanostructured composites can produce and/or

enhance multifunctionality in ways that conventional composites could not. For example, “Thostenson *et al* (2001)” and “Chou *et al.* (2010)” reviewed recent advances related to the science and technology of carbon nanotubes and their composites, “Breuer and Sundararaj (2004)” reviewed recent studies on polymer/carbon nanotube composites, “Li *et al* (2008a)” surveyed the recent advances related to the use of carbon nanotubes and their composites as sensors and actuators, while “Gibson *et al* (2007)” reviewed recent publications dealing with vibrations of carbon nanotubes and their composites, and “Sun *et al* (2009)” reviewed articles dealing with various types of energy absorption in nanocomposites. With the addition of very small amounts of carbon nanotubes, nonconducting polymers and polymer composites can be transformed to conducting materials, thus enhancing their multifunctionality. Accordingly, “Bauhofer and Kovacs (2009)” have reviewed relevant research on electrical percolation in carbon nanotube polymer composites. Modeling and analysis of functionally graded materials (FGM) have been reviewed by “Birman and Byrd (2007)”. “Montalvao *et al* (2006)” reviewed vibration-based SHM of composite materials, while a similar review with emphasis on composite delamination identification had been published earlier by “Zou *et al* (2000)”.

All the results on the status of nanocomposite incorporations into aeronautic structures highlight the need to further investigate on the possibility to transfer the very interesting nanostructure properties to specific composites. The aim of this project is situate in this context; in fact, while there is no doubt about the enormous potentiality of the nanotechnology to develop new multifunctional materials, not many projects have been developed with the intent to use the advantages of the recent discoveries in a specific sector such as the aeronautic field. For example, it can be observed that many papers dealing with the advantage of carbon nanostructured forms (CNTs, graphene sheets, etc) in the thermosetting matrix relay results on epoxy formulations entirely inappropriate for aeronautic components. Only very recently, the technological benefits of such systems have begun to be identified for targeted applications, and demonstrators are under construction for a wide range of applications from space and aerospace, to civil engineering and domestic products. For this project, the technological benefits will be direct toward the development of a new generation of aeronautic composites.

### **I.3 Research strategies**

The multifunctional composite has been developed in such a way as to impart to the materials specific abilities and functions to increase electrical conductivity, and simultaneously flame resistance.

A particular attention has been focused on the manufacturing aspects related to the integrations of multifunctional materials into real carbon fiber reinforced panels. This is a revolutionary approach that should lead to the

creation of novel generation of materials with desired properties and design flexibilities.

### ***1.3.1 Reduced electrical conductivity: Current technology***

Most aircraft skins are made primarily of aluminium, which is a very good conductor of electricity. By making sure that there are no gaps in this conductive path, the engineer can assure that most of the lightning current will remain on the exterior skin of the aircraft. These designs are thoroughly tested before they are incorporated in an aircraft. Some modern aircrafts are made of advanced composites which are significantly less conductive than aluminium. Then, the composites are reinforced with conductive metal fibers or metal screens in order to dissipate lightning currents.

But many of these solutions add additional weight and reduces composite advantage.

The research strategy proposed to overcome this drawback consists in the use of conductive nanofillers into the polymeric matrix to enhance mechanical and electrical properties and improve additional properties such as flame retardant behaviour. In this work, appropriate carbon based nanofillers have been embedded inside on epoxy resin specifically formulated for aeronautic application to boost the electrical properties of the composite. Materials such as carbon nanotubes, carbon nanofibers, and carbon nano sheets (graphene) were investigated. Carbon nanotubes and graphene show remarkable thermal and mechanical features as well as extraordinary electrical properties. A critical point in order to transfer these excellent filler properties to the composite material is the homogeneous inclusion of the nanostructured materials in the polymeric matrix. Carbon nanotubes and graphene sheets form agglomerated bundles and pillars, respectively, due to very strong inter-tubular and inter-layer Van der Waals interactions. A critical issue in obtaining the desired composite properties is in the complete and uniform dispersion of nanoparticles within the matrix. The dispersion has been optimized through an appropriate choice of both the mixing techniques and the selection and treatment of the components in such a way as to exploit the synergy of their chemical interactions in order to realize a multifunctional material.

#### ***1.3.1.1 Research activity***

In particular, thermosetting nanocomposites, including nanofillers (MWCNTs and graphene sheets) have been prepared. Epoxy resin, as a polymer matrix, has been used to manufacture the thermosetting nanocomposites.

This activity has been articulated following different approaches:

A- choice of the carbon nanotubes

B- preparation of graphene sheets

C- incorporation of the nanostructured materials into the polymeric matrix.

A- choice of the carbon nanotubes

The most relevant issues to be considered in the development of innovative CNT-based composites with improved mechanical and electrical properties are: i) the possibility to achieve an effective dispersion of CNTs ii) the capability to create a strong adhesion to the polymeric matrix leading to the formation of strong interfacial bonding. The two effects are not strictly related, because one can have a good dispersion without achieving strong adhesion; moreover the second effect, determinant for mechanical properties, is less important for electrical conductivity. An optimization of the composite may be pursued by varying the CNT type, preparation technique and processing parameters. Although several research groups have analyzed these relevant issues by considering either the basic physical phenomena or the technological aspects, there are still different questions to clarify “Xie *et al.* (2005); Martin *et al.* (2005); Sandler *et al.* (2003); Moisala *et al.* (2006); Kovacs *et al.* (2007); Kim *et al.* (2005); Du *et al.* (2005); Spitalsky *et al.* (2009)”. For example the oxidation of CNT performed to create a more homogeneous dispersion into the polymer, can induce nanotube damage considerably affecting both mechanical and electrical properties and depending on the oxidative treatment “Kim *et al.* (2005); Spitalsky *et al.* (2009)”.

Recent reviews considering most of the published results on this topic pointed out some interesting results, regarding the maximum achievable conductivity. Interestingly, type (SWCNT or MWCNT) and treatment (purification, oxidation) of the nanotubes do not show a clear impact on the maximum conductivity, whereas contradicting results about the dependence of the conductivity on the aspect ratio are reported. Indeed, dispersion seems the determinant factor to reach higher conductivity. As an example, it was reported that the epoxy composites filled with well dispersed CNTs yield much higher values of electrical and thermal conductivity than samples with poor dispersion “Xie *et al.* (2005)”. It is suggested that this happens because the well dispersed CNTs can effectively form conductive paths even at lower loading. However, it is emphasized that the best dispersion not necessarily leads to the highest conductivities, since a good dispersion can imply the formation of a polymer layer around the carbon nanotubes, which encapsulate and insulate it, thus preventing the formation of a high-conductance percolation path “Guadagno *et al.* (2011a)”. In reference “Guadagno *et al.* (2011a)” it has been shown that the nanotube functionalization with  $-COOH$  has a strong influence on the electrical properties and results in a remarkable reduction of the conductivity of the composite. For this reason, in developing the PhD project, to impart good electrical properties, very accurate controls were performed on the nature of

CNTs, functional groups and interactions between nanotubes and epoxy matrix.

#### B- preparation of graphene sheets

Graphene has emerged as a subject of enormous scientific interest due to its exceptional electron transport, mechanical properties, and high surface area. When incorporated appropriately, these atomically thin carbon sheets can significantly improve physical properties of host polymers at extremely small loading.

Because of the great interest generated by the exceptional properties of graphene sheets and the discovery of methods for their production, researchers all over the world are studying graphene “Kim *et al.* (2010)”.

Among the methods for preparation of graphene sheets, the “Bottom-Up” methods to produce graphene sheets were excluded.

In bottom-up processes, graphene is synthesized by a variety of methods such as chemical vapour deposition (CVD), arc discharge, epitaxial growth on SiC, chemical conversion, reduction of CO, unzipping carbon nanotubes, and selfassembly of surfactants. CVD and epitaxial growth often produce tiny amounts of large-size, defect-free graphene sheets. They may be more attractive than the mechanical cleavage method for production of graphene sheets for fundamental studies and electronic applications but are not a suitable source for polymer nanocomposites that require a large amount of graphene sheets preferably with modified surface structure. The main disadvantages of these methods (existence of defects, small production scale, low yield of graphene, carbonaceous impurities, expensive starting materials, oxidized graphene, contamination with  $\alpha$ -Al<sub>2</sub>O<sub>3</sub> and  $\alpha$ -Al<sub>2</sub>S) “Kim *et al.* (2010)” lead us to count on “Top-Down” methods to produce Graphene sheets.

In developing the PhD project “graphene sheets” were produced by top-down processes.

In order to fully exploit the outstanding properties of graphene-based composites, a mass production method of the graphene sheets is necessary. The approach that has been used consists in the preparation of graphene-polymer composites via complete exfoliation of graphite and molecular-level dispersion of individual, chemically modified graphene sheets within oligomer host. The method of preparation of this nanofiller consists of oxidizing the graphite to obtain the graphite oxide whose exfoliation is the only way to produce suspensions of two-dimensional carbon sheets. In literature, it has already been demonstrated that the exfoliation behavior of graphite oxide using top-down processes allows to obtain a large amount of nanofiller.

In top-down processes, graphene or modified graphene sheets are produced by separation/exfoliation of graphite or graphite derivatives (such as graphite oxide (GO) and graphite fluoride). In general, these methods are suitable for

large scale production required for polymer composite applications. Starting from graphite or its derivatives offers significant economic advantages over the bottom-up methods; graphite is a commodity material with current annual global production of over 1.1 million tons at \$825/ton. Therefore, the top-down approaches will be discussed in more detail. Figure I.5 shows a block diagram which summarizes the different routes reported for production of graphene or modified graphene starting from graphite or GO. Alkali metal- or acid-intercalated graphite can be expanded upon heat treatment to produce a thicker (also <100 nm) form of 2-D carbon known as expanded graphite (EG), which is commonly used as a filler for polymer composites.

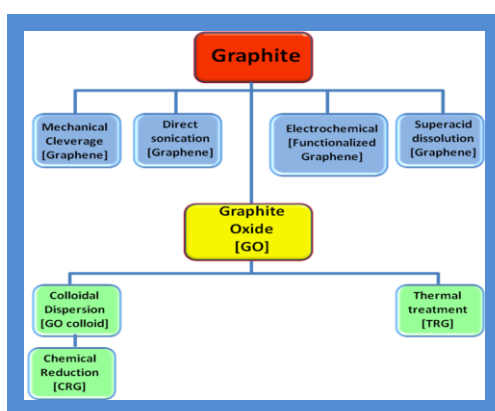


**Figure I.5** Top-down methods for production of graphene and modified graphene starting from graphene or via graphene oxide (GO)

The graphite oxide (graphite oxide - GO) can be prepared according to the already published method “Staudenmaier (1898)” from the high surface area graphite (graphite - G), dispersing the graphite nitrating mixture and using  $\text{KClO}_3$  as oxidizing agent. The chemical oxide can be reduced (CRGO) using hydrazine monohydrate as a reducing agent (see Figure I.6). The layers of GO are functionalized with carboxyl groups, phenolic and epoxy, while the chemical reduction of graphite oxide provides a partially reduced product, which still functions hydroxyl and epoxy “Stankovich *et al.* (2007)”. The functions of GO and GRGO can be used to bind chemically a polymerizations initiators, and the polymers can be grown directly on graphene sheets.

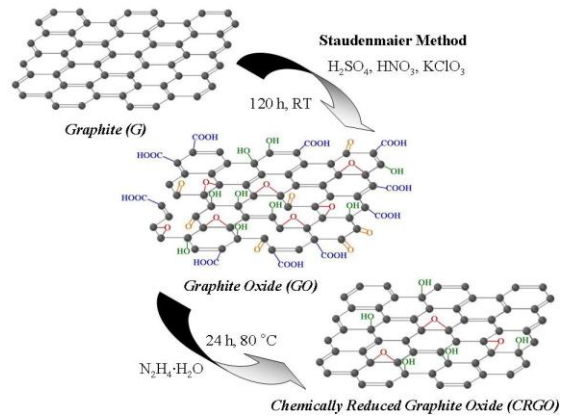


**Figure I.6** Synthesis scheme of chemically reduced graphite oxide

### 1.3.2 Poor flame resistance: Current Technology

Currently no fire resistance requirements exist for exterior polymer composite structures on airplanes. However, the aircraft manufacturer will be required to demonstrate that polymer structural composites provide high or equivalent safety with respect to the traditional material system (aluminium alloy). For this reason the development of efficient strategies to overcome this critical point is strongly desired.

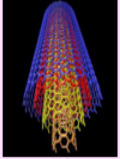
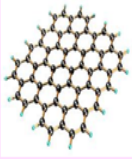
#### 1.3.2.1 Research strategy

Two work strategies (the second of these is to reach the goal without adding new nanofillers to simplify the composition of a multifunctional epoxy matrix) have been proposed.

The first approach involved the inclusion of new molecular fillers (POSS) with reactive epoxy groups in the formulated thermosetting aeronautic resins. For this approach the experimental results are shown in the chapter VIII.

The second approach concerned the identification of reactive organophosphorus compounds that could be incorporated into epoxy formulations to provide fire-resistant structural composites without to compromise the processing conditions and handling, physical, and mechanical properties. In this regard, the intention was to replace part of the common hardener agent (DDS) with a mixture of Bis(3-aminophenyl)phenylphosphine oxide (BAPPO) and Bis(3-aminophenyl)methylphosphine oxide (BAMPO). Actually these hardener agents are not commercial products, they were synthesized and characterized. For this approach the experimental results are shown in the

chapter IX. The Figure I.7 summarizes the aim and the research strategies designed to overcome drawbacks related to technical targets required for aeronautical composite.

<b>TARGET OF THE PROJECT</b>	
<b>OVERCOME DRAWBACKS RELATED TO TECHNICAL TARGETS REQUIRED FOR AERONAUTICAL COMPOSITE</b>	
<b>Reduced Electrical Conductivity</b> <b>Poor Flame Resistance</b>	<b>HOW TO OVERCOME THESE DRAWBACKS?</b>
<b>RESEARCH STRATEGIES:</b>	
<b>REDUCED ELECTRICAL CONDUCTIVITY</b>	<b>POOR FLAME RESISTANCE</b>
<p>Use of <u>conductive nanofiller into polymeric matrix to enhance mechanical and electrical properties and to improve additional properties such as flame retardant behaviour.</u></p> <div style="display: flex; justify-content: space-around; align-items: center;">    </div>	<p><u>First Approach</u> Inclusion of <u>new molecular fillers (POSS) with reactive epoxy groups</u></p> <p><u>Second Approach</u> Identification of <u>reactive organophosphorus compounds that could be incorporated into epoxy formulations to provide fire-resistant structural composites without to compromise the processing conditions and handling, physical, and mechanical properties.</u></p>
<p><u>How to combine two different functionalities?</u></p> <p><u>Use of nanofiller (carbon nanostructured forms) as conductive network inside an epoxy resin hardened and/or filled with new molecules</u></p>	

**Figure I.7** Scheme of research strategies

### 1.3.2.2 Motivation of the chosen work strategies

One of the main disadvantage of epoxy resins, as generally of other organic polymers, is their flammability. In order to meet application requirements their flame retardant properties have to be improved by maintaining other important characteristics as thermal and mechanical properties, and also considering environmental issues as risks for human life and environment, waste treatment and recycling “Toldy (2007a)”.

Successful strategies to reduce the flammability of a material involve breaking the complex combustion process at one or more stages to reduce the rate and/or change the mechanism. A flame retardant interferes with one

or more steps of the combustion cycle, which include heating the polymeric material, subsequently degrading it, and further combusting the volatiles.

There are two ways to interrupt the burn cycle. One method, solid phase inhibition, involves the polymer substrate. In this method, a flame retardant inhibits combustion by forming a glass-like coating, preferably of low thermal conductivity, on the surface of the material exposed to heat. The coating layer consists of highly crosslinked carbonaceous char that insulates the underlying polymer from the heat of the flame, thus inhibiting the production of new fuel. The retardant may also degrade endothermally, thereby absorbing the energy needed to maintain the flame.

The second method of interrupting the flame cycle, vapor phase inhibition, involves changing the flame's chemistry. A flame retardant may be transformed into a volatile free-radical inhibitor, thus deactivating the highly active propagating radicals that result from chain scission during the combustion process to quench the flame.

Flame retardants are classified into two main categories: additives, which are mechanically blended with the polymeric substrate, and reactives, which are chemically bonded to the polymer either by copolymerization or by modification of the parent polymer. Although often cheaper and more widely used, additives can result in more detrimental side effects. For example, simple additives do not become an integral part of the polymer matrix, so the material's physical and mechanical properties may be adversely affected. In addition, the additives may leach out of the plastic over time.

Flame retardant additives used with synthetic polymers include organic phosphorus compounds, organic halogen compounds, and combinations of organic halogen compounds with antimony oxides. Inorganic flame retardants include hydrated alumina, magnesium hydroxide, borates, et. al. "Williams (2010)".

The use of phosphorus (P) as a flame retardant, particularly in epoxy resins, has been widely studied and is the subject of recent review articles with the aim to develop new structural materials with improved fire resistance and reduced smoke and toxicity. My effort concentrated on the use of bis(3-aminophenyl)methylphosphine oxide as a curing agent for epoxies (see Figure I.8).

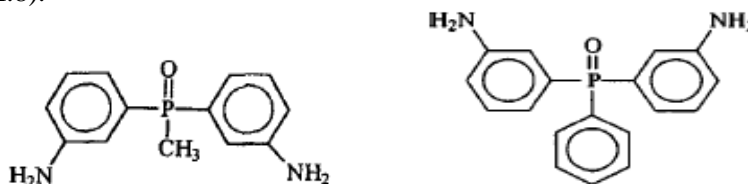


**Figure I.8** Structural formula of bis(3-aminophenyl)methylphosphine oxide and bis(3-aminophenyl)phenylphosphine oxide

Phosphorus, when incorporated in polymers as an additive or reactive comonomer, is known to impart fire retardation by condensed phase and gas

phase mechanisms. In the condensed phase, P catalyzes char formation that protects the underlying material from heat and acts as a barrier to the release of fuel gases from the surface. When acting in the condensed phase as a char catalyst, P retards the spread of fire with minimal release of toxic gases. In the gas phase, P acts as a flame poison with PO species participating in a kinetic mechanism that is analogous to that of halogens in flames. Phosphorus has been incorporated into polymeric materials both as an additive and as part of the polymeric chain. Additives are normally more economical but tend to leach out and have a negative impact on processability and mechanical properties. Cured epoxy resins have a high concentration of hydroxyl (OH) groups and, therefore, P-containing flame-retardant compounds are particularly effective because P tends to react with OH groups “Hergenrother *et al.* (2005)”.

In particular, the phosphine oxide groups have the advantage of containing the hydrolytically stable P-C bond (compared to P-O-C) and the oxidatively stable P=O bond (compared to phosphine). Polymers containing phosphine oxide moieties typically display good flame resistance, high thermal oxidative stability, enhanced solubility, and improved miscibility and adhesion “Zhuang (1998)”.

#### First approach (inclusion of POSS molecules)

Polyhedral oligomeric silsesquioxanes, POSS, are a unique class of materials that have the general formula  $(\text{RSiO}_{1.5})_n$  “Li *et al.* (2002)”. At least some of the R groups are usually unreactive, as phenyl, methyl, *etc.*, but one can also incorporate one or more reactive groups, *e.g.*, styryl, methacrylate, *etc.* The presence of a polymerizable substituent enables the formation of polymers, either by direct polymerization or co-polymerization with another monomer. The diameter of the POSS is typically on the order of 15 Å and they are, in general, easily incorporated into a polymer matrix. The generalized structure of a POSS system is shown in Figure I.9. This consists of substituents R, which are unreactive and provide for compatibilization and solubility, and reactive groups X (only one of which is shown in this figure but more are possible) attached to a chemically and thermally robust hybrid framework. The composition is intermediate between that of silica and silicon; it offers a precise three-dimensional structure for reinforcement at the molecular level of polymer segments. There has been much less work in fire retardancy with POSS than with clays, one US patent “Lichtenhan and Gilman (2002)” and one paper “Devaux *et al.* (2002)”. The patent shows that POSS significantly reduces the PHRR for a polyether-block-polyamide system (50–70% reduction), for polypropylene (a 40% reduction) and a styrene-butadiene-styrene (SBS) triblock polymer (40–60% reduction).

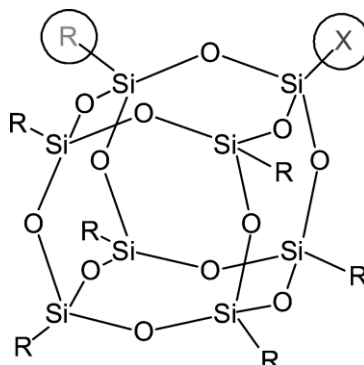


**Figure I.9** Generalized structure of a POSS material

The decrease in the time to ignition has not been experimented for aeronautic epoxy resins. For POSS with polyurethane fabrics 30 the reduction in peak heat release rate (PHRR) is about 55%. It appears that POSS materials should be more widely studied as fire retardant systems, since the reduction in PHRR is quite large and the time to ignition shows a more useful behavior.

Due to these benefits, in this work POSS compounds were solubilized or embedded in the formulated epoxy mixture, and then the finished properties of the material were analysed.

Second approach (identification of reactive organophosphorus compounds)

This work started with the synthesis, characterization and efficiency evaluation of reactive organophosphorus compounds that have been incorporated into epoxy formulations to provide fire-resistant structural composites. These new hardener agents (mixture of Bis(3-aminophenyl)phenylphosphine oxide and/or Bis(3-aminophenyl)methylphosphine oxide) replace part of the common hardener agent (DDS) (see Figure I.10)

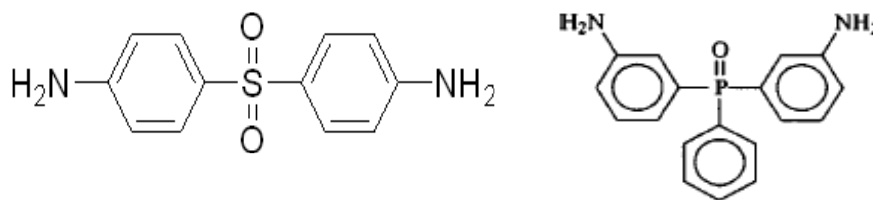


**Figure I.10** 4,4'-Diaminodiphenyl sulfone (DDS) and bis(3-aminophenyl)phenylphosphine oxide (BAPPO)

Why new syntheses?

Advantages of these new products: these synthesized molecules become an integral part of the thermosetting matrix also acting as hardener agents (with

the same initial reactions as those activated by DDS, a hardener agent already used to manufacture resins in the aeronautic field). It is worth noting that this partial replacement should contribute to fabricate fire retardant composites preserving the good mechanical performances due to the DDS hardener agent with a very similar molecular structure.



---

## Chapter II

---

# Development of epoxy mixtures for application in aeronautics and aerospace

### II.1 Preface

In this chapter I will describe a successful attempt toward the development of aeronautic materials based on nanofilled epoxy resins. The epoxy matrix was prepared by mixing a tetrafunctional epoxy precursor with a reactive diluent which allows to reduce the moisture content and facilitate the nanofiller dispersion step. The reactive diluent also proves to be beneficial for improving the cure degree of nanofilled epoxy mixtures. It increases the mobility of reactive groups resulting in a higher cure degree than the epoxy precursor alone. This effect is particularly advantageous for nanofilled resins where higher temperature treatments need, compared to the unfilled resin, to reach the same cure degree. As nanofiller, different carbon nanostructured fiber-shaped fillers were embedded in the epoxy matrix with the aim of improving the electrical properties of the resin. The results highlight a strong influence of the nanofiller nature on the electrical properties especially in terms of electrical percolation threshold (EPT) and electrical conductivity beyond the EPT. Among the analyzed nanofillers, the highest electrical conductivity is obtained by using multiwall carbon nanotubes (MWCNTs) and heat-treated carbon nanofibers (CNFs). The achieved results have been analyzed by considering the nanofiller morphological parameters and characteristics with respect to the impact on their dispersion effectiveness.

### II.2 General remarks

In order to choose an effective epoxy mixture, it is necessary to consider that the structure of the resin strongly governs its chemical and some of the physical properties. The number of reactive sites in the epoxy precursors controls the functionality directly acting on the cross-linking density. This,

combined with the nature of hardener agent, the functionality, the stoichiometry and the curing cycle determines the final properties of the cured resin especially in terms of mechanical and thermal properties. Conversely, some of the physical properties, such as electrical conductivity can be quite improved by embedding very small amount of conductive nanoparticles. The use of conductive nanofillers inside of polymeric matrices to enhance electrical properties seems to be a very useful strategy to increase the performance of the composite. In this way when used to form structural parts (e.g. the aircraft fuselage) if a sufficiently high (around 10 S/m) conductivity is reached, the material is able to dissipate lightning currents without employing conductive metal fibers or metal screens which are detrimental in terms of overall weight. Along this stream, in these last few years, various nanofillers or nanostructured conductive materials have been made commercially available which offer a significant chance to reach such a technological goal. By selecting the appropriate resin system with specific nanofillers, critical points in the properties of aeronautical materials might be solved. Among the nanofillers, a particular attention has been addressed to carbon nanostructured fibre-shaped fillers, as CNTs and CNFs. Indeed, since Iijima's landmark paper in 1991 "Iijima (1991)", carbon nanotubes (CNTs) have spurred many researchers on developing advanced CNT composite materials to transfer some of their excellent physical properties to polymeric matrices "Andrews and Weisenberger (2004); Coleman *et al.* (2006a); Moniruzzaman and Winey (2006); Coleman *et al.* (2006b); Xie *et al.* (2005); Guadagno *et al.* (2009b); Guadagno *et al.* (2011a)". Actually, CNTs are considered one of the strongest materials known and very promising to manufacture a very versatile class of composites for structural applications. CNTs in polymeric matrices offer the possibility to combine complementary interesting properties. As conductive filler with high aspect ratio, CNTs are more effective than traditional carbon black "Sandler *et al.* (2003); Khare and Bose (2005)", thus allowing to obtain composite materials with high electrical conductivity at lower filler concentrations "De Vivo *et al.* (2009a); Guadagno *et al.* (2010c); Iannuzzo *et al.* (2008)". CNFs, though not perfect in the structure and less conductive, are fairly more economical than CNTs for manufacturing epoxy-based systems because they are easier to disperse, process and functionalize. Simultaneously they provide mechanical and electrical property enhancements but with a lower overall cost. These composites are increasingly used for aircraft structures and need to be engineered for efficient lightning strike protection to achieve tolerance similar to that of traditional metal-alloys. The aim of this work is situated in this contest. We have tried to increase the electrical conductivity of a nanofilled epoxy resin tailored to meet specific needs of the aeronautic field. We have chosen carbon fibre-shaped fillers as MWCNTs and CNFs because they have proven to be very effective in improving electrical conductivity of polymeric matrices. In particular, we have examined the properties of a

nanofilled resin obtained by dispersing MWCNTs and CNFs inside of an epoxy mixture based on a tetrafunctional epoxy precursors, the TetraGlycidyl-MethyleneDiAniline (TGMDA), cured with 4,4'-diaminodiphenyl sulfone (DDS). This precursor was selected among several solutions because it shows suitable properties for fibrous composites in aerospace applications. Generally, the physical properties of epoxy resins strongly depend on the functionality of the epoxy precursor, a tetrafunctional precursor assures good properties of the cured resin due to the high level of crosslinking density. Unfortunately, this advantage also causes inconveniences resulting from the brittleness and poor resistance to crack propagation. In this work, the toughness of the tetrafunctional epoxy precursor has been increased by blending the epoxy precursor with a reactive modifier that performs a double function, as flexibilizer and regulator of viscosity for a best dispersion of MWCNTs and CNFs. Preliminary results on the physical properties of unfilled and nanofilled resins appear very promising. In particular, the use of reactive diluent in the epoxy mixture reduces the moisture content, eases the step of nanofiller dispersion and allows to reach higher curing degree compared to the epoxy precursor alone. The electrical conductivity values obtained for the epoxy mixture filled with two nanofillers are compared to identify the most promising systems and understand the relations between the electric transport property and the morphological characteristics of the materials. In particular, the role of electron tunneling is discussed on the basis of the dc conductivity measurements "Connor *et al.* (1998); Mdarhri *et al.* (2008)". Moreover, the ac characteristics are analyzed in the frequency range [0.1,1000] kHz in order to highlight the effect of the diverse aggregation and dispersion of the adopted fillers inside the matrix. The interpretation of the different performances are congruent with the morphological observations. The properties of the cheaper and easy-to-process CNFs-based composites appear to be promising for the considered aeronautic application.

## II.3 Experimental section

### II.3.1 Materials and sample preparation

The epoxy matrix was prepared by mixing an epoxy precursor (TGMDA) (*Epoxy equivalent weight 117-133 g/eq*), with an epoxy reactive monomer 1,4-Butandioldiglycidylether (BDE) that acts as flexibilizer and reactive diluents. These resins, both containing an epoxy, were obtained by Sigma-Aldrich. The curing agent investigated for this study is 4,4'-diaminodiphenyl sulfone (DDS). Figure II.1 shows the chemical structures of these compounds.

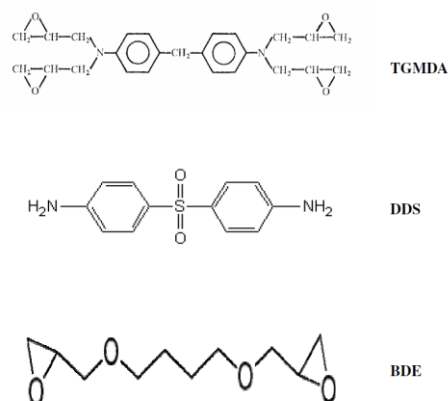


**Figure II.1** Chemical structures of compounds used for the epoxy matrix composite

The MWCNTs (3100 Grade) was obtained from Nanocyl S.A. The specific surface area of both multi-wall carbon nanotubes determined with the BET method is around 250–300 m<sup>2</sup>/g, the carbon purity is >95% with a metal oxide impurity <5% as it results by thermogravimetric analysis (TGA). TEM investigation has shown for the CNTs a diameter around 20 nm. CNFs were produced at Applied Sciences Inc. and were from the Pyrograf III family. The pristine CNFs are labelled as PR25XTPS1100 where XT indicates the debulked form of the PR25 family, PS indicates the grade produced by pyrolytically stripping the as-produced fiber to remove polyaromatic hydrocarbons from the fiber surface and 1100 is the temperature in the process production. Sample PR25XTPS1100 was thermally treated to 2500°C to provide the sample named PR25XTPS2500. The epoxy matrix was obtained by mixing TGMDA with BDE monomer at a concentration of 80%:20% (by wt) epoxide to flexibilizer. DDS was added at a stoichiometric

concentration with respect to the epoxy rings. Epoxy blend and DDS were mixed at 120°C and the nanofillers (MWCNTs or CNFs) were added and incorporated into the matrix by using a ultrasonication for 20 minutes (Hielscher model UP200S-24KHz high power ultrasonic probe). All the mixtures were cured by a two-stage curing cycles: a first isothermal stage was carried out at the lower temperature of 125°C for 1 hour and the second isothermal stage at higher temperatures up to 180°C or 200°C for 3 hours. These samples are named TGMDA+DDS+BDE(20%)+CNT(X%)(Y°C) where X is the CNT percentage and Y is the temperature of the second stage.

### ***II.3.2 Methods***

Thermal analysis was performed with a Mettler DSC 822 differential thermal analyzer in a flowing nitrogen atmosphere. SEM micrographs were obtained using a Field Emission Scanning Electron Microscope (FESEM, mod. LEO 1525, Carl Zeiss SMT AG, Oberkochen, Germany).

Some of the nanofilled sample sections were cut from the solid samples by a sledge microtome. These slices were etched before the observation by FESEM microscopy. The etching reagent was prepared by stirring 1.0 g potassium permanganate in a solution mixture of 95 ml sulphuric acid (95-97%) and 48 ml orthophosphoric acid (85%). The filled resins were immersed into the fresh etching reagent at room temperature and held under agitation for 36 hours. Subsequent washings were done using a cold mixture of 2 parts by volume of concentrated sulphuric acid and 7 parts of water. Afterwards the samples were washed again with 30% aqueous hydrogen peroxide to remove any manganese dioxide. The samples were finally washed with distilled water and kept under vacuum for 5 days. The nanofilled sample sections were placed on a carbon tab previously stuck to an aluminum stub (Agar Scientific, Stansted, UK). The samples were covered with a 250-Å-thick gold film using a sputter coater (Agar mod. 108 A). TEM images were recorded on high-resolution transmission electron microscopy (HRTEM) JEM-2100 (JEOL, Japan) operating at 100 kV accelerating voltage. Nanofilled cured samples were sectioned by microtome with a section thickness down to 150 nm and collected on a 400 mesh holey carbon-coated copper grid.

Dynamic mechanical properties of the samples were performed with a dynamic mechanical thermo-analyzer (TA instrument-DMA 2980).

Solid samples with dimensions 4x10x35 mm<sup>3</sup> were tested by applying a variable flexural deformation in dual cantilever mode. The displacement amplitude was set to 0.1%, whereas the measurements were performed at the frequency of 1 Hz. The range of temperature was from -60°C to 300°C at the scanning rate of 3°C/min.

Infrared spectra were performed at room temperature by using a Bruker

Vertex 70 FTIR spectrophotometer with a  $2\text{ cm}^{-1}$  resolution (64 scans collected).

Water transport properties were analyzed for unfilled and nanofilled resins. The samples were cut into samples with dimensions of  $40\times 20\times 0.50\text{ mm}^3$  immediately after the curing cycle. The thickness of the water absorption test samples was made small, deliberately, compared to its width and length, such as edge effects can be ignored and simple one-dimensional diffusion model analysis can be applied without incurring significant error. The specimens were placed into distilled water chambers maintained at constant temperatures of  $25^\circ\text{C}$ . The specimens were weighed periodically using a digital balance with  $0.01\text{ mg}$  resolution to determine the percent weight change, and, thus, water uptake. The specimens were periodically removed, dried and immediately weighed, and then returned to the water bath. The drying step was performed to ensure the removal of excessive surface (superficial) water, specimens were gently wiped dry using clean, lint-free tissue paper. The measurements of the DC volume conductivity were performed on disk-shaped specimens of about  $2\text{ mm}$  thickness and  $50\text{ mm}$  diameter by using circular metalized electrodes with a diameter of about  $22\text{ mm}$ . The samples were coated by employing a silver paint with a thickness of about  $50\text{ }\mu\text{m}$  and a surface resistivity of  $0.001\text{ }\Omega\cdot\text{cm}$  in order to reduce the contact resistance and their eventual surface roughness. The measurement system, remotely controlled by the software LABVIEW®, is composed of a suitable shielded cell with temperature control, of multimeter Keithley 6517A with function of voltage generator (max  $\pm 1000\text{V}$ ) and voltmeter (max  $\pm 200\text{ V}$ ) and the ammeter HP34401A (min current  $0.1\text{ }\mu\text{A}$ ) for samples above the percolation threshold. For ones below the percolation threshold the system is composed only of multimeter Keithley 6517A with function of voltage generator (max  $\pm 1000\text{V}$ ) and pico-ammeter (min current  $0.1\text{ fA}$ ). For sensitivity purposes the applied electric field has been  $0.5\text{ MV/m}$  for samples below the percolation threshold, whereas in order to avoid Joule heating of samples it has been set to  $5.0\text{ kV/m}$  for samples above the percolation threshold. Impedance measurements were carried out in the frequency range  $[0.1\text{-}1000]\text{ kHz}$  by using a Quadtec7600 LCR meter (0.05% Slow Measurement Accuracy) and by applying a sinusoidal voltage stress of amplitude  $0.1\text{V}$  or  $1\text{V}$  for the sample above or below the EPT respectively, in order to avoid measurements around the current saturation limit ( $100\text{mA}$ ) of the instrument for the samples with low resistivity.

### II.3.3 Results and discussions

#### II.3.3.1 Choice of the curing cycle: Thermal analysis

The cure behavior of the epoxy matrix was studied by Differential Scanning Calorimetry (DSC). This technique is especially useful for studying the cure of reactive epoxy systems because the curing is accompanied by the liberation of heat. DSC experiments can provide information on reaction rates, cure rates, and cure degree (DC) “Maas (1978); Pappalardo (1974); Sanjana and Sampson (1981)”.

In this work, DSC has been used for the estimation of the DC of the samples under the assumption that the exothermic heat evolved during cure is proportional to the extent of reaction. This assumption has already been adopted by other authors “Horie *et al.* (1970); Edwards and Ng (1968)”. The DC can be determined from the total heat of reaction ( $\Delta H_T$ ) of the curing reaction and the residual heat of reaction ( $\Delta H_{resid}$ ) of the partially cured epoxy resin as follows:

$$DC = \frac{\Delta H_T - \Delta H_{resid}}{\Delta H_T} \times 100$$

To obtain fraction reacted at various temperatures, a series of isothermal experiments was performed. To secure accurate total  $\Delta H$  values from isothermal studies, dynamic runs were made after the isothermal curing cycle to obtain the residual heat of reaction. The total heat of reaction was considered as follow:

$$\Delta H_T = \Delta H_{iso} - \Delta H_{resid}$$

where  $\Delta H_{iso}$  and  $\Delta H_{resid}$  are the areas under the isothermal and dynamic thermograms, respectively.

In this work the cure degree of the system TGMDA+DDS and TGMDA+DDS+BDE(20%) after a two stage curing cycle composed of a first step of 125°C for 1 hour and a second step at the higher temperature of 180°C for 3 hours was analyzed. The results of calorimetric analysis performed on the two formulations are reported in Figure II.2, where we reported the DSC curve of each formulation before (uncured sample) and after the curing cycle (cured sample). A comparison of the DSC traces highlights a reduced  $\Delta H_{resid}$  for the sample wit BDE.

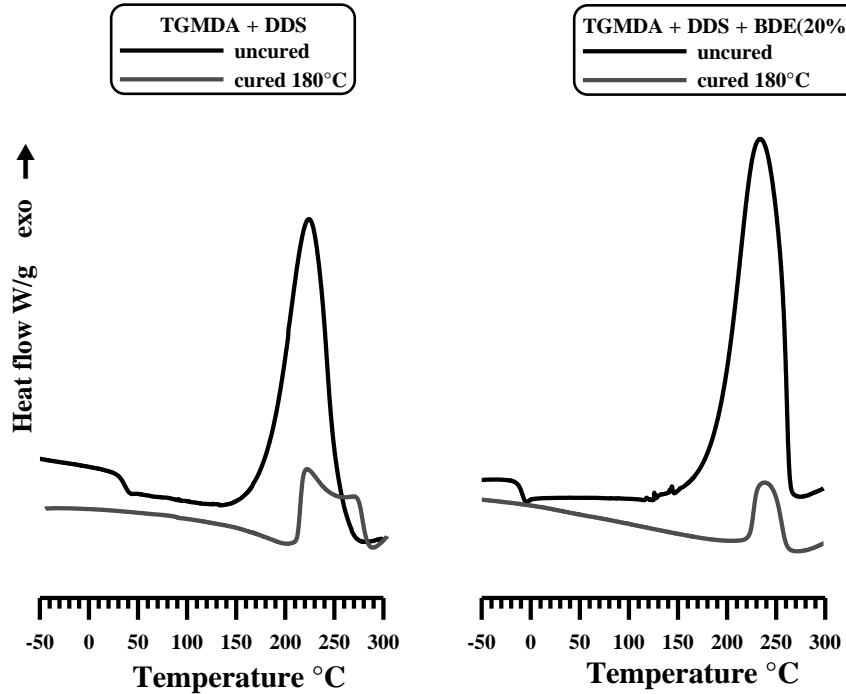


**Figure II.2** DSC curves of: a) the uncured and cured epoxy resin TGMDA+DDS (without reactive diluent) on the left side, and b) the uncured and cured epoxy mixture TGMDA+DDS+BDE(20%)(TGMDA with reactive diluent/DDS) on the right side

The cure degrees for TGMDA+DDS and TGMDA+DDS+BDE(20%) were found to be 80% and 91% respectively. This result has proven that, in the case of TGMDA+DDS+BDE(20%) system, the presence of reactive diluent BDE imparts to the segments of epoxy precursor higher mobility than the epoxy precursor alone; this in turn causes an increase in the efficiency of the curing process increasing the cure degree of about 14% using the same curing cycle.

The inclusion of MWCNTs (0.32%) in the epoxy formulation TGMDA+DDS+BDE(20%) highlighted that this gain is not enough when this formulation also includes MWCNTs. In fact, the DC decreases from 91% to 86% by adding CNTs. To increase the value of the curing degree of the nanofilled formulation, the sample was tested after a curing cycle with the second step at the higher temperature of 200°C for 3 hours. The DC value was found to be 94%, an acceptable value for aeronautic epoxy formulations (see Figure II.3). The curing degree for all the nanofilled formulations was always found higher than 92% for the curing cycle with the second step at higher temperature.

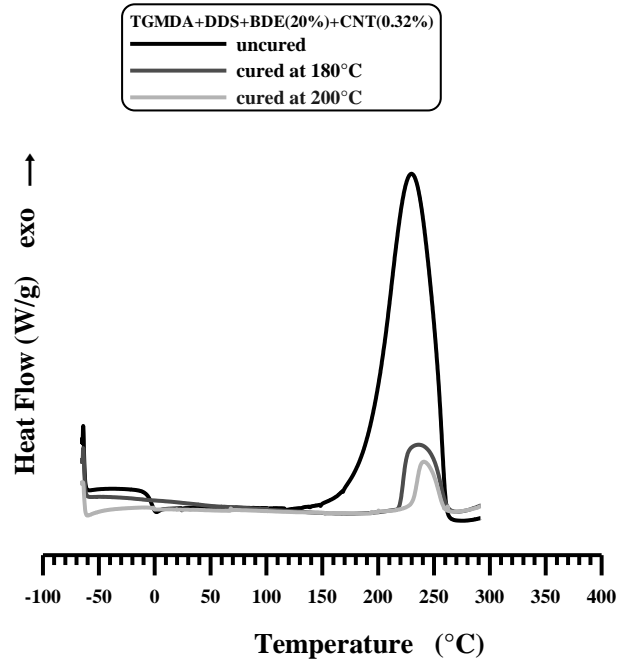


**Figure II.3** DSC curves of: the uncured epoxy mixture TGMDA+DDS+BDE(20%)+CNT(0.32%), and the same epoxy mixture cured by two different curing cycles

Temperatures higher than 220°C are necessary to obtain similar values in same curing degree of nanofilled epoxy mixtures in absence of reactive diluent.

### II.3.3.2 Dynamic Mechanical Results

Dynamical mechanical data provide useful information on the relaxation processes that become operative in the polymer in a temperature range depending on the examined system. The graphics in Figure II.4 show that the incorporation of a small concentration of MWCNTs (0.32%) in the temperature range of  $-60 \div 180^\circ\text{C}$  causes an increase in the elastic modulus value with respect to the epoxy matrix. The different temperature of the second stage of the curing cycle changes the curve profiles at temperature higher than 70°C. For the lower temperature of the curing cycle (second stage), the nanofilled composite shows a non-progressive decrease in the value of the elastic modulus with an unforeseen increase between 210 and 240°C before again decreasing. This behavior is very likely due to an increase in the cross-linking density during the heating. This increase is not observed from the pure resin (unfilled sample) with the same history of the

curing cycle, see sample TGMDA+DDS+BDE(20%)(180°C). This behavior can be explained if one assumes that the inclusion of carbon nanotubes well dispersed inside the matrix causes a reduction of the cross-linking density in a fraction of the epoxy matrix in close contact with the nanofiller. This also explain two peaks in the  $\tan \delta$  of the sample TGMDA+DDS+BDE(20%)+CNT(0.32%)(180°C) indicating the presence of a lower temperature glass transition (at 215°C), beside the main transition at the same temperature as the pristine resin (260°C).

It is very likely that this second lower transition is due to unreacted molecular segments that cause inhomogeneities from regions of varying crosslink density; since the samples TGMDA+DDS+BDE(20%)+CNT(0.32%)(180°C) and TGMDA+DDS+BDE(20%)(180°C) are formulated with the same stoichiometry and curing history, the lower cross-linking density can be ascribed only to the nanoinclusions. This secondary peak, active at a lower temperature disappears for the same composite cured up to 200°C, see sample TGMDA+DDS+BDE(20%)+CNT(0.32%)(200°C). A more effective curing cycle at higher temperature up to 200°C allows to overcome the drawback due to the inclusion of nanofiller inside the epoxy matrix. It was also observed that a different percentage of MWCNTs (data not reported here) is reflected in both the location and magnitude of the transition peak at lower temperature. These results indicate that, for the nanofilled composites, the curing history must to be optimized with respect to the unfilled formulations.

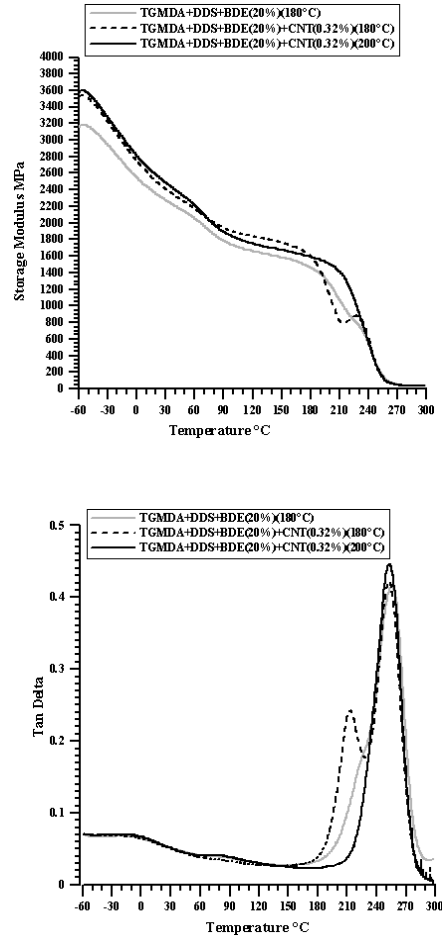


**Figure II.4** Storage modulus (MPa) (at the top), and Loss factor ( $\tan\delta$ ) (at the bottom) of the pure epoxy and the composites 0.32 wt% MWCNTs solidified up to 180 and 200°C respectively

For the reason above described, all the formulations (filled and unfilled) have been cured with a two-stage curing cycle, a first step at 125°C for 1 hour and a second step at 200°C for 3 hours.

### *II.3.3.3 Water Transport Properties*

Water vapor absorption decreases the performance of aircraft materials for the negative effects on mechanical properties, corrosion and weight. Data concerning the effect of water absorption on the mechanical properties of epoxy resins show a dramatic lowering of the glass transition temperature and the consequent degradation of high-temperature properties. Petherick et al. proposed that this depression of T<sub>g</sub> is caused by disruption of the strong hydrogen bonds in the cured network, and their replacement with weaker water-related hydrogen bonds “Maxwell and Pethrich (1983)”. In the field of structural materials for aircraft/aerospace applications more work has been done on the moisture content of TGMDA+DDS system for its properties which allow higher operating temperatures maintaining the mechanical performance. Despite these excellent properties, the water content absorbed is reported to be higher than other common epoxy resins applied as structural resins. In fact, TGMDA+DDS systems (without BDE) are reported to absorb as much as 6.5 wt% water; “Liu et al. (2005)” reported for this system a value of 7.76% (at 23°C) and “Li et al. (2009)” the value of 6.48% (at 35°C). A higher water content results in a dramatic drop in T<sub>g</sub> “Sarti (1979a); Sarti (1980b); Thomas and Windle (1980)”.

For the epoxy mixture where a reactive diluent is in the network, no data are available from the literature, therefore measurements of sorption and diffusion of liquid water at 25°C for the unfilled resin (epoxy mixture), the resin with 0.5% of MWCNT, the resin with 0.64% of heat-treated CNFs and the resin with 1% of as-received CNFs were performed. In addition, because the cured samples (without BDE) reported in literature are related to samples hardened with different curing cycles, in this work TGMDA+DDS(200°C) samples (without BDE) cured with the same curing cycle of TGMDA+DDS+BDE(20%)(200°C) epoxy system have been tested and the results are shown in Figure II.5 for water activity (a=1) at the temperature of 25°C.

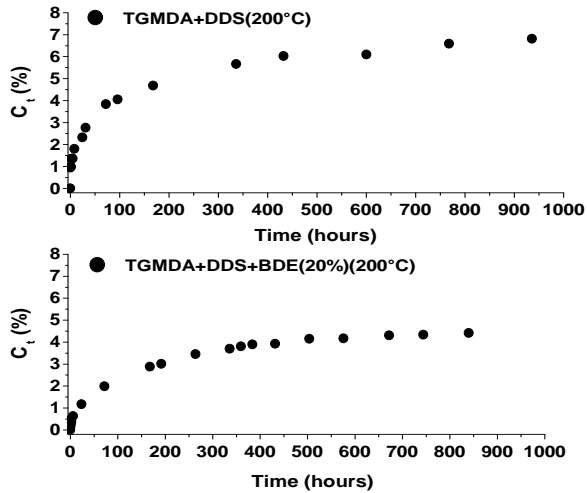


**Figure II.5** The concentration at time ( $C_t$ ) as a function of the time (hours) of the epoxy resin (without BDE), and the epoxy mixture containing the diluent

It can be seen that the presence of reactive diluent in the epoxy mixture reduces the sorption at equilibrium of liquid water ( $C_{eq}$ ) from 6.81 to 4.41. In conclusion, a percentage of 20% wt of BDE reduces the value in  $C_{eq}$  of about 35%.

The sorption at equilibrium of liquid water  $C_{eq}$  into the five samples and the diffusion parameter,  $D$  ( $\text{cm}^2/\text{s}$ ), are shown in Table II.1, while in Figure II.6 the reduced curves,  $C_t/C_{eq}$ , as a function of square root of time, normalized for the thickness  $d$  of both the unfilled resin and the nanofilled resins are shown. The concentration of water adsorbed at  $25^\circ\text{C}$  is reported as a function of time for samples having the same thickness.

**Table II.1** Diffusion parameters ( $D$ ) and Sorption values at equilibrium of liquid water ( $C_{eq}$ ) of the epoxy resin (without BDE), the epoxy mixture containing the diluent and the nanofilled mixtures

sample	$C_{eq}$ (%)	$D$ ( $\text{cm}^2/\text{s}$ )
TGMDA+DDS+BDE(20%)(200°C)	4,41	1,11E-09
TGMDA+DDS(200°C)	6,81	1,29E-09
TGMDA+DDS+BDE(20%)+ PR25XTPS2500(0,64%)(200°C)	5,04	1,25E-09
TGMDA+DDS+BDE(20%)+MWCNT(0,5%)(200°C)	5,25	1,11E-09
TGMDA+DDS+BDE(20%)+PR25XTPS1100(1,0%)(200°C)	4,92	1,35E-09
DGEBA+DDS	4,03	2,00E-09

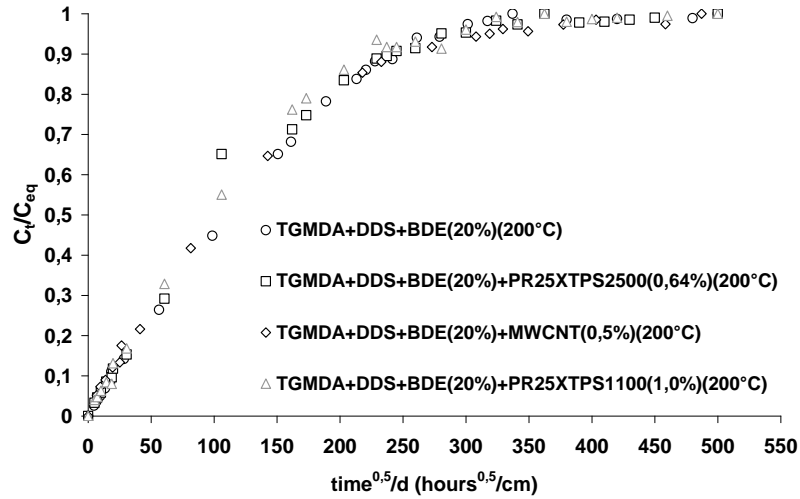


**Figure II.6**  $C_t/C_{eq}$  against the square root of time of unfilled and nanofilled mixtures

Data in Table II.1 show that at high water activity ( $a = 1$ ) the nanofilled samples are characterized by values of  $C_{eq}$  only slightly higher. This result was already found for a different epoxy matrix, DiGlycidil-Ether Bisphenol-A (DGEBA) cured with DDS at stoichiometric concentration. The thermodynamic interaction of the amorphous resin with liquid water is almost not changed by the presence of the carbon nanotubes and/or heat-treated and untreated CNFs.

The resin is highly plasticized and the most part of water molecules form clusters inside the network. It is worth recalling that, in liquid water, at activity  $a = 1$ , the plasticizing effect is in the highest degree and hides differences that could be evaluated at lower activity of water. Indeed different behavior was observed for the resin (DGEBA) cured with a different hardener agent and filled with CNT at low water vapor activity “Guadagno *et al.* (2009b)”. In this work the aim is to evaluate the difference in the more critical case ( $a=1$ ) to compare the behavior of this epoxy system with the system without BDE already studied in literature. In Figure II.6, we observe a Fickian behavior, that is a linear dependence of the reduced sorption on square root of time, a curvature for  $C_t/C_{eq} > 0.7$  and a constant value at equilibrium. This Fickian behavior gives the possibility to derive the diffusion parameter,  $D$ , by the first linear part of the curve, by the Eq. (1).

$$\frac{C_t}{C_{eq}} = \frac{4}{d} \left( \frac{Dt}{\pi} \right)^{\frac{1}{2}} \quad (1)$$

where  $C_{eq}$  is the equilibrium concentration of water,  $C_t$  the concentration at time  $t$ ,  $d$  (cm) is the thickness of the sample, and  $D$  ( $cm^2/s$ ) the mean diffusion coefficient. The value of  $D$  is between  $1.11 \times 10^{-9}$  and  $1.35 \times 10^{-9}$   $cm^2/s$ . If we consider the very small deviations on the points (attributable to experimental errors), it is evident that the diffusion of water molecules into the samples with different nanofillers follows the same curve. These results lead us to think that the small percentage of nanofiller (max 1%) has no effect on the transport behavior of the samples.

If one compares the results related to the sample TGMDA+DDS+BDE(20%) with data reported for the TGMDA+DDS system (without BDE) it can note that a lower value of absorbed water is obtained for the epoxy mixture TGMDA+DDS+BDE(20%) and also for the nanofilled epoxy resins. This value is almost comparable with the value obtained for DGEBA cured with DDS in stoichiometric amount as we can see for all the analyzed samples in Table II. 1.

#### *II.3.3.4 Thermogravimetric analysis*

Thermogravimetric analysis (TGA) can be used to study the oxidative stability of the components and formulated resins. Thermal degradation in air of the unfilled epoxy formulation TGMDA+DDS (without reactive diluent) and the reactive diluent BDE are shown in Figure II.7. The unfilled epoxy mixture begins to degrade at 320°C, while the reactive diluent at 120°C. Figure II.8 shows the thermogravimetric curves of the uncured TGMDA+DDS+BDE(20%) formulation together with the curve of the same epoxy mixture after the two step curing cycle, TGMDA+DDS+BDE(20%)(180°) and TGMDA+DDS+BDE(20%)(200°). The curve of the uncured mixture shows at 120°C the beginning of a first step of degradation involving a very small fraction of materials due to the degradation of the reactive diluent. Fortunately, the cured mixture begins to degrade at 320°C which is the temperature at which the epoxy mixture composed of only the epoxy precursor TGMDA starts to degrade. This is a very useful result which also highlights that when the reactive diluent is in the epoxy network, it is thermally stable up to 320°C. Figure II.7, on the right side, also shows the thermogravimetric curves in air of the same epoxy formulation nanofilled with a percentage of 0.32% of MWCNTs. It can see that no change in the thermogravimetric curves are shown, as the previous results, in the cured nanofilled formulation, the reactive diluent does not constitute a problem for the thermal stability of the formulation.

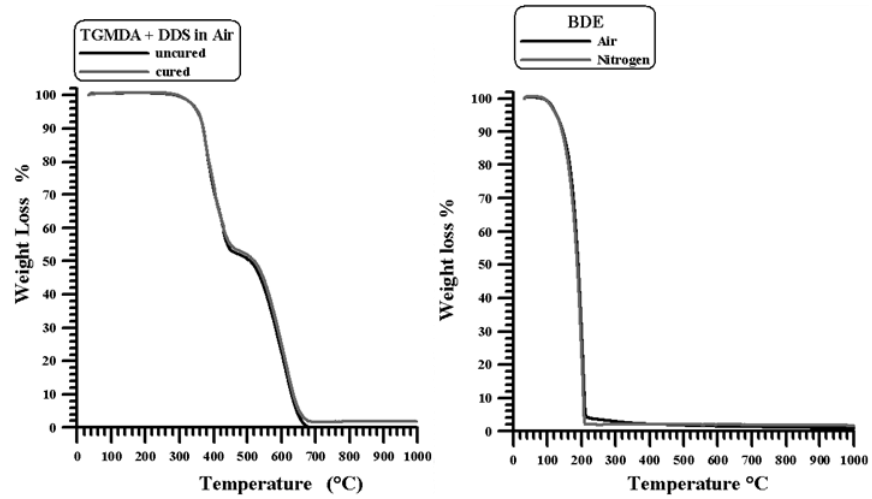


**Figure II.7** Thermogravimetric curves in air of: a) the uncured and cured unfilled epoxy resin TGMDA/DDS (without reactive diluent) on the left side, and b) the reactive diluent BDE on the right side

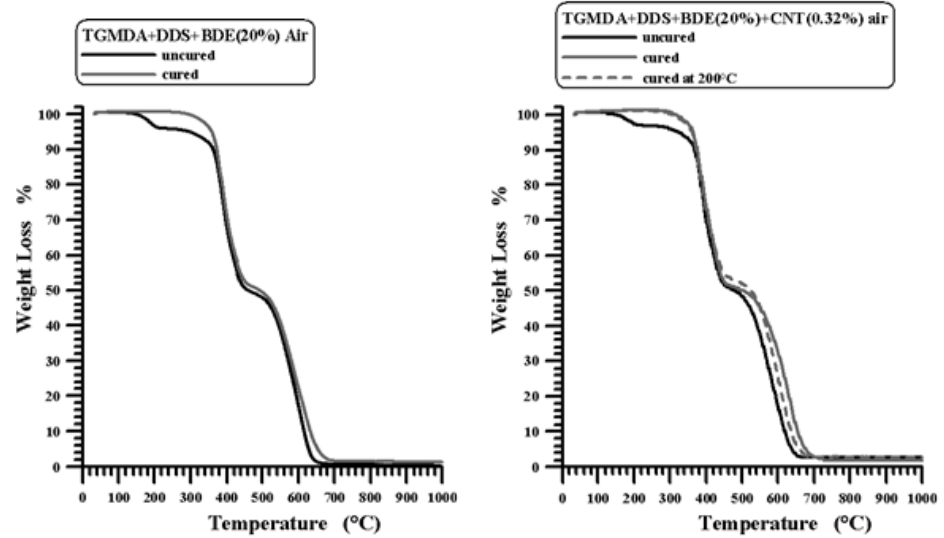


**Figure II.8** Thermogravimetric curves in air of : a) the uncured and cured unfilled epoxy mixture TGMDA+DDS+BDE(20%) (TGMDA with reactive diluent/DDS) on the left side, and b) the same epoxy formulation nanofilled with a percentage of 0.32% of MWCNTs on the right

Very similar results were obtained for the epoxy resins filled with untreated and heat treated CNFs; in addition, the different thermal treatment of CNFs does not have an appreciable effect on the degradation behaviour. On the contrary, the electrical properties here shown demonstrate the strong influence of the thermal treatment on the conductivity and electrical percolation threshold of the two different samples.

#### *II.3.3.5 Morphological investigation*

In order to analyze the homogeneity of the nanofiller dispersion in the polymeric matrix, the nanofilled samples with MWCNTs, as received CNFs and heat-treated CNFs were investigated by means SEM. Morphological analysis was carried out on etched samples to remove the resin surrounding the nanofibers, leaving them bare as described in the section “Experimental”. SEM investigation was also carried out to study the dispersion of MWCNTs at different concentration of MWCNTs. Figure II.9 shows SEM images of nanofilled epoxy composites at loading rate of 0.64 (see Figure II.9A), 0.32 (see Figure II.9B) and 0.05 (see Figure II.9C) per cent by weight. A careful observation evidences a homogeneous structure in the samples with nanofiller percentage of 0.64% and 0.32% in which the CNTs are uniformly distributed into the epoxy matrix (see Figure II.9A and Figure II.9B). In fact, for this CNT percentage, whole lengths of the carbon nanotube segments released from the residual resin fraction are observed. Figure II.9C shows the fracture surface of the epoxy composite at a nanofiller percentage of 0.05%. In this sample, the effect of etching procedure generates small “islands” of nanofilled resin which are not interconnected by CNTs as observed in Samples A and B where single nanotubes besides touching each other also create contacts in the whole mass of the sample crossing the areas where the resin was completely removed by the etching procedure. This observation was also confirmed by TEM investigation as it can be seen in Figure II.10. for sample B (0.32% of CNTs) which confirmed that single nanotube are distributed along the sample. TEM investigation for the sample filled with a lower percentage of 0.05% (not reported here) confirmed that completely separated nanotubes are embedded in the matrix. In this case the dispersion state is very different with respect to the samples A and B. In the section of Electrical Behavior it will show that this different dispersion state strongly influence the nature of the electrical interaction between nanotubes inside the epoxy matrix and therefore their conductive paths.

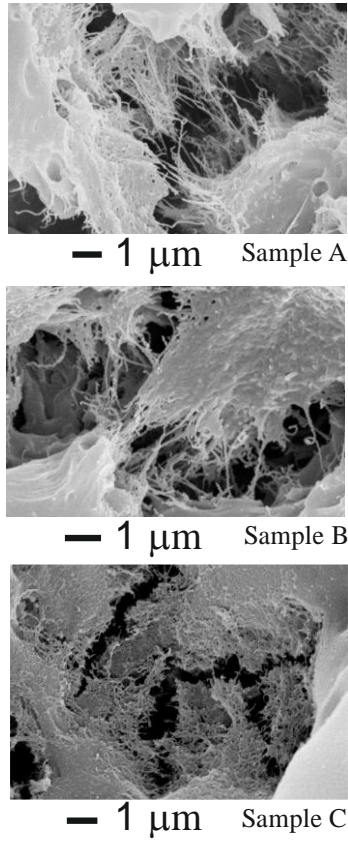


**Figure II.9** Fracture surface SEM images of the nanofilled epoxy composites at loading rate of A) 0.64, B) 0.32 and C) 0.05 per cent by weight of CNTs

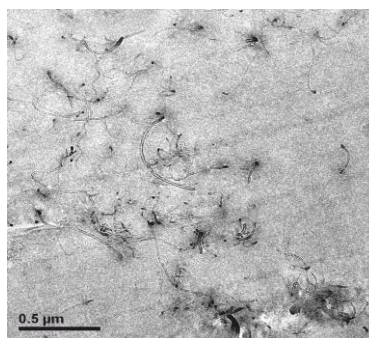
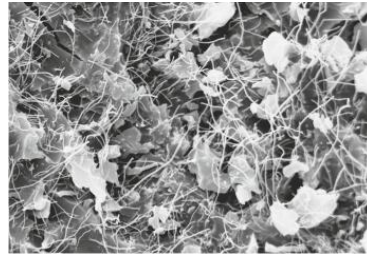
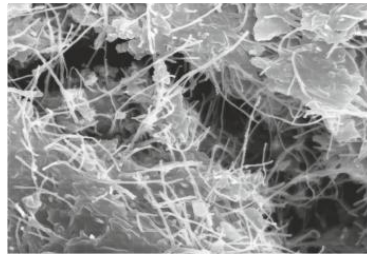


**Figure II.10** TEM image of sample B (epoxy resin at loading rate of 0.32 per cent by weight of CNTs)

Figure II.11 shows SEM images of nanofilled epoxy composites at loading rate of 0.64 per cent by weight of CNFs. The as-received CNFs filled composites are on the top and those with heat-treated CNFs are on the bottom.



— 3  $\mu\text{m}$



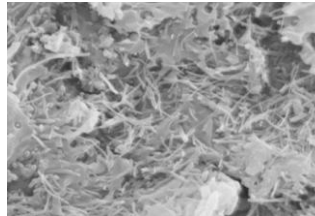
— 3  $\mu\text{m}$

**Figure II.11** Fracture surface SEM images of the nanofilled epoxy composites at loading rate of 0.64 per cent by weight: as received CNFs filled resin is on the top, heat-treated CNFs filled resin is on the bottom

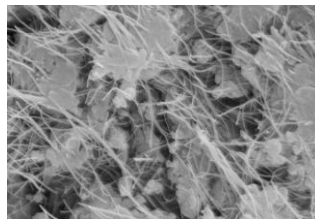
A careful observation of the SEM images seems to highlight the following:

- 1) SEM investigations highlight that CNFs are uniformly distributed in the epoxy matrix in both the samples; in fact they cover the entire surface of the samples where they are even observable as single nanofibers in each zone of the fracture surface.
- 2) heat-treated CNFs seem to be characterized by a more straight structure than un-treated CNFs. This morphological characteristic is most probably due to a more perfect rigid structure which results in a less tendency to bend with respect to untreated CNFs; as expected, the straight morphological feature is statistically observed for all the concentrations of heat-treated CNFs, as it can also be observed in Figure II.11 for the samples filled with a higher percentage of CNTs;
- 3) heat-treated CNF seems statistically to show a narrowing of the diameter, this effect can be well observed in Figure II.12 where the samples filled with untreated and heat-treated CNFs were acquired with the same magnification;
- 4) heat-treated CNF seems statistically less bonded to the epoxy matrix; this effect can be also observed in the enlargements of Figure II.13,

where it can be seen that, in the case of untreated CNFs, the majority of the CNFs is tightly tied to the epoxy matrix.

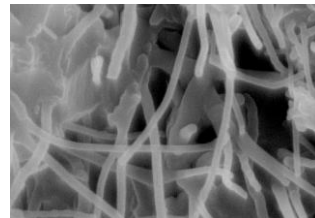


— 3 μm

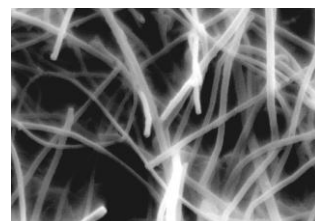


— 3 μm

**Figure II.12** Fracture surface SEM images of the nanofilled epoxy resins at loading rate of 1.0 per cent by weight: as received CNFs filled resin is on the top, heat-treated CNFs filled resin is on the bottom



- 300 nm



- 300 nm

**Figure II.13** Fracture surface SEM images (enlargement) of the nanofilled epoxy resins at loading rate of 1.0 per cent by weight: as received CNFs filled resin is on the top, heat-treated CNFs filled resin is on the bottom

The difference in the interaction CNF-matrix can be understood considering the analysis performed on the effect of heat-treatments on CNFs in previous

papers “Endo *et al.* (2003a); Guadagno *et al.* (2013d)”. In particular, Endo *and al.* to understand the effect of heat treatment on the nanofibers performed different tests using various analytic techniques, such as high-resolution transmission electron microscopy (HRTEM), Raman spectroscopy, X-ray diffraction and the electrical conductivity in the bulk state. They found that the untreated CNF shows a morphology, termed "stacked cup" that generates a fiber with carbon planes' exposed edges along the entire interior and exterior surfaces of the nanofiber. The most prominent feature upon heat treatment of these nanofibers is the formation of energetically stable loops between adjacent active end planes both on the inner and outer surfaces. These loops can contribute to round the walls, thus eliminating the exposed edges. The FTIR spectra of untreated and heat-treated CNFs show that a less number of chemical groups are attached on the wall of heat-treated CNFs. These groups, more numerous on the wall of untreated CNFs, are most probably responsible of covalent and/or non-covalent bonds such as intermolecular forces due to hydrogen bonds. It was found that these stronger interactions also favor the mechanical reinforcement. The stronger interaction of un-treated CNF with the matrix than the heat treated CNF could be due to a synergic combination of these two effects: on the one hand the carbon planes' exposed edges of the untreated CNFs and on the other hand the number of functional groups attached to the walls of the nanofibers. These groups (most of all hydroxyl and ether groups) are available for chemical and physical interactions between the walls and the epoxy matrix.

### *II.3.3.6 Electrical Behavior*

#### *II.3.3.6.1 Dielectric properties of the resin*

The measurements of dielectric properties of the neat resins and of filled ones are required in order to achieve a compact and reliable design of electromagnetic shielding (EMI or RFI) and radar absorbing materials (RAM) and structural components for the automotive, aviation and aerospace applications.

The permittivity of the unfilled resins are measured in the range of [0.1-100] kHz. During the measurements, the temperature was kept constant at room temperature, therefore its possible influence can be considered negligible. The real part ( $\epsilon_r$ ) of the complex effective permittivity of the samples based on TGMDA epoxy formulation with and without BDE diluent (labeled as TGMDA+DDS+BDE(20%)(200°C) and TGMDA+DDS(200°C), respectively), and of the sample based on DGEBA epoxy formulation (labeled as DGEBA+DDS) are shown in Figure II.14. There is a slight

decrease in the effective permittivity of the three different resins with increasing frequency in the entire measured frequency range.

Generally, in an epoxy resin system, the permittivity is characterized by the number of dipoles present in the structure and by their capability to orient under an applied electric field “Sheppard and Senturia (1986); Eloundou (2002)”.

As in the epoxy chain, most of them can be oriented at low frequency. Thus, in the lower frequency range, the epoxy composites tend to show their highest value of permittivity due to the free dipolar functional groups and/or a interfacial polarization due to the presence of conducting impurities. When the frequency of the applied voltage increases, both mechanisms become negligible and the permittivity progressively decreases. The two TGMDA based systems are characterized by a relative permittivity (around 4) similar to what it has been found for another thermosetting resin (LY556) based on bisphenol-A cured with the hardener HY917 (anhydride type hardener) “Wang and Chen (2012)”. The DGEBA based system shows instead a higher value (>5). In the case of this last sample we performed the measurements to obtain a sample cured in the same condition of the TGMDA based systems (with a stoichiometric amount of DDS and using the same curing cycle). The similar behavior of the two TGMDA systems is reasonably due to similar electrical polarization effects. A clear difference is evident for the DGEBA based system, which exhibit a higher electrical polarization. The dipole moments contribute to the polarization mechanisms in the epoxy resins which in turn influence their permittivity. The density of such dipolar groups in a cured epoxy system can be significantly different due to the nature of epoxy precursors and hardeners. Therefore, this occurrence could justify the discrepancy in the value of the permittivity of the two kinds of resin.

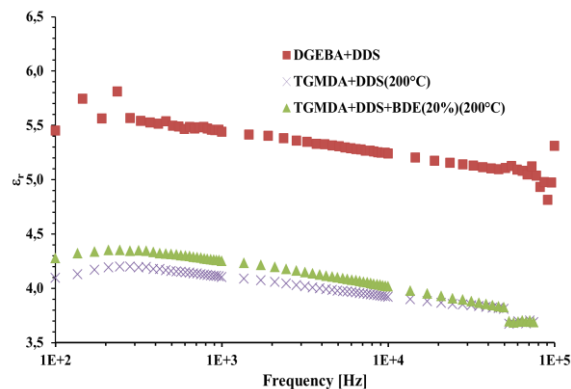


**Figure II.14** AC behaviour of the relative electric permittivity for the TGMDA epoxy formulations (with and without diluent) compared with the formulation based on DGEBA at  $T=30^{\circ}\text{C}$

For sake of completeness the electrical conductivity is investigated as a function of the frequency in the range [1-100] kHz.

Regardless of the chemical formulation of the resin, the electrical conductivity (Figure II.15) is typical of an insulator material.

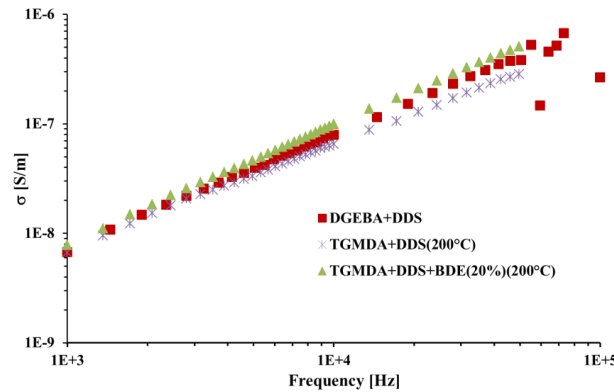


**Figure II.15** AC behaviour of the electrical conductivity for the TGMDA epoxy formulations (with and without diluent) compared with the formulation based on DGEBA at  $T=30^{\circ}\text{C}$

The AC conductivity is generally dominated by the dielectric losses, rather than by the charge transport inside the material. The losses are associated to the part of the energy of the applied field which is dissipated as heat due to the “friction” between the molecules that are perturbed from their equilibrium condition by the applied electric field and forced to a continuous orientation. For this reason the ac conductivity increases as the frequency increases “Murphy and Morgan (1939)”.

The values for the different systems are of the same order of magnitude and vary from about 10ns/m at 100Hz to about 1 $\mu\text{S/m}$  at 100kHz.

### II.3.3.6.2 DC conductivity of nanofilled resins

Figure II.16 shows the DC volume conductivity of the composite as a function of filler loading (%wt). The results obtained, for the composite with MWCNT and heat-treated CNFs, above the percolation threshold are among the highest values obtained for epoxy systems “Bauhofer and Kovacs (2009)”.

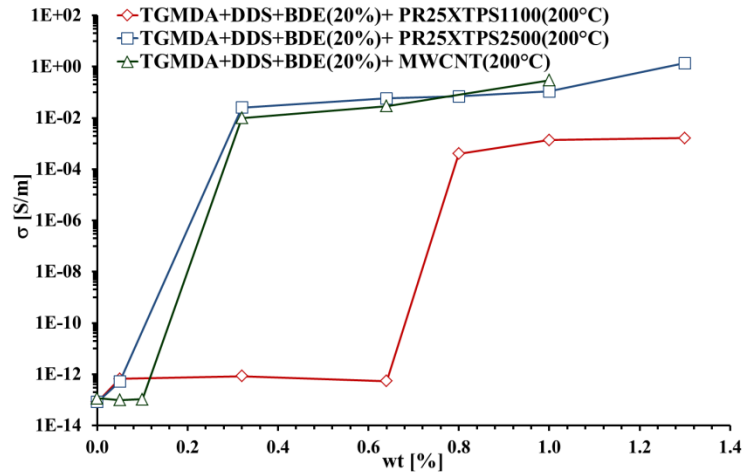


**Figure II.16** DC volume conductivity of the nanofilled composites as a function of the nanofiller concentration

In previous papers, the authors have investigated separately the electrical properties of composites filled with different type and functionality of carbon nanotubes (i.e. SWCNT, MWCNT, DWCNT) “Guadagno *et al.* (2011a); De Vivo *et al.* (2012b)” or composites with different carbon fibers (as-received or heat treated) “Guadagno *et al.* (2012e)”. In this paper the best electrical performance of the CNT-based composites are compared to those obtained with carbon fibers. As provided by the percolation theory, at low filler contents, the composite exhibits an electrical conductivity comparable to that of the pure polymer. Instead, near the percolation threshold, the composite exhibits a transition from an insulating to a conducting behavior, whereas at higher filler concentrations, the electrical conductivity reaches a plateau at a value several orders (generally more than four/five) of magnitude above that the neat resin.

The dependence of the conductivity of the carbon-based filled composites above the percolation threshold as a function of the filler concentration is described by the classical power law “Guadagno *et al.* (2011a); Guadagno *et al.* (2010c); McLachlan *et al.* (2005); Sandler *et al.* (2003)”:

$$\sigma = \sigma_0 (\phi - \phi_c)^t$$

where  $\sigma_0$  is the intrinsic conductivity of the filler,  $\phi$  is the filler concentration (in weight or volume fraction),  $\phi_c$  is the percolation threshold and  $t$  an exponent depending on the dimensionality of the percolating structure.

If the filler content in the composite is homogenous, the composite conductivity, above the percolation threshold, can be described by the behavior of a single tunnel junction. This suggests the DC conductivity

should follow the following rule “Connor *et al.* (1998); Mdarhri *et al.* (2008); Kilbride and Coleman (2002)”:

$$\ln(\sigma_{DC}) \propto \phi^{-1/3} \quad (2)$$

The detection of a linear relation between the DC conductivity (in logarithmic scale) and  $\phi^{-1/3}$ , as shown in Figure II.17, is a classic approach adopted to confirm that electron tunneling is the main responsible for the electrical conductivity in such nanofilled resins.

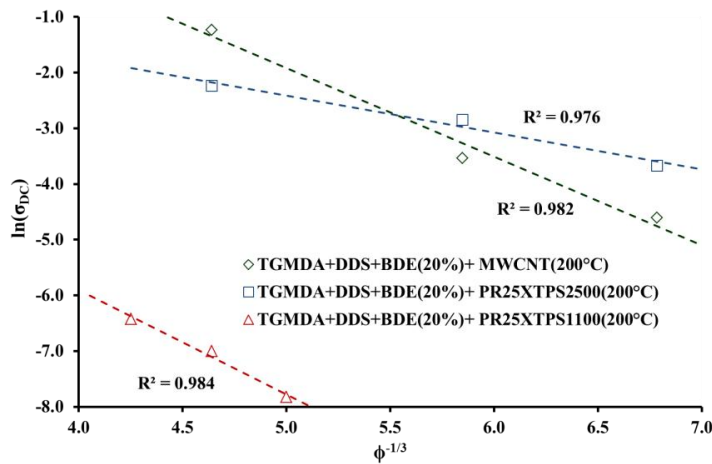


**Figure II.17** Plot of the log of conductivity against  $\phi^{-1/3}$

The dashed line is a fit of the DC data to Eq. (2), the value of  $R^2$  very close to 1 is indicative that the tunneling effect is the involved conduction mechanism. This supports the idea that the current is limited by potential barriers between nanotubes due to the resin coating, or conductivity above the percolation threshold depends largely on the interaction matrix-filler and not on the conductivity of the filler.

Theoretical and experimental studies available in the literature “Bauhofer and Kovacs (2009); Spinelli *et al.* (2012); Hu *et al.* (2008); Eken *et al.* (2011); Li et Chou (2007b)” put in evidence the correlations between material characteristics (polymeric matrices, CNT type) and process parameters, (synthesis method, treatment, etc.) with the electrical performances of the resulting composites. In particular, a previous work “Guadagno *et al.* (2012f)”, concerning the influence of the cure temperature of the resin, has put in evidence that quite similar values of electrical conductivity can be obtained for the samples cured at 180 and 200°C. In fact, the conductivities of the samples TBD-MWCNT(0.32%)(cured at 200°C) and TBD-MWCNT(0.32%)(cured at 180°C) are 0.029 S/m and 0.023 S/m respectively. The EPT for the composites filled by MWCNT and heat-treated

CNFs (PX25XTP2500), falls in the range [0.1,0.32] %wt. Instead, for the composite filled by as-received CNFs (PR25XTP1100) the electrical percolation threshold is detected in the range [0.64, 0.80]% wt.

The remarkable difference in the EPT between the two type of nanofibers may be attributed to the different morphological feature and the high structural integrity of the heat-treated filler, as highlighted in the section Section II.3.3.1. As it concerns the geometrical aspects, the theoretical prediction of the EPT for randomly-dispersed hard particles can be obtained with reference to the excluded volume theory associated to these objects “Balberg *et al.* (1984)”. According to this theory, the EPT of a composites filled with cylindrical conductive particles of diameter  $W$  and length  $L$  can be estimated as the inverse of the Aspect Ratio ( $AR=L/W$ ). For the as-received CNFs, having  $L=[20,200]$   $\mu\text{m}$  and  $D=[125,150]$   $\text{nm}$ , as reported in the manufacturer data-sheet, this theory indicates EPT less than 0.75% (i.e. the EPT obtained for  $L$  at minimum and  $D$  at maximum value respectively), a value which is very close to the experimentally detected (i.e.  $EPT_{PR25XTPS1100} \in [0.64,0.8]\%$ ). Instead a lower electrical percolation threshold is observed for the heat-treated CNFs-based composite. One plausible reason could be attributed to the thermal treatment that leads to the alignment of the fibers while the increased structural order induced by the graphitization of the fibers confers to them an higher rigidity, as the SEM images of Figure II.11 and Figure II.12 confirm. This involves an increase of the “equivalent length” of the CNFs which determine a higher value of the  $AR$  and, as a consequence, a lower EPT. The same mechanism may also justify the higher conductivity of heat-treated CNF for the same filler concentration. In fact, a larger number of electrical contacts can be produced by the longer, straight heat-treated fibers. Therefore, the electrical experimental results confirm the strong influence of the different filler-resin interactions on the final electrical performance of the composites (i.e. electrical percolation threshold and conductivity at high filler loading). The use of heat-treated CNFs rather than the more expensive and hard to disperse (especially for high concentrations) CNTs, could be an advantageous alternative for the production of conductive polymers satisfying also mechanical and thermal constraints required by the different applications.

### *II.3.3.7 Impedance spectroscopy of nanocomposites*

Detailed studies of AC electrical properties play an important role in the characterization of the nanocomposites for design and performance optimization purposes. The impedance spectroscopy (IS) is classically adopted tool for this aim. This technique is based on analyzing the ac response of the impedance parameters of a material to a sinusoidal stimulus

as a function of the frequency. In this study the impedance ( $\dot{Z}$ ) is represented by its magnitude ( $|Z|$ ) and phase ( $\phi$ ).

This technique enables to detect the changing electrical response of the samples, and, for composites with conducting inclusions, the insulator to conductor transition. In particular, a critical frequency,  $f_c$  “Connor *et al.* (1998)” can be found where the frequency-independent behaviour changes to a frequency-dependent one.

The most commonly used model of a physical system involving these AC electrical parameters can be represented by a  $R_p C_p$  parallel electrical circuit. The relations between the impedance parameters and the electrical parameters of the equivalent circuit are:

$$|Z| = \frac{R_p}{\sqrt{1 + \omega^2 R_p^2 C_p^2}} \quad \phi = \arctan(\omega R_p C_p) \quad (3)$$

where  $\omega = 2\pi f$  is the angular frequency and  $f$  is the frequency.

Therefore, the impedance spectroscopy of AC electrical behavior of neat resin and nanofilled resins is presented. The aim is to investigate how the addition, in different concentrations, of nanoparticles and their conducting behavior alters the electrical properties of the resulting materials. The results highlight a strong influence of the nanofiller nature on the electrical properties especially in terms of electrical percolation threshold (EPT) and electrical conductivity beyond the EPT. Among the analyzed nanofillers, the highest electrical conductivity is obtained by using multiwall carbon nanotubes (MWCNTs) and heat-treated carbon nanofibres (CNFs).

The frequency analysis of the composites is carried out by considering three filler concentrations [0.05, 0.32 and 1] wt. These concentrations are chosen since 0.05 wt% is a value below the percolation threshold for all the three types of fillers, 0.32 wt% is a loading close to the percolation threshold for the nanotubes (MWCNT) and the heat treated fibers (PR25XTPS2500) and finally 1% wt is a concentration fairly above the threshold for all composites regardless of the type of filler.

Figure II.18 shows the plots of the magnitude of the normalized impedance ( $|Z_{norm}| = |Z| \cdot d/A$  in  $\Omega/m$  where  $d$  is the thickness of the sample and  $A$  is the area of the electrode) and relative phase angle (degree) as function of the frequency.

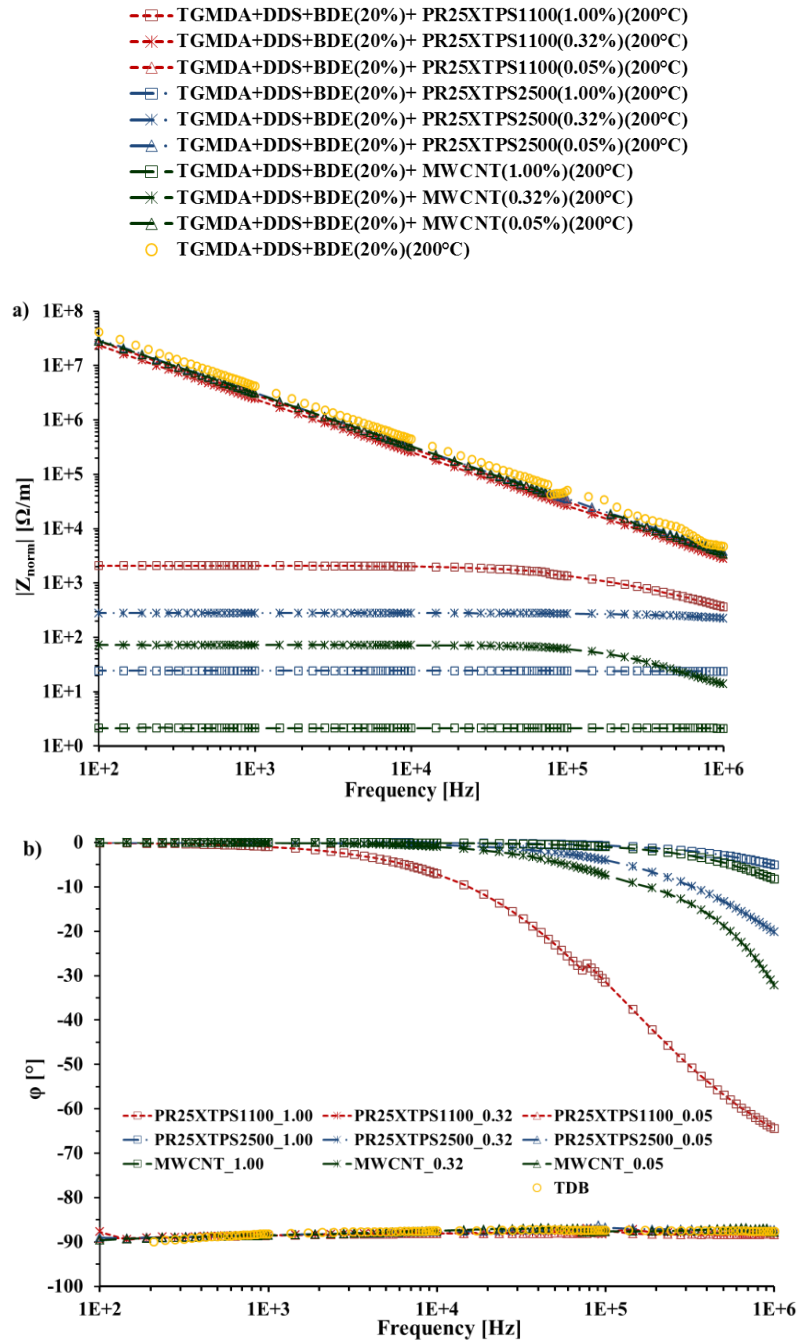
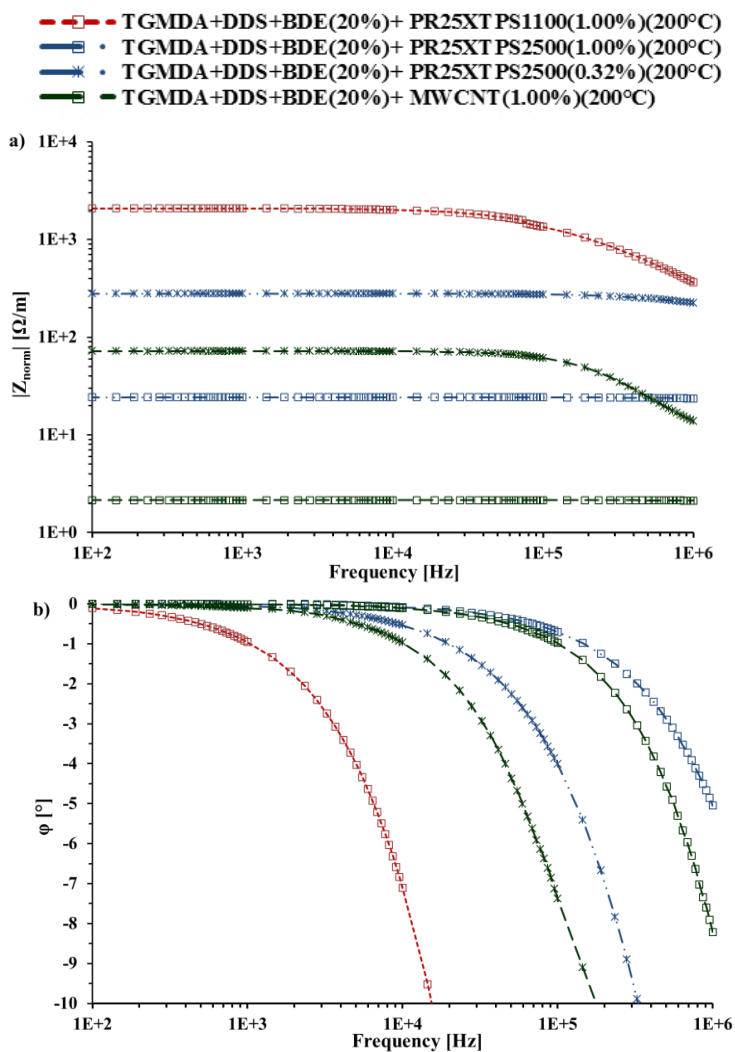


Figure II.18 Normalized impedance a) and phase angle b) vs frequency

For the composites below the percolation threshold the  $|Z_{norm}| \propto 1/f$  (in log-log scale is a straight line) and  $\varphi \cong -90^\circ$ , as for a typical insulating material, are strictly close to the behavior of the neat resin (yellow marker).

Instead, for the composite above the percolation threshold, it is interesting to note that both the modulus and phase exhibit a constant value until the frequency reaches a critical value  $f_c$  after which it decreases highlighting that at high frequency the electrical behavior of the composite is dominated by the capacitance of the system.

This aspect is most noticeable from the Figure II.19 which shows the plots of  $|Z_{norm}|$  and  $\varphi$  related to composites above the percolation threshold.



**Figure II.19**  $|Z_{norm}|$  and  $\varphi$  vs frequency for composites at filler loadings beyond percolation threshold

At the same concentration, the composite made with MWCNT presents the lowest value of normalized impedance. In fact, the value of  $|Z_{norm}|$  for the MWCNT is about one order of magnitude lower than that obtained with the heat-treated CNFs and 3 orders compared to as received CNFs, for the 1% concentration. Instead, the difference is about one order of magnitude for the concentration to 0.32% between MWCNTs and heat-treated CNFs.

As regards the frequency-dependent behavior it becomes less pronounced and the characteristic frequency  $f_c$  shift forward slightly with increasing filler loading indicating a transition of the material from a resistive-type to capacitive one according to the so called *universal dynamic response model* suitable to describe the electrical behavior in many disordered solids “Dyre (1988a); Dyre and Schröder (2000b); Jonscher (1990)”.

This critical frequency is strictly correlated to the tunneling effect between carbon nanotubes in which both the (tunneling) distance and the height of energy barrier are somehow altered with respect to the stationary condition by the frequency of the applied electrical field. Synthetically, frequencies greater than this critical value ( $f_c$ ) lead to a decrease of these parameters that in turn modulate the tunneling effect and consequently the electrical performance of the composites “Connor *et al.* (1998)”.

However, the value of  $f_c$  is greater for the composites loaded with heat-treated CNFs compared to those with MWCNTs, as it is evident in Figure II.19a. This distinction is particularly evident in Figure II.19b, where it is possible to observe that, for a given frequency, the value of the filler loading for the composite PR25XTPS2500 is lower than that of the composite with MWCNT.

This suggests that the composites with heat-treated CNFs are characterized by a purely resistive behavior in a wider frequency range compared to that exhibited by other filled-composites. This interesting topic will be the object of a forthcoming paper where the behavior of the composites will be investigated in a wider frequency range.

## II.4 Conclusions

An epoxy resin mixture based on a tetrafunctional epoxy precursors, the TetraGlycidyl-MethyleneDiAniline (TGMDA) has been formulated, prepared and characterized. The presence of reactive diluent 1,4-Butandiol diglycidylether (BDE) in the epoxy mixture reduces the sorption at equilibrium of liquid water ( $C_{eq}$ ) of about 35% “Guadagno *et al.* (2013g); Guadagno *et al.* (2013h)”. This percentage is very relevant for epoxy mixtures to apply in the aeronautics because absorbed moisture reduces the matrix-dominated mechanical properties. Absorbed moisture also causes the matrix to swell. This swelling relieves locked-in thermal strains from elevated temperature curing. These strains can be large and large panels, fixed at their edges, can buckle due to the swelling strains. In addition,

during freeze-thaw cycles, the absorbed moisture expands during freezing and can crack the matrix. In addition, during thermal spikes, absorbed moisture can turn to steam. When the internal steam pressure exceeds the flatwise tensile strength of the composite, the laminate will delaminate. The reduction in the water absorption was also found for nanofilled epoxy mixtures formulated to increase the electrical conductivity. The presence of the reactive diluent allows to reach higher curing degree compared to the epoxy precursor alone providing an efficient strategy for energy-saving “Guadagno *et al.* (2013g); Guadagno *et al.* (2013h)”.

The morphological feature of the nanofillers has proven to play a relevant role in determining the electrical properties of the analyzed nanofilled resins. The composites obtained with heat treated CNF are characterized by the lowest value, among all considered systems, of the percolation threshold and by a dc conductivity of the same order of the more expensive and hard to disperse (especially for high concentrations) CNTs. Also the frequency behavior of the composites put in evidence that CNF composites could be advantageously employed for the production of materials for aeronautic components since they are also suitable for managing mechanical and thermal constraints required by such applications “Guadagno *et al.* (2013g); Guadagno *et al.* (2013h)”.



---

## Chapter III

---

# Role of the CNF defects on the electrical and mechanical properties of *CNF-Based* Resins

### III.1 Preface

In the previous chapter a different behaviour of the CNFs on the electrical properties of the nanocomposite has been shown. In particular, the results highlighted a strong influence of the nanofiller nature on the electrical properties especially in terms of electrical percolation threshold (EPT). For this reason, an in-depth study aimed to understand the influence of the thermal treatment of the fibers on the finished properties of the nanocomposite has been done. In this chapter the role of the CNF defects on the electrical and mechanical properties of CNF-based resins has been investigated. In particular, heat treatment of carbon nanofibers has proven to be an effective method in removing defects from carbon nanofibers causing a strong increase in their structural perfection and thermal stability. It affects the bonding states of carbon atoms in the nanofiber structure and causing a significant transformation in the hybridization state of the bonded carbon atoms.

Nanofilled resins made of heat-treated CNF show significant increase in the electrical conductivity even at low concentration. This confirms that enhancement in the fiber structural perfection with consequent change in the morphological features plays a prominent role in affecting the electrical properties. Indeed heat-treated CNFs display stiff structure and smooth surface which tends to lower the thickness of the unavoidable insulating epoxy layer formed around CNF which, in turn, plays a fundamental role in the electrical transport properties along the conducting clusters. This might be very beneficial in terms of electrical conductivity but negligible for the mechanical properties.

### III.2 General remarks

Carbon based nano-fillers inside epoxy formulations, as previously described, represent one of the key components of an emerging technological revolution. Among the carbon nanostructured forms, carbon nanotubes (CNTs) have spurred many researchers on developing advanced CNT-based materials in order to transfer some of their excellent physical properties to epoxy matrices “Coleman *et al.* (2006a); Xie *et al.* (2005); Guadagno *et al.* (2009b); Guadagno *et al.* (2011a); De Vivo *et al.* (2012b); Prolongo *et al.* (2012); Kim *et al.* (2011); Bai (2003); Cadek *et al.* (2003)”. CNTs in polymeric matrices offer the possibility to combine complementary interesting properties. As conductive filler with high aspect ratio, CNTs are more effective than traditional carbon black “Sandler *et al.* (2003); Khare and Bose (2005); Spitalsky *et al.* (2010b); Martone *et al.* (2011)” which results in nanofilled materials with high electrical conductivity at lower filler concentrations “Guadagno *et al.* (2011a); De Vivo *et al.* (2012b)”. Despite these benefits, there are still several issues to be considered in the development of innovative CNT-based resins. These issues are related to the high cost and the possibility to achieve an effective dispersion of CNTs in the polymeric matrix due to the very strong interactions among CNTs with respect to the interactions between nanofiller and epoxy matrix. Functionalization of CNTs performed for the purpose of enhancing the interactions between polymeric matrix and nanofillers can induce nanotube damage and, depending on the functionalization treatment, considerably affects both mechanical and electrical properties “Kim *et al.* (2005); Du *et al.* (2005); Spitalsky *et al.* (2009a)”. Many material researchers are looking for answers to overcome these inconveniences by using other nanotubes, such as carbon nanofibers (CNFs) characterized by physical properties comparable to those of CNTs “Hirsch (2002); Eitan *et al.* (2003)”. CNFs can be manufactured with morphological parameters suitable to reduce the interactions among their walls “Lafdi *et al.* (2007a); Lafdi *et al.* (2008b)”. In fact, unlike CNTs for which Van der Waals forces cause the nanotubes to form ropes or reassemble after being dispersed, CNFs are less affected by Van der Waals forces and tend to stay dispersed for longer period of time. In addition, they can be used as effective low cost replacements for carbon nanotubes in high performance resins formulations. The structure of vapor-grown CNFs gives rise to some excellent mechanical properties, very high electrical and thermal conductivity “Endo *et al.* (2001b); Uchida *et al.* (2006); Al-Saleh and Sundararaj (2009); Zhou *et al.* (2007)”. These nanomaterials are very promising to manufacture for efficient lightning strike protection and mechanical resistance. At room temperature, the intrinsic resistivity of highly graphitic vapor-grown carbon fiber is approximately  $5 \times 10^{-5} \Omega \cdot \text{cm}$  “Endo *et al.* (1976c)” which is a value comparable to the resistivity of graphite “Lincoln and Popowich (1976)”.

Due to their particular properties like low electrical resistivity and high aspect ratio, CNFs allows to obtain nanofilled thermosetting materials with high electrical conductivity. In such a way, it is possible to produce composites with different electrical resistivity values by controlling their concentration and interaction inside the matrix “Lincoln and Popowich (1976)”. This feature is suitable for applications that require variation of the electrical resistivity in different ranges such as electrostatic dissipation (ESD) ( $10^6 - 10^8 \Omega \cdot \text{cm}$ ), electrostatic painting ( $10^4 - 10^6 \Omega \cdot \text{cm}$ ), EMI shielding ( $10^1 - 10^3 \Omega \cdot \text{cm}$ ), and lightning strike protection ( $< 10 \Omega \cdot \text{cm}$ ) “Burton *et al.* (2011)”.

The aim of this work is to study (1) the potential use of CNF as filler to produce new polymer nanocomposites (2) the changes in structural ordering of CNF during carbonization and graphitization processes and how these changes will influence the physical properties of the final resins as a function of filler concentration. In such a way it might be possible to overcome some drawbacks related to the electrical properties of typical epoxy-based composites in the field of aeronautic and aerospace materials.

### **III.3 Experimental section**

#### ***III.3.1 Materials***

##### *III.3.1.1 Carbon nanofibers*

Vapor-grown carbon nanofibers in the form of powders used in this study were produced at Applied Sciences Inc. and were from the Pyrograf III family, as previously reported in the experimental section of the chapter II.

The nanofibers have an Average Bulk Density of Product ( $\text{g}/\text{cm}^3$ ) ranging from 0.0192 to 0.0480; b) a Nanofiber Density (including hollow core) ( $\text{g}/\text{cm}^3$ ) from 1.4 to 1.6; c) a Nanofiber Wall Density ( $\text{g}/\text{cm}^3$ ) from 2.0 to 2.1; d) an Average Catalyst (Iron) Content (ppm)  $< 14,000$ ; e) an Average Outer Diameter (nm) from 125 to 150; f) an Average Inner Diameter (nm) from 50 to 70; g) an Average Specific Surface Area,  $\text{m}^2/\text{g}$  from 65 to 75; h) a Total pore volume ( $\text{cm}^3/\text{g}$ ) of 0.140 ; g) an Average Pore Diameter (angstroms  $\text{\AA}$ ) of 82.06 and lengths ranging from 50 to 100  $\mu\text{m}$ .

Sample PR25XTPS1100 was heat treated to 2500°C to provide the best combination of mechanical and electrical properties giving the sample named PR25XTPS2500.

The heat-treatment was performed in an atmosphere controlled batch furnace. Approximately 300 g of nanofibers were placed in a ceramic crucible for the heat-treatment. The furnace was purged with nitrogen gas for

one hour prior to heating. The heating rate was 100°C per hour, and the furnace was held at the temperature of 2500°C for one hour prior to cooling.

### *III.3.1.2 Nanofilled Epoxy Resins*

CNFs were dispersed within the chosen epoxy mixture (see experimental section of the chapter II) at loading rates of 0.05, 0.32, 0.64, 0.8, 1.00 and 1.3 per cent by weight. Our experiments show that nanofilled resins with loads beyond 1.3 per cent by weight become difficult in establishing a homogenous mixture.

All the mixtures were cured by a two-stage curing cycles, as described in the experimental section of the chapter II. The as-received carbon nanofibers, designated as PR25XTPS1100, and the neat resin were used as a baseline for this study.

### *III.3.2 Characterizations*

Raman spectra were collected at room temperature with a microRaman spectrometer Renishaw inVia operating with a 514-nm laser source.

X-ray diffraction was performed with a Bruker D8 Advance diffractometer with Ni-filtered CuK $\alpha$  radiation ( $\lambda=1.54050 \text{ \AA}$ ).

The infrared spectra were obtained in absorbance by using a Bruker Vertex 70 FTIR-spectrophotometer with a resolution of 2 cm<sup>-1</sup> (32 scans collected).

Thermogravimetric Analysis was carried out in air using a thermal analyzer Mettler TGA/SDTA 851. Temperature range was 25°C – 1000°C at heating rate of 10°C min<sup>-1</sup>. SEM micrographs were obtained using a Field Emission Scanning Electron Microscope (FESEM, mod. LEO 1525, Carl Zeiss SMT AG, Oberkochen, Germany).

Some of the nanofilled sample sections were cut from the solid samples by a sledge microtome. These slices were etched (the etching procedure is reported in the experimental section of the chapter II) before the observation by FESEM microscopy. Transmission Electron Microscopy (TEM) was carried out on a Philips CM-20 model equipped with a 200 kV accelerating voltage and a high brightness LaB6 gun for high coherence and small probe. As previously reported, the measurements of the *dc* volume conductivity were performed on disk-shaped specimens of about 2 mm thickness and 50 mm diameter by using metalized electrodes with a diameter of about 22 mm. The metallization is obtained by employing a silver paint (RS 186-3600) with a thickness of about 50  $\mu\text{m}$  and a surface resistivity of 0.001  $\Omega \text{ cm}$ . The measurement system, remotely controlled by the software LABVIEW®, is composed of a suitable shielded cell with temperature control, of multimeter Keithley 6517A with function of voltage generator (max  $\pm 1000\text{V}$ ) and voltmeter (max  $\pm 200 \text{ V}$ ) and the ammeter HP34401A (min current 0.1 $\mu\text{A}$ )

for samples above the percolation threshold. For samples below the percolation threshold the system is composed only of multimeter Keithley 6517A with function of voltage generator (max  $\pm 1000\text{V}$ ) and pico-ammeter (min current  $0.1\text{fA}$ ). For sensitivity purposes the applied electric field has been  $0.5\text{ MV/m}$  for samples below the percolation threshold, whereas in order to avoid Joule heating of samples it has been set to  $5.0\text{ kV/m}$  for samples above the percolation threshold.

Dynamic-mechanical properties were performed using a Tritec 2000 DMA - Triton Technology. DMA experiments were performed to identify transition regions in the formulated resins, such as the glass transition temperature ( $T_g$ ) and any other small transitions.

Storage modulus  $E'$  and damping coefficient,  $\tan \delta$ , given by the ratio between the loss modulus and the storage modulus, are recorded as a function of temperature. The specimens with  $30 \times 10 \times 2\text{ mm}^3$  are fixed between a movable and a stationary clamp fixture and then enclosed in a thermal chamber. Frequency and load amplitude and temperature range, appropriate for the tested material are inputted. A sinusoidal oscillatory three points bending (3PB) load is applied to the specimen in programmed temperature range, which generates a sinusoidal strain. The frequency was fixed at  $1\text{ Hz}$ . Oscillation displacement amplitude of  $0.03\text{ mm}$  was thus chosen. The ramp experiments were performed at heating rates of  $3^\circ\text{C/min}$  in the temperature range from  $-90^\circ\text{C}$  to  $315^\circ\text{C}$ .

### ***III.3.3 Results and discussion***

#### *III.3.3.1 Carbon nanofibers characterization*

##### *III.3.3.1.1 Morphological and structural investigation*

In order to fully understand the influence of heat treatment on the physical properties of nanofilled epoxy resins, the morphologies of both nanofibers and nanofilled samples were characterized. FESEM investigation on the nanofibers was performed to analyze the morphology of the nanofibers before their incorporation into the epoxy precursors. The images shown in Figure III.1(a) indicate that as-received CNFs are debulked enough to avoid additional treatment.

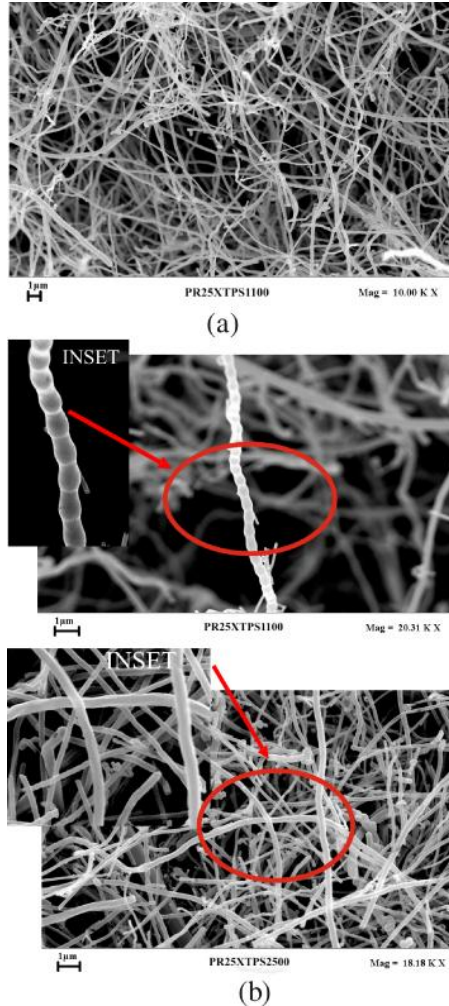


**Figure III.1(a)** An SEM image of as-received CNFs (PR25XTPS1100); **(b)** SEM images of as-received CNFs (PR25XTPS1100) and CNFs heat treated at 2500°C (PR25XTPS2500); the inset shows higher magnifications for each sample

The influence of heat treatment on the nanofiber morphology can be seen in Figure III.1(b) where also the as-received CNFs at the same magnification are shown for comparison. The insets at higher magnification show that the as-received CNFs are characterized by a nested configuration. The heat treatment seems able to statistically reduce this effect; in fact, heat-treated CNFs appear to be characterized by straighter walls where the nested configuration is not clearly visible. Changes in morphology due to heat treatment can be better analyzed by means of the TEM technique. Figure III.2 on the left side shows the TEM micrograph of the CNFs used in this

study. The individual pristine nanofiber has a hollow core that is surrounded by a cylindrical fiber comprised of highly crystalline, graphite basal planes stacked at about  $25^\circ$  from the longitudinal axis of the nanofiber. This structure, termed 'stacked cup' or 'herringbone', generates a fiber with exposed edge planes along the entire interior and exterior surfaces of the nanofiber. In the section III.3. 3.2.4 on the dynamic mechanical properties of the nanofilled epoxy resins we will see that the exposed edge planes determine stronger interactions with the epoxy matrix than CNFs with straight external walls, leading to a more evident increase in the storage modulus in the entire range of investigated temperatures.

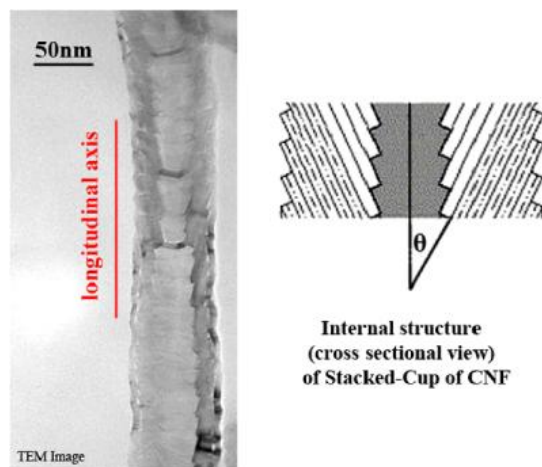


**Figure III.2** Bright field micrograph of the 'Dixie cup' carbon nanofiber structure on the left side and a cross-sectional view of the CNF

This particular morphology as also referred to as a nested configuration or as fishbone type. Nested carbon nanofibers have an orientation similar to that of a set of stacked Dixie cups with a hollow core. The Dixie cups of the pristine CNFs are also clearly visible in the inset of Figure III.1(b) (see PR25XTPS1100 sample). The as-received CNFs exhibit only local molecular ordering. As they are heat treated, an increase in temperature results in the aromatic molecules becoming stacked in a column structure; after heat treating the pristine nanofibers to a temperature of  $2500^\circ\text{C}$ , the graphene layers became straight, and the minimum interlayer spacing was reached for the PR25XTPS2500 nanofibers. As shown by the TEM micrograph in Figure III.3, the layers within the Dixie cup carbon nanofiber have coalesced following heat treatment.

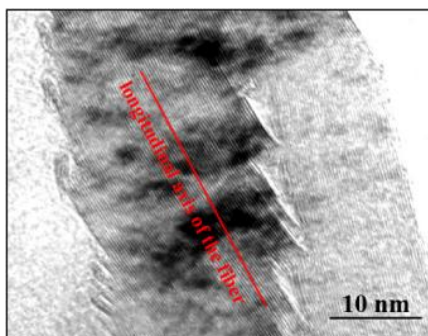


**Figure III.3** High-resolution imaging of the localized area of the coalesced Dixie cup structure

At this magnification the inclination angle of each 'cup' is apparent. Within each cup it can be seen that the localized ordering of the graphene planes has been changed due to coalescence resulting in continuous planes. The stacking effect is shown through the use of a gray scale. The walls of the nanofibers are dark due to their high electronic density. The surrounding regions are starkly lighter with low electronic densities. The graphene layers appear very straight without any disclination defects. However, there is no change in the inclination angle to the central core axis. The edges of any pair of graphene layers have been rounded encapsulating the carbon planes' exposed edge. This allows the exposed graphene planes to attain a level of maximum structural stability.

#### III.3.3.1.2 Structural investigation

Figure III.4 shows that the wide-angle x-ray diffractograms of the two samples further clarify the differences in the structural features of the different heat-treated carbon nanofibers. The profile of the (002) reflection at  $2\theta = 26^\circ$  in the pristine CNFs indicates characteristics of the disordered and amorphous carbon; whereas the higher sharp peak of the same reflection in the x-ray diffractogram of the PR25XTPS2500 sample indicates that the heat treatment causes a very high degree of carbon nanofiber graphitization. In addition, the heat treatment increases the  $2\theta$  angle of the (002) peak from  $26.0^\circ$  for the as-received PR25XTPS1100 carbon nanofibers to  $26.2^\circ$  for heat-treated PR25XTPS2500 nanofibers with a change in the interlayer spacing  $d_{(002)}$  from 0.343 to 0.340 nm.

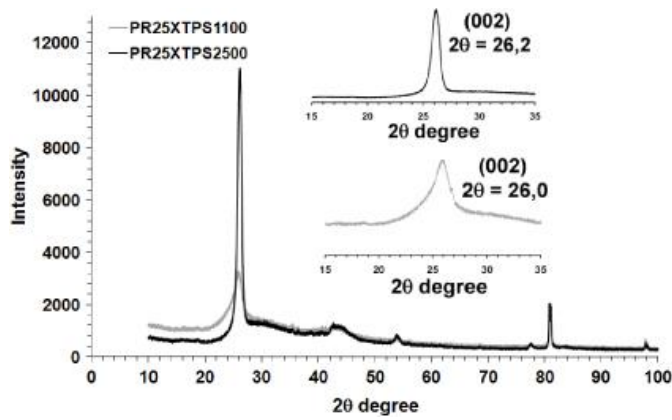


**Figure III.4** X-ray diffraction patterns of pristine and annealed nanofibers

This result agrees with the TEM and Raman results, indicating that the graphene layers became more tightly packed and highly graphitic after heat treatment.

### III.3.3.1.3 Raman and FT/IR spectroscopy

The Raman spectra collected for samples PR25XTPS1100 and PR25XTPS2500 are shown in Figure III.5.

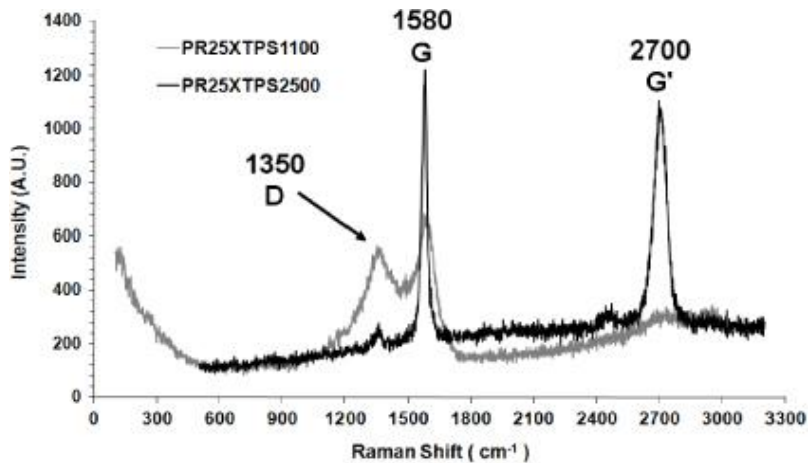


**Figure III.5** Raman spectra of samples PR25XTPS1100 and PR25XTPS2500

Generally the Raman spectra for carbonaceous material is divided into first- and second-order regions. The first-order region lies in the interval of 1100–1800 wavenumbers. In this region we can observe the main graphite band, the G band at  $\sim 1580 \text{ cm}^{-1}$ . This band is observable with different intensities

for the two samples. Additional bands at  $\sim 1350\text{--}1355\text{ cm}^{-1}$ , at  $1500$  and  $1622\text{ cm}^{-1}$  are observed for more poorly crystalline graphite. The band at  $\sim 1350\text{ cm}^{-1}$  is known as the disorder-induced D band (D for defect or disorder) “Lucchese *et al.* (2009)” and it is observable when defects are present in the carbon aromatic structure. Also the band  $1500\text{ cm}^{-1}$  observable as a shoulder on the right of the G band in the PR25XTPS1100 sample is attributed to defects outside the plane of aromatic layers like tetrahedral carbons. In the second-order region (from  $2200$  to  $3300\text{ cm}^{-1}$ ), we can observe the band at  $\sim 2700\text{ cm}^{-1}$  (G' band) which is indicative of graphite crystallinities. This band is almost absent in the PR25XTPS1100 sample, indicating a very low crystallinity degree. A very important parameter that can be used for quantifying disorder is the ratio ( $I_D/I_G$ ) between the intensities of the disorder-induced D band ( $1350\text{ cm}^{-1}$ ) and the first-order graphite G ( $1580\text{ cm}^{-1}$ ) band “Lucchese *et al.* (2009)”. The  $I_D/I_G$  values of the two samples are  $0.8$  for PR25XTPS1100 and  $0.08$  for PR25XTPS2500. An analysis of such characteristics has also been performed in “Endo *et al.* (2003a)”. If we compare the previous data with those reported there we can observe that the  $R$  value is the same for the as-received CNFs ( $0.8$ ), while for the CNFs treated at  $2500^\circ\text{C}$  it is  $0.3$  for those employed in “Endo *et al.* (2003a)” and  $0.08$  for those used in our paper. A good agreement is, indeed, found for the TEM investigation and x-ray diffraction. In fact, the value of  $d_{(002)}$  is  $0.339\text{ nm}$  in “Endo *et al.* (2003a)” and  $0.340\text{ nm}$  in this paper. We may hypothesize that the observed differences could be ascribed to the different treatment times at the considered temperature. In conclusion the black spectrum shows a profile corresponding to carbon fibers characterized by a high level of order with two intense signals (G and G' bands) characteristic of graphitic  $\text{sp}^2$  materials, as already evidenced by TEM investigation. Figure III.6 shows the FTIR spectra of untreated and heat-treated CNFs.

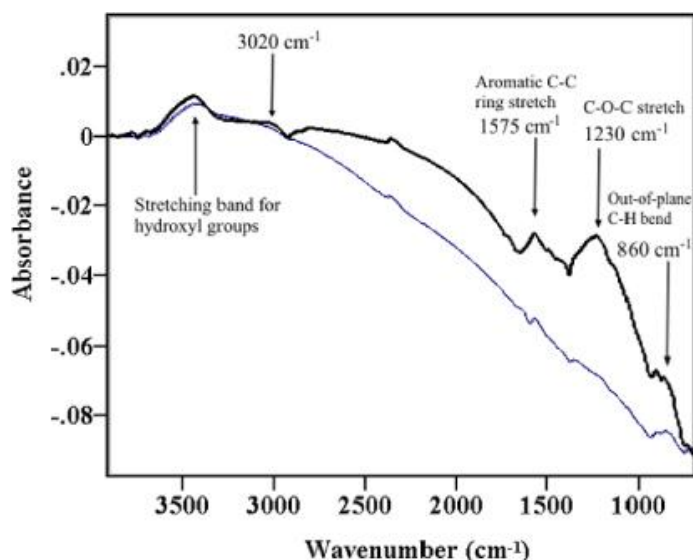


**Figure III.6** FTIR spectra of the samples PR25XTPS1100 (thick line) and PR25XTPS2500 (thin line)

The heat treatment influences the surface of the nanofibers in several regions of the spectrum. The intensity of the weak broad band corresponding to the hydroxyl groups ( $\text{O-H}$  stretching vibration) between  $3306$  and  $3665\text{ cm}^{-1}$  decreases in the spectrum of heat-treated CNFs; in addition, many bands corresponding to non-aromatic vibrations and aromatic  $\text{C-H}$  signals reduce their intensity or disappear completely after heat treatment at high temperature. Among these bands there are: (1) the aromatic  $\text{C-H}$  stretching signal of arenes (several bands at around  $3020\text{ cm}^{-1}$ ); (2) different small bands at about  $1493$  and  $1443$  appearing as shoulders on the right of the band at  $1575\text{ cm}^{-1}$  corresponding to an aromatic  $\text{C=C}$  ring stretch; these bands can be attributed to the asymmetrical bending vibration of methyl groups that overlap with the scissoring vibration of methylene groups; (3) the  $\text{O-H}$  bending (in-plane) between  $1380$  and  $1430\text{ cm}^{-1}$ ; (4) the  $\text{C-O-C}$  and  $\text{C-O}$  stretch vibrations at  $1230\text{ cm}^{-1}$ ; (5) the signal corresponding to the out-of-plane  $\text{C-H}$  vibration at about  $860\text{ cm}^{-1}$  that overlaps with the signal corresponding to the  $\text{O-H}$  bend (out-of-plane). These last results agree with TEM, RX and Raman data, and also evidence that a lower number of chemical groups are attached on the wall of heat-treated CNFs.

#### III.3.3.1.4 Thermogravimetric analysis

Thermogravimetric analysis (TGA) can be used to study the oxidative stability of carbon nanostructured forms. Thermal degradation in air of samples PR25XTPS1100 and PR25XTPS2500, depicted in Figure III.7, shows that after heat treatment at  $2500^\circ\text{C}$ , CNFs are more stable toward

thermal oxidative destruction than the untreated CNFs. The oxidative stability enhancement is of about 200°C; in fact for sample PR25XTPS2500 the beginning of the degradation occurs at about 750°C with respect to the temperature of 550°C corresponding to the untreated CNFs. The treatment at high temperature reduces the defect density, producing more perfect CNFs and therefore stabilizing the carbon nanofibers toward thermal oxidative destruction.

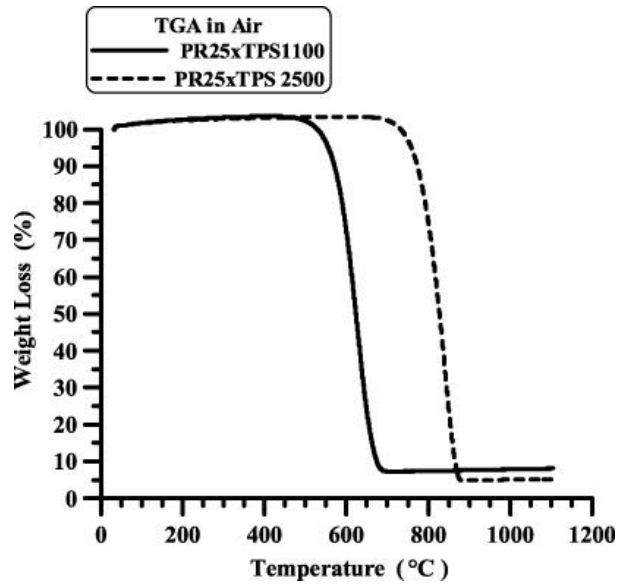


**Figure III.7** TGA of samples PR25XTPS1100 and PR25XTPS2500

### III.3.3.2 CNF/epoxy resin characterization

#### III.3.3.2.1 Thermogravimetric analysis

Figure III.8 shows the thermogravimetric curves in air of the unfilled epoxy formulation and the same resin filled with PR25XTPS2500 carbon nanofibers.

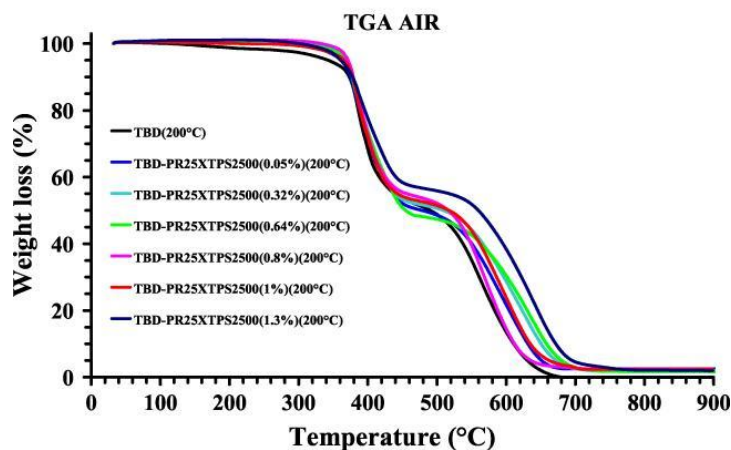


**Figure III.8** TGA curves of the unfilled and PR25XTPS2500 filled epoxy resins

A two-step thermal degradation process can be observed for all the samples. The first stage of thermal degradation of the nanofilled samples substantially occurs in the temperature range of 380–480°C, highlighting a stabilizing effect of the CNFs in the first stage of the degradation; in fact the unfilled sample TBD shows a slight weight loss (~5%–6%) in the temperature range between 150 and 380°C. The end of the first stage at about 460°C involves a lower mass loss for samples loaded with a higher percentage of CNFs. The beginning of the first stage is most probably due to degradation processes which do not involve oxygen (dehydration, random scission etc), whereas the second step is strongly dependent on the oxygen availability. This hypothesis is supported by the different trend of the thermogravimetric curves in inert ( $N_2$ ) atmosphere (not reported here). There are two distinct and well-separated turns also for TGA curves in nitrogen; the first step is in the same temperature range, whereas the second step is much slower with respect to the degradation in air. A very interesting result is the different mass loss at the end of the first stage; it is between 60–70% in nitrogen and 45–50% in air, this effect is not influenced by the presence of CNFs.

Very similar results were obtained for the epoxy resins filled with untreated CNFs; the different thermal treatment of CNFs does not have an appreciable effect on the degradation behavior. On the contrary, the electrical properties shown in section III.3.3.2.3 demonstrate the strong influence of the thermal treatment on the conductivity and electrical percolation threshold of the two different samples.

#### III.3.3.2.2 Morphological analysis

In order to analyze the homogeneity of the nanofiller dispersion in the polymeric matrix, the samples with as-received CNFs and with heat-treated

CNFs were investigated by means of SEM. The analysis was carried out on etched samples to remove the resin surrounding the nanofibers, leaving them bare as described in section III.3. Figure III.9 shows SEM images of nanofilled epoxy resins at a loading rate of 0.64% by weight. The as-received CNF filled resins are on the left side and those with heat-treated CNFs are on the right side.

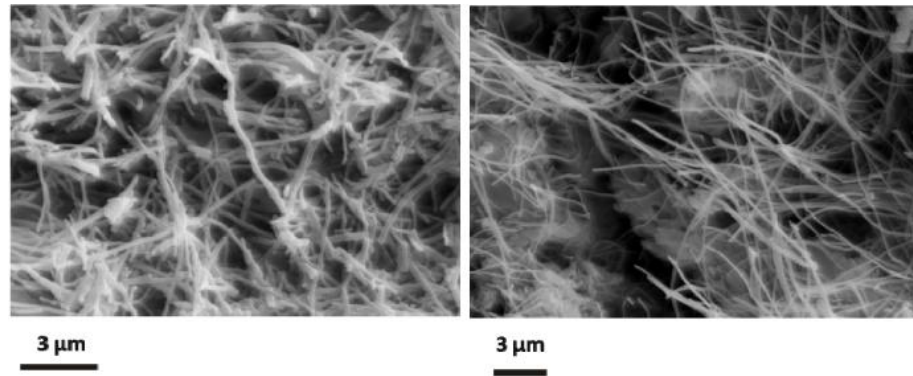


**Figure III.9** Fracture surface SEM images of the nanofilled epoxy resins at a loading rate of 0.64% by weight: as-received CNF filled resins are on the left side, heat-treated CNFs filled resins are on the right side

Careful observation highlights an homogeneous structure for both the samples, in which the CNFs are uniformly distributed in the epoxy matrix. CNFs heat treated at 2500°C seem stiffer with the straight morphology, compared to the as-received CNFs.

#### III.3.3.2.3 Electrical behavior

Figure III.10 shows the measured dc volume conductivity as a function of the CNFs' weight percentage for the as-received CNF nanofilled resin (gray curve) and the heat-treated CNF nanofilled resin (black curve).

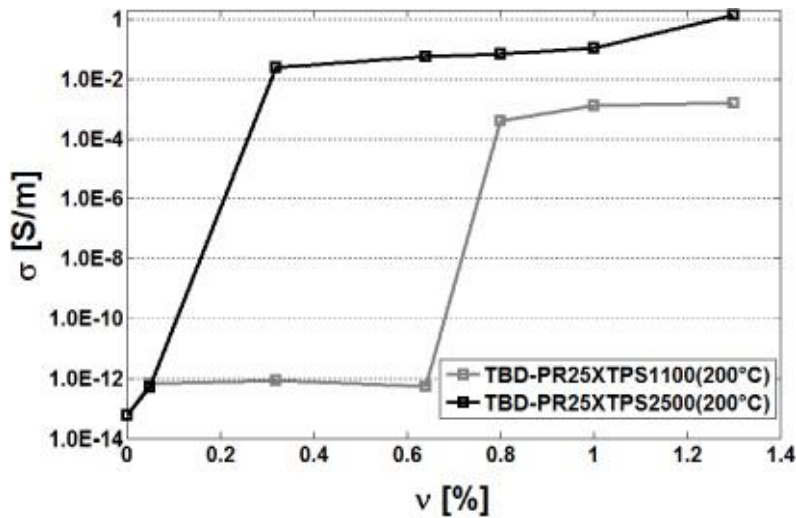


**Figure III.10** DC volume conductivity of the samples versus CNF weight percentage

Remarkable differences between the two samples are evident. In fact, although both samples exhibit a conversion from the behavior of an insulator to that of a conductor with a jump of more than five to six orders of magnitude in the dc electric conductivity, the CNF concentration at which the transition occurs is very different for the two systems. In particular, the CNF concentration for the sample filled with the heat-treated filler is much lower (less than 0.32%) than that pertaining to the sample filled with untreated CNFs for which a more than double value is found. Hence a lower amount of heat-treated filler is enough to obtain higher values in the electrical conductivity of the resin. Moreover, the value reached by the conductivity beyond the percolation region is three orders of magnitude lower for the epoxy matrix filled with the as-received CNFs with respect to the heat-treated CNFs. For example, if the percentage of 1.3% of CNFs is considered, the conductivity is around  $1.6 \text{ mS m}^{-1}$  for the PR25XTPS1100-based system, whereas the epoxy matrix filled with PR25XTPS2500 is higher than  $1.37 \text{ S m}^{-1}$ .

In a previous paper, the authors analyzed the electrical conductivity of resins filled with CNFs subjected to heat treatment at temperatures ranging from 1500 to 3000°C “Lafdi *et al* (2007a)”. They obtained similar results for a different epoxy matrix and for a CNF concentration of 4%. In particular, they found that heating treatment at a temperature of 3000°C causes an increasing in the electrical conductivity from about  $10^{-3} \text{ S m}^{-1}$  (for the untreated CNF loaded sample) to  $1.0 \text{ S m}^{-1}$  for the heat-treated CNFs. Generally, the heat treatment leads to resins characterized by higher conductivity. In the same paper, the authors show that when the loading of

CNFs was increased at 8% or 12%, no remarkable differences were observed between the untreated and the heat-treated CNF loaded samples. If the present results are compared with the already published data, it can be deduced that the observed remarkable differences in the conduction properties of the two analyzed systems (PR25XTPS1100- and PR25XTPS2500-based systems) are not associated with different values of the conductivity of the different CNFs but, most probably, to other occurrences which are effective at low filler concentrations. In particular, the geometrical properties of the two fillers and the characteristics of their distribution inside the matrix may be analyzed for this purpose. Concerning the geometrical aspects, the theoretical prediction of the electrical percolation threshold (EPT) for randomly dispersed hard particles can be obtained with reference to the excluded volume associated with these objects “Balberg *et al.* (1984)”. According to this theory, the EPT of a resin filled with cylindrical conductive particles of diameter  $W$  and length  $L$  can be estimated as the inverse of the aspect ratio ( $AR = L/W$ ), whereas the conductivity of the nanofilled resin beyond the EPT increases with  $AR$ . For the pristine CNFs, having  $L = [20,200]$   $\mu\text{m}$  and  $D = [125,150]$   $\text{nm}$ , this theory indicates EPT less than 0.75% (i.e. the EPT obtained for  $L$  at minimum and  $D$  at maximum value respectively), a value which is very close to the detected one (i.e.  $EPT_{PR25XTPS1100} \in [0.64, 0.8]\%$ ). The thermal treatment, leading to the alignment of the fibers, as the SEM images of Figures III.1(b) and III.9 confirm, induces a narrowing of the diameter and an increase of the length of the CNFs which determine a higher value of the  $AR$  and a lower EPT. Moreover, the increased structural order induced by the graphitization after heat treatment at 2500°C determines a higher rigidity of the obtained fibers. The increased rigidity is in turn responsible for a lower tendency of the heat-treated fibers to bend with respect to the pristine ones. As far as the percolation mechanism is concerned, the lower curvature determines a greater 'equivalent length' of the heat-treated fibers (the span covered by the fiber inside the resin) which, therefore, may lower the EPT. The same mechanism may also be responsible of the higher conductivity of heat-treated CNFs for the same filler concentration. In fact, a larger number of electrical contacts can be produced by the longer, straight heat-treated fibers. It is known that in nanofilled resins with a filler concentration over the EPT, the predominant conduction mechanism is the tunneling effect between neighboring conducting structures in which a great role is played by the interaction of the filler matrix. Numerical simulations presented in a recent study “Spinelli *et al.* (2012)” show that a variation as large as three orders of magnitude in the conductivity of a nanosized cylindrical filler does not affect the resulting conductivity of the resin when the tunneling effect is considered. This can be modeled with a resistance  $R_{\text{tunnel}}$ , depending exponentially on the distance between the conductive filler structures belonging to the percolation path;

$$R_{\text{tunnel}} = \frac{h^2 d}{Ae^2 \sqrt{2m\lambda}} \exp\left(\frac{4\pi d}{h} \sqrt{2m\lambda}\right) \quad (1)$$

In equation (1)  $h$  is Planck's constant,  $A$  and  $d$  are the cross-sectional area and the distance between the filler respectively,  $e$  the electron charge,  $m$  the mass of an electron and  $\lambda$  represents the height of the barrier which typically takes values of a few eV. The heat-treated CNFs are characterized by a greater smoothness of the external surface of the fibers (with respect to the pristine fibers). The smoother surface may indeed provide fewer linking points for the epoxy matrix thus inducing a lower thickness of the insulating layer around the fibers. Finally, it can be considered that a good filler dispersion is observed during the production process and is shown in the SEM images of Figure III.9 for both the nanofilled resins. This suggests that the nanofiber agglomeration does not have a significant impact on the obtained conductivity characteristics. Summing up, the better conduction performances exhibited by the nanofilled systems based on heat-treated CNF may be reasonably ascribed to their lower tendency to bend due to graphitization and to their smoother surface, which determines a lower thickness of the insulating layer around the fibers, which in turn controls the value of the resistance associated with the tunneling between conducting clusters forming the percolating paths inside the resin. Moreover, it can be observed that the values of electrical conductivity are quite similar to those found for the same epoxy matrix filled with CNTs “De Vivo *et al.* (2012c)”.

### III.3.3.2.4 Dynamic mechanical properties

Dynamic mechanical analyses (DMAs) on the nanofilled samples were carried out with the aim of understanding the influence of the different CNFs on the storage modulus and  $\tan\delta$  of the samples. Figures III.11(a) and (b) show the storage modulus of the epoxy resin filled with untreated and heat-treated CNFs.

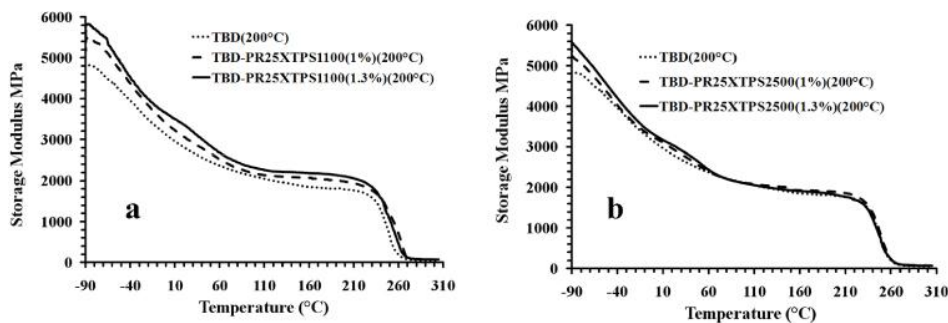


**Figure III.11** Storage modulus of the epoxy resin filled with untreated and heat-treated CNFs

We can observe a value in the storage modulus higher than 2000 MPa up to 110°C for all the samples. The principal drop, due to the glass transition, is evident for all the curves in the temperature range of 230–260°C. In this range also the  $\tan \delta$  curves show a peak, indicating the main transition ascribable to the glass transition temperature (see Figure III.12). All the samples show almost identical peak height and position in the loss factor curves. This indicates that the CNFs have no particular effect on the relaxation phenomena leading to the glass transition temperature of the samples. As far as the storage modulus is concerned, heat-treated CNFs show a reinforcing effect up to 60°C. Untreated CNFs show a stronger reinforcing effect than the heat-treated CNFs. This effect can be observed in the entire analyzed temperature range (–90–260°C). Considering the results related to  $\tan \delta$  curves, this very interesting result is most likely due to the different morphological features of the CNFs; in particular, the exposed edges in the untreated CNFs cause a more efficient interaction of the nanofiller matrix, improving the effectiveness of the load transfer between the two components.

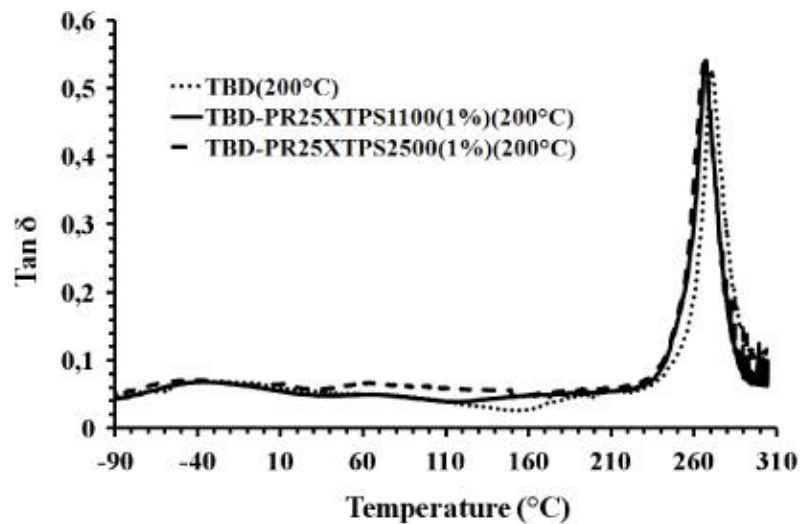


**Figure III.12** Loss factor ( $\tan \delta$ ) of the unfilled epoxy mixture and its resins filled with 1% (weight percentage) of untreated and heat-treated CNFs

### III.4 Conclusions

Graphitization of carbon nanofibers has proven to be an effective method in removing defects from carbon nanofibers, causing a strong increase in their structural perfection and stability. Raman spectroscopy, in fact, shows that the heat treatment strongly influence the degree of structural ordering and

therefore the bonding states of carbon atoms in the nanofiber structure. It causes a significant transformation in the hybridization state of the bonded carbon atoms “Guadagno *et al.* (2013d)”. TGA shows that nanofibers annealed at 2500°C (PR25XTPS2500) are more stable in air than the pristine nanofibers (PR25XTPS1100). The oxidative stability enhancement of 200°C was observed. The presence of defect sites along the fibers highlights the role of the defects on the electrical properties of CNFs/epoxy-amine resins. The enhancement in the fiber structural perfection very positively affects the electrical conductivity of the nanofiber-reinforced resins leading to an increase in the conductivity at very low filler concentration. The investigation on the dc conductivity around the percolation threshold shows a significant difference between the two different nanofibers. The lower percolation threshold and higher conductivity exhibited by the nanofilled resins based on heat-treated CNF can be justified on the basis of their stiffness and smoothness of surface graphitized CNFs which determines a lower thickness of the insulating epoxy layer around the fibers. This hypothesis is also supported by FTIR analysis of untreated and heat-treated CNFs. FTIR data have shown that fewer chemical groups are attached on the wall of heat-treated CNFs. These groups, more numerous on the wall of as-received CNFs, are most probably responsible for covalent and/or non-covalent bonds such as intermolecular forces due to hydrogen bonds. These stronger interactions should favor the mechanical reinforcement and, conversely, decrease the electrical conductivity. The morphological features and the chemical changes on the CNFs walls affect the electrical conductivity and the dynamic mechanical properties, causing a lower reinforcing effect in the storage modulus of the resin nanofilled with heat-treated CNFs than for the samples filled with untreated CNFs “Guadagno *et al.* (2013d)”. The heat treatment at high temperature also causes an increase in the oxidative stability of the nanofillers and their loaded resins. The oxidative stability of the reinforced resin tends to increase with increasing nanofiller percentage. A very interesting result observed for CNFs is that the value of the electrical conductivity of the resin filled with CNFs treated at 2500°C is the higher value obtained for epoxy resins filled with a low percentage of CNTs. The values of electrical conductivity are only slightly different from those found for the same epoxy matrix filled with CNTs “Guadagno *et al.* (2013d)”. However, it has to be considered that CNFs/epoxy resins are obtained by an easier production process mainly in the step of nanofiller dispersion inside the epoxy liquid mixture, which is a very difficult step before the curing process.



---

## Chapter IV

---

# Viscoelastic Properties of CNT/Epoxy-Amine Resins for Structural Applications

### IV.1 General remarks

The ability to homogeneously disperse nanotubes throughout a matrix depends on the method of nanotube incorporation into the resin and, most of all, on the chemical nature and viscosity of the initial epoxy precursors. By choosing the appropriate control of the matter structure as well as the specific CNT, material scientists can work to overcome several critical points related to the industrial application of nanofilled resins. In fact, the results reported in literature highlight that epoxy resins with CNTs embedded in the network offer tremendous potential to improve the properties of advanced composites with modest or without additional weight and easy integration into current processing schemes. Carbon-based fillers, like MWCNTs or CNFs, are the most widely used carbon nanofillers to enhance physical properties of epoxy matrix. In order to achieve superior performance of nano-filled epoxy resins, many issues related to the nature of epoxy matrix have to be analyzed.

In this chapter, the effect of the chosen epoxy reactive diluent on the viscosity of a tetrafunctional epoxy precursor has been analyzed for unfilled and nanofilled epoxy matrices. Despite very good mechanical performance of the chosen multifunctional epoxy resin, one of the current limitations of this epoxy precursor is related to the high value of the viscosity. This is a very critical point to manufacture CFRCs. In this chapter an epoxy formulation able to overcome this drawback is shown. In order to optimize the dispersion of MWCTs inside the epoxy mixture, the initial epoxy precursors were fluidified with an epoxy reactive monomer which has proven to be very effective to lower the viscosity of the nanoparticles/resin mixture and therefore in facilitating the nanofiller dispersion step.

## IV.2 Materials and Methods

The preparation of the epoxy matrix was reported in the experimental section of the chapter II.

The MWCNTs (3100 Grade), added and incorporated into the matrix by using an ultrasonication for 20 min, were obtained from Nanocyl S.A. Transmission electron microscopy investigation (TEM) has shown for the CNTs a diameter around 20 nm.

The epoxy blend with DDS is named TBD in the following.

Dynamic mechanical properties of the samples were performed with a dynamic mechanical thermo-analyzer (TA instrument-DMA 2980). Solid samples with dimensions 4x10x35 mm<sup>3</sup> were tested by applying a variable flexural deformation in dual cantilever mode. The displacement amplitude was set to 0.1%, whereas the measurements were performed at the frequency of 1 Hz. The range of temperature was from -60°C to 300°C at the scanning rate of 3°C/min.

The rheological measurements were carried out in a Physica MCR 301 (Anton Paar) rotational rheometer equipped with a parallel plate geometry (50 mm diameter, 1mm gap) on the pure epoxy resins, on the TBD system and on the MWCNT-TBD nanocomposite with 0.5 wt% nanotube content. Strain sweep tests, at the frequency of 1 rad/s, were previously performed on the 0.5wt% MWCNT-TBD at the temperatures of 50 and 75°C to determine the linear viscoelastic region. Small amplitude oscillatory shear measurements at 1% strain, within the linear viscoelasticity regime, were, then, performed in the frequency range comprised between 10<sup>-2</sup> and 10<sup>2</sup> rad/s at the temperatures of 50 and 75°C

Atomic Force Microscopy (NanoScope V multimode AFM - Digital Instruments) AFM images were collected in tapping mode (TMAFM) which reaches lateral resolution < 1nm and height resolution of less than 1 Å. The data were acquired in an ambient atmosphere (30% - 40% humidity), using microfabricated silicon tips/cantilevers. All the images have been recorded simultaneously in height and in amplitude. For morphological investigation, the composite sections were cut from the solid samples by a sledge microtome. These slices were etched before the observation by AFM microscopy.

## IV.3 Results and discussion

### *IV.3.1 Rheological, dynamic mechanical and morphological properties*

The complex viscosity ( $\eta^*$ ) versus the frequency ( $\omega$ ) of the TGMDA epoxy resin at different temperatures is shown in Figure IV.1. The results clearly evidence the Newtonian behaviour for the pure TGMDA epoxy resin, as

expected. The complex viscosity is, in fact, constant in the whole frequency range tested. Moreover, increasing the temperature the complex viscosity decreases, following an Arrhenius type behaviour. The inclusion of the flexibilizer BDE diluent decreases the viscosity of the TGMDA epoxy resin, as requested; then, the further addition of the DDS curing agent significantly increases the complex viscosity of the TBD system. All these systems show the Newtonian behaviour, similarly to the TGMDA resin.

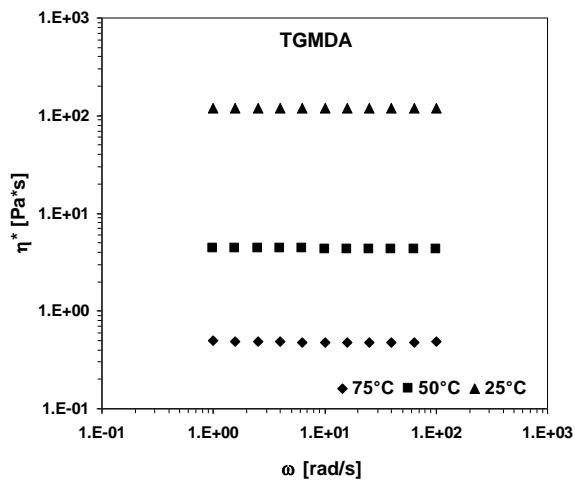


**Figure IV.1** Complex viscosity vs frequency for TGMDA epoxy resin at different temperatures

The inclusion of the multi-walled carbon nanotubes in the formulated epoxy resin mixture with DDS (indicated as TBD) significantly modifies the rheological behaviour of the TBD mixture itself. In fact, at 0.5 wt % MWCNT content the complex viscosity clearly shows a shear thinning behaviour with  $\eta^*$  values much higher at the lower frequencies, as reported in Figure IV.2.

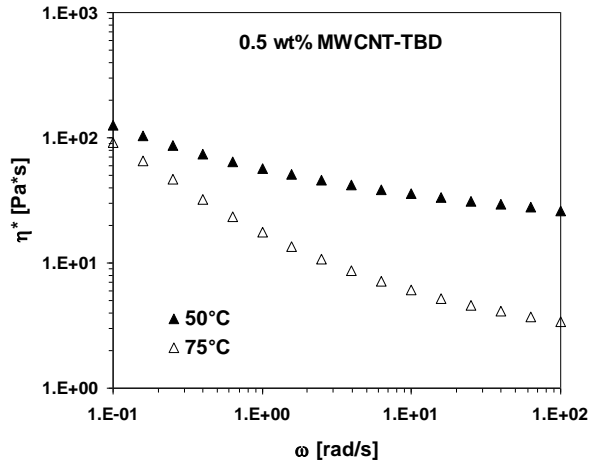


**Figure IV.2** Complex viscosity vs frequency for the 0.5 wt% MWCNT-TBD nanocomposite at different temperatures

In Figure IV.3 the storage ( $G'$ ) and loss ( $G''$ ) moduli vs. frequency for the 0.5wt% MWCNT-TBD nanocomposite at  $T=75^\circ\text{C}$  are reported. The tendency to a plateau in  $G'$ , clearly detected at the lower frequencies, can be attributed to the formation of a percolation network in the nanocomposite. Large scale polymer relaxations in the nanocomposites are, in fact, restrained by the presence of the nanotubes indicating that the 0.5 wt % MWNT content is higher than the nanocomposite rheological percolation threshold “Pötschke *et al.* (2002); Nobile (2011a)”.

Preliminary results on the dynamic mechanical properties of nanofilled epoxy mixture, as measured on the cured epoxy mixture, appear very promising. Indeed, the values of the storage modulus of the cured resin range between 3.56 and 2.21 GPa in the temperature window between  $-60^\circ\text{C}$  and  $60^\circ\text{C}$ . This result indicates that the nanofilled epoxy mixture at the loading rate of 0.32 wt % of CNTs allows to use the formulated material also when a storage modulus higher than 2 GPa is required. The glass transition temperature measured by dynamic mechanical properties of the solidified sample is between  $250\text{-}260^\circ\text{C}$ .

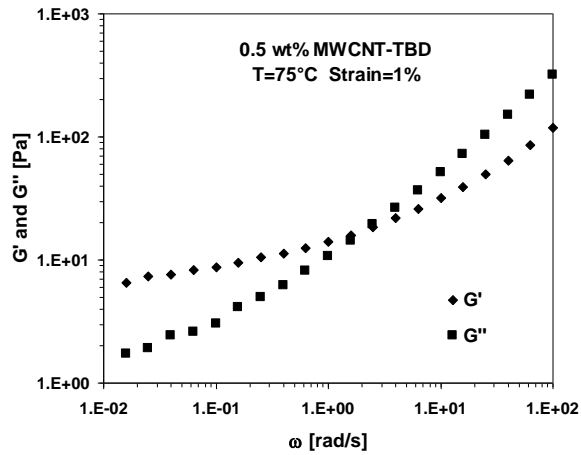


**Figure IV.3** Storage ( $G'$ ) and Loss ( $G''$ ) moduli vs. frequency for the 0.5 wt% MWCNT-TBD composite at  $T= 75^\circ\text{C}$

Figure IV.4 shows the AFM micrograph of 0.64 wt% MWCNT-TBD( $200^\circ\text{C}$ ); the height image is on the left and amplitude image is on the right. The formulated material has shown a strong ability to withstand chemical action of the etching solution that has allowed the nanotubes to appear on the surface, forming a homogeneous structure in which CNTs uniformly cover the entire surface. The image clearly shows that the nanofillers were well dispersed in the polymeric matrix. The obtained results demonstrate that the method used for CNT dispersion into the epoxy mixture was very efficient for this investigated composite.

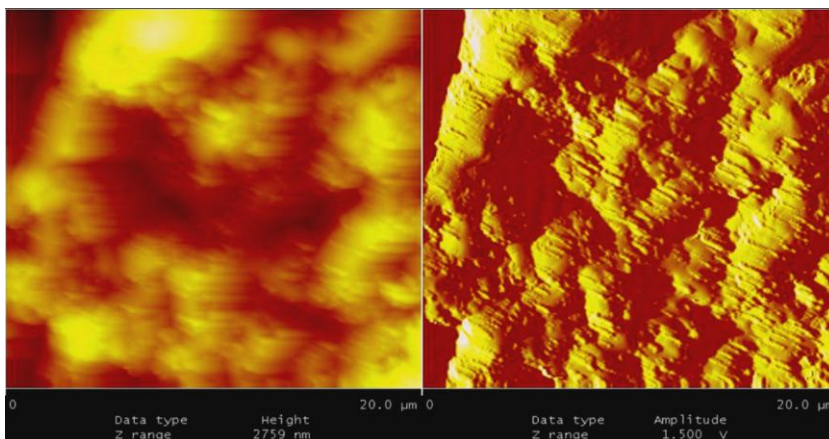


**Figure IV.4** Tapping mode AFM image of 0.64wt% MWCNT-TBD( $200^\circ\text{C}$ )

#### **IV.4 Conclusions**

The presence of the reactive diluent 1,4-Butandiol diglycidylether in the epoxy mixture reduces the viscosity values without decreasing the mechanical properties “Nobile *et al.* (2013b)”. The complex viscosity of the 0.5 wt% MWCNT-TBD nanocomposite evidences a shear thinning behavior at the lower frequencies “Nobile *et al.* (2013b)”. The storage modulus values of the cured resins indicate that the nanofilled epoxy mixture at 0.32 wt % CNT content allows to use the formulated material as structural material in a wide range of temperature

---

## Chapter V

---

# Influence of Nanofiller Morphology on the Viscoelastic Properties of CNF/Epoxy Resins

### V.1 General remarks

As previously described, resins filled with conductive nanofillers were proposed in literature to overcome drawbacks related to insulating properties of the epoxy resins used to manufacture carbon fiber reinforced composites (CFRCs) “Guadagno *et al.* (2011a); B.De Vivo *et al.* (2012b); Sandler *et al.* (2003); Khare and Bose (2005); Guadagno *et al.* (2013d)”.

Nanofilled resins made of conductive nanostructured forms of carbon show significant increases in their electrical conductivity even at low nanofiller concentrations. Among mono-dimensional shaped forms of carbon, carbon nanofibers (CNFs) offer very promising results. The values of electrical conductivity of nanofilled epoxy resins are similar to those found for epoxy matrices filled with CNTs. However, it has to be considered that CNFs/epoxy resins are obtained by an easier production process mainly in the step of nanofiller dispersion inside the epoxy liquid mixture, which is a very difficult step before the curing process. Further criticalities are related to the processing methods employed to manufacture CFRCs. Economic and efficient means of producing high performance fibre-reinforced composites, containing nanofiller embedded in the resin which impregnates CFs, are critically limited by the initial viscosity of epoxy precursors. Generally, the physical properties of epoxy resins strongly depend on the functionality of the epoxy precursor; a tetrafunctional precursor for example assures good properties of the cured resin due to the high level of crosslinking density. Unfortunately, this advantage also causes inconveniences resulting from the high viscosity of the tetrafunctional precursor, the brittleness and poor resistance to crack propagation. In this chapter the first results on the rheological properties of an aeronautic formulation “Guadagno *et al.*

(2013g); Guadagno *et al.* (2013i)” obtained by blending the epoxy precursor with a reactive modifier that performs a double function, as flexibilizer and regulator of viscosity for a best dispersion of nanoparticles are shown.

## V.2 Materials

The morphological parameters of the pristine CNFs (labeled as PR25XTPS1100) are shown in Table V.1.

As previously said, sample PR25XTPS1100 was heat treated to 2500°C to provide the best combination of mechanical and electrical properties, giving the sample the name PR25XTPS2500.

The preparation of the epoxy matrix was reported in the experimental section of the chapter II.

*The epoxy matrix* was prepared in accord with a procedure already previously described. The epoxy blend with DDS is named TBD in the following. The CNFs (samples PR25XTPS1100 and PR25XTPS2500) were added and incorporated into the matrix by using an ultrasonication for 20 min. The experiments show that nanofilled resins with loads beyond 1.3% by weight have difficulty in establishing a homogeneous mixture.

**Table V.1** Morphological parameters of PR25XTPS1100 CNFs

Average Bulk Density of Product, (lb/ft <sup>3</sup> )	1.2-3.0
Nanofiber Wall Density, (g/cm <sup>3</sup> )	2.0-2.1
Nanofiber Density (including hollow core), (g/cm <sup>3</sup> )	1.4-1.6
Average Catalyst (Iron) Content, (ppm)	<14,000
Average Outer Diameter, (nm)	125-150
Average Inner Diameter, (nm)	50-70
Average Specific Surface Area, m <sup>2</sup> /g	65-75
Total pore volume (cm <sup>3</sup> /g)	0.140
Average Pore Diameter (angstroms Å)	82.02

Micrographs of nanofilled epoxy composites were obtained using a Field Emission Scanning Electron Microscope (FESEM, mod. LEO 1525, Carl Zeiss SMT AG, Oberkochen, Germany). Nanofilled sample sections were cut from solid samples by a sledge microtome. These slices were etched before the observation by FESEM. The nanofilled sample sections were placed on a carbon tab previously stuck to an aluminum stub (Agar Scientific, Stansted, UK). The samples were covered with a 250-Å-thick gold film using a sputter coater (Agar mod. 108 A).

The rheological measurements were carried out in a Physica MCR 301 (Anton Paar) rotational rheometer equipped with a parallel plate geometry (50 mm diameter, 1mm gap) on the pure TGMDA epoxy precursor, on the binary TGMDA-BDE system (named TB blend), on the ternary TGMDA-BDE-DDS system (named TBD in the following) and on the CNFs-TBD

nanocomposites with 0.5 wt % nanofiber content. Nanocomposites with PR25XTPS1100 nanofibers as well as nanocomposites with PR25XTPS2500 nanofibers have been tested. Strain sweep tests, at the frequency of 1 rad/s and  $T=75^{\circ}\text{C}$ , were previously performed to determine the linear viscoelastic region. Small amplitude oscillatory shear measurements at 1% strain, within the linear viscoelasticity regime, were, then, performed in the frequency range comprised between  $10^{-2}$  and  $10^2$  rad/s, at the temperature of  $75^{\circ}\text{C}$ .

### V.3 Morphological analysis

As previously described (see figure II.13) FESEM investigations of nanofilled epoxy composites at loading concentration of 1.0 per cent by weight of CNFs, highlight that heat-treated CNFs seem to be characterized by a more straight structure than un-treated CNFs. In addition, heat-treated CNF seems statistically less bonded to the epoxy matrix; in fact, in the case of untreated CNFs, the majority of the CNFs is tightly tied to the epoxy matrix.

### V.4 Rheological analysis

The complex viscosity ( $\eta^*$ ) values versus the frequency ( $\omega$ ) for the TGMDA epoxy precursor and for the binary TGMDA-BDE blend 80%:20% (by wt), named TB, are reported in Figure V.1. The results evidence that  $\eta^*$  is constant in the whole frequency range tested, showing a Newtonian behaviour for the pure TGMDA epoxy precursor and for the binary TB blend. The inclusion of the flexibilizer BDE diluent, then, decreases the viscosity of the TGMDA, so that the dispersion of the nanofibers in the high viscosity TGMDA epoxy precursor is improved

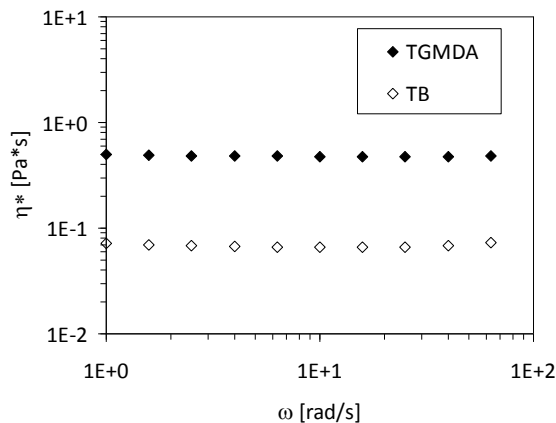


**Figure V.1** Complex viscosity ( $\eta^*$ ) vs frequency ( $\omega$ ) for the TGMDA epoxy precursor and for the TGMDA-BDE blend (TB);  $T= 75^{\circ}\text{C}$

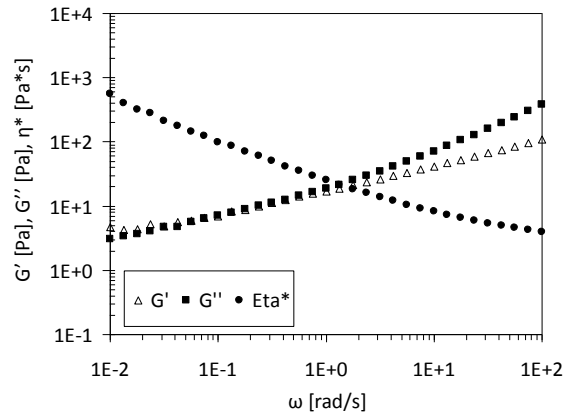


**Figure V.2** Complex viscosity ( $\eta^*$ ), storage ( $G'$ ) and loss ( $G''$ ) moduli vs frequency ( $\omega$ ) for the 0.5 wt% PR25XTPS2500-TBD nanocomposite;  $T = 75^\circ\text{C}$

The inclusion of the heat-treated PR25XTPS2500 carbon nanofibers in the formulated TBD epoxy mixture (TGDMA-BDE-DDS) significantly modifies the rheological behaviour of the TBD mixture itself. In fact, at 0.5 wt % PR25XTPS2500 nanofiber content, the complex viscosity clearly shows a shear thinning behaviour with  $\eta^*$  values much higher at the lower frequencies, as shown in Figure V.2 for the temperature  $T = 75^\circ\text{C}$ . On the contrary, the nanocomposite with 0.5 wt % of the as received PR25XTPS1100 carbon nanofibers behaved essentially as a Newtonian fluid with complex viscosity values only slightly higher than those exhibited by TBD epoxy system.

In Figure V.2 the storage ( $G'$ ) and loss ( $G''$ ) moduli values vs. frequency for the 0.5 wt% PR25XTPS2500-TBD nanocomposite are also reported. The tendency to a plateau in  $G'$ , clearly detected at the lower frequencies, can be attributed to the formation of an interconnected network between carbon nanofibers. Large scale relaxations in the nanocomposite are, in fact, restrained by the presence of the CNFs indicating that the 0.5 wt % content of the heat-treated PR25XTPS2500 CNFs is higher than the rheological percolation threshold “Pötschke *et al.* (2002); Nobile *et al.* (2007c); Nobile (2011<sup>o</sup>); Nobile (2012d); Rahatekar *et al.* (2006)”.

In Figure V.3 the  $G'$  and  $G''$  values of the filled epoxy with the untreated and treated CNFs are compared at  $T = 75^\circ\text{C}$ . The results clearly evidence that the filled epoxy with the heat-treated CNFs show very high elasticity, while the nanocomposite with as received CNFs are essentially characterized by a viscous behaviour. In the case of filled epoxy with as received PR25XTPS1100 CNFs, the rheological percolation threshold is, therefore, higher than 0.5 wt % CNFs. Such a difference in the rheological behaviour

can be attributed to the different morphology observed in the filled epoxy with the as received and heat-treated CNFs. Indeed, in both nanocomposites a good dispersion of the CNFs at 0.5 wt % is achieved, but the heat-treated CNFs seem statistically less bonded to the epoxy matrix as well as more straight compared to the as received CNFs and the interconnected network between PR25XTPS2500 carbon nanofibers is obtained.

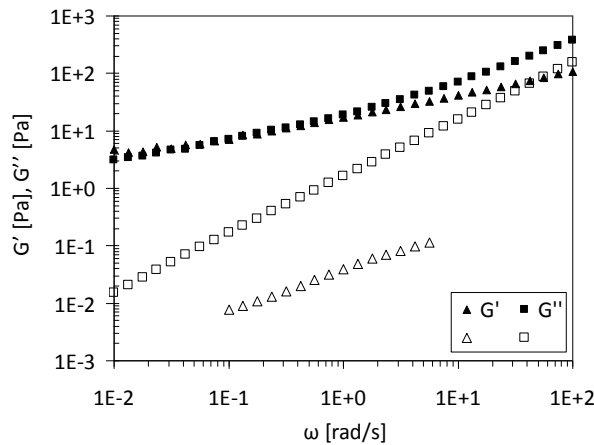


**Figure V.3** Storage ( $G'$ ) and loss ( $G''$ ) moduli vs frequency ( $\omega$ ) for the 0.5 wt% PR25XTPS2500-TBD nanocomposite (filled symbols) and for the 0.5 wt% PR25XTPS1100-TBD nanocomposite (empty symbols);  $T = 75^\circ\text{C}$

## V.5 Conclusions

In this chapter it has been shown that the inclusion of the reactive diluent BDE in the epoxy resin based on the TGMDA precursor reduces the viscosity values of the TGMDA “Guadagno *et al.* (2013j)”. The viscoelastic properties of the nanofilled epoxy composites at 0.5 wt% content of as received and heat-treated CNFs evidence the formation of an interconnected network between CNFs only in the case of the heat-treated PR25XTPS2500 carbon nanofibers, which seem statistically less bonded to the epoxy matrix than the as received CNFs “Guadagno *et al.* (2013j)”.



---

## Chapter VI

---

# Exfoliated graphite as conductive filler in aeronautic epoxy mixtures

### VI.1 Preface

Exfoliated graphite-filled epoxy composites were prepared with load levels from 0.1% to 6.5% by weight. In particular, nanocomposites filled with graphite, characterized by 56% of the amorphous phase (AP) and Brunauer-Emmett-Teller (BET) specific surface area of 14.7 m<sup>2</sup>/g, exhibit an electrical percolation threshold (EPT) less than 3% wt and an electrical conductivity of about 0.18 S/m and 0.66 S/m in the case of samples filled at 4% wt and 6% wt, respectively. The electrical conductivity of the resin filled with exfoliated graphite is resulted strongly dependent on the AP percentage. AFM, SEM and TEM investigations have shown that the AP is characterized by exfoliated graphite composed of blocks containing few layers of graphene sheets together with completely exfoliated graphite. A small increase in the percentage of AP leads to an appreciable decrease in the EPT and an increase of the electrical conductivity. In fact, for a sample filled with graphite characterized by 60% of the AP percentage and BET of 16.3 m<sup>2</sup>/g, the electrical conductivity is about 0.4 S/m for a filler concentration of 1.8% wt, highlighting an EPT corresponding to a concentration value lower than 1.8% wt. Values related to EPT so small are never found in literature for aeronautic epoxy resins loaded with this low concentration of exfoliated graphite.

### VI. 2 General Remarks

Epoxy resins may be attractive because they have high strength to weight ratios, are inexpensive, and are easy to process but, over the years, they have been neglected in many applications where their insulation property was

undesirable characteristic. However, several carbon nanoparticles can be embedded in this type of resins with the aim of improving some of their chemical and physical properties among which the electrical conductivity “Guadagno *et al.* (2013k); Gojny Florian *et al.* (2005)”. For this purpose, the use of graphite and/or exfoliated graphite was extensively investigated in literature “Guadagno *et al.* (2013k); Gojny Florian *et al.* (2005); Lu *et al.* (2006); Bhagat and Verma (2013)”. It has been demonstrated that exfoliated graphite, obtained by means of fast heating and vaporization of a gas within a graphite intercalation, represents a possible and interesting filler for producing conductive polymers “Debelak and Lafdi (2007); Sengupta *et al.* (2011)”. In fact, the extent of graphite surface modification, namely the interaction between the matrix and nano-particles, strongly influences the electrical and mechanical properties of the graphite/polymer nanocomposites “Miller *et al.* (2007)”. Therefore, significant scientific and industrial interest has been focused on the applicability of exfoliated graphite/polymer composites especially as electromagnetic interference shielding, antistatic coating, electromagnetic interference (EMI) suppression “Panwar *et al.* (2009); Chung (2001)”, or electrode materials “McCreery (2008)”. In many cases, due to the micrometer size of the graphite, relatively large amount of this 2-dimensional filler needs to reach the electrical percolation threshold and high electrical conductivity respect to the values typically obtained to impart these properties to the polymeric matrix by means of traditional mono-dimensional conductive nanofillers such as carbon nanotubes, carbon nanofibers, etc. High concentrations of filler may lead to a degradation of some desired basic features of the resin, among which viscosity, processability, homogeneous nanofiller distribution, reproducibility in the chemical and physical properties and costs. “Ganguli *et al.* (2008)” in order of improving chemical interaction between nanofiller and matrix, focused on chemically functionalized exfoliated graphite-filled epoxy composites prepared using filler amount varying from 2% to 20% by weight. Despite the thermal conductivity improvement observed by increasing nanofiller concentration, the electrical property of the chemically functionalized graphite/epoxy composite was found deteriorated as already observed for the functionalization of mono-dimensional conductive nanofillers “Guadagno *et al.* (2011a)”. “Nigrawal *et al.* (2010)” have investigated possible variations in the dc conductivity for exfoliated graphite powder filled epoxy developed using centrifugation technique. Their study highlights that the dc conductivity value increased from centre to periphery due to the increase in the exfoliated graphite concentration. Furthermore, a significant enhancement of electrical conductivity with increasing temperature is detected. Even if the concentration of exfoliated graphite is 3% by weight, the electrical conductivity of the different developed composites was relatively low. In this chapter the influence of the graphite amorphous phase

on the electrical properties of an epoxy formulation tailored to meet specific needs of aeronautic materials was explored. Preliminary results here presented show that an higher degree of AP allows to improve the electrical performance of the nanocomposite suggesting that this controllable feature can be an alternative parameter to design epoxy resins where high electrical conductivity is required at very low filler concentration.

### VI.3 Material and Experimental Part

The considered filler has a two dimensional (2D) predominant shape and it is obtained with an exfoliation procedure from natural graphite, that leads to obtain 2D conductive particles with an average diameter of 500  $\mu\text{m}$ . The graphite used is characterized by two different degree of AP: 56% and 60%. The graphite/matrix nanocomposites obtained are called EG and HEG, respectively. Exfoliated graphite particles were prepared as follows: a mixture containing nitric and sulphuric acid and natural graphite was used. After 24 h of reaction, intercalation within graphene sheets took place to form intercalated graphite compound. Then the mixture was filtered, washed with water, and dried in an oven at low temperatures. The intercalated graphite compound was subjected to sudden heat treatment temperature of 900  $^{\circ}\text{C}$  and rapid expansion then occurred. The expansion ratio was as high as 300 times. The changes in the degree of AP was obtained by changing the resident time in the fluidized bed; as the time increases, the trapped intercalate and/or gases would have a second the chance to escape causing further expansion and exfoliation. The high temperature gas creates enormous pressure within the stacked layers. Fig.VI.1 shows the schematic of the intercalation/exfoliation process. All the mixtures were cured by two-stage curing cycles: a first isothermal stage was carried out at the lower temperature of 125 $^{\circ}\text{C}$  for 1 hour and then a second isothermal stage at higher temperatures up to 200 $^{\circ}\text{C}$  for 3 hours was performed.

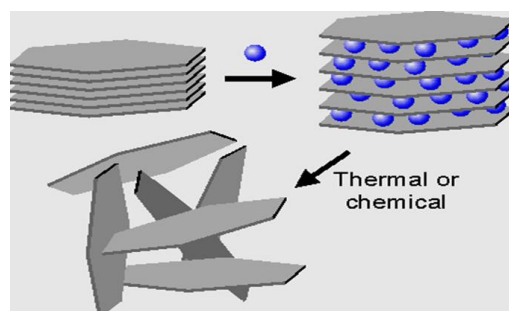


**Figure VI.1** Schematic of the intercalation/exfoliation process (2006 Princeton University, Ceramic Materials Laboratory)

## VI.4 Methods

Scanning electron microscope micrographs were obtained using a Field Emission Scanning Electron Microscope (FESEM, mod. LEO 1525, Carl Zeiss SMT AG, Oberkochen, Germany). TEM analyses were performed with a Philips CM100 apparatus using an acceleration voltage of 100kV. AFM images were acquired in an ambient atmosphere (30%-40% humidity) with a NanoScope V multimode AFM (Digital Instruments), Santa Barbara (CA), using microfabricated silicon tips/cantilevers. All the images have been recorded simultaneously in height, in amplitude and in phase. Some of the nanocomposites section were cut from the solid samples by a sledge microtome. These slices were etched before the morphological analyses. The measurements of the dc volume conductivity were performed by using disk-shaped specimens of about 2 mm thickness and 50 mm diameter, the measurement electrode is circular with a diameter of about 22 mm. The measurement system, remotely controlled by the software LABVIEW®, is composed of a suitable shielded cell with temperature control, of multimeter Keithley 6517A with function of voltage generator (max  $\pm 1000V$ ) and voltmeter (max  $\pm 200 V$ ) and the ammeter HP34401A (min current  $0.1\mu A$ ) for samples above the percolation threshold. For ones below the percolation threshold the system is composed only of multimeter Keithley 6517A with function of voltage generator (max  $\pm 1000V$ ) and pico-ammeter (min current  $0.1fA$ ). Wide-angle X-ray diffraction (WAXD) patterns in reflection were obtained by an automatic Bruker D8 Advance diffractometer operating at 35 KV and 40 mA. The nickel filtered Cu-K $\alpha$  radiation ( $1.5418 \text{ \AA}$ ) was used. d-spacings were calculated using Bragg's law. The correlation lengths (D) of the graphitic nanofiller were determined using Scherrer's equation (eq. 1)

$$D = \frac{K\lambda}{\beta \cos \theta} \quad (1)$$

where K is the Scherrer constant, assumed = 1,  $\lambda$  is the wavelength of the incident X-rays,  $\theta$  is the diffraction angle and  $\beta$  is the corrected integral breadth, obtained by subtracting the instrumental broadening of the closest silicon reflection from the observed integral breadths, as follows:  $\beta = \beta_{\text{obs}} - \beta_{\text{inst}}$ .  $\beta_{\text{obs}}$  were determined through a fit with a Lorentzian function of the intensity corrected diffraction patterns, adopting the procedure according to "Iwashita *et al.* (2004)". The instrumental broadening ( $\beta_{\text{inst}}$ ) was also determined through a fitting of Lorentzian function to line profiles of a standard silicon powder 325 mesh (99%). The degree of crystallinity ( $\chi_c$ ) of the graphitic nanofiller was evaluated from X-ray diffraction data, applying the standard procedure of resolving the diffraction pattern into two areas, Ac and Aa, that can be taken as proportional to the crystalline and the amorphous fraction (AP) of EG, respectively, and calculated, for the  $2\theta$  range  $15-40^\circ$ , using the equation (eq. 2)

$$\chi_c = \frac{A_c}{A_c + A_a} \times 100 \quad (2)$$

according to the classical Hermans-Weidinger method “Hermans and Weidinger (1961)”.

Raman spectra were collected at room temperature with a microRaman spectrometer Renishaw inVia operating with a 514-nm laser source.

Dynamic-mechanical properties were performed using a Tritec 2000 DMA -Triton Technology.

## VI. 5 Results

### VI.5.1 Carbon nanofiller characterization (Raman Spectroscopy)

The Raman spectrum of the exfoliated graphite (EG) sample is shown in Figure VI.2.

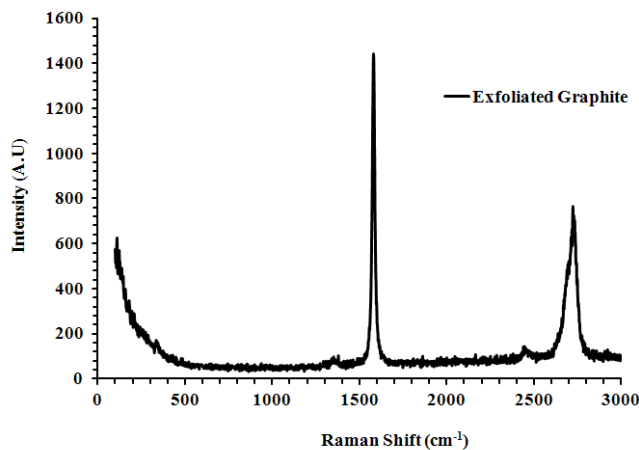
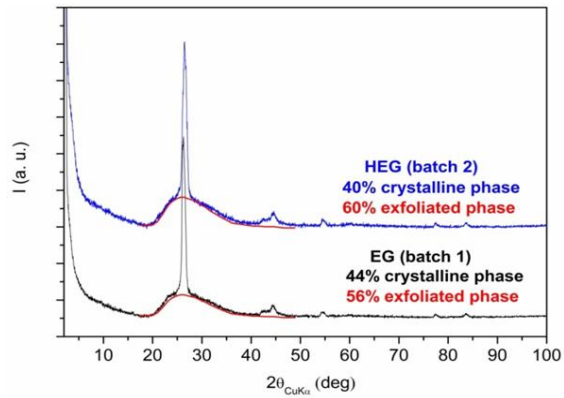


**Figure VI.2** Raman spectrum of exfoliated graphite (EG) sample

The Raman spectrum for carbonaceous material is divided into first and second order regions. The first-order region lies in the interval of 1100 to 1800 wave numbers. In this region we can observe the main graphite band, the G band at  $\sim 1580 \text{ cm}^{-1}$ . This band is observable with different intensity for all the samples. Additional bands at  $\sim 1350\text{-}1355 \text{ cm}^{-1}$ , at  $1500 \text{ cm}^{-1}$  and  $1622 \text{ cm}^{-1}$  are observed for more poorly crystalline graphite. The band at  $\sim 1350 \text{ cm}^{-1}$  is known as the disordered-induced D band and it is observable when defects are present in the carbon aromatic structure. In the second order region (from 2200 to  $3300 \text{ cm}^{-1}$ ), we can observe the band at  $\sim 2700 \text{ cm}^{-1}$  which is indicative of graphite crystallinities.

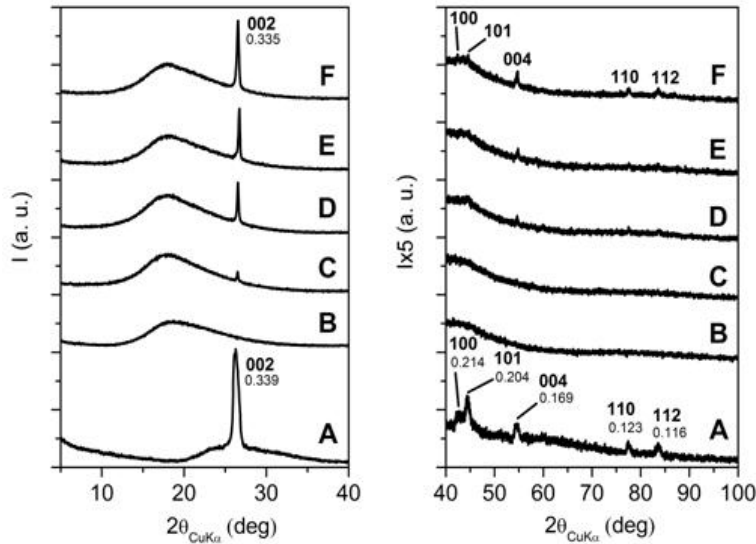
### VI.5.2 Exfoliated graphite and epoxy/exfoliated graphite nanocomposites: X-Ray Diffraction Analysis

Figure VI.3 shows XRD plot of EG and HEG samples where we can see that EG sample is characterized by 56% of the AP percentage and HEG sample is characterized by 60% of the AP percentage.



**Figure VI.3** XRD plots of EG and HEG samples

Figure VI.4 shows XRD patterns of: A) EG sample, B) TBD unfilled epoxy resin, C) TBD\_EG 1% wt, D) TBD\_EG 2% wt, E) TBD\_EG 4% wt, F) TBD\_EG 6.5% wt nanofilled epoxy composites at different percentage by weight of exfoliated graphite (EG).



**Figure VI.4** XRD patterns of: A) EG, B) TBD, C) TBD\_EG 1%wt, D) TBD\_EG 2%wt, E) TBD\_EG 4%wt, F) TBD\_EG 6.5%wt

The exfoliated graphite shows a well defined graphitic structure. Between 20 and 40 degrees of 2theta we can observe a broad amorphous phase below the reflection 002, which might be associated with exfoliated and stacked in a disorderly fashion graphitic layers. The size of the crystals in the direction perpendicular to the planes 002, evaluated by the Scherrer's equation, is about 12 nm. The average number of graphitic layers stacked in an orderly manner is approximately 35. This mean dimension of a stacked graphene sheets was calculated from the width of the individual peaks using the Debye-Scherrer equation. In all the composites with TBD, the crystal size of EG in the direction perpendicular to the planes 002 is 40-45 nm, therefore, during the process of formation of the composite, the EG particles reaggregate and the crystals become more ordered. Furthermore, the reflection 002 shows a shift from 26.3 in the pristine EG to 26.6 degrees of 2 theta in the composites.

### VI.5.3 Epoxy/exfoliated graphite nanocomposites: Dynamic Mechanical Analysis

Figure VI.5 shows a strong increase in the storage modulus in a wide range of temperatures, in particular in the range of temperature between -90 and 210°C for the T20BD+1.8%HEG sample with respect to the T20BD+2% EG sample. No significant decrease is observed in the Tg. Tg of the nanofilled formulations is between 240÷280°C; similar results are obtained for the same epoxy matrix nanofilled with CNFs and CNTs.

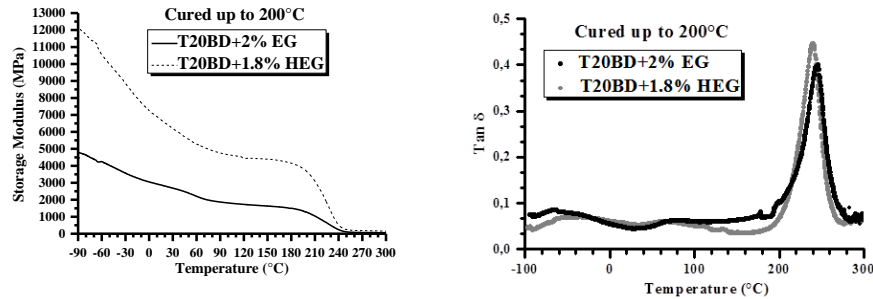
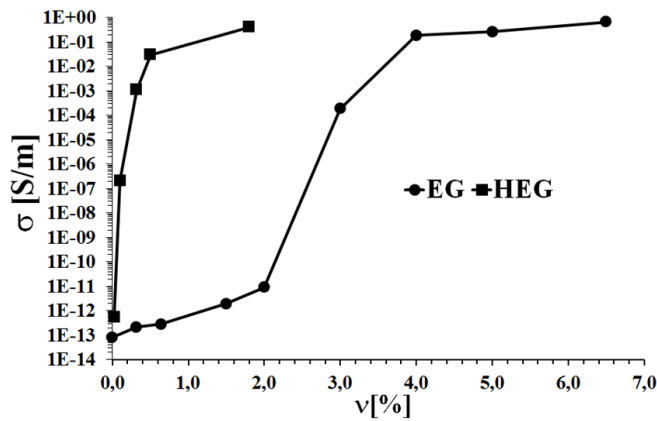


**Figure VI.5** Storage modulus (see graphic on the left) and loss factor ( $\tan\delta$ ) (see graphic on the right) of the sample T20BD+2% EG (AP 56%), and sample T20BD+1.8 % HEG (AP 60%)

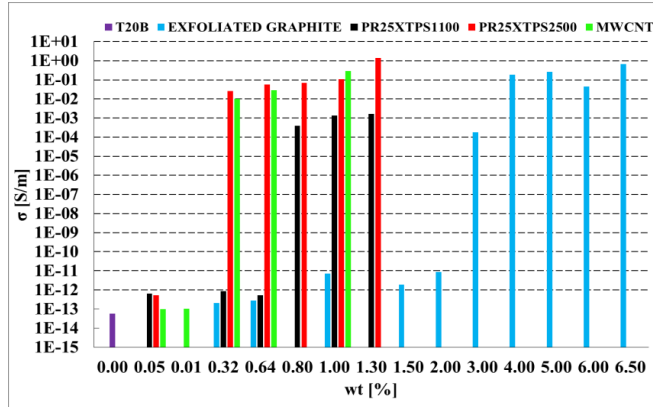
#### VI.5.4 Epoxy/exfoliated graphite nanocomposites: Electrical Characterization

Figure VI.6 shows the electrical percolation curves for two nanocomposites as a function of nanofiller percentage : EG (filled circles) - nanocomposite filled with exfoliated graphite (AP 56%); HEG (square dots) - nanocomposite filled with exfoliated graphite (AP 60%). The results shown in Figure VI.6 demonstrate that, by using bi-dimensional, cheaper and easier to be processed exfoliated graphene sheets, it is possible formulating composites characterized by the same values in the electrical conductivity found for mono-dimensional conductive nanofillers (MWCNTs and CNFs). In particular, a very small concentration of exfoliated graphite can be used in the case of graphite characterized by high value in the AP degree as evidenced by the very small value in the electrical percolation threshold (EPT) (between 0.1% – 0.4 %). The value in EPT shown in Figure VI.6 (see the HEG -square dots-curve) was never found in literature for epoxy resin loaded with this low concentration of graphene layers. Of course, this advantage is additional to other advantages found for epoxy resins loaded with graphene layers. From the graphic, it is possible to observe that for EG-based nanocomposite the electrical percolation threshold (EPT) is less than 3% wt and that the DC conductivity reaches the value of about 0.66 S/m at the highest tested filler concentration (6.5% wt). The rapid increase of the electric conductivity around of the percolation threshold indicates the formation of the conductive network between the sheets of the exfoliated graphite. For aspects concerning the application of these nanofilled resins, Figure VI.7 is very indicative, it shows the electrical conductivity of the nanocomposites for all the fillers analyzed in this PhD thesis. The conductivity is very similar for heat-treated CNFs and MWCNTs. In particular, for the same filler percentage, the epoxy resin filled with heat-treated CNFs presents nearly always higher electrical conductivity than other fillers. The higher value for the conductivity is achieved for the epoxy mixture filled with a percentage CNFs (1.3 wt%) for which a comparison

with MWCNTs is not possible because nanofilled composites with loads beyond 1.3 per cent by weight of MWCNTs become difficult in establishing a homogenous mixture.



**Figure VI.6** Electrical conductivity of two nanocomposites as a function of nanofiller percentage: EG (filled circles) - nanocomposite filled with exfoliated graphite (AP 56%); HEG (square dots) - nanocomposite filled with exfoliated graphite (AP 60%)



**Figure VI.7** Electrical conductivity of nanofilled resins at different nanofiller percentage

The electrical conductivity of nanocomposites with exfoliated graphite appears strongly dependent on the AP percentage degree of the nanofiller. In particular, in the Table VI.1 the comparison between the EG and HEG with 1.8% of the filler is reported.

**Table VI.1** *Physical properties of the EG and HEG for a filler amount of 1.8%wt*

Sample	AP [%]	S <sub>BET</sub> [m <sup>2</sup> /g]	σ [S/m]
EG	56	14.7	<10 <sup>-12</sup>
HEG	60	16.3	0.4

Table VI.1 shows that the Brunauer-Emmett-Teller specific surface area (S<sub>BET</sub>) increases with increasing the AP percentage. This result is in line with other investigations on the correlation between specific surface area and exfoliation degree “Stankovich *et al.* (2007)”. Another very important result in Table VI.1 is that a very small increase in the AP percentage leads to a strong increase in the conductivity and a very relevant decrease in the EPT. The nanocomposite HEG with 1.8% wt of the filler shows an electrical conductivity of about 0.4 S/m and an EPT lower than 1.8% wt (see also Figure VI.6). Similar results on the effect of the AP degree were reported for PMMA expanded graphite nanocomposites “Zheng *et al.* (2002)”, although lower values in the dc conductivity were found for this type thermoplastic polymeric matrix. These values of electrical conductivity and EPT are, to the best of the authors’ knowledge, never found in literature for the thermosetting epoxy resin loaded with this low concentration of graphene layers. In sum, the employment of exfoliated graphite characterized by high values in the fraction of the filler is of particular benefit in order to simultaneously satisfy two requirements: a) high electrical conductivity at very low percentage of exfoliated graphite, and b) strong increase in the storage modulus in a wide range of temperatures, in particular in the range of temperature between -90 and 210°C.

### ***VI.5.5 Exfoliated graphite and epoxy/ exfoliated graphite nanocomposites: Morphological investigation***

SEM investigation on the exfoliated graphite with different AP percentage was performed to analyze the morphology of the nanofiller before its incorporation into the epoxy precursors. The Figure VI.8 shows SEM images of EG and HEG samples respectively. We can see that the exfoliated graphite sheets are highly agglomerated with a fluffy morphology, as already observed in literature “McAllister *et al.* (2007)”. While the layered structure of graphite persists after oxidation, the change in hybridization of the carbon atoms upon oxidation produces a wrinkled morphology observable in Figure VI.8, characteristic of graphite subjected to heat treatment. A very similar result was found for an other polymeric matrix “Abdala *et al.* (2006)”.

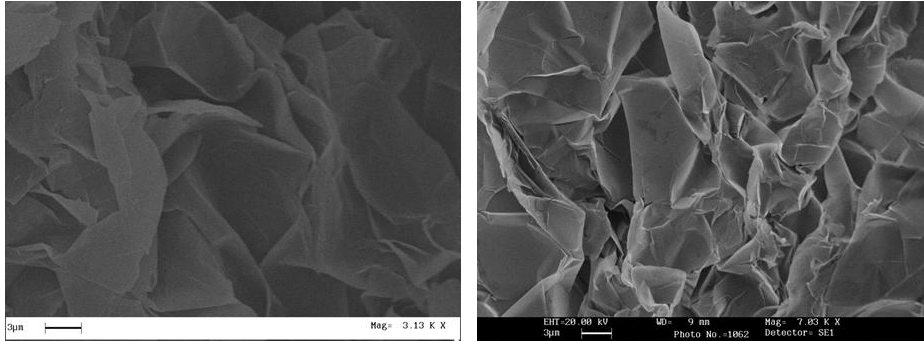


**Figure VI.8** SEM images of EG (on the left) and HEG (on the right) samples

In order to analyze the homogeneity of the nanofiller dispersion in the polymeric matrix, the nanofilled samples with exfoliated graphite were investigated by means of SEM, FESEM, AFM and TEM.

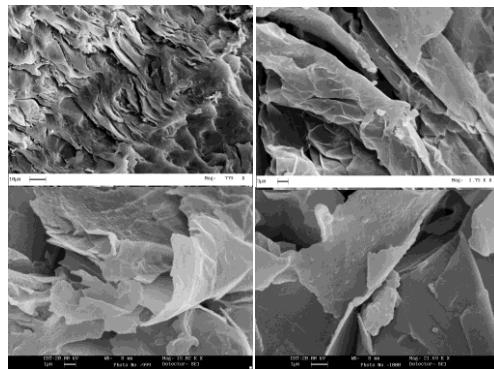


**Figure VI.9** Fracture surface SEM images of the nanofilled epoxy composites at two different loading rates: 0.64% by weight (see images on the top) and 5% by weight (see images on the bottom) of exfoliated graphite EG

Graphene nanosheets are uniformly distributed inside the sample. SEM investigation highlighted that folds in graphene sheets are always present. The image at lower magnifications (see image in the left side on the top) provides a very clear idea on the distribution of GNSs inside the epoxy sample; the morphological features are continuously repeated throughout the entire surface of the sample. The same morphological characteristics related to the folding structure of graphene sheets are also evident in the FESEM images with high resolution, shown in Figure VI.10, of the sample nanofilled with 3% by weight of EG (see image on the right), and the sample loaded at 0.5% (see image on the left) and 1.8% (see image in the middle) by weight of HEG respectively.

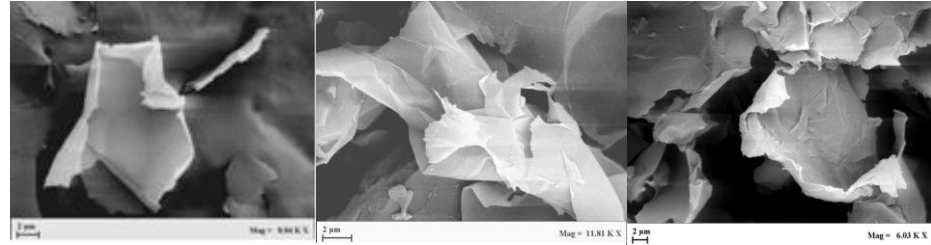


**Figure VI.10** Fracture surface FESEM images of the epoxy composites nanofilled with EG and HEG at different loading rates: 3% by weight of EG (see image on the right), and the sample loaded at 0.5% (see image on the left) and 1.8% (see image in the middle) by weight of HEG respectively

Figure VI.11 shows the AFM images of the nanofilled epoxy composite at loading concentration of 3% by weight of EG. These AFM images were collected after a strong etching procedure that has allowed the packets of exfoliated graphite layers of different thickness to appear on the surface. It's possible to observe folded graphene sheets resembling the draping of a textile, as also reported by "Pereira *et al.* (2010)".

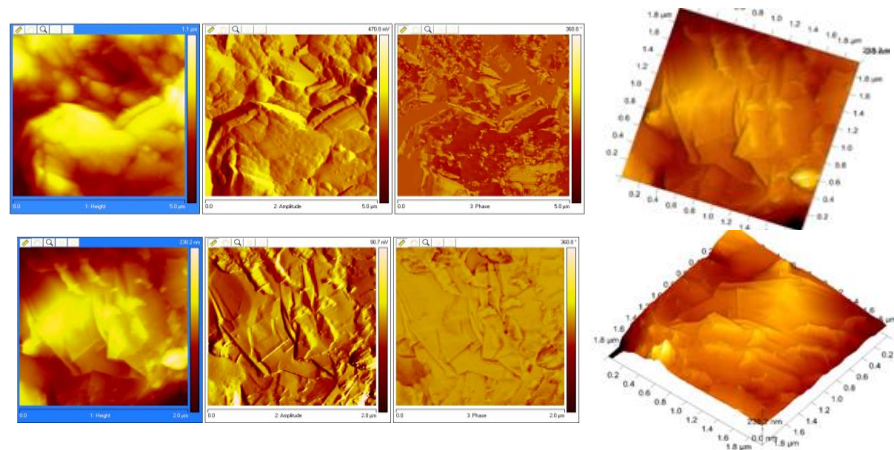


**Figure VI.11** Fracture surface AFM images of the nanofilled epoxy composite at loading concentration of 3% by weight of EG

Figures VI.12 and VI.13 show TEM images of the nanofilled epoxy composite at 1.8 wt% of HEG and 2 wt% of EG respectively. Exfoliated graphite nano-platelets (xGnPs) are new types of nanoparticles made from graphite. These nanoparticles consist of small stacks of graphene that are 1 to 15 nanometers thick, with diameters ranging from sub-micrometer to 100 micrometers. We can see TEM images of a multilayer graphene stack. In particular, thin arrows indicate the edges of the individual layers, and the bold arrow indicates a folded off-plane fragment of layer. From the high

magnification TEM image (see image on the top of Figure VI.13), the thickness of xGnPs can be estimated to be about 16 nanometers. TEM images of exfoliated graphite powder show the crumpled morphology of the few layer graphene sheets. We can observe the wrinkled and disordered graphene sheet-like structure. From the folded edge of exfoliated graphite nanoplatelets in the TEM images, the thickness can be estimated to be several nanometers. Packets of graphite layers of different thickness are observed in the cross-section images.

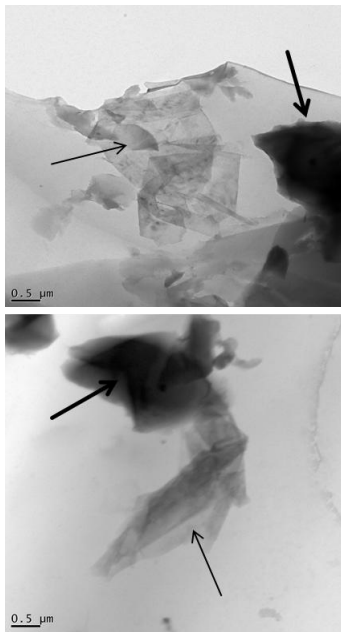


**Figure VI.12** TEM images of the nanofilled epoxy composite at 1.8 wt% of HEG

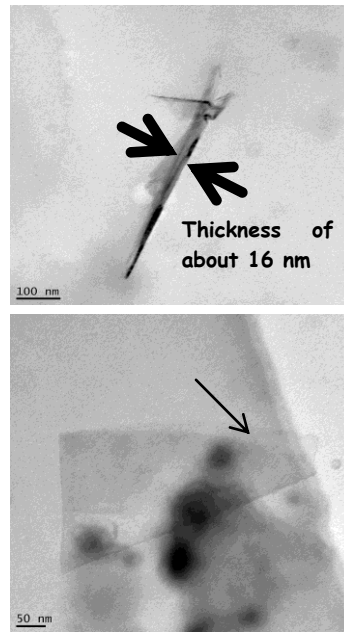


**Figure VI.13** TEM images of the nanofilled epoxy composite at 2 wt% of EG

## VI.6 Conclusions

In this chapter the electrical behaviour of a resin filled with exfoliated graphite was studied. The dc electrical conductivity and the EPT were found to be strongly influenced by the AP percentage of the exfoliated graphite “Guadagno *et al.* (2013)”. In particular, a small increase in the AP percentage and therefore in the exfoliated percentage of graphite, as well as the specific surface area (BET) very positively affect the electrical parameters. A very important result of this study is that the values detected for the electrical parameters were found very similar to those obtained with mono-dimensional shaped nanofillers. This good result can be obtained thanks to the possibility to act on the percentage of the exfoliated graphite.

## Chapter VI

---

Concerning this last point, other tests are in progress and some of the morphological parameters of the nanofillers here analyzed are under evaluation to better investigate the correlation between AP and the exfoliation percentage of graphite. This work is still in progress, but we think, a giant step towards understanding the electrical behavior of resins filled with bi-dimensional shaped carbon forms (more inexpensive and easy to process graphene layers) was taken.

---

# Chapter VII

---

## Fire retardancy concepts

### VII.1 Preface

The massive use of polymer materials in our everyday life is driven by their remarkable combination of properties, low weight and ease of processing. However, polymers are also known for their relatively high flammability; most often accompanied by the production of corrosive or toxic gases and smoke during combustion. Consequently, improving the fire retardant behavior of polymers is a major challenge for extending their use to most applications.

Safety requirements are currently becoming more and more drastic in terms of polymers' reaction to fire and their fire resistance performance, while various flame retardant additives, such as halogenated additives, are being phased out for their proven or suspected adverse effects on the environment. The combined challenge thus consists in developing effective and environmentally friendly flame retardant systems for polymer materials “Laoutid *et al.* (2009)”. A flame retardant should inhibit or suppress a combustion process and that's why they are used in products which would otherwise have a high risk of fire. Including flame retardant into products is one way to improve their fire safety relatively cheap way. Depending on their nature, flame retardants can act chemically and/or physically in solid, liquid or gas phase. They interfere with combustion during a particular stage of this process, e.g.during heating, decomposition, ignition or flame spread “Troitzsch (1990)”.

### VII.2 Polymer combustion

Due to their chemical structure, made up mainly of carbon and hydrogen, polymers are highly combustible “Pal *et al.* (1991)”.

The combustion reaction involves two factors: one or more combustibles (reducing agents) and a combustive (oxidizing agent). The combustive is generally the oxygen in the air. The whole process usually starts with an

increase in the temperature of the polymeric material due to a heat source, to such an extent that it induces polymer bond scissions. The volatile fraction of the resulting polymer fragments diffuses into the air and creates a combustible gaseous mixture (also called fuel). This gaseous mixture ignites when the auto-ignition temperature (defined as the temperature at which the activation energy of the combustion reaction is attained) is reached, liberating heat. Alternatively, the fuel can also ignite at a lower temperature (called the flash point) upon reaction with an external source of intense energy (spark, flame, etc.). The life span of the combustion cycle depends on the quantity of heat liberated during the combustion of the fuel. When the amount of heat liberated reaches a certain level, new decomposition reactions are induced in the solid phase, and therefore more combustibles are produced. The combustion cycle is thus maintained, and called a *fire triangle* (Figure VII.1).

This global process is complex and involves several reactions and transport phenomena in the solid, gaseous and interfacial phases. Heating can be caused by a contribution of thermal energy from an external heat source (radiation, convection or conduction), by a chemical process induced inside the material (fermentation, oxidation, etc.) or by the exothermicity of the combustion reaction initiated. In polymers, the amount of energy required to initiate combustion varies in function of the physical characteristics of the material. For instance, during the heating of semi-crystalline thermoplastics, the polymer softens, melts and drips. The energy stored by the polymer during these processes depends on both its heat-storage capacity and its enthalpy of fusion and degree of crystallinity. Therefore, the increase in polymer temperature and the related rate depend primarily on the heat flow, the difference in temperature due to the exothermicity of the reactions involved, and the specific heat and thermal conductivity of the semicrystalline thermoplastic. In contrast, in the case of amorphous thermoplastics and most thermosets, due to the absence of a melting point, the heating step leads directly to polymer decomposition. The thermal decomposition of a polymer (i.e. covalent bond dissociation) is an endothermic phenomenon, which requires an input of energy. The energy provided to the system must be higher than the binding energy between the covalently linked atoms (200 to 400 kJ/mol for most C-C polymers). The decomposition mechanism is highly dependent on the weakest bonds, and also on the presence or absence of oxygen in the solid and gas phases. Generally, thermal decomposition is the result of a combination of the effects of heat and oxygen. We can therefore distinguish between non-oxidizing thermal degradation and oxidizing thermal degradation “Pal *et al.* (1991)”. Non-oxidizing thermal degradation is generally initiated by chain scissions under the simple effect of temperature (pyrolysis). This scission involves varying degrees of material depolymerization. The initial scission depends on several factors: the presence of oxygen atoms in the chain and

catalyst residues, former residues of oxidation, chemical defects in polymer chains and the existence of weak bonds along the chain, particularly at the end, which can initiate unzipping reactions.

Chain scission can occur in two ways:

- by formation of free-radicals ( $R_1-CH_2-CH_2-R_2 \rightarrow R_1-CH_2^\bullet + \bullet CH_2-R_2$ ), in this case, the reaction does not stop at this stage because these radicals start a chain/cascade reaction, which occurs under both oxidizing and nonoxidizing conditions.

- by migration of hydrogen atoms and the formation of two stable molecules one of which has a reactive carbon-carbon double bond ( $R_1-CH_2-CH_2-CH_2-R_2 \rightarrow R_1-CH=CH_2 + CH_3-R_2$ ).

In oxidizing thermal conditions, the polymer reacts with oxygen in the air and generates a variety of low molecular weight products: carboxylic acids, alcohols, ketones, aldehydes, etc. This degradation also releases very reactive species, i.e.  $H^\bullet$  and  $OH^\bullet$ , particularly in polyolefins. Oxidation can lead to crosslinking through recombination reactions of the macromolecular radicals. However, bond scission usually remains the dominant reaction. The propagation rate of the degradation process is controlled by the wrenching reaction of hydrogen atoms from the polymer chains. The oxidation stability of the polymer thus depends on the C-H bond energy.

Some researchers "Tkac (1981)" suggest that at combustion temperatures above 300°C polymer degradation takes place via non-oxidizing thermal decomposition. Under these conditions, the rate of pyrolysis is much faster than the diffusion of oxygen in the solid phase. Oxidation therefore only occurs in the gas phase due to the presence of low molecular weight compounds produced by thermal decomposition. The decomposition gases generated by pyrolysis first mix with oxygen by both convection and diffusion into the layer close to the surface, create free radicals, and then ignite. This ignition can be triggered by an external flame (flash-ignition) or self-induced (self-ignition) when the temperature is sufficiently high. Ignition depends on several parameters, in particular oxygen concentration. The combustion of the gases increases the polymer temperature and thus supports the pyrolysis and production of new combustible gases. Combustion thus continues even in the absence of an external heat source.

### ***VII.2.1 Mechanism of action***

Fire is the result of three ingredients:

- heat
- fuel
- oxygen

as you can see in the fire triangle (SpecialChem4Polymers), shown in Figure VII.1.

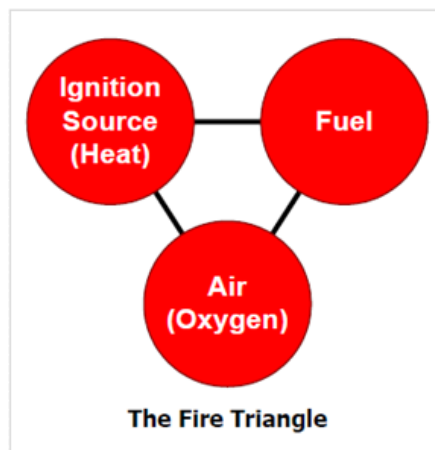


**Figure VII.1** *The fire triangle*

Heat produces flammable gases from the pyrolysis of polymer. Then, an adequate ratio between these gases and oxygen leads to ignition of the polymer.

The combustion leads to a production of heat that is spread out ( $\Delta H_1$ ) and fed back ( $\Delta H_2$ ). This heat feedback pyrolyses the polymer and keeps the combustion going “SpecialChem4Polymers” (see Figure VII.2).

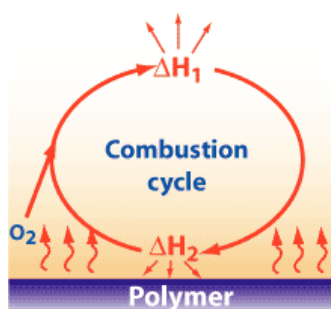


**Figure VII.2** *Combustion cycle*

To limit the establishment of this combustion circle, one (or several) ingredient has to be removed. Several techniques are available in order to break down this combustion circle. To limit the establishment of this combustion circle, one (or several) ingredient has to be removed. Several techniques are available in order to break down this combustion circle.

Flame retardants have to inhibit or even suppress the combustion process. Depending on the polymer and the fire safety test, flame retardants interfere

into one or several stages of the combustion process: heating, decomposition, ignition, flame spread, smoke process. Flame retardants can act chemically and/or physically in the condensed phase and/or in the gas phase. However, we have to remember that both of them occur during a complex process with many simultaneous reactions.

#### VII.2.1.1. Chemical Effect Condensed Phase

In condensed phase two types of reactions can take place:  
 1) Breakdown of the polymer can be accelerated by flame retardants. It leads to pronounced flow of the polymer which decreases the impact of the flame which breaks away.  
 2) Flame retardants can cause a layer of carbon (charring) on the polymer's surface. This occurs, for example, through the dehydrating action of the flame retardant generating double bonds in the polymer. These processes form a carbonaceous layer via cyclizing and cross-linking processes cycle "SpecialChem4Polymers" (see figure VII.3).

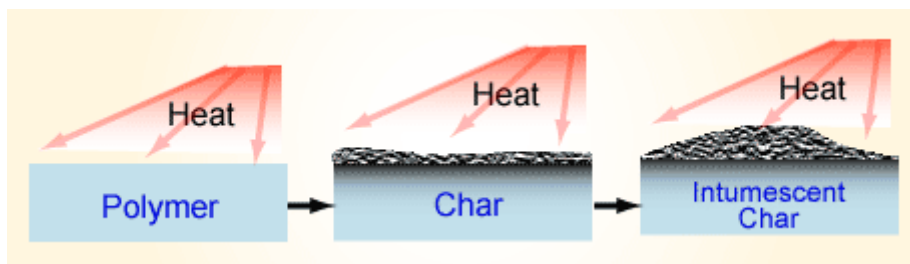


**Figure VII.3** Char and intumescence formation

Flame retardants can be classified in two categories:

- *additive flame retardants*: these are generally incorporated during the transformation process and do not react at this stage with the polymer but only at higher temperature, at the start of a fire; they are usually mineral fillers, hybrids or organic compounds, which can include macromolecules.
- *reactive flame retardants*: unlike additive flame retardants, these are usually introduced into the polymer during synthesis (as monomers or precursor polymers) or in a post-reaction process (e.g. via chemical grafting). Such flame retardants are integrated in the polymer chains. There are four main groups of flame retardant chemicals:
  - Inorganic flame retardants including aluminium trioxide, magnesium hydroxide, ammonium polyphosphate and red phosphorous.
  - Halogenated flame retardants, primarily based on chlorine and bromine. The brominated flame retardants are included in this group.
  - Organophosphorous flame retardants are primarily phosphate esters. Organophosphorous flame retardants may contain bromine or chloride.

- Nitrogen-based organic flame retardants are used for a limited number of polymers.

#### *VII.2.1.2 Intumescence*

Flame retarding polymers by intumescence is essentially a special case of a condensed phase mechanism. The activity in this case occurs in the condensed phase and radical trap mechanism in the gaseous phase appears to not be involved. In intumescence, the amount of fuel produced is also greatly diminished and char rather than combustible gases is formed. The intumescent char, however, has a special active role in the process. It constitutes a two-way barrier, both for the hindering of the passage of the combustible gases and molten polymer to the flame as well as the shielding of the polymer from the heat of the flame. In spite of the considerable number of intumescent systems developed in the last 15 years, they all seem to be based on the application of 3 basic ingredients:

- a "catalyst" (acid source)
- a charring agent and
- a blowing agent (Spumific)

Chemical reactions between these ingredients lead to the formation of the protective intumescent char. A general mechanism has been widely accepted: the acid source decomposes and yields a mineral acid, then it takes part in the dehydration of the carbon source and finally the blowing agent produces gaseous products. These gases are trapped in the char resulting from the carbon source dehydration and make it swell. Intumescence is therefore a physical protection solution chemically created. The char contains free radicals able to trap those generated during polymer burning. It is also a support for catalytic acidic species that react with oxidized compounds formed during polymer degradation. This also permits to maintain these species in the condensed phase.

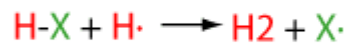
Additives combining the last three ingredients leading to intumescent effect are commercially available. However, intumescent formulations can simply be developed and are more suitable than some commercial grades for some specific applications. Table VII.1 "SpecialChem4Polymers" below summarize usual catalyst, charring and blowing agents.

**Table VII.1** Main components of intumescent systems

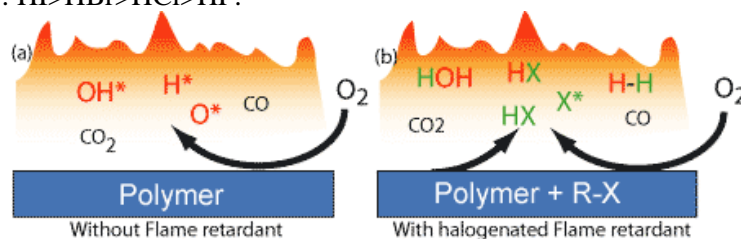
Catalyst (Acid source)	Charring agents	Blowing agents (Spumific)
Ammonium salts Phosphates, polyphosphates	Polyhydric compounds	Amines/amides
Sulfates Halides	Starch Dextrin Sorbitol Pentaerythritol, monomer, dimer, trimer Phenol-formaldehyde resins Methylol melamine	Urea Urea-formaldehyde resins Dicyandiamide Melamine Polyamides
Phosphates of amine or amide	Others Charring	
Products of reaction of urea or Guanidyl urea with phosphoric acids Melamine phosphate Product of reaction of ammonia with P2O5	Polymers (PUR, PA, ...)	
Organophosphorus compounds Tricresyl phosphate		
Alkyl phosphates Haloalkyl phosphates		

### VII.2.1.3 Chemical Effect Gas Phase

The flame retardant or their degradation products stop the radical mechanism of the combustion process that takes place in the gas phase. The exothermic processes, which occur in the flame, are thus stopped, the system cools down, the supply of flammable gases is reduced and eventually completely suppressed. The high-reactive radicals HO and H· can react in the gas phase with other radicals, such as halogenated radicals X· resulted from flame retardant degradation. Less reactive radicals which decrease the kinetics of the combustion are created “SpecialChem4Polymers” (see Figure VII.4)



Flame inhibition studies have shown that the effectiveness decreases as follow:  $\text{HI} > \text{HBr} > \text{HCl} > \text{HF}$ .

**Figure VII.4** Mechanism of action of halogenated flame retardants

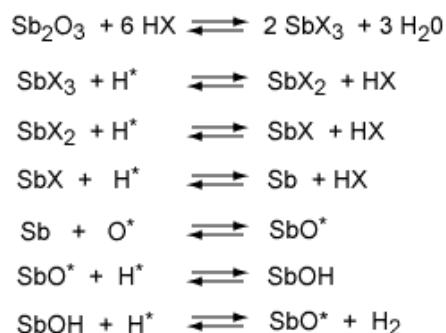
Brominated compounds and chlorinated organic compounds are generally used because iodides are thermally unstable at processing temperature and effectiveness of fluorides is too low. The choice depends on polymer type. The behaviour of the halogenated fire retardant in processing conditions (stability, melting, distribution, etc...) and/or effect on properties and long-term stability of the resulting material are among the criteria that have to be considered. Moreover it is particularly recommended to use an additive that produces halide to the flame at the same range of temperature of polymer degradation into combustible volatile products. Then, fuel and inhibitor would both reach the gas phase according to the "right place at the right time" principle. The most effective fire retardant (FR) polymeric materials are halogen-based polymer (PVC, CPVC, FEP, PVDF...) and additives (CP, TBBA, DECA, BEOs...). However the improvement of fire-performance depends on the type of fire tests i.e. the application.

They perfectly illustrate the previously described chemical modes of action. Severe perturbations of the kinetic mechanism of the combustion lead to incomplete combustion.

#### VII.2.1.4 Synergism with Antimony trioxide ( $Sb_2O_3$ )

To be efficient the trapping free radicals needs to reach the flame in gas phase. Addition of antimony trioxide allows formation of volatile antimony species (antimony halides or antimonyoxyhalide) capable to interrupt the combustion process by inhibiting  $H^*$  radicals via a serie of reactions proposed bellow. This phenomenon explains the synergistic effect between halogenated compounds and  $Sb_2O_3$ .

For most applications, these two ingredients are present in the formulations.



### VII.2.1.5 Physical Effect

#### VII.2.1.5.1 Formation of a protective layer

The additives can form a shield with low thermal conductivity, through an external heat flux, that can reduce the heat transfer  $\Delta H_2$  (from the heat source to the material). It then reduces the degradation rate of the polymer and decreases the "fuel flow" (pyrolysis gases from the degradation of the material) that feeds the flame. Phosphorus additives may act the same way. Their pyrolysis leads to thermally stable pyro- or polyphosphoric compounds which form a protective vitreous barrier "SpecialChem4Polymers" (see Figure VII.5). The same mechanism can be observed using boric acid based additives, zinc borates or low melting glasses.

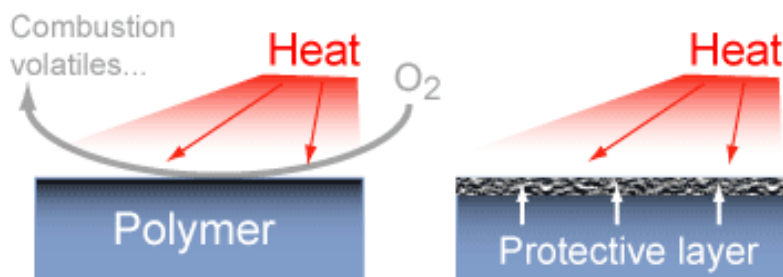


**Figure VII.5** Formation of protective layer inhibiting, combustion and volatiles

#### VII.2.1.6 Cooling effect

The degradation reactions of the additive can influence the energy balance of combustion. The additive can degrade endothermally which cools the substrate to a temperature which is below the one required for sustaining the combustion process. Different metal hydroxides follow this principle and its efficiency depends on the amount incorporated in the polymer.

#### VII.2.1.7 Dilution

The incorporation of inert substances (e.g. fillers such as talc or chalk) and additives (which evolve as inert gases on decomposition) dilutes the fuel in the solid and gaseous phases so that the lower ignition limit of the gas mixture is not reached. In recent work, the isolating effect of a high amount of ash (resulting from certain silica-based fillers) has been shown in fire-retarded systems. Moreover, it highlights also an opposite effect as thermal degradation of the polymer in the bulk is increased by heat conductivity of the filled material.



---

## Chapter VIII

---

# Effect of Incorporation of POSS Compounds on Thermal and Fire Resistance of Aeronautic Resins

### VIII.1 Preface

The aim of the work reported in this chapter is to evaluate the effect of different POSS compounds to act as flame retardants in epoxy mixtures for application in the aeronautic field. Four series of POSS: DPHPOSS, ECPOSS, GPOSS and TCPOSS were dispersed into an epoxy-amine mixture by ultrasonication and magnetic stirring. Visual assessment and optical microscopy were performed to analyze the dispersion/dissolution of POSS inside the epoxy formulation. Thermal degradation of POSS was found to be different for the four samples, whereas no significant differences were observed for the epoxy resins containing POSS compounds. Flame retardancy tested by the LOI indicated that GPOSS has meaningful effects on the flame retardancy of the epoxy mixture. The incorporation of 5 wt% GPOSS into epoxy matrix resulted in a LOI value 33 with respect to 27 of the pure epoxy mixture. The trend observed by LOI tests was confirmed by mass loss calorimetry measurements: a decrease from 540 kW/m to 327 kW/m was observed in the peak of heat release rate (PHRR).

### VIII.2 General remarks

Successful strategies to reduce the flammability of a material are extremely important in the field of aeronautic and aerospace applications. Currently, the material scientists have the possibility "to use" the advantages of the nanotechnologies in addition to the classical methods to protect the materials. Typically, structural composites are carbon fiber or graphite reinforced epoxy resins. Their major advantages over traditional metallic materials like steel and aluminium are their favourable mechanical and

physicochemical properties, and high strength to weight ratio. However, a limitation of epoxy composites is their poor fire resistance “Chatterjee (2009)”. This problem is a major concern in applications where fire can occur. In this context, the subject of fire retardant composites became a source of interest for both academic and industrial researches “Kandola *et al.* (2009); Varley *et al.* (2006); Durga *et al.* (2009); Chiu *et al.* (2009); Husain *et al.* (2004)”. Since inorganic fibres, used for reinforcement in composites are heat resistant and organic polymers are flammable, the fire properties of matrix resin play an important role in determining the fire properties of the related composites. Successful strategies to reduce the flammability of epoxy resins thus appear extremely important in the field of aeronautic applications. The manufacture of fire retardant materials is an extensive area of research “Kandola *et al.* (2009); Varley *et al.* (2006); Durga *et al.* (2009); Chiu *et al.* (2009); Husain *et al.* (2004)”, the understanding of which can improve safety as well as the marketability of a product.

The most common aeronautic grade epoxy resin types includes tetraglycidyl diamino diphenyl methane (TGMDA) cured with diamine diphenyl sulfone (DDS) because such a system shows a high glass transition temperature and the tetrafunctionality of TGMDA leads to high density crosslinked network allowing the manufacture of high performance light-weight composites of interest for aeronautic applications “Rose *et al.* (1993); Levchik *et al.* (1995)” but epoxy networks are known to be sensitive to thermo-oxidation, especially of their aliphatic segments. Indeed, amine crosslinked epoxies are known to undergo dehydration at relatively low temperature (200-300°C) and chain scission can also occur although the presence of aromatic groups in the cured resin network tends to increase its thermal stability “Grassie *et al.* (1986)”. More specifically for TGMDA/DDS system, around 300°C, Delobel and coll. and Camino and coll. observed scission of non-allylic C-N bonds and acetone release. Sulphur containing species and formation of thermostable char are found to occur in the range 300-400°C. Delobel and coll. noticed that at high temperature (>310°C), there are scission reactions along the macromolecule leading to the formation of polyaromatic structures and under air, an oxidation process, which leads to oxygenated aromatic structures. These last structures are favoured when the temperature increases. In addition, they observed that the amount of residue between 250°C and 520°C is higher in thermo-oxidative conditions than under inert gas. In fact, oxygen is found to take part in the degradation and it leads to the formation of a material with good thermal properties until 460°C. However, at higher temperatures, in air, a complete degradation of the material occurs whereas in nitrogen atmosphere, the amount of residue remains constant (around 20-30 wt%). The authors conclude that there is a competition between the carbonization process and the oxidative degradation at high temperature “Rose *et al.* (1993); Levchik *et al.* (1995)”. Several strategies to improve the fire behaviour (i.e. reduce combustibility, smoke and toxic fume production)

of epoxy resins and more specifically TGMDA/DDS system have been developed over the last decades “Ratna (2005); Lu and Hammerton (2002); Weil and Levchik (2004)”. Mainly two approaches have been considered so far “Lu and Hammerton (2002); Toldy *et al.* (2007a)”. The first one concerns the introduction of additive type flame retardant within the polymer by physical and mechanical approach. This provides the most economical way of promoting flame retardancy for commercial polymers. Nevertheless, a variety of problems, such as poor compatibility, leaching and a reduction in mechanical properties makes this approach less attractive. The second approach concerns either the design of new intrinsically flame retarding polymers or modification of existing polymers through copolymerisation with a flame retarding unit either in the main chain or as a pendent group. Many researches focus on this last approach as even a few weight percent of the unit into the polymer chains can lead to remarkable improvements in the overall flame retardancy of the polymer. Historically, halogen containing compounds were commonly applied as flame retardants in epoxy resins either by blending or chemical modification to improve their thermal and flame retardant properties, but because of their toxic and corrosive fumes released during combustion and the apparition of new directives from the European Union which restrict their use, they are becoming much less favoured and the development of halogen-free flame retardants is becoming the main focus of research attention “Lu and Hammerton (2002)”. A wide variety of flame retardants have been reported for epoxy resin including boron, phosphorous and silicon containing compounds “Chiu *et al.* (2009); Lu and Hammerton (2002); Toldy *et al.* (2008b)”. Moreover, in the last decade, nanoparticles, which exhibit a high aspect ratio, specific surface in combination with their low density, high strength, stiffness and other specific properties (electrical conductivity for instance) and which do not generate toxic smoke or corrosive fumes during combustion, have been considered as good candidates as retardant additives for thermoplastics and are recently attracting much interest in epoxy resins “Toldy *et al.* (2007a); Lee *et al.* (2010)”. Indeed, compared to conventional fillers, they are incorporated at low loadings that enable to not degrade mechanical properties of the polymer matrix while enhancing other properties such as fire resistance. Recently Polyhedral Oligomeric Silsesquioxanes (POSS) are emerging as a particle of interest for research because it was shown that the addition of relatively small amount of silicon compounds within polymer matrices can efficiently improve their flame retardancy through both char forming in the condensed phase and the trapping of active radicals in the vapour phase “Lu and Hammerton (2002)”. POSS are also found to interact synergistically with phosphorous compounds to enhance flame retardancy of epoxy systems “Zhang *et al.* (2011a); Zhang *et al.* (2012b); Hsiue *et al.* (2001); Gerard *et al.* (2012)”.

“Franchini *et al.* (2009)” studied the influence of POSS structure on fire behaviour of epoxy hybrid systems. They observed that POSS nanoparticles induced an effective fire retardant effect which efficiency depends on POSS structure. POSS bearing phenyl ligands were found to be more effective than POSS with isobutyl ligands. In addition, the presence of a chemical linkage between phenyl based POSS nanoparticles and the epoxy matrix is found to favour the dispersion of POSS which results in enhanced fire retardancy. “Zhang *et al.* (2013c)” have also studied the influence of POSS structure. They observed that cage-type POSS exhibit a more adapted structure which can make an epoxy system self extinguishing whereas the ladder type has a negligible effect on the fire performances of the epoxy matrix.

In a recent paper the authors investigate the effects of the incorporation of OctaMethylOligomericSilsequioxanes (OMPOSS) and Carbon NanoTubes (CNTs) on the reaction to fire of an epoxy resin containing ammonium polyphosphate (APP) (a conventional intumescent flame retardant) cured with diethylenetriamine (DETA) “Gerard *et al.* (2012)”. They found that the combination of APP and CNTs provides no enhancement of the reaction to fire of this system; whereas using OMPOSS in combination with APP, a large synergistic effect via an intumescence phenomenon is observed. Other authors have formulated epoxy composite with 2 wt% of octa-aminophenyl polyhedral oligomeric silsequioxanes-reduced graphene oxide (OapPOSS-rGO) by using as cross-linking agent 4,4'-diamino diphenylmethane (DDM) “Wang *et al.* (2012)”. They found that with the incorporation of 2 wt% of OapPOSS-rGO, the onset thermal degradation temperature of epoxy composite was increased by 43°C. In addition, the peak heat release rate, total heat release and CO production rate were reduced by 49%, 37% and 58%, respectively, compared to those of neat epoxy. The positive influence of POSS materials to act as fire retardant was found also for thermoplastic polymer for example for polyether-block-polyamide system (50–70% reduction of the PHRR), for polypropylene (40% reduction of PHRR) and a styrene - butadiene-styrene (SBS) triblock polymer (40–60% reduction of PHRR) “Lichtenhan and Gilman (2002)”. Considering these promising results, we have undertaken a study aimed at understanding the effect of different nanostructured carbon forms on the fire behaviour of aeronautic resins containing functionalized and unfunctionalized POSS compounds.

Interestingly not many studies can be found concerning the ability of carbon nanotubes (CNT) to improve flame retardancy and thermal stability of epoxy resins and they present contradictory conclusions. Indeed, “Tao *et al.* (2006)” report that CNT negatively affect the thermal stability of epoxy matrices. More specifically, they found the incorporation of CNT in epoxy accelerates the thermal degradation of epoxy and lowers its degradation temperature. The authors explain the lowered degradation temperature by an effect of the CNT on the extent of curing of the epoxy matrix yielding an epoxy/CNT nanocomposite containing unreacted components that

decompose at lower temperatures. In addition, the presence of metallic catalyst residues in the CNT might also catalyze the decomposition of the epoxy. Other studies “Jyotishkumar *et al.* (2013)” confirm the decrease in overall curing density of epoxy matrices by the addition of CNT. Contrary to Tao and coll., “Katsoulis *et al.* (2011)” observe no significant alteration of the thermal stability of the epoxy system in presence of double-wall carbon nanotubes but they do not notice a significant effect on the fire reaction properties of the epoxy composite whereas “Lee *et al.* (2010)” obtain an improvement of the flame retardant and anti-oxidation properties of epoxy systems with addition of CNT or layered clay. “Rahatekar *et al.* (2010)” studied the effect of CNT or layered clay (MMT type) on the flammability of epoxy systems. They found that integrity of the residue/char formed from epoxy/CNT composites was superior to that of epoxy/MMT composites. They also observed a significant increase in thermal conductivity of epoxy/CNT composites with high loading of CNT which leading to a decrease of the shielding ability of the protective layer and a heat up of the underlying polymer. This enhanced thermal conductivity of epoxy/CNT composites is found to be responsible for the initial mass loss reduction. “Gerard *et al.* (2012)” studied the effect of two types of nanoparticles (CNT and POSS) on the reaction to fire of an epoxy resin modified with a phosphorous flame retardant. They observed that combination of an intumescent phosphorus-based flame retardant and POSS particles provides a large synergistic effect via an intumescent phenomenon. More precisely, they observed the trapping of degradation gases is enhanced resulting in the creation of an intumescent protective layer earlier than when phosphorus flame retardant is used alone. In addition, the presence of POSS allows the creation of silicophosphates that reinforce the residue. On the contrary, they observe no synergy to fire resistance of epoxy system for the combination of the intumescent phosphorous-based flame retardant and CNT. The residue resulting from the formulation is found to be excessively stiff and it cracks during combustion, hindering the proper formation of the protective layer. Functionalization of CNT has also been considered in the literature. For instance, “Shen *et al.* (2007)” prepared amino-functionalized CNT that were found to enhance the thermal stability of the resulting epoxy composites whereas “Jin *et al.* (2011)” observe that their acid-treated and amino-functionalized CNT have little effect on the decomposition temperature of epoxy resins. “Ma *et al.* (2007)” who studied the effect of silane-functionalization of CNT, observed an enhancement of CNT dispersion within epoxy and an increase of thermal properties of the composites. More precisely, silane-functionalized CNT are found to retard the thermal decomposition of the composite and higher residual yields are obtained. “Yu *et al.* (2011)” have modified CNT with molybdenum phenolic resin and they obtained improved CNT dispersion and improved fire behaviour. It appears from the above results that the potential of CNT towards epoxy resins in

terms of fire properties is not fully demonstrated. In this chapter we show the first results on the effect of POSS compounds to act as fire retardant of a high performance epoxy mixture for aeronautic applications for the development of new multifunctional composites containing protecting nanofillers.

### **VIII.3 Experimental**

#### ***VIII.3.1 Materials***

The epoxy matrix T20B was prepared by mixing an epoxy precursor, tetraglycidyl methylene dianiline (TGMDA) (Epoxy equivalent weight 117-133 g/eq), with an epoxy reactive monomer 1-4 Butanediol diglycidyl ether (BDE) at a concentration of 80%: 20% (by wt) respectively.

Four different POSS compounds were dispersed in the epoxy matrix: GPOSS, TCPOSS and ECPOSS functionalized with a different number of oxirane rings, and DPHPOSS functionalized with phenyl groups. The structure of the used organic substituted POSS compounds are shown in Table VIII.1. POSS/epoxy composites were prepared with 5 wt% of POSS. The curing agent used for the curing was 4,4'-diaminodiphenyl sulfone (DDS). This hardener agent was added at a stoichiometric concentration with respect to all the epoxy rings (TGMDA, BDE and POSS – in the case of POSS with epoxy rings). TGMDA, BDE and DDS were obtained from Sigma-Aldrich, while POSS compounds from Hybrid Plastics Company.

#### ***VIII.3.2 Characterizations and Experimental procedure***

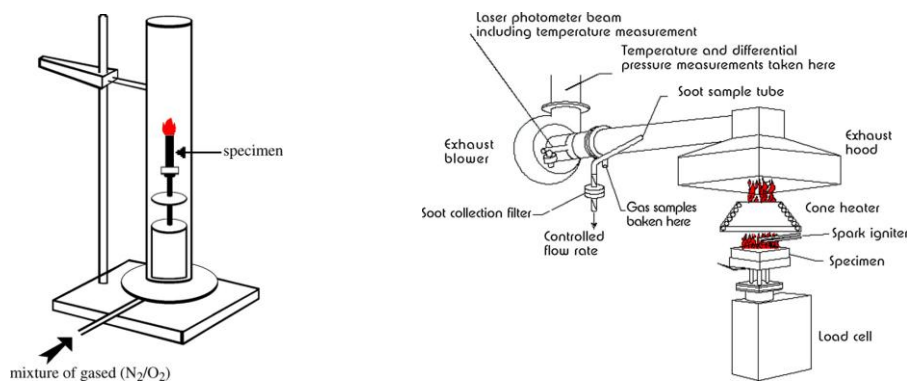
Epoxy blends and DDS were mixed at 120°C and all the samples were cured by a two-stage curing cycles: a first isothermal stage was carried out at the lower temperature of 125°C for 1 hour and the second isothermal stage at higher temperatures up to 200°C for 3 hours.

Fire resistance of POSS based epoxy samples was characterized by limiting oxygen index measurement (LOI) and mass loss calorimetry.

Experimental conditions for LOI tests: barrels of 80x10x3 mm<sup>3</sup> are fixed in a vertical position and their top is inflamed with a burner. The mixture of gases flows upstream through this chimney and is homogenized by being passed through layers of glass beads. After a 30-second purge of the column, the top of the specimen is ignited, like a candle. LOI, the minimum concentration of oxygen in a nitrogen/oxygen mixture required to just support the sample combustion (that either maintains flame combustion of the materials for 3 minutes or consumes a length of 5 cm of the sample), was measured following standard ASTM 2863. The LOI is expressed as:

$$LOI = 100 \frac{[O_2]}{[O_2] + [N_2]}$$

The higher the LOI the better the flame retardant property. Air contains approximately 21% oxygen and therefore any material with an LOI of less than 21 will probably support burning in an open-air situation. These materials are classified as “combustible”, whereas those with an LOI above 21 are classified as “self-extinguishing”, because their combustion cannot be sustained at ambient temperature without an external energy contribution. Experimental conditions for Mass loss calorimeter: plates of  $100 \times 100 \times 3 \text{ mm}^3$  are exposed to a radiant cone ( $50 \text{ kW/m}^2$ ) using a forced ignition. The heat of combustion released was measured using a thermopile according to standard ISO 13927. The principle of mass loss calorimeter experiments is based on the measurement of the decreasing oxygen concentration in the combustion gases of a sample subjected to a given heat flux (in general from 10 to  $100 \text{ kW/m}^2$ ). The sample is placed on a load cell in order to evaluate the evolution of mass loss during the experiment. A conical radiant electrical heater uniformly irradiates the sample from above. The combustion is triggered by an electric spark. The combustion gases produced pass through the heating cone and are captured by means of an exhaust duct system with a centrifugal fan and a hood. The gas flow, oxygen, CO and  $\text{CO}_2$  concentrations and smoke density are measured in the exhaust duct. Experimental set-up for LOI measurement and Mass loss calorimeter measurement is shown in Figure VIII.1.

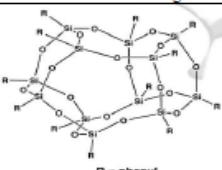
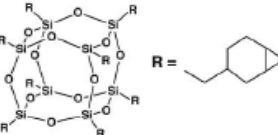
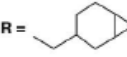
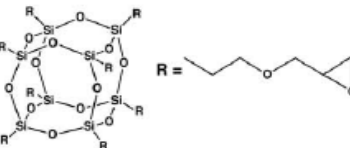
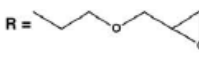
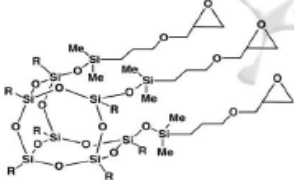


**Figure VIII.1** Experimental set-up for LOI measurement (see image on the left) and Mass loss calorimeter measurement (see image on the right)

Thermogravimetric analysis (TGA) was carried out with a Mettler TGA/SDTA 851 thermobalance. Resin samples were heated from  $25^\circ\text{C}$  to  $900^\circ\text{C}$  at a  $10^\circ\text{C}/\text{min}$  heating rate under air and nitrogen flow. The weight loss was recorded as a function of temperature. POSS dispersion methods were evaluated with aim of choosing the best procedure to obtain the

optimal dispersion of these compounds inside the epoxy formulation. An efficient method to obtain a good dispersion was developed consisting in one or two steps; in the first step POSS compounds were ultrasonicated inside the liquid epoxy formulation at 90°C, in the second step, the dispersion was optimized by magnetic stirring at 120°C. Optical stereo-microscope analysis was performed in order to evaluate the dispersion level of the POSS in the epoxy mixture.

**Table VIII.1** POSS compounds investigated in this chapter

Acronym	Configuration	Characteristics and aspect
<b>DPHPOSS</b>	 <p>R = phenyl</p>	1) Appearance: Powder 2) Color: White; 3) Molecular/Chemical Formula: $C_{72}H_{40}O_{18}Si_{12}$ 4) Molecular Weight: 1550.26 FW
<b>ECPOSS</b>	 <p>R = </p>	1) Appearance: Semi-solid 2) Color: Light Yellow; 3) Molecular/Chemical Formula: $(C_9H_{13}O)_n(SiO_{1.5})_n$ $n=8,10,12$ 4) Molecular Weight: 1418.20 (for n = 8)
<b>GPOSS</b>	 <p>R = </p>	1) Appearance: Viscous liquid 2) Color: Colorless to Slightly Yellow; 3) Molecular/Chemical Formula: $(C_9H_{17}O_2)_n(SiO_{1.5})_n$ $n=8,10,12$ 4) Molecular Weight: 1337.88 (for n = 8)
<b>TCPOSS</b>	 <p>R = cyclohexyl</p>	1) Appearance: Clear Oil 2) Color: Yellow 3) Molecular/Chemical Formula: $C_{60}H_{128}O_{18}Si_{10}$ 4) Molecular Weight: 1490.58 FW

## VIII.4 Results and discussion

### VIII.4.1 Dispersion of POSS inside the epoxy mixture

POSS dispersion inside the epoxy mixture was tested for all the analyzed POSS using two step of mechanical agitation: 1) ultrasonication for 20 minutes (Hielscher model UP200S-24KHz high power ultrasonic probe) at 90°C and 2) magnetic stirring in oil bath at 120°C for 1h.

*VIII.4.1.1 Results on the dispersion of DPHPOSS in the epoxy mixture.*

DPHPOSS powder was dispersed at a percentage of 5 wt% in the epoxy mixture T20BD obtaining the sample T20BD+5%DPHPOSS; before to apply the mechanical agitation via ultrasonic waves, a preliminary analysis of the sample T20BD+5%DPHPOSS was performed by optical microscopy (see Figure VIII.2).

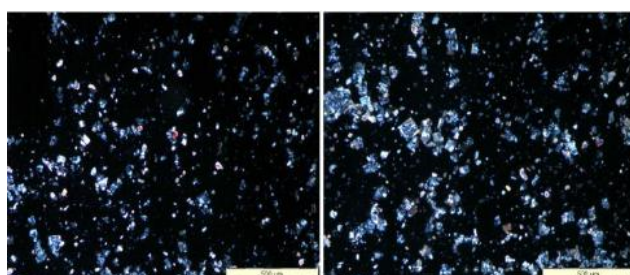


**Figure VIII.2** *Optical image of T20BD+5%DPHPOSS sample (before ultrasonication).*

As expected, several aggregates of DPHPOSS molecules are detectable, indicating that POSS's cage crystalline aggregates were almost intact. A relevant average size reduction of dispersed POSS phase was achieved by ultrasonication for 20 minutes (see Figure VIII.3)

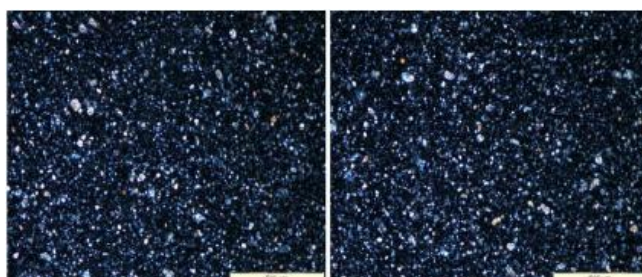


**Figure VIII.3** *Optical image of T20BD+5%DPHPOSS sample (after ultrasonication)*

The followed magnetic stirring step performed at 400 rpm in oil bath at 120°C for 1 hour, did not lead to any relevant differences in the POSS dispersion. The microscope images showed phenomena of re-aggregation (see Figure VIII.4). The results on the dispersion of DPHPOSS in the T20B mixture indicate that this POSS is not epoxy-soluble and only the first step

must be applied to ensure a better dispersion of POSS powder in the epoxy matrix.

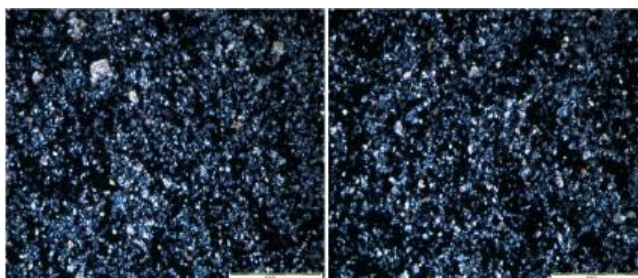


**Figure VIII.4** Optical image of T20BD+5%DPHPOSS sample (after ultrasonication and magnetic stirring in oil bath at 120°C for 1h)

#### VIII.4.1.2 Results on the dispersion of ECPOSS in the epoxy mixture

ECPOSS was dispersed at a percentage of 5 wt% in the epoxy mixture T20BD obtaining the sample T20BD+5%ECPOSS. Visual assessment of this sample (see Figure VIII.5) after ultrasonication (on the left) and after 1h in a stirred oil bath at 120°C (on the right) showed a clear mixture.



**Figure VIII.5** Photos of T20BD+5%ECPOSS mixture after ultrasonication (on the left) and after 1h in a stirred oil bath at 120°C (on the right)

In support of these results, optical stereo-microscope examination of sample was performed by using high resolution stereo inspection. It was found that few small aggregates (not visible to the naked eye) were present after the ultrasonication, the heating stirring action at 120°C further reduces the dimension of these aggregates improving the dispersion; consequently the final material appears as a random few POSS aggregates in the liquid epoxy mixture (see Figure VIII.6).

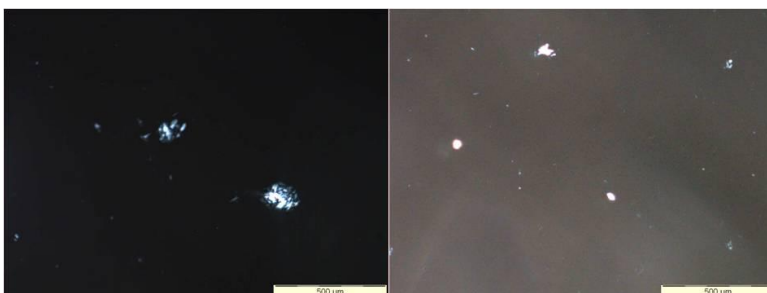


**Figure VIII.6** Optical image of T20BD+5%ECPOSS sample after ultrasonication (on the left) and magnetic stirring in oil bath at 120°C for 1h (on the right)

#### VIII.4.1.3 Results on the dispersion of GPOSS in the epoxy mixture

GPOSS in the form of viscous liquid was dispersed at a percentage of 5 wt% in the epoxy mixture T20BD obtaining the sample T20BD+5%GPOSS.

Visual assessment of sample after ultrasonication highlighted the presence filamentous residues (see Figure VIII.7 – on the left). The subsequent stirring step in heated oil bath causes the dissolution of the filamentous residues, consequently the sample becomes clear (see Figure VIII.7 – on the right).

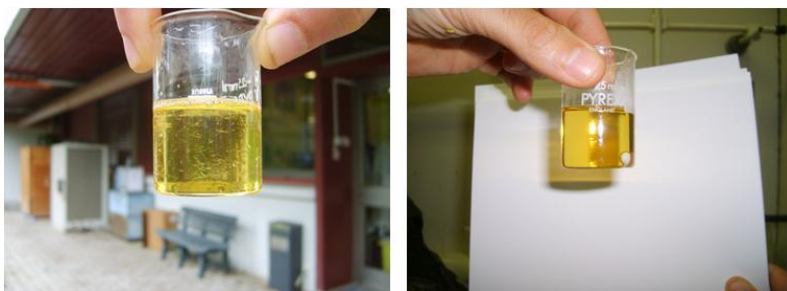


**Figure VIII.7** Photos of T20BD+5%GPOSS mixture after ultrasonication (on the left) and after 1h in a stirred oil bath at 120°C (on the right)

As for the previous sample, optical stereo-microscope examinations of sample by using high resolution *stereo* inspection have shown a very good level of GPOSS solubility inside the matrix after the second step.



**Figure VIII.8** *Optical image of T20BD+5%GPOSS sample after ultrasonication and magnetic stirring in oil bath at 120°C for 1h*

#### *VIII.4.1.4 Results on the dispersion of TCPOSS in the epoxy mixture*

TCPOSS liquid was dispersed at a percentage of 5 wt% in the epoxy mixture T20BD obtaining the sample T20BD+5%TCPOSS.

Visual assessment of T20BD+5%TCPOSS sample shows particle suspensions in the sample detectable also after sonication. Nevertheless, the subsequent stirring step in the heated oil bath causes dissolution of this residue making clear the sample with no particles visible to the naked eye. Optical stereo-microscope examinations of sample by using high resolution *stereo* inspection have shown very small aggregates well distributed into the epoxy formulations after the two steps of ultrasonication and magnetic stirring in oil bath at 120°C for 1h (see Figure VIII.9).



**Figure VIII.9** *Optical image of T20BD+5%TCPOSS sample after ultrasonication and magnetic stirring in oil bath at 120°C for 1h*

In conclusion, data on the dispersion of the analyzed POSS inside the epoxy mixture T20B show that the structure of POSS plays an important role on the dissolution/dispersion of these compound into the matrix. In particular, GPOSS that is fully epoxidized with glycidyl groups is compatible with

epoxy precursors and shows good level of dissolution into the initial liquid epoxy mixture after the two steps of ultrasonication and magnetic stirring at 120°C. DPHPOSS which contains no epoxy group does not dissolve into the epoxy formulations. However, the only ultrasonication step allows to obtain an homogeneous dispersions of very small aggregates inside the formulation.

#### VIII.4.2 Thermogravimetric analysis

Thermogravimetric curves for POSS, epoxy T20BD and POSS/epoxy mixture (POSS/EPM) as a function of temperature are shown in Figure VIII. 10. The thermal degradation process of pure POSS compounds is different for the four samples, DPHPOSS appears to be the most thermostable than other POSS, while these considerable differences are not reflected in the POSS/EPM samples.

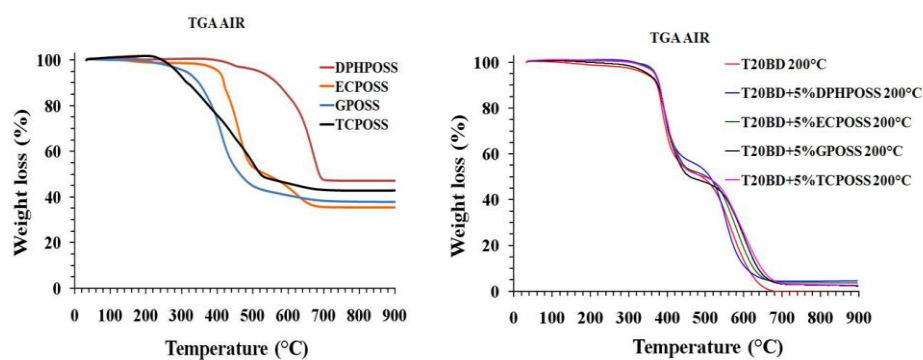


**Figure VIII.10** TG profiles for POSS (on the left side), EPM and POSS/EPM (on the right side)

Thermogravimetric analysis shows that all the POSS/EPM samples are thermostable up to 300°C.

### VIII.4.3 Fire behavior of POSS/EPM

The HRR versus time curves for the different samples are shown in Figure VIII.11.

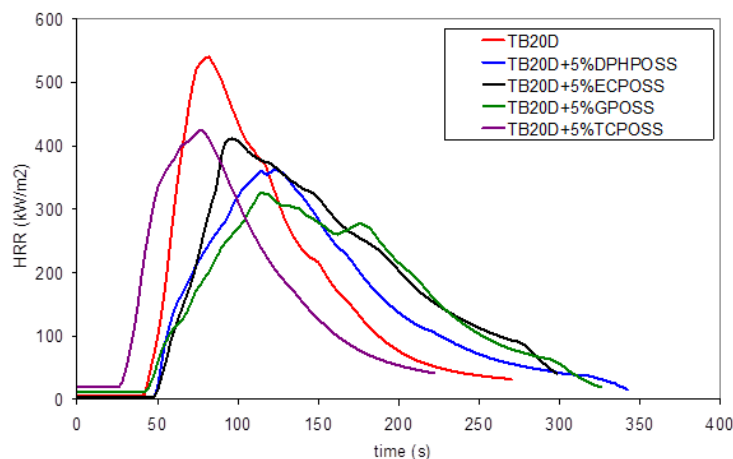


**Figure VIII.11** HRR of T20BD and POSS/EPM formulations

Fire behavior of T20BD is clearly modified in presence of POSS. In addition to the significant decrease of the peak of heat release rate, the time of ignition is slightly increased for DPHPOSS, ECPOSS and GPOSS. Table VIII.2 shows the *limiting oxygen index* (LOI) and the values of the peak of heat release rate (PHRR). It appears that the presence of POSS compounds undoubtedly acts as flame retardant for T20BD epoxy system as shown by the increase of LOI and the decrease of the PHRR. GPOSS leads to the best increase of LOI (22% with respect to T20BD value). The best behavior is also confirmed by the larger decrease in the PHRR value; in fact, a decrease from 540 kW/m<sup>2</sup> to 327 kW/m<sup>2</sup> was observed in the PHRR of the T20BD+5%GPOSS sample for which we can observe the smallest value. These results are to be related to the fully epoxidized structure of GPOSS which allows a better dispersion of the POSS particles due to complete dissolution within T20BD and chemical linkages with the epoxy system. It is interesting to point out that DPHPOSS which exhibits the most thermostable structure (see Figure VIII.10) also leads to a significant increase of LOI and decrease of PHRR. However DPHPOSS particles does not bear any reactive functions towards T20BD epoxy system and their lack of compatibility with T20BD can represent a limiting factor to disperse them properly at a nanoscale. These results indicate a similar trend as observed by “Franchini *et al.* (2009)” on an other epoxy system (DGEBA/MDEA) filled with non soluble phenyl based POSS and phenyl or isobutyl epoxidized POSS.

**Table VIII. 2** LOI and PHRR of the POSS/EPM samples

Sample	LOI (%O <sub>2</sub> )	PHRR (kW/m <sup>2</sup> )
T20BD	27	540
TB20D+5%DPHPOSS	30	362
TB20D+5%ECPOSS	28	411
TB20D+5%GPOSS	33	327
TB20D+5%TCPOSS	26	425

**Figure VIII.12** Photographs of residues from left to right (neat T20BD, T20BD+5%DPHPOSS, T20BD+5%ECPOSS, T20BD+5%GPOSS, T20BD+5%TCPOSS)

From the pictures, it can be seen that the neat T20BD system exhibits a continual crispy char relevant of quite a good thermo-stability of the neat system. Nevertheless, no intumescence is observed for this system. For the systems containing POSS particles, to the exception of TCPOSS based system, intumescent chars are obtained highlighting that the incorporation of POSS enhance significantly the thermostability of the char in an efficient way and GPOSS and DPHPOSS lead to the best intumescent chars.

### VIII.5 Conclusions

The incorporation of 5% of POSS into T20BD epoxy resins is beneficial for improving its flame retardancy “Raimondo *et al.* (2013a); Raimondo *et al.* (2013b); Guadagno *et al.* (2013i)”. The most promising POSS are GPOSS and DPHPOSS. Data on the dispersion of the analyzed POSS inside the epoxy mixture T20B show that the structure of POSS plays an important role on the dissolution/dispersion of these compound into the matrix. GPOSS was

solubilized in the matrix using two steps: ultrasonication at 90 °C and magnetic stirring in oil bath at 120°C for 1h.

The chosen procedure allows a good level of dissolution into the initial liquid epoxy mixture. This result is most probably due to the structure of GPOSS that is fully epoxidized with glycidyl groups which make compatible the POSS molecule with epoxy precursors and reactive diluent. In addition its structure allows to react and participate to the T20BD network formation during the curing cycle. This could be one the reasons of the better fire behavior of GPOSS compared to the other analyzed POSS. Another relevant result of this work regards the fire behavior of DPHPOSS which is satisfactorily although it does not solubilize in initial epoxy precursors and for which only the ultrasonication step was used to obtain an homogeneous dispersions of very small aggregates inside the formulation.

---

## Chapter IX

---

# Multifunctional epoxy resin with enhanced flame resistance

### IX.1 General remarks

The development of multifunctional materials or “smart materials” is currently a challenge involving an increasing number of material scientists.

The increased interest in multifunctional materials and structures is driven by the need for the development of new materials and structures that simultaneously perform multiple structural functions, combined non-structural and structural functions, or both. Multifunctional materials are necessarily composite materials, and the strong growth in the use of composites has been greatly influenced by multifunctional design requirements. Until now, the traditional approach to the development of structures is to address the load-carrying function and other functional requirements separately, resulting in a suboptimal load-bearing structure with add-on attachments which perform the non-structural functions with the penalty of added weight. Recently, however, there has been increased interest in the development of load-bearing materials and structures which have integral non-load-bearing functions, guided by recent discoveries about nanofillers and nanotechnology that can help to project materials working as multifunctional systems.

In the last decades the use of composite in the primary structures in the aeronautics is rapidly increased. As previously mentioned, the most representative example is the Boeing 787 Dreamliner built with more than 50% of composites. Unfortunately, the epoxy resin between the carbon fiber layers which constitute the composite can burn under accidental aircraft fire conditions. in the flame condition. Successful strategies to reduce the flammability of structural materials are extremely important in the field of aeronautic and aerospace applications.

On the other hand, some modern aircrafts are made of advanced composites which are significantly less conductive than aluminum. Then, the composites

are reinforced with conductive metal fibres or metal screens in order to dissipate lightning currents. But many of these solutions add additional weight and reduces composite advantage.

In sum, the aeronautic composites hitherto developed suffer of limitations, as far as the properties of flame resistance and electrical conductivity are concerned. The object of the invention “Guadagno *et al.* (2013i)” is thus to overcome such limitations of the prior art.

Such object is attained by an epoxy resin having a limiting oxygen index (LOI) measured according to standard ASTM 2863, which is at least 28%.

The resins of the invention “Guadagno *et al.* (2013i)” are able to increase flame resistance and their use in several industrial processes allows to produce a new generation of composites able to perform multiple functions and, in addition, also the single functions. In particular, the resins of the invention can be developed with the following aims:

1) to apply a resin resistant to the flame and thermal degradation in aeronautics, aerospace, automotive, nautical and infrastructural applications; other applications in aircraft manufacture are in the production of cabin walls, overhead bins, galleys and lavatories, among other interior parts.

2) to apply a resin resistant to the flame and thermal degradation able to simultaneously overcome some of the drawbacks related to the insulating properties of the resin used to manufacture carbon fiber reinforced composites (CFRC). Such material is applicable in aeronautics, aerospace, automotive, nautical and infrastructural applications.

According to a first embodiment of the invention “Guadagno *et al.* (2013i)”, the epoxy resin is obtainable by curing an epoxy precursor formulation with an hardening agent which is an organophosphine oxide of general formula  $R_3PO$ , wherein at least two R moieties are amino-phenyl and one R moiety is alkyl, phenyl or amino-phenyl, wherein each phenyl ring may have independently one or more electrophile substituents.

Preferably, according to the invention, the ratio by weight between said epoxy precursor formulation and said hardening agent is in the range 40% to 100%, and more preferably 60% to 100%.

The hardening agent may preferably be Bis(3-aminophenyl)phenyl phosphine oxide (BAPPO), Bis(3-aminophenyl)methyl phosphine oxide (BAMPO), Tri(3-aminophenyl)phenyl phosphine oxide (TAPPO) or a mixture thereof.

Further advantageous hardening agents are (alkyl-bis-amino-aryl)phosphine oxide or tri-amino-arylphosphine oxide, having one or more than one electron withdrawing agents as substituents on the aryl groups, as indicated in the following compounds 1 to 6 of Figure IX.1.

## Multifunctional epoxy resin with enhanced flame resistance

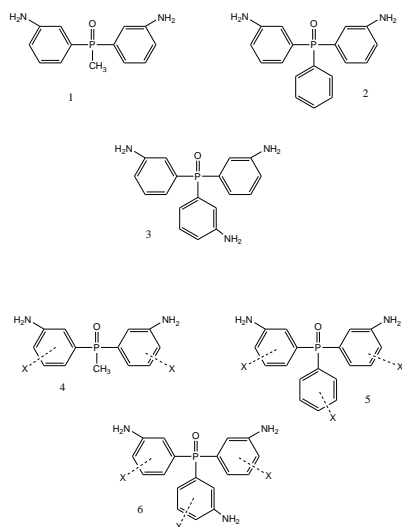


**Figure IX.1** Hardening agents

It is also possible using such hardening agents in combination with hardening agents which are not organophosphine compounds, such as the conventional 4,4'-diaminodiphenyl sulfone (DDS) or any other.

Bis(3-aminophenyl) phenyl phosphine oxide (BAPPO) (3) is well-known and may e.g. be synthesized via a two-step route. Firstly, the bis(3-nitrophenyl) phenyl phosphine oxide (2) is obtained as an intermediate by reacting compound (1) with nitric acid/sulfuric acid. Then BAPPO is obtained by reduction of the intermediate (2) by means of hydrazine monohydrate. In sum, a possible synthesis route may be represented as follows (see Figure IX.2):

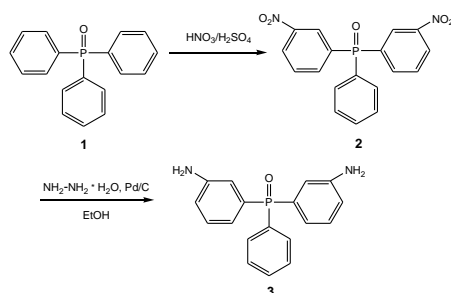


**Figure IX.2** Scheme of synthesis of bis(3-aminophenyl) phenyl phosphine oxide (BAPPO) 3

Bis(3-aminophenyl) methyl phosphine oxide (BAMPO) (4) is well-known and may e.g. be synthesized through a process involving the following synthesis route (see Figure IX.3):

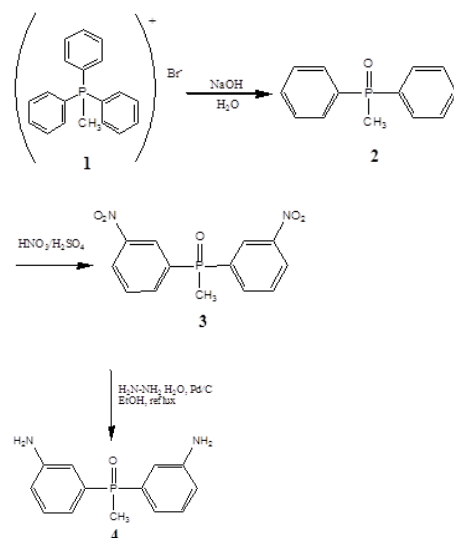


**Figure IX.3** Scheme of synthesis of bis(3-aminophenyl) methyl phosphine oxide (BAMPO) 4

Electrophilic aromatic substitution on BAMPO, BAPPO and TAPPO by electron withdrawing groups on aryl amine rings produces the organophosphine oxides 4, 5 and 6 of Figure IX.1 (where X=NO<sub>2</sub>, Cl, Br, CN, RCO). Any formulation known in the art may be used as epoxy precursor formulation: e.g. such formulation may contain tetrafunctional epoxy precursors and flexibilizer and/or reactive diluents.

Advantageously, a resin of the invention “Guadagno et al. (2013i)” further incorporates conductive nanofillers, such as carbon nanotubes, e.g. functionalized and unfunctionalized SWCNTs, DWCNTs, MWCNTs, untreated and heat treated carbon nanofibers, carbon black, functionalized and unfunctionalized exfoliated graphite and graphene layers, whereby the insulating properties of the epoxy resin are changed and the latter becomes multifunctional.

It is demonstrate that the use of an organophosphine oxide as hardening agent or the incorporation of a POSS compound allows to obtain epoxy resins with flame retardants properties, which are improved in respect of the conventional resins “Guadagno et al. (2013i)”.

The invention “Guadagno et al. (2013i)” embraces also the above-mentioned epoxy resins further containing conductive nanofillers embedded inside the respective matrix, which resins are in particular suitable for application in the aeronautic field “Guadagno et al. (2013i)”.

## IX.2 Synthesis of new hardener agents

Flame retardation of epoxy resins can be achieved using fire-resistant curing agents. At this purpose two flame retardant have been synthesized: the Bis (3-aminophenyl) phenylphosphine oxide (BAPPO) and the Bis (3-aminophenyl) methylphosphine oxide (BAMPO) and used as hardener agents. Dissolution methods to solubilize these hardeners in the epoxy matrix have been evaluated and optimized in order to obtain a new epoxy formulation with improved fire properties. This chapter also concerned the chemical-physical characterization of the new formulations and the evaluation of the fire properties and more specifically of their limited oxygen index and the heat release rate.

A phosphorus-containing diamine compound, bis(3-aminophenyl)phenyl phosphine oxide (BAPPO), was synthesized for its use as curing agent of epoxy resins. The synthesis was performed using a two-step route procedure with the preparation of bis(3-nitrophenyl) phenyl phosphine oxide as intermediate "Liu *et al* (1997)". Then BAPPO was obtained by reduction of the intermediate by means of hydrazine monohydrate following the procedure suggested by "Zhuang (1998)" with slight modifications. The obtained compounds were recognized and characterized using the Magnetic resonance.  $^1\text{H}$ ,  $^{13}\text{C}$ ,  $^{31}\text{P}$  NMR spectra of the synthesized compounds confirmed the obtained structures.

### IX.2.1 Materials

#### Solvents

- Chloroform (Sigma Aldrich) stabilized with ethanol
- Ethanol (Sigma Aldrich, absolute).
- Deuterated Dimethyl Sulfoxide (DMSO-d<sub>6</sub>)

#### Reagents

- Hydrazine Monohydrate (Sigma Aldrich) 64-65 %, reagent grade+ 98%  $\rho=1.032$  [g/cm<sup>3</sup>]
- Nitric Acid (Carlo Erba) 69.5%  $\rho=1.413$  [g/cm<sup>3</sup>]
- Sulphuric Acid (Sigma Aldrich) 95-97%  $\rho=1.84$  [g/cm<sup>3</sup>]
- Palladium on Activated Carbon (Pd/C) (Fluka, Pd 10%, +C)
- Triphenyl phosphine oxide (Sigma Aldrich)

### IX.2.2 Characterization

Proton, Carbon  $^{13}$  and Phosphorous  $^{31}$  Nuclear Magnetic Resonance ( $^1\text{H}$ ,  $^{13}\text{C}$  and  $^{31}\text{P}$  NMR) to check the structure of the compounds were used. Samples were dissolved in deuterated solvents DMSO-d<sub>6</sub>. NMR spectra were

obtained on a Bruker Spectrometer Avance 400.  $^1\text{H}$  and  $^{13}\text{C}$  NMR spectra were referred to tetramethylsilane (TMS) and  $^{31}\text{P}$  NMR spectra were referred to  $\text{H}_3\text{PO}_4$ .

### IX.2.3 Synthesis procedure of BAPPO

BAPPO **3** was synthesized via a two-step route (see Figure IX.2) .

*1<sup>st</sup> step: Preparation of bis(3-nitrophenyl) phenyl phosphine oxide 2*

Triphenyl phosphine oxide **1** (5 g, 0.018 mol) was charged into a 250 ml two necked round bottom flask equipped with a magnetic stirrer and a reflux condenser, then 36 ml of sulphuric acid were added. In a salt/ice bath was placed a two necked round bottom flask containing nitric acid (2.61g), and sulfuric acid (18 ml) was introduced drop-wise. The amount of nitric acid that is required must be carefully controlled in order to obtain a high yield of the dinitro compound. The acid mixture was then transferred into the addition funnel and it was added drop-wise to the reaction mixture over a period of 2 hours, taking care to keep the temperature in a range of  $[-5;0]^\circ\text{C}$ , then it was left to room temperature overnight. After this time, the reaction mixture was poured in a beaker containing ice, obtaining a fluorescent yellow precipitate. After the ice melted, the mixture was extracted with chloroform and washed with a sodium bicarbonate aqueous solution until neutral pH. The solvent was removed under vacuum obtaining a viscous residuum, then EtOH was added. This caused the obtainment of a precipitate. The soluble fraction was recovered from the mixture and the solvent was removed under vacuum. A white powder was obtained, which became green when dissolved in deuterated DMSO- $d_6$ .

$^1\text{H}$ ,  $^{13}\text{C}$ ,  $^{31}\text{P}$  NMR spectra confirmed the structure of **2** shown in figure IX.4 (see Figures IX.5 and IX.6). The yield was 60%.

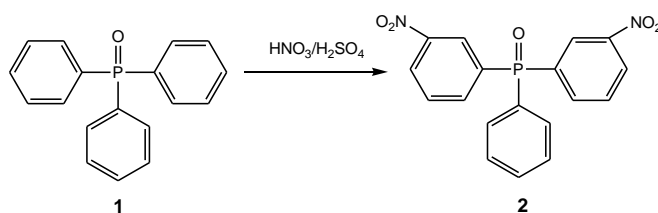


**Figure IX.4** Scheme of synthesis of bis (3-nitro phenyl) phenyl phosphine oxide 2

$^1\text{H}$  NMR (400 MHz, DMSO- $d_6$ , ppm):  $\delta$ : 8.50-8.48 (2H), 8.43-8.40(2H); 8.15-8.10(2H), 7.90-7.85 (2H), 7.76-7.70 (3H), 7.64-7.59 (2H);  $^{31}\text{P}$  NMR (161.97 MHz, DMSO- $d_6$ , ppm) shown a single peak (28.7 ppm);  $^{13}\text{C}$ (100 MHz, DMSO- $d_6$ , ppm):147.8, 137.6; 134.4, 133.1; 131.5, 131, 129.2, 127.2; 126.0;

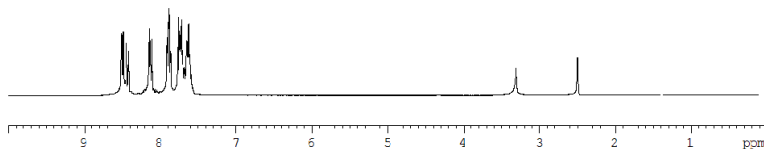


**Figure IX.5**  $^1\text{H}$  spectrum of bis(3-nitrophenyl) phenyl phosphine oxide 2 in DMSO- $d_6$

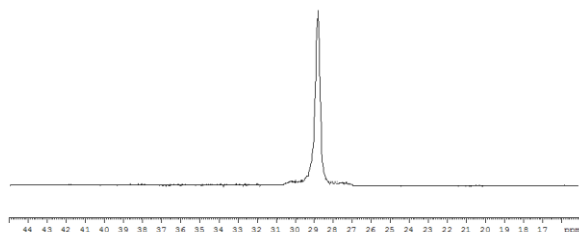


**Figure IX.6**  $^{31}\text{P}$  spectrum of bis(3-nitrophenyl) phenyl phosphine oxide 2 in DMSO- $d_6$

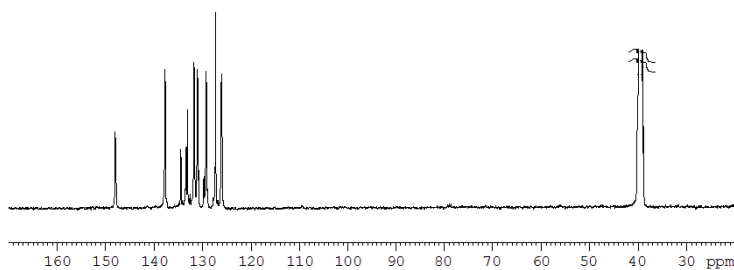


**Figure IX.7**  $^{13}\text{C}$  spectrum of bis(3-nitrophenyl) phenyl phosphine oxide 2 in DMSO- $d_6$

2<sup>o</sup>step: Preparation of bis(3-aminophenyl) phenyl phosphine oxide 3 (BAPPO)

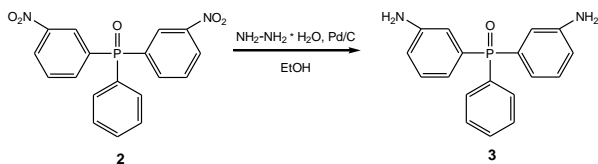


**Figure IX.8** Scheme of synthesis bis(3-aminophenyl)phenyl phosphine oxide 3 (BAPPO)



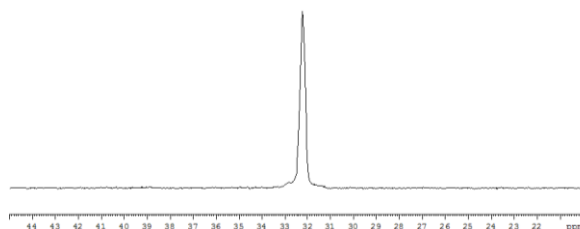


**Figure IX.10**  $^{31}\text{P}$  spectrum of bis(3-aminophenyl)phenyl phosphine oxide 3 (BAPPO) in DMSO-d<sub>6</sub>

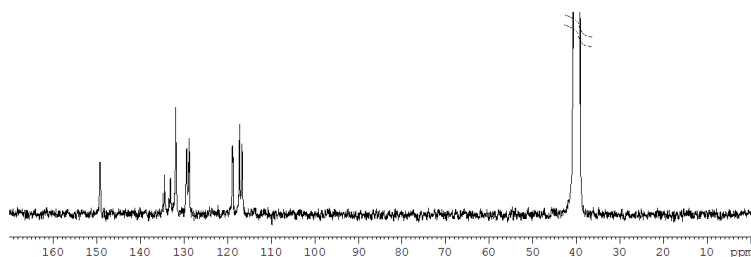


**Figure IX.11**  $^{13}\text{C}$  spectrum of bis(3-aminophenyl)phenyl phosphine oxide 3 (BAPPO) in DMSO-d<sub>6</sub>

#### **IX.2.4 Synthesis procedure of BAMPO**

##### *Solvents*

- Chloroform (Sigma Aldrich) stabilized with ethanol
- Ethanol (Sigma Aldrich, absolute).
- Methanol (Fisher Scientific)
- Deuterated Dimethyl Sulfoxide (DMSO-d<sub>6</sub>)

##### *Reagents*

- Hydrazine Monohydrate (Sigma Aldrich) 64-65 %, reagent grade+ 98%  $\rho=1.032$  [g/cm<sup>3</sup>]
- Methyltriphenylphosphonium Bromide (Sigma Aldrich) 98%
- Nitric Acid (Carlo Erba) 69.5%  $\rho=1.413$  [g/cm<sup>3</sup>]
- Sulphuric Acid (Sigma Aldrich) 95-97%  $\rho=1.84$  [g/cm<sup>3</sup>]
- Palladium on Activated Carbon (Pd/C) (Fluka, Pd 10%, +C)
- Sodium Hydroxide (Sigma Aldrich), pellets

*Characterization*

Proton, Carbon 13 and Phosphorous 31 Nuclear Magnetic Resonance ( $^1\text{H}$ ,  $^{13}\text{C}$  and  $^{31}\text{P}$ ) were used to check the structure of the compound. Samples (about 10 mg) were dissolved in deuterated solvents DMSO- $d_6$ . NMR spectra were recorder on a Bruker AVANCE 400 operating at 400 MHz for  $^1\text{H}$ . The  $^1\text{H}$  and  $^{13}\text{C}$  NMR chemical shifts are referenced to tetramethylsilane ( $\text{SiMe}_4$ ) at 0 ppm and  $^{31}\text{P}$  NMR spectra were referenced using  $\text{H}_3\text{PO}_4$  at 0 ppm as an external standard. Spectra are reported as follows: chemical shift ( $\delta$  ppm), multiplicity, coupling constant (Hz), and integration. Multiplicities were abbreviated as follows: singlet (s), doublet (d), triplet (t), quartet (q), multiplet (m), and broad (br).

**Synthesis**

Bis(3-aminophenyl) methyl phosphine oxide **4** (BAMPO) was synthesized through four sequential steps “Liu *et al* (1997)” (see Figure IX.3).

*1<sup>o</sup> step: preparation of biphenyl methyl phosphine oxide (2)*

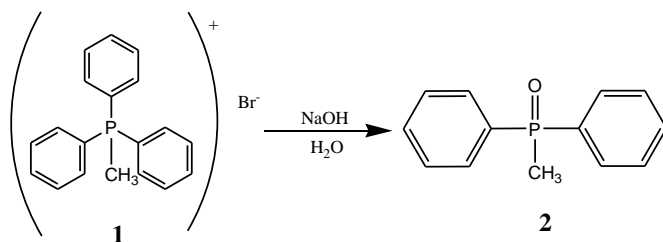


**Figure IX.12** Scheme of synthesis of biphenyl methyl phosphine oxide (2)

Methyltriphenylphosphonium bromide (10 g, 0.028 mol ) was charged to a 250 ml two necked round bottom flask, equipped with a reflux condenser and a magnetic stirrer. Water (50 ml) was then added and the mixture was heated to reflux until the starting material was dissolved (about 30 minutes). Meanwhile sodium hydroxide (5.6 g, 0.14 mol) was dissolved in 50 ml of water in a beaker and then transferred to the mixture and further refluxed for two hours. After the addition of sodium hydroxide solution a slightly yellow organic layer was observed on the top of the mixture. The completion of the reaction was monitored by TLC (chloroform: methanol\_ 9:1). The product was extracted with chloroform and then washed several times with water, dried over a night on magnesium sulfate and chloroform was removed under vacuum, obtaining 5 g of a white powder. The yield was of 82%.

The product structure was checked by NMR spectra:  $^1\text{H}$  NMR (400 MHz, DMSO- $d_6$ ,ppm): d 7.77-7.73 (4H), 7.66-7.55 (6H), 2.02 (d,3H) (Figure IX.13);  $^{31}\text{P}$  NMR (161.97 MHz, DMSO- $d_6$ , ppm) shown a single peak (32.8) (Figure IX.14);  $^{13}\text{C}$  (100 MHz, DMSO- $d_6$ ,ppm): d : 135.6-134.7 (d, $J(\text{C},\text{P})$ ), 131.4 (s), 130.1(s), 128.5 (s), 16.2-15.5 (d, $J(\text{C},\text{P})$ ) (Figure IX.15).

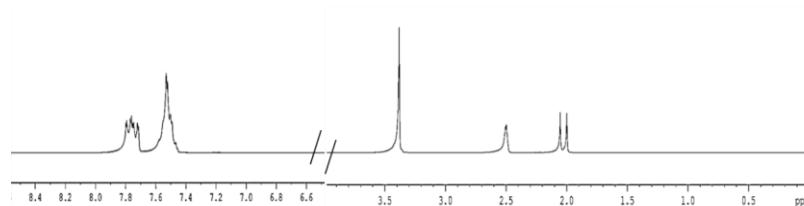


**Figure IX.13**  $^1\text{H}$  spectrum of biphenyl methyl phosphine oxide (2) in  $\text{DMSO-}d_6$

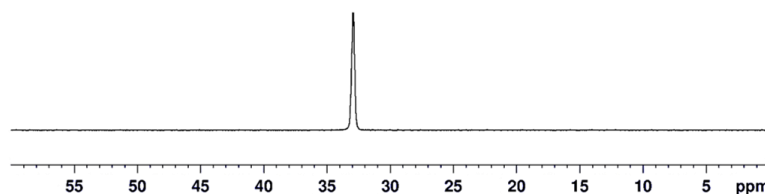


**Figure IX.14**  $^{31}\text{P}$  spectrum of biphenyl methyl phosphine oxide (2) in  $\text{DMSO-}d_6$

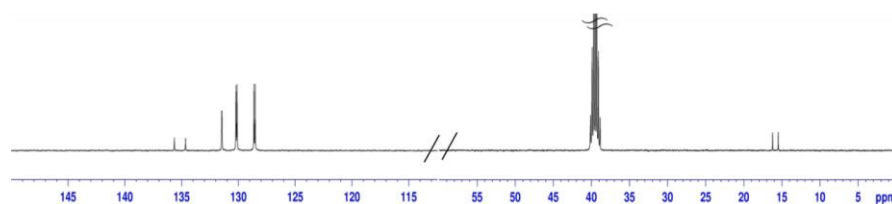


**Figure IX.15**  $^{13}\text{C}$  spectrum of biphenyl methyl phosphine oxide (2) in  $\text{DMSO-}d_6$

*2<sup>o</sup>step Preparation of binitro phenyl methyl phosphine oxide (3)- Nitration*

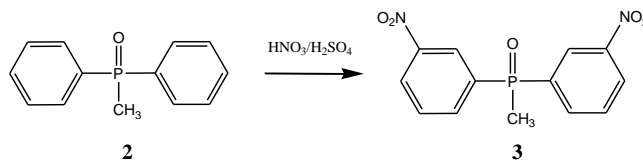


**Figure IX.16** Scheme of synthesis of binitro phenyl methyl phosphine oxide (3)

The biphenyl methyl phosphine oxide **2** (5 g, 0.023 mol) was charged into a 100 ml two necked round bottom flask equipped with a magnetic stirrer, a

reflux condenser and an addition funnel. The flask was placed in an ice bath and concentrated sulfuric acid (14.6 ml) was introduced drop-wise. The mixture was stirred until the starting material dissolved. In a separate ice bath was placed a two necked round bottom flask containing nitric acid (4.31g), and sulfuric acid (9.8 ml) was introduced drop-wise. The total amount of sulfuric acid was ten times than of nitric acid by weight, which in turn was 5% excess of the stoichiometric amount. The acid mixture was then transferred into the additional funnel and it was added drop-wise to the reaction mixture, which start to become slight yellow. The reaction was allowed to continue for two hours taking care to keep temperature into a range of 0-5°C, then it was left to room temperature for another 3 hours. After this time the reaction mixture was poured in a beaker containing ice, obtaining a fluorescent yellow precipitate, which was filtered and washed with water. Ethanol was added to the washed product and then evaporated under vacuum. The obtained powder appeared white, but when it was dissolved in DMSO-d<sub>6</sub> it became green. In the <sup>1</sup>H NMR spectrum all signals related to the product **3** were found, but not all the water was removed. In order to eliminate water, the product **3** was again dissolved in ethanol and dried over magnesium sulfate, but the <sup>1</sup>H NMR shown the presence of impurity; the product was then dissolved in dichloromethane and filtered, but it was not possible obtain the clear product. The synthesis was repeated in the same condition as reported above and the crude product after filtration and washing with water was heated at 35°C. Warming did caramelize the product, so it was necessary to wash it with ethanol: the solvent was evaporated under vacuum regaining a white product, but still containing water. However, it was decided to use the product for the next step. The yield was 85%.

<sup>1</sup>H NMR (400 MHz, DMSO-d<sub>6</sub>, ppm): δ: 8.62-8.59 (2H), 8.47-8.39(2H);8.34-8.19 (2H), 7.87-7.82 (2H), 2,50-2.28 (d, 3H), (Figure IX.17); <sup>31</sup>P NMR (161.97 MHz, DMSO-d<sub>6</sub>, ppm) shown a single peak (32.28 ppm) (Figure IX.18); <sup>13</sup>C(400 MHz, DMSO-d<sub>6</sub>, ppm): d:147.8 (s) 137.1-135.8 (d, J(C,P)) ; 136.6 (s), 130.7 (s), 126,7 (s), 124,9 (s), 15.71-14.73 (d,J(C,P)) (Figure IX.19)

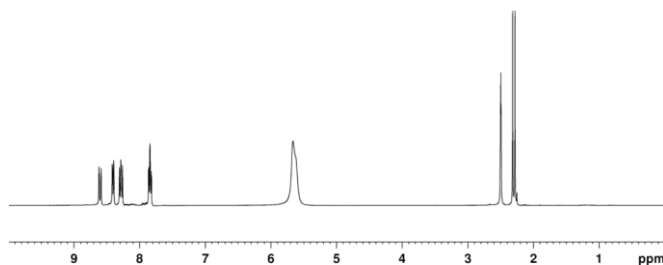


**Figure IX.17** <sup>1</sup>H spectrum of binitro phenyl methyl phosphine oxide (**3**) in DMSO-d<sub>6</sub>

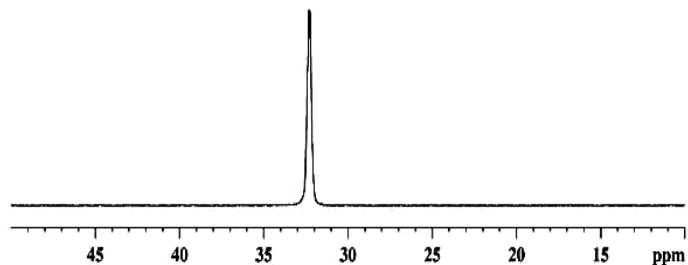


**Figure IX.18**  $^{31}\text{P}$  spectrum of binitro phenyl methyl phosphine oxide (**3**) in  $\text{DMSO-d}_6$

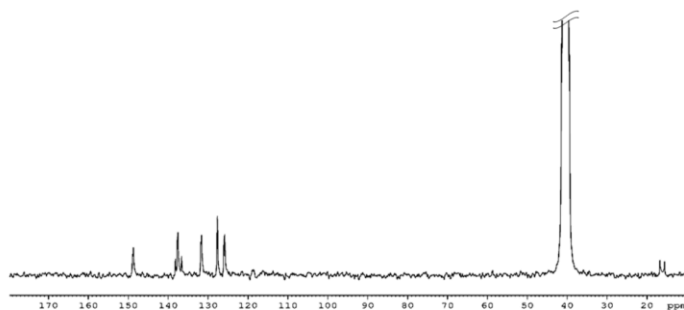


**Figure IX.19**  $^{13}\text{C}$  spectrum of binitro phenyl methyl phosphine oxide (**3**) in  $\text{DMSO-d}_6$

*3<sup>o</sup>step: Preparation of bis(3-aminophenyl)methyl phosphine oxide (**4**) BAMPO*

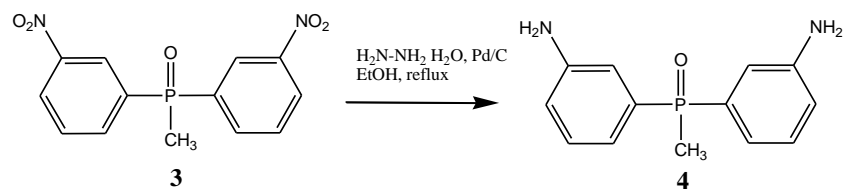


**Figure IX.20** Scheme of synthesis of bis(3-aminophenyl)methyl phosphine oxide

Bis(3-nitrophenyl) methyl phosphine oxide **3** (6.09 g, 0.0198 mole) was charged in a three-necked round bottom flask, equipped with an overhead stirrer, an addition funnel and a reflux condenser, and 61 mL of absolute ethanol was added, heating the mixture at 50 °C until the starting material dissolved (~30 minutes). The mixture was purged with nitrogen. A small

amounts of catalyst Pd/C (0.0345 g) was added and hydrazine monohydrate (10.35 g, 0.207 mol) was added dropwise from the addition funnel. This reaction step did not require heating since the reaction is exothermic. During the evolution of the reaction were observed several changing in the color of the mixture. From dark green to yellow to black, furthermore the evolution of gas from the mixture denoted that the reaction was occurring. When the reaction slowed down as indicated by a slowing of gas evolution, a second portion of Pd/C (0.0345 g) was added and the reaction was heated to reflux for one hour, the completion of the reduction was determined by  $^1\text{H}$  spectra. After then discoloring activated carbon (0.1 g) was added to the mixture and the reaction was left to reflux for an hour. The black solution was then cooled and filtered through celite on a filter funnel with drip-tip. A yellow solution was obtained; the solvent was evaporated under vacuum and the product 4 was obtained with a yield of 72%. During the synthesis of BAMPO, several attempts were made changing the amount of catalysts in order to obtain a solid. High temperature-time treatment were used, but a high viscous residue was obtained, which was insoluble in the majority of solvents; an equi-volume hexane-benzene mixture was added to this residue but it was not possible to separate the desired product. Separation on silica gel using a mixture of chloroform and methanol (9:1) was successful, but gave very low yields (lower than 35% of recovered product). The best solution was found in adding chloroform to the red oily liquid residue. The red oil solution was not soluble in chloroform, whereas solvent resulted yellow. A separator funnel was used and the solution was filtered several times. Solvent was then evaporated under vacuum, with a yield of 65%.

$^1\text{H}$ ,  $^{31}\text{P}$ , and  $^{13}\text{C}$  spectra of bis(3-aminophenyl) methyl phosphine oxide are reported in Figure IX.21, Figure IX.22, and Figure IX.23 respectively.

$^1\text{H}$  NMR (400 MHz, DMSO- $d_6$ , ppm): d: 7.13-7.06 (2H); 6.89-6.64 (6H) 5.3 (s, 4H), 1.79(d, 3H) (Figure IX.21) ;

$^{31}\text{P}$  NMR (161.97 MHz, DMSO- $d_6$ , ppm) shown a single peak (33.6 ppm) (Figure IX.22);

$^{13}\text{C}$  100 MHz, DMSO- $d_6$ , ppm): d :148.7-148.6 (d, $J(\text{C},\text{P})$ )129.1-128.9-117.01-116.4, 115.1-115.0, 16.3,15.6 (d,  $J(\text{C},\text{P})$ ) (Figure IX.23)

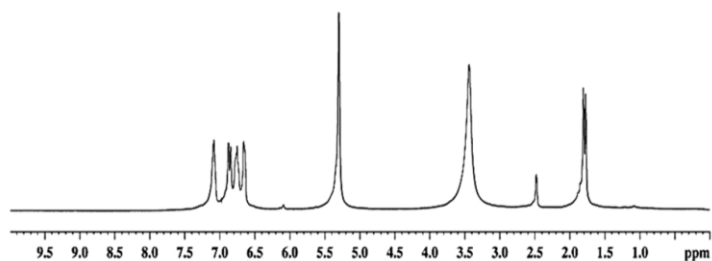


**Figure IX.21**  $^1\text{H}$  spectrum of bis(3-aminophenyl)methyl phosphine oxide (4) BAMPO in DMSO- $d_6$

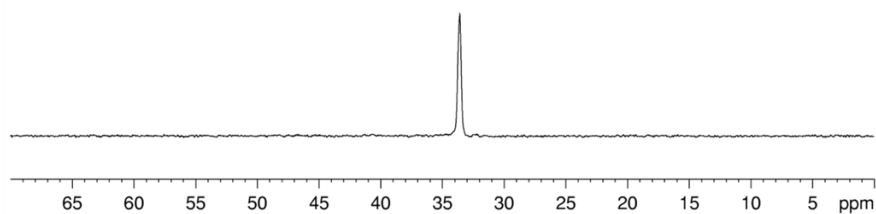


**Figure IX.22**  $^{31}\text{P}$  spectrum of bis(3-aminophenyl)methyl phosphine oxide (4) BAMPO in DMSO- $d_6$

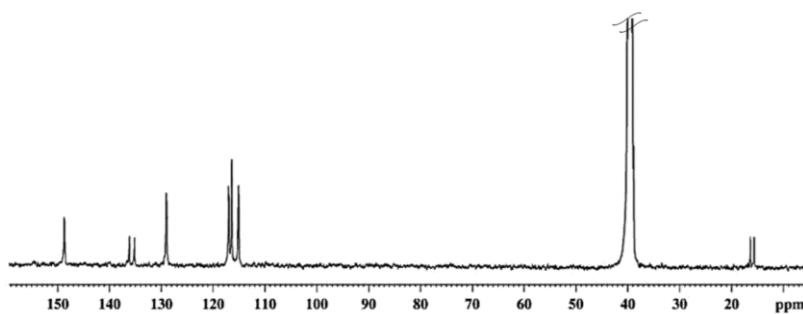


**Figure IX.23**  $^{13}\text{C}$  spectrum of bis(3-aminophenyl)methyl phosphine oxide (4) BAMPO

### IX.3 Thermal and oxidative degradation of BAPPO and BAMPO

Thermal degradation both in air and in nitrogen of the samples BAMPO and BAPPO, depicted in Figure IX.24, shows that BAPPO is more stable toward thermal oxidative destruction than BAMPO. The oxidative stability

enhancement is of about 240°C; in fact, for sample BAPPO the beginning of the degradation occurs at about 340°C with respect to the temperature of 100°C corresponding to BAMPO. The presence of *phenyl group attached to the double bond P=O* most likely determines an increase of the thermal stability of BAPPO with respect to that observed for BAMPO. First derivative TGA curves (in air and nitrogen) of BAMPO and BAPPO, shown in Figure IX.25, highlight some stages of degradation that in the TGA curves are not readily seen. In this regard in air a four-step and a three-step thermal degradation processes can be observed for BAMPO and BAPPO respectively, in nitrogen instead a three-step for BAMPO and a single-step for BAPPO thermal degradation processes can be observed. TGA in air of BAMPO sample (see graphic on the left in Figure IX.24 ) shows that at the end of the third stage at about 400°C a weight loss of 55% was recorded. For both compounds BAMPO and BAPPO, the first stages of degradation are most probably due to degradation processes which do not involve oxygen (dehydration, random scission etc), whereas the last steps are strongly dependent on the oxygen availability. This hypothesis is supported by the different trend of the thermogravimetric curves in inert (N<sub>2</sub>) atmosphere (see graphic on the right in Figure IX.24).

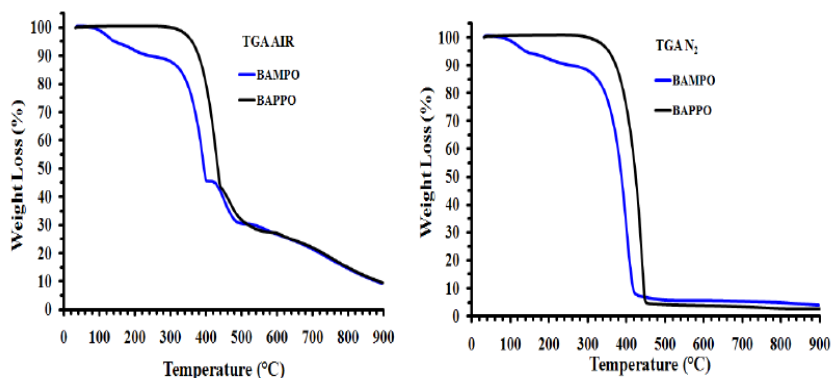


**Figure IX.24** TGA curves of BAMPO and BAPPO

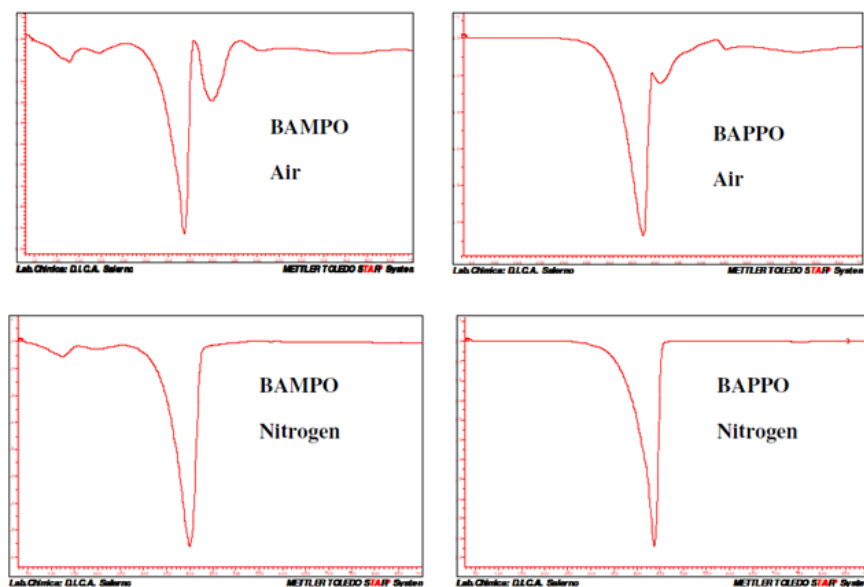


**Figure IX.25** First derivative TGA curves (in air and nitrogen) of BAMPO and BAPPO

Chemical structure of the synthesized organophosphorus compounds was characterized by FTIR spectroscopy.

FTIR spectra of BAMPO and BAPPO are depicted in Figure IX.26. The formation of aromatic primary amine groups in these molecules is confirmed by IR absorption peaks in the range of values of about  $3462\text{--}3220\text{ cm}^{-1}$  (N-H stretching vibration). Other peaks at  $1172$  and  $1157\text{ cm}^{-1}$  (P=O group in the BAPPO and BAMPO spectra respectively) and  $1437$  and  $1442\text{ cm}^{-1}$  (P-Ph group in the BAPPO and BAMPO spectra respectively) confirm the presence of phosphine oxide moiety in these compounds.

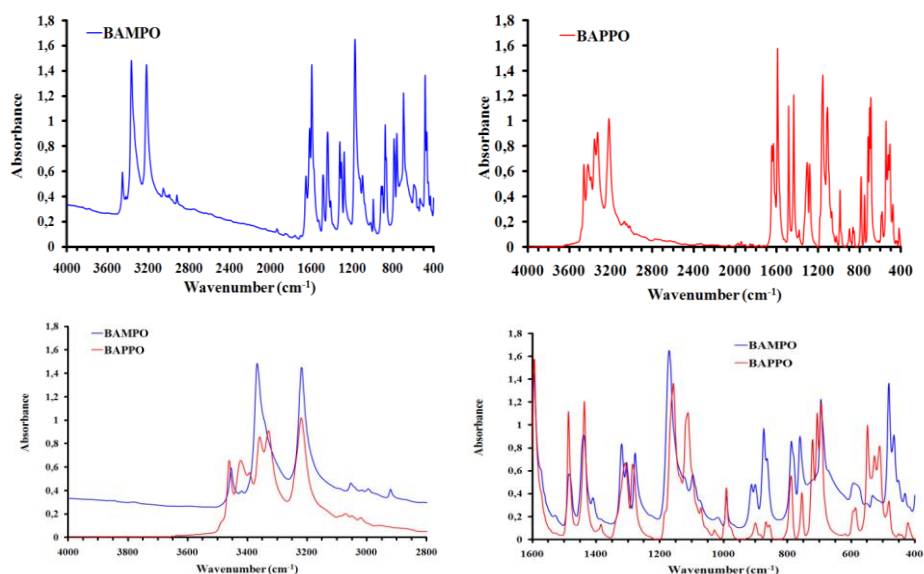


**Figure IX.26** FTIR spectra of BAMPO and BAPPO

#### IX.4 Dissolution of BAMPO and BAPPO in epoxy matrix

A preliminary dynamic thermogravimetric analysis (TGA) test was performed to be sure that no thermal degradation of components occurs during the tests. This analysis showed that the beginning of the thermal decomposition for TGMDA occurred at 300°C (if no curing agent is added) (see the following Figure IX.27) - therefore, bath oil temperature was set to 70°C and 80°C for these tests. As we will see later in this report, the same temperature was chosen also for the dissolution tests of POSS in the same matrix.

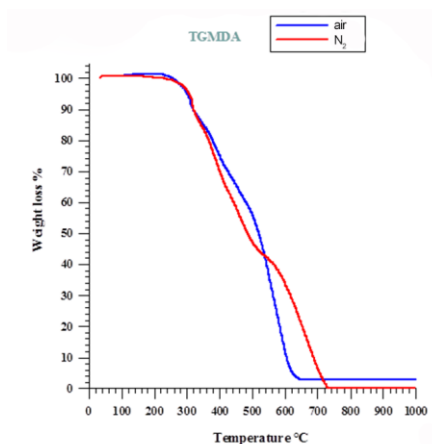


**Figure IX.27** Thermogravimetric analysis of TGMDA

### ***Dissolution of BAMPO in epoxy matrix***

#### ***Solubility test – BAMPO in TGMDA+BDE at 70°C***

Bampo and Bappo were used in stoichiometric amount with respect to epoxy rings (epoxy rings of epoxy precursors + epoxy rings of reactive diluent).

In order to facilitate the dissolution in the epoxy mixture, the two synthesized organophosphorus molecules have been previously finely pulverized by mechanical stirring for several hours with a stirring speed of about 450 rpm. The pulverized molecules were held under vacuum for 3 hours in order to remove moisture before being inserted in the epoxy mixture. Figure IX.28 shows finally pulverized BAMPO.



**Figure IX.28** Finely pulverized BAMPO

The dissolution of BAMPO inside the epoxy blend was carried out through mechanical agitation using a magnetic stirrer (400 rpm) in an heated oil bath (70°C) for about 2 hours. After 2 hours, the mixture appeared to be fluid, caramel-colored and BAMPO particles were not visible to the naked eye. In

Figure IX.29 we can see the mixture poured into molds used for the fire testing that have been pre-heated to preserve its fluidity. Before the beginning of the curing process, the mixture was degassed at 45°C for about 15 minutes. In Figure IX.30 we can see the tested BAMPO based epoxy samples after the curing process, before (see image on the left) and after (see image on the right) extraction from the molds.



**Figure IX.29** BAMPO based uncured epoxy mixture poured into molds used for fire testing

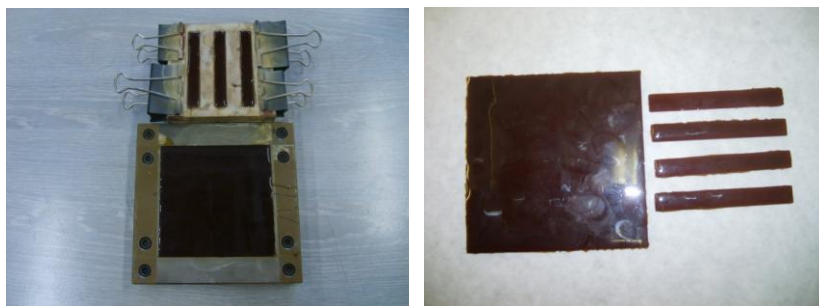


**Figure IX.30** Tested BAMPO based epoxy samples after the curing process, before (see image on the left) and after (see image on the right) extraction from the molds

It is worth noting that different temperatures (120, 100, 90, 80°C) and different times of dissolution were tested. In all these cases the epoxy mixture became very viscous and partially cross-linked, thus preventing the solubilisation of BAMPO. In Figure IX.31 we can see the cross-linked BAMPO based epoxy sample after mechanical agitation in oil bath at 120°C for 5 minutes.



**Figure IX.31** *Cross-linked BAMPO based epoxy sample at 120°C*

***Dissolution of BAPPO in epoxy matrix***

***Solubility test – BAPPO in TGMDA+BDE at 80°C***

The dissolution of BAPPO in the epoxy blend was carried out through mechanical agitation using a magnetic stirrer (400 rpm) in an heated oil bath (80°C) for about 3 hours. After 2 hours, the mixture showed a creamy consistency and had a light brown color. Several particle aggregates and lumps of BAPPO molecules are detectable. However, it was possible to avoid the formation of aggregates by slowly adding pulverized BAPPO particles in the epoxy mixture which was mechanically stirred (400 rpm) in an heated oil bath at a higher temperature (95°C) for about 3 hours. In this way, we obtained a homogeneous dispersion of the BAPPO particles in the epoxy mixture. It is worth noting that the solubility test performed at 120°C in an oil bath resulted in the crystallization and partial crosslinking of the BAPPO in the mixture after 1H. Before the beginning of the curing process, the mixture was degassed at 55°C for about 15 minutes. In Figure IX.32 we can see the tested epoxy samples containing BAPPO particle aggregates and lumps (solubilized in an oil bath at 80°C for 3H) after extraction from the molds subsequently to the curing process.



**Figure IX.32** *Tested epoxy samples containing BAPPO particle aggregates and lumps*

Figure IX.33 shows the tested epoxy sample containing BAPPO particles (solubilized in an oil bath at 95°C for 3H) homogeneously dispersed after extraction from the molds subsequently to the curing process .



**Figure IX.33** Tested epoxy sample containing BAPPO particles homogeneously dispersed

## **IX.5 Evaluation of the BAPPO and BAMPO as hardeners for improving fire properties**

### ***IX.5.1 Materials***

The epoxy matrix T20B was prepared, as previously already said, by mixing an epoxy precursor, tetraglycidyl methylene dianiline (TGMDA) (*Epoxy equivalent weight 117-133 g/eq*), with an epoxy reactive monomer 1-4 Butanediol diglycidyl ether (BDE) at a concentration of 80%: 20% (by wt) respectively.

*The curing agents* used for the curing were BAMPO or BAPPO. These hardener agents were added at a stoichiometric concentration with respect to all the epoxy rings (TGMDA and BDE).

TGMDA, BDE were obtained from Sigma-Aldrich, while Bampo and Bappo were synthesized with the experimental procedures before described.

### ***IX.5.2 Sample preparation***

Epoxy blends and BAMPO were mixed by magnetic stirring at 70°C (the mixing temperature is strongly recommended). The degassing of the mixture is recommended at 45°C.

Epoxy blends and BAPPO were mixed by magnetic stirring at 95°C (the mixing temperature is strongly recommended). The degassing of the mixture is recommended at 55°C.

As above already reported, all the mixtures were cured by a two-stage curing cycles: a first isothermal stage was carried out at the lower temperature of 125°C for 1 hour and the second isothermal stage at higher temperatures up to 200°C for 3 hours.

### IX.5.3 Characterizations

Fire resistance of the solidified epoxy samples was characterized by limiting oxygen index measurement (LOI) and mass loss calorimetry.

Experimental conditions for LOI tests: barrels of 80x10x3 mm<sup>3</sup> are fixed in a vertical position and their top is inflamed with a burner. LOI, the minimum concentration of oxygen in a nitrogen/oxygen mixture required to just support the sample combustion, was measured following standard ASTM 2863.

Experimental conditions for Mass loss calorimeter: plates of 100x100x3 mm<sup>3</sup> are exposed to a radiant cone (50kW/m<sup>2</sup>) using a forced ignition. The heat of combustion released was measured using a thermopile according to standard ISO 13927.

Thermogravimetric analysis (TGA) was carried out with a Mettler TGA/SDTA 851 thermobalance. Resin samples were heated from 25°C to 900°C at a 10°C/min heating rate under air and nitrogen flow. The weight loss was recorded as a function of temperature. Thermal and oxidative degradation of BAMPO and BAPPO based composites was evaluated (see Figure IX.34)

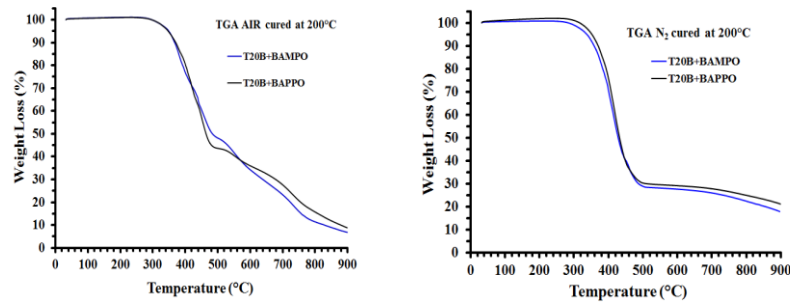


**Figure IX.34** TGA curves of BAMPO and BAPPO based composites

The thermal degradation begins at about 320°C for BAMPO and BAPPO based composites. In nitrogen the resin filled with BAPPO curing agent shows a slight increase in the thermal stability.

**Table IX.1** LOI and PHRR of the T20B formulation cured with BAMPO and BAPPO

Sample	LOI(%O <sub>2</sub> )	PHRR (kW/m <sup>2</sup> )
T20BD	27	540
T20B/BAMPO	40	447
T20B/BAPPO	36	379

Data shown in Table IX.1 demonstrated that BAMPO and BAPPO hardeners are more efficient than DDS to increase epoxy system LOI. The PHRR of the epoxy system decrease when BAMPO or BAPPO are used in comparison to DDS. Moreover, Figure IX.35 shows that BAMPO and BAPPO lead to important intumescence of the systems when compared to DDS based system.



**Figure IX.35** Char aspect of T20B systems with different hardeners

CNTs embedded inside the epoxy matrix to increase electrical conductivity do not lead to the formation of intumescent charring (see Figure IX.36 ) (on the contrary the presence of the nanotubes seems to favour some densification of the char), not improve PHRR of the epoxy system because CNTs could act as heat conductors, CNTs however exhibit an interesting potential to improve LOI of epoxy systems at low amount of CNTs, as you can see in Table IX.2.

The last three samples refer to resins with conductive nanofillers embedded inside the respective matrix and the sample according to the invention (line 6 in Table IX.2.) shows an improvement in the PHRR - namely a decrease of this value – with respect to nanofilled samples hardened with DDS (lines 4 and 5 in Table IX.2). It has to be noticed that a low concentration of CNTs (0.5wt%) is advisable to reach the electrical percolation threshold.

**Table IX.2** LOI and PHRR values of the epoxy samples

Sample	LOI(%O <sub>2</sub> )	PHRR (kW/m <sup>2</sup> )
T20BD	27	540
T20B/BAMPO	40	447
T20B/BAPPO	36	379
T20BD+0.5%CNT(3100)	28	603
T20BD+1%CNT(3100)	28	629
T20B+BAMPO+0.5%CNT(3100)	38	561

**Figure IX.36** Char aspect of T20BD+CNTs composites

HEG embedded inside the epoxy matrix to increase electrical conductivity not improve PHRR and LOI of the epoxy system because exfoliated graphite could act as heat conductors (see Table IX.3).

In Table IX.3 it is evident that in nanofilled composites when GPOSS is used as flame retardant the LOI parameter is high (30 with respect to 25 of the same resin containing only HEG and 27 that is already the highest value found for epoxy matrices in aeronautics) and the PHRR exhibits a significant decrease with respect to 882 of the nanofilled sample without GPOSS.

Another important aspect is that in the GPOSS-based epoxy composites the inclusion of the HEG (as well as of CNT3100) determines a significant increase in the time of ignition (80s with respect to 64s of the nanofilled sample without GPOSS).

We have obtained an efficient flame-retardant composite because it provide low value of PHRR/Tig, allowing a decrease of the fire growth rate.

**Table IX.3** LOI and PHRR values of the epoxy samples

Sample	LOI(%O <sub>2</sub> )	PHRR (kW/m <sup>2</sup> )	Tig (s)
T20BD	27	540	40
T20BD+ 5%GPOSS	33	327	42
T20BD+ 1.8%HEG	25	882	64
T20BD+5%GPOSS+1.8%HEG	30	560	80

DMA analysis was performed on TA instruments DMA2980 under the following conditions:

- Dual cantilever mode to avoid sample sliding,
- Temperature scan from 25°C to 320°C at 3°C/min,
- amplitude: 18µm,
- Frequency: 1Hz,
- Preload force: 0.01N,
- Specimen dimensions: 50mmx10mmx3mm

Table IX.4 indicates the maximum of temperature of the main mechanical transition T<sub>m</sub> associated to the glass transition temperature of the epoxy samples. BAPPO and BAMPO hardeners lead to a decrease of the epoxy network glass transition with respect to the DDS, but such decrease does not hinder the use of the respective resins as structural materials.

**Table IX.4** Maximum of temperature of the main mechanical transition T<sub>m</sub> associated to the glass transition temperature of the epoxy systems

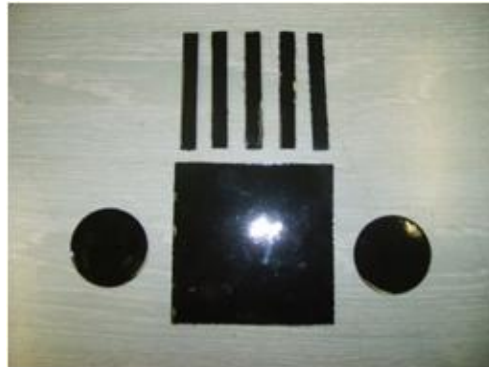
Sample	DMA-T <sub>g</sub> (°C)
T20BD	270
T20B+BAMPO	218
T20B+BAPPO	227
T20BD+ 0.5%CNT(3100)	258
T20BD+ 1%CNT(3100)	263
T20BD+ 5%DPHPOSS+0.5%CNT(3100)	258
T20BD+ 5%GPOSS+ 0.5%CNT(3100)	261
T20BD+ 5%GPOSS+ 0.5%PR25XTPS2500	272
T20BD+ 5%GPOSS+ 1.8%HEG	260
T20BD+ 5%GPOSS+ 1%CNT(3100)	261
T20BD+ 5%DPHPOSS+ 1%CNT(3100)	264
T20BD+ BAMPO+ 0.5%CNT(3100)	222
T20BD+ BAPPO(ns)+ 0.5%CNT(3100)	212

Table IX.5 containing DC conductivities data of nanofilled epoxy resin samples proves that nanofilled samples of the invention [1] have multifunctional properties, i.e. both of fire resistance and electrical conductivity. In particular, the GPOSS-based epoxy resins nanofilled with exfoliated graphite (HEG) and heat-treated at 2500°C carbon nanofibers (PR25XTPS2500) provide the best combination of mechanical and electrical properties.

**Table IX.5** DC conductivities data of nanofilled epoxy resin samples

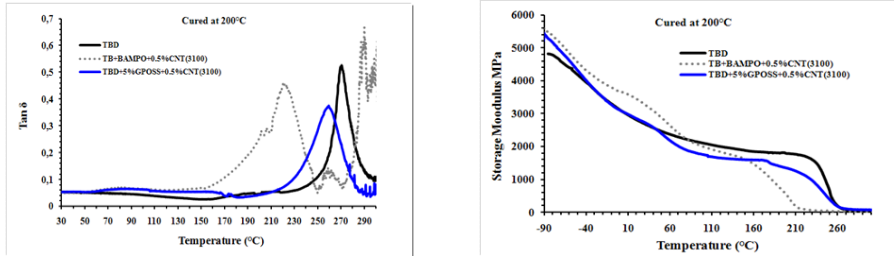
Sample	Conductivity values (S/m)
T20BD	8.00E-13
T20B+BAMPO+0.5%CNT(3100)	1.68E-1
T20B+BAPPO(n.s)+0.5%CNT(3100)	1.10E-1
T20BD+5%GPOSS+0.5%CNT(3100)	3.54E-3
T20BD+5%GPOSS+0.5%PR25XTPS2500	1.35E-1
T20BD + 5%GPOSS+ 1.8%HEG	1.33

Figure IX.37 shows photos of multifunctional tested samples.



**Figure IX.37** Photo of multifunctional tested samples

Dynamic mechanical analysis performed on BAMPO and GPOSS-based multifunctional composites show high values of the glass transition temperature (see graphic on the left of Figure IX.38), we can also observe a value in the storage modulus higher than 2000 MPa up to 80°C for all the samples. At -55°C the multifunctional composites show a value in the storage modulus higher than 4400 MPa which is the value of the unfilled epoxy resin (see graphic on the right of Figure IX.38). In sum the multifunctional composites meet the process requirements that make them suitable for structural applications in the aeronautical field.



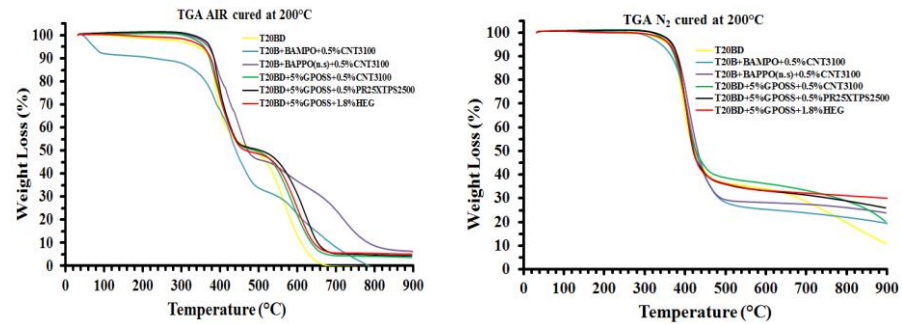
**Figure IX.38** Loss factor ( $\tan\delta$ ) and storage modulus (Mpa) of the unfilled epoxy mixture and its multifunctional resins

Table IX.6 contains LOI and PHRR values of the multifunctional composites. In particular, we can observe that the GPOSS-based epoxy resin nanofilled with CNT(3100) shows the lowest value of PHRR. It is worth noting that a reduction of pHRR means that the fire spread over the entire area is slowed down. Instead BAPPO-based nanofilled epoxy resin shows the highest value of PHRR most likely due to a poor dispersion of the CNTs in the polymer matrix.

**Table IX.6** LOI and PHRR values of the multifunctional composites

Sample	LOI (%O <sub>2</sub> )	PHRR (kW/m <sup>2</sup> )
T20BD	27	540
T20B+BAPPO(ns)+0.5%CNT(3100)	30.2	753
T20BD+5%GPOSS+0.5%CNT(3100)	30	293
T20BD+5%GPOSS+0.5%PR25XTPS2500	29	506
T20BD+5%GPOSS+1.8%HEG	30	560

In TGA curves of multifunctional composites (see graphics in Figure IX.39) we show a general stabilizing effect in the multifunctional composites in the first stage of the thermal degradation with respect to unfilled resin T20BD. The T20BD+BAMPO+0.5%CNT3100 sample instead shows in air a weight loss of about 10% in the temperature range between 40-100°C. The same sample appears in nitrogen thermally stable up to about 300°C.



**Figure IX.39** TGA curves of multifunctional composites

## IX.6 Conclusions

BAMPO and BAPPO have been synthesized and used as curing agent for the epoxy system based on the TGMDA. The obtained formulations have been characterized and the fire properties have been studied. The results show that these new synthesized phosphorus based hardeners are more efficient than DDS to increase epoxy system LOI. The PHRR of the epoxy system decrease when BAMPO or BAPPO are used in comparison to DDS. BAMPO and BAPPO lead to important intumescence of the systems when compared to DDS based system. The nanofilled samples of the invention “Guadagno *et al.* (2013i)” have multifunctional properties, i.e. both of fire resistance and electrical conductivity. In sum the multifunctional composites meet the process requirements that make them suitable for structural applications in the aeronautical field.

---

## Chapter X

---

# Development of Multifunctional Carbon Fiber Reinforced Composites (CFRCs) - Manufacturing Process

### X.1 Preface

The work reported in this chapter describes a successful attempt toward the development of CFRCs based on nanofilled epoxy resins. The epoxy matrix was prepared by mixing a tetrafunctional epoxy precursor with a reactive diluent which allows to reduce the viscosity of the initial epoxy precursor and facilitate the nanofiller dispersion step. As nanofiller, multiwall carbon nanotubes (MWCNTs) were embedded in the epoxy matrix with the aim of improving the electrical properties of the resin used to manufacture CFRCs. Panels were manufactured by *Resin Film Infusion* (RFI) using a non-usual technique to infuse a nano-filled resin into a carbon fiber dry preform.

### X.2 General remarks

In recent years the use of fiber reinforced resin composites has continuously expanded, particularly in weight-sensitive materials, such as aircraft and space vehicles. The bring into play of epoxy-based thermosetting composite materials to the *aircraft industry* was driven by the increase in performance and most of all by weight reduction. However, composites exhibit some rather poor inherent characteristics, such as low electrical, thermal and mechanical properties. A simple solution is to modify matrix molecular structure or add compatible conductive fillers that eventually improve the resulting composite system. In order to choose an effective epoxy mixture, it is necessary to consider that the structure of the resin strongly governs its chemical and some of the physical properties. The number of reactive sites in the epoxy precursors controls the functionality directly acting on the cross-linking density. This, combined with the nature of hardener agent, the

functionality, the stoichiometry and the curing cycle determines the final properties of the cured resin especially in terms of mechanical and thermal properties. Conversely, some of the physical properties, such as electrical conductivity can be quite improved by embedding very small amount of conductive nanoparticles “Guadagno *et al.* (2011a); De Vivo *et al.* (2012b); Guadagno *et al.* (2013d)”. The use of conductive nanofillers inside of polymeric matrices to enhance electrical properties seems to be a very useful strategy to increase the performance of the composite. Nanofilled resins made of conductive nanostructured forms of carbon show significant increases in their electrical conductivity even at low nanofiller concentrations. MWCNTs offer very promising results; however, some criticalities are related to the processing methods employed to manufacture CFRCs. Economic and efficient means of producing high performance fibre-reinforced composites, containing nanofiller embedded in the resin which impregnates CFs, are critically limited by the initial viscosity of epoxy precursors. In this paper, we show the first results on the process manufacturing of an aeronautic formulation “Guadagno *et al.* (2013g); Guadagno *et al.* (2013i)” obtained by blending the epoxy precursor with a reactive modifier that acts as regulator of viscosity for a best dispersion of nanoparticles embedded in the resin used to manufacture CFRCs.

### **X.3 Materials**

The preparation of the epoxy matrix was reported in the experimental section of the chapter II.

The MWCNTs (3100 Grade), added and incorporated into the matrix by using an ultrasonication for 20 min, were obtained from Nanocyl S.A.

Epoxy resin was filled with MWCNTs at 0.5% concentration w/w%. This concentration was chosen because the curves of dc volume conductivity vs. CNTs concentration highlighted that the electrical percolation threshold (EPT) is lower than 0.3 %.

### **X.4 CFRCs –Manufacturing Process**

CFRCs were manufactured by *Resin Film Infusion* (RFI) using a non-usual technique to infuse a nano-filled resin into a carbon fiber dry preform “Hussain *et al.* (2006)”. This new technique allows to overcome drawbacks related to no optimal values in the viscosity for a RFI process and is therefore particularly advantageous for nanofilled resins where the presence of nanofillers increases the viscosity values hindering the injection of the nanofilled epoxy formulation. A well-known process for the manufacturing of high performance resin-based composite materials is the resin film infusion. In this process, a dry carbon fiber preform is placed in a vacuum bag and the resin is injected from an edge of preform while in the other is

vent the vacuum so the resin flow through the length of the preform. The scheme can be seen in Figure X.1.

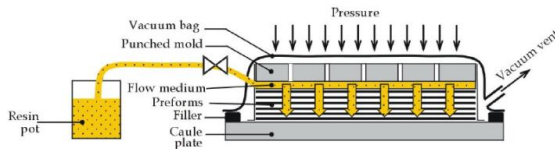


**Figure X.1** Scheme of Liquid resin infusion technique

Optimum value of viscosity required for this process is lower than 0.3 Pa s. In literature is possible to find a theoretical maximum limit of 0.8 Pa s “Becker, (no data)”. Often a nanofilled resin exceeds the limit of 0.8 Pa s; then the usual liquid infusion becomes unfeasible.

To overcome this critical point, a thin layer of liquid epoxy mixture containing MWCNTs (0.5%wt) was spread on a release films (*Release Ease 234 TFP-HP Airtech*); then a dry preform (400mm x 400mm ) made laminating 7 plies of carbon fiber cloths (SIGMATEX (UK) LDT 193GSM (*grams square meter*) /PW (*plain wave*) /HTA40 E13 3K(3000 fibres each tow) ) was placed on mixture forcing it to flow through the thickness of the preform using an external supplementary pressure inside an autoclave. In this way the length of the impregnation path is considerably reduced and the process can be forced by means of the pressure application. A further advantage of this technology is due to the smaller length of the infiltration path which reduces the effects of infiltration through the preform. In fact, the edges of the preform were sealed to force the resin to only flow through the thickness (see Figure X.2A). The laminate was covered by a porous release film and a distribution media to allow to the resin to escape from the upper side and a breather media to receive the excesses of the resin (see Figure X. 2B). Finally it was made a vacuum bag and the laminate was putted into the autoclave (see Figure X.2C).



**Figure X.2** Steps of laminate preparation

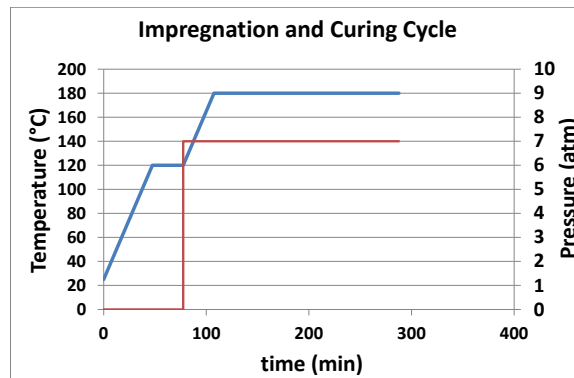
## X.5 Results and discussion

Table X.1 shows the values of the viscosity  $\eta^*$  (Pa s) at three different temperatures.

**Table X.1** Values of the viscosity  $\eta^*$  (Pa s) at three different temperatures

Temperature (°C)	$\eta^*$ (Pa s)
90	1.43
120	0.68
140	0.59

Data shown in Table X.1 highlight that the usual liquid infusion process could be applied only for infusion temperature higher than 120°C. These high values of temperature would increase the costs and difficulties. The technic above described allows to overcome these criticalities. Impregnation conditions and curing cycle of CFRC panels is shown in Figure X.3.



**Figure X.3** Impregnation and curing cycle

A picture of the manufactured panels is shown in Figure X.4. All the manufactured panels show a volume fiber fraction calculated  $V_f$  between 0.55 and 0.56.



**Figure X.4** *Manufactured panel*

### **X.6 Morphological investigation**

Strips of panels were observed by an optical microscope along the section to evaluate the infiltration effects and eventually the presence of voids. The samples were encapsulated into a special resin and observed by means of a metallographic optical microscope LEICA DM RXE. Figure X.5 shows the methodology used to analyze the sections of the manufactured panels.



**Figure X.5** *Sections of the manufactured panels*

The bottom side of panel 1100X is shown in Figure X.6A, whereas Figure X.6B shows the upper side of the panel 2745X which was in contact with the release film and the distribution media.

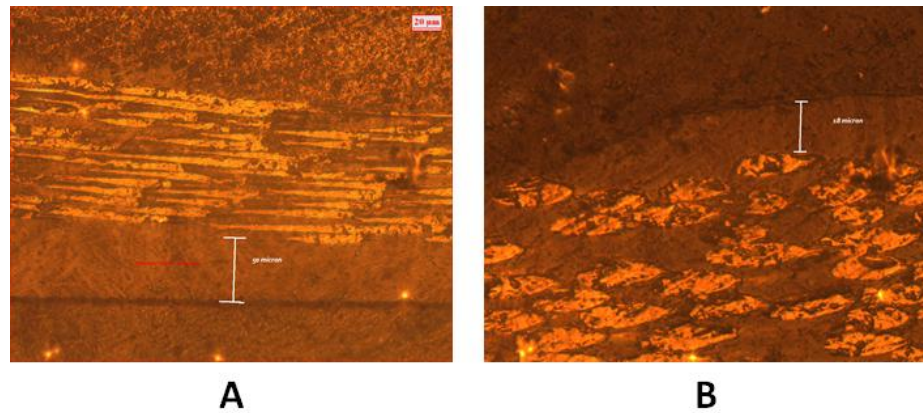


**Figure X.6** *Optical images of the section of the manufactured panels*

The optical micrographs show the absence of voids and inhomogeneities.

### **X.7 Conclusions**

In this chapter we have shown the first results obtained using a new technique to manufacture CFRCs “Guadagno *et al.* (2013m)”. This technique is particularly advantageous to impregnate CFs with aeronautic resins filled with conductive nanofillers. In particular, the impregnation can be obtained also using an epoxy mixture characterized by viscosity values higher than 0.3 Pa s.

---

# General conclusions

---

Detailed conclusions are drawn at the end of any chapter containing experimental results. In this section only the general conclusions are described.

- An epoxy mixture based on a tetrafunctional epoxy precursor (TGMDA) and the reactive diluent (BDE) tailored to meet specific needs of aeronautical materials has been formulated, prepared and characterized.
- The results on the physical properties of unfilled and nanofilled samples are very promising. In particular, the use of reactive diluent in the initial epoxy precursors as proven to be of benefit for many aspects: a) it reduces the moisture content (see results of chapter II), b) it eases the step of nanofiller dispersion (due to the decrease in the viscosity value), as it can be seen in the chapters IV and V, c) it allows to reach higher curing degree compared to the epoxy precursor alone (see results of the chapter II).
- Several conductive nanostructured forms of carbon were embedded inside the epoxy matrix to enhance electrical and, if possible, also mechanical properties. Nanocomposites filled with nanofiber-shaped forms (MWCNTs and untreated and heat-treated CNFs) and bidimensional shaped nanofillers (exfoliated graphite) were prepared and characterized. The electrical percolation curves filled with these different nanofillers show that beyond the EPT the dc conductivity is almost the same for all the analyzed nanofillers (see results shown in the chapters II, III, VI). On the contrary, the concentration range where the EPT is observed is very different for each nanofiller and it is strongly dependent on the morphology and then on the preparation procedure of the filler. For example, in the case of exfoliated graphite, a small increase in the exfoliation degree, caused by slightly changing the preparation procedure, determines a strong

## General conclusions

---

decrease in the EPT range, and then very positively also affects the analysed mechanical properties.

- BAMPO and BAPPO have been synthesized and used as curing agent for the formulated epoxy matrix. The results show that these new synthesized phosphorus based hardeners are more efficient than DDS to increase epoxy system LOI. The PHRR of the epoxy system decrease when BAMPO or BAPPO are used in comparison to DDS. BAMPO and BAPPO lead to important intumescence of the systems when compared to DDS based system (see results shown in the chapter IX).
- The incorporation of 5% by weight of POSS compounds into the epoxy resins is beneficial for improving its flame retardancy. The structure of POSS plays an important role on the dissolution/dispersion of these compounds into the matrix (see results shown in the chapter VIII).
- Multifunctional epoxy resins characterized by improved flame resistance incorporating conductive nanofillers were formulated. Dc conductivity (S/m) values of the multifunctional resins range between  $3.5 \times 10^{-3}$  and 1.33. LOI (% O<sub>2</sub>) values range between 30.2 and 29 and PHRR (kW/m<sup>2</sup>) range between 293 and 753. These results are shown in the chapter IX. The nanofilled samples behave as multifunctional systems.
- One of the most promising systems (a multifunctional system capable of bearing mechanical loads) was used to manufacture a first multifunctional panel (CFRCs) (see results shown in the chapter X).

---

## References

---

- Abdala A., Adamson D. H., McAllister M. J., Milius D.L., Herrera-Alonso M., “Research: Thermally exfoliated graphite oxide: An alternative to CNTs”, 2006 Princeton University, Ceramic Materials Laboratory.
- Al-Saleh M H and U. Sundararaj (2009) A review of vapor grown carbon nanofiber/polymer conductive composites. *Carbon*, **47**(1), 2-22.
- Andrews R. and MC. Weisenberger. (2004) Carbon nanotubes polymer composites. *Current Opinion in Solid State and Materials Science*, **8**(1), 31-37.
- Bai J B.( 2003) Evidence of the reinforcement role of chemical vapour deposition multiwalled carbon nanotubes in a polymer matrix. *Carbon*, **41**(6), 1325-1328.
- Balberg I., Anderson CH., Alexander S., Wagner N. (1984) Excluded volume and its relation to the onset of percolation. *Phys. Rev. B*, **30**(7),3933-3943.
- Bauhofer W. and JZ. Kovacs (2009) A review and analysis of electrical percolation in carbon nanotube polymer composites. *Compos Sci Technol*, **69**(10), 1486-1498.
- Baur J. and E. Silverman (2007) Challenges and opportunities in multifunctional nanocomposite structures for aerospace applications. *MRS Bulletin*, **32**(4), 328-334.
- Becker DW. Tooling for Resin Transfer Moulding, Wichita State University, Wichita Kansas, no data.
- Bhagat S. and P. K. Verma (2013) Effect of Graphite Filler on Mechanical Behavior of Epoxy Composites. *International Journal of Emerging Technology and Advanced Engineering*, **3**(2),427-430.

## References

---

- Birman V and LW. Byrd (2007) Modeling and analysis of functionally graded materials and structures. *Appl Mech Rev*; **60**, 195-216.
- Breuer O and U Sundararaj (2004) Big returns from small fibers: A review of polymer/carbon nanotube composites. *Polymer Composites*, **25**(6), 630-645.
- Burton D., Lake P., Palmer A. (2011) Properties and Applications of Carbon Nanofibers (CNFs) Synthesized using Vapor-grown Carbon Fiber (VGCF) Manufacturing Technology (Cedarville, OH: Applied Sciences)
- Cadek M., Coleman J N., Ryan K P., Nicolosi V., Bister G. et al. (2003) Reinforcement of polymers with carbon nanotubes: the role of nanotube surface area. *Nano Letters.*, **4**(2), 353-356.
- Chatterjee A. (2009) Thermal Degradation Analysis of Thermoset Resins. *J. Appl. Polym. Sci.*, 114(3), 1417-1425.
- Chiu Y.C., Ma C.C.M., Liu F.Y., Chou I.C., Chiang C.L., Yang J.C. (2009) Thermal degradation and flammability of P/Si Polysilsesquioxane epoxy nanocomposites. *J. Appl. Polym. Sci.*, 114(3), 1435-1443.
- Chou T-W., Gao L., Thostenson E T., Zhang Z., Byun J-H. (2010) An assessment of the science and technology of carbon nanotube composites. *Compos Sci Technol*, 70(1), 1-19.
- Chung D.D.L. (2001) Electromagnetic interference shielding effectiveness of carbon materials. *Carbon*, 39, 279–285.
- Coleman JN., Khan U., Gun'ko YK. (2006) Mechanical reinforcement of polymers using carbon nanotubes. *Adv Mater.*, 18(6):689–706.
- Coleman JN., Khan U., Blau WJ., Gun'ko YK. (2006) Small but strong: a review of the mechanical properties of carbon nanotube-polymer composites. *Carbon*, 44(9), 1624–1652.
- Connor MT., Roy S., Ezquerra TA., Balta-Calleja FJ. (1998) Broadband AC conductivity of conductor-polymer composites. *Phys Rev B*, 57(4):2286-2294.
- Debelak B. and K. Lafdi. (2007) Use of exfoliated graphite filler to enhance polymer physical properties. *Carbon*, 45(9), 1727-1734.
- Devaux E., Rochery M., Bourbigot S. (2002) Polyurethane/clay and polyurethane/POSS nanocomposites as flame retarded coating for polyester and cotton fabrics. *Fire Mater.*, 26(4-5), 149-154.
- De Vivo B., Guadagno L., Lamberti P., Raimo R., Sarto MS. et al. Electromagnetic properties of Carbon NanoTube/epoxy nanocomposites. Extended abstracts, IEEE Conference Proceeding, International Symposium

- 
- on Electromagnetic Compatibility - EMC Europe 2009, Athens (Greece), 11-12 June 2009; p.1-4, DOI 10.1109/EMCEUROPE.2009.5189674.
- De Vivo B., Lamberti P., Tucci V., Guadagno L., Vertuccio L., Vittoria V., Sorrentino A. (2012) Comparison of the Physical Properties of Epoxy-Based Composites Filled with Different Types of Carbon Nanotubes for Aeronautic Applications. *Adv Polym Tech*, 31(3), 205–218.
  - De Vivo B. et al (2012) Electrical properties of multi-walled carbon nanotube/tetrafunctional epoxy-amine composites. *AIP Conference Proceedings*, 1459 (1), 199-201.
  - Du F., Fischer JE., Winey KI. (2005) Effect of nanotube alignment on percolation conductivity in carbon nanotube/polymer composites. *Phys. Rev. B*; 72(12), 121404(R) [4 pages].
  - Durga G., Singh D., Kukreja P., Narula A.K. (2009) Synthesis, characterization, curing and thermal studies of phosphorylated epoxy resins. *Indian J. Eng. Mat. Sci.*, 16(2), 133-139.
  - Dyre JC. (1988) The random free- energy barrier model for ac conduction in disordered solids. *J Appl Phys*; 64(5), 2456-2468.
  - Dyre JC. and TB.Schrøder (2000)Universality of ac conduction in disordered solids. *Rev. Mod. Phys.*, 72(3), 873-892.
  - Edwards GD. and QY. Ng. (1968) Elution behavior of model compounds in gel permeation chromatography. *Journal Polymer Science: Part C*, 21, 105–117.
  - Eitan A., Jiang K., Dukes D., Andrews R., Schadler L. (2003) Surface modification of multiwalled carbon nanotubes: toward the tailoring of the interface in polymer composite. *Chem. Mater.*, 15(16), 3198-3201.
  - Eken AE., Tozzi EJ., Klingenberg DJ., Bauhofer W. (2011) A simulation study on the combined effects of nanotube shape and shear flow on the electrical percolation thresholds of carbon nanotube/polymer composites. *Journal of Applied Physics*, 109(8), 084342-9.
  - Eloundou J P. (2002) Dipolar relaxations in an epoxy–amine system. *European Polymer Journal*, 38(3), 431–438.
  - Endo M., Kim YA., Hayashi T., Yanagisawa T., Muramatsu H. et al. (2003). Microstructural changes induced in “stacked cup” carbon nanofibers by heat treatment. *Carbon*, 41(10), 1941- 1947.
  - Endo M. et al (2001) Vapor-grown carbon fibers (VGCFs) basic properties and their battery applications. *Carbon*, 39(9), 1287-1297.
  - Endo M., Koyama T., Hishiyama Y. (1976) Structural improvement of carbon fibers prepared from benzene. *Japan. J. Appl. Phys.*, 15, 2073-2076.

## References

---

- Franchini E., Galy J., Gérard J.F., Tabuani D., Medici A. (2009) Influence of POSS structure on the fire retardant properties of epoxy hybrid networks. *Polym. Deg. And Stab.*, 94, 1728-1736.
- Ganguli S., Roy A. K., Anderson D. P. (2008) Improved thermal conductivity for chemically functionalized exfoliated graphite/epoxy composites. *Carbon*, 46(5), 806–817.
- Gerard C., Fontaine G., Bellayer S., Bourbigot S. (2012) Reaction to fire of an intumescent epoxy resin: Protection mechanisms and synergy. *Polym. Deg. Stab.*, 97, 1366-1386.
- Gibson RF., Ayorinde EO., Wen Y-F. (2007) Vibrations of carbon nanotubes and their composites: a review. *Compos Sci Technol*; 67(1), 1-28.
- Gojny Florian H., Wichmann Malte H.G., Fiedler B., Schulte K. (2005) Influence of different carbon nanotubes on the mechanical properties of epoxy matrix composites – A comparative study. *Composites Science and Technology* , 65(15–16), 2300–2313.
- Grassie N. and M.I. Guy (1986) Degradation of epoxy polymers: Part 4 – Thermal Degradation of Bisphenol-A Diglycidyl Ether cured with Ethylene Diamine. *Polymer degradation and stability*, 14(2), 125-137.
- Guadagno L., De Vivo B., Di Bartolomeo A., Lamberti P., Sorrentino A., Tucci V., Vertuccio L., Vittoria V. (2011) Effect of functionalization on the thermo-mechanical and electrical behaviour of multi-wall carbon nanotube/epoxy composites. *Carbon*, 49(6), 1919-1930.
- Guadagno L., Vertuccio L., Sorrentino A., Raimondo M., Naddeo C. et al. (2009) Mechanical and barrier properties of epoxy resin filled with multi-walled carbon nanotubes. *Carbon*, 47(10), 2419-2430.
- Guadagno L., Naddeo C., Vittoria V., Sorrentino A., Vertuccio L., Raimondo M. et al. (2010) Cure Behavior and Physical Properties of Epoxy Resin Filled with Multiwalled Carbon Nanotubes. *Journal of Nanoscience and Nanotechnology*, 10(4), 2686-2693.
- Guadagno L., Raimondo M., Vittoria V., Lafdi K., De Vivo B. et al. (2013) The Role of the carbon nanofiber defects on the electrical and mechanical properties of CNF-based resins. *Nanotechnology*, 24(30), 305704 (10pp).
- Guadagno L., Raimondo M., Vittoria V., Lafdi K., De Vivo B. et al. Role of The Carbon Nanofiber Defects On The Electrical Properties of CNF-Based Composites. *ACMA 2012, International Symposium on Aircraft Materials*. May 09-12, 2012 Fez, Morocco (Editors: A. Menou, M. Karama, A. Moudden, A. Benejedou, A. Saouab, El Ham; ISBN:9782953480429)

- 
- Guadagno L., Raimondo M., Vertuccio L., Naddeo C., Vittoria V., De Vivo B., Lamberti P., Spinelli G., Tucci V. Electrical, and dynamic mechanical properties of MWCNTs/epoxy composite for high performance aerospace applications. ECCM 15 – 15th European Conference on Composite Materials. June 24-28, 2012 Venice-Italy - ISBN:9788888785332
  - Guadagno L., Raimondo M., Vittoria V., Vertuccio L., Naddeo C., Lamberti P., Tucci V. Italian Patent Resina epossidica con basso tenore di umidità. Filing number: TO2013A000926 Filing date: 15.11.2013.
  - Guadagno L., Raimondo M., Longo P., Bonnaud L., Murariu O., Dubois Ph. Italian Patent Resina epossidica multifunzionale con accresciuta resistenza alla fiamma. Filing number: TO2013A001021 Filing date: 13.12.2013
  - Guadagno L., Raimondo M., Vittoria V., Vertuccio L., Naddeo C., Russo S. et al. Development of epoxy mixtures for application in aeronautics and aerospace. RCS Advances (submitted).
  - Guadagno L., Raimondo M., Lafdi K., Fierro A., Rosolia S., Nobile M.R. Influence of Nanofiller Morphology on the Viscoelastic Properties of CNF/Epoxy Resins. 7th International Conference on Times of Polymers (TOP) and composites. June 22-26, 2014, Ischia (Italy) (submitted paper).
  - Guadagno L., Raimondo M., Vittoria V., Vertuccio L., Lafdi K., De Vivo B., Lamberti P., Spinelli G., Tucci V. Effect of conductive nanofiller structures on electrical properties of epoxy composite for aeronautic applications. ICEAF III 3rd International Conference of Engineering Against Failure. 26-28 June, 2013 - Kos island, Greece, Patras Spiros Pantelakis Vol.III, Pag. 527-533 ISBN:9789608810433.
  - Guadagno L., Raimondo M., Vittoria V., Vertuccio L., Lafdi K., De Vivo B., Lamberti P., Spinelli G., Tucci V. Exfoliated graphite as conductive filler in aeronautic epoxy mixtures. 3rd EASN Association International Workshop on AeroStructures Proc. 9th- 11th October 2013, Milan, Italy (ISSN 2309-7213).
  - Guadagno L., Raimondo M., Vietri U., Barra G., Vertuccio L., Volponi R., Cosentino G., De Nicola F., Grilli A., Spena P. Development of Multifunctional Carbon Fiber Reinforced Composites (CFRCs) - Manufacturing Process. 7th International Conference on Times of Polymers (TOP) and composites. June 22-26, 2014, Ischia (Italy) (submitted paper)
  - Hermans P. H. and A. Weidinger. (1961) On the determination of the crystalline fraction of polyethylenes from X-ray diffraction. Die Makromol. Chem., 44(1), 24-36.

## References

---

- Hergenrother Paul M., Thompson Craig M., Smith Jr. Joseph G., Connell John W., Hinkley Jeffrey A., Lyon Richard E., and Moulton Richard. (November 2005) Flammability of Epoxy Resin Containing Phosphorus. Technical Report.
- Hirsch A. (2002) Functionalization of single-walled carbon nanotubes. *Angew. Chem. Int. Edn.*, 41(11), 1853-1859.
- Horie K., Hiura H., Sawada M., Mita I., Kambe H. (1970) Calorimetric investigation of polymerization reactions. III. Curing reaction of epoxides with amines. *J Polym Sci Part A-1: Polym Chem*, 8(6), 1357–1372.
- Hsiue G.H., Liu Y.L., Liao H.H. (2001) Flame-retardant epoxy resins: an approach from organic-inorganic hybrid nanocomposites. *J. Polym. Sci. Part A: Polym. Chem.*, 39, 986- 996.
- Hu N., Masuda Z., Yan C., Yamamoto G., Fukunaga H., et al. (2008) The electrical properties of polymer nanocomposites with carbon nanotube fillers. *Nanotechnology*, 19(21), 215701.
- Husain M., Varley R.J., Cheng Y.B., Simon G.P. (2004) Effect of organo-phosphorous and nano-clay materials on the thermal and fire performance of epoxy resins. *J. Appl. Polym. Sci.*, 91, 1233-1253.
- Hussain F. et al. (2006) Review article: Polymer-matrix Nanocomposites, Processing, Manufacturing, and Application: An Overview. *Journal of Composite Materials*, 40(17), 1511-1575.
- Iannuzzo G., Calvi E., Russo S., Guadagno L., Naddeo C. et al. Smart Carbon Nanotubes/Epoxy Composite Materials for Advanced Aerospace Applications. Extended abstracts, SAMPE Europe 29th Int. Conf. and Forum 2008, Paris (France) , 31 March-2 April 2008:246-51.
- Iijima S. (1991) Helical microtubules of graphitic carbon. *Nature*, 354(6348),56-58.
- Iwashita N., Park C. R., Fujimoto H., Shiraishi M., Inagaki M.(2004) Specification for a standard procedure of X-ray diffraction measurements on carbon materials. *Carbon*, 42(4),701-714.
- Jin F.L., Ma C.J., Park S.J.(2011) Thermal and mechanical interfacial properties of epoxy composites based on functionalized carbon nanotubes. *Mat. Sci. Eng. A*, 528, 8517-8522.
- Jonscher AK. (1990) The universal dielectric response. I. *Electrical Insulation Magazine, IEEE*, 6(2), 16 -22.
- Jyotishkumar P., Logakis E., George S.M., Pionteck J., Haussler L., Hassler R., Pissis P., Thomas S. (2013) Preparation and properties of Multiwalled

- 
- Carbon Nanotubes/Epoxy-Amine Composites. *J. Appl. Polym. Sci.*, 127(4), 3063-3073.
- Kandola B.K., Biswas B., Price D., Horrocks A.R (2010) Studies on the effect of different levels of toughener and flame retardants on thermal stability of epoxy resin. *Polym. Deg. Stab.*, 95(2),144-152.
  - Katsoulis C., Kandare E., Kandola B.K. (2011) The combined effect of epoxy nanocomposites and phosphorous flame retardant additives on thermal and fire reaction properties of fiber reinforced composites. *J. Fire. Sci.*, 29, 361-383.
  - Khare R. and S. Bose (2005) Carbon nanotube based composites-a review. *Journal of Minerals & Materials Characterization & Engineering* , 4(1),31-46.
  - Kilbride BE., Coleman JN.et al (2002) Experimental observation of scaling laws for alternating current and direct current conductivity in polymer-carbon nanotube composite thin films. *J Appl Phys*, 92(7), 4024-4030.
  - Kim H., Abdala A.A., Macosko C.W. (2010) Graphene/Polymer Nanocomposites. *Macromolecules*, 43, 6515–6530.
  - Kim I T., Tannenbaum A., Tannenbaum R. (2011) Anisotropic conductivity of magnetic carbon nanotubes embedded in epoxy matrices. *Carbon*, 49(1), 54-61.
  - Kim YJ., Shin TS., Choi HD., Kwon JH., Chung YC., Yoon HG. (2005) Electrical conductivity of chemically modified multiwalled carbon nanotube/epoxy composites. *Carbon*, 43(1), 23–30.
  - Kovacs JZ., Velagala BS., Schulte K., Bauhofer W. (2007) Two percolation thresholds in carbon nanotube epoxy composites. *Composites Science and Technology*, 67(5), 922–928.
  - Lafdi K., Fox W., Matzek M., Yildiz E. (2007) Effect of carbon nanofiber heat treatment on physical properties of polymeric nanocomposites—part I. *J. Nanomater.* Article ID 52729, 6 pages.
  - Lafdi K., Fox W., Matzek M., Yildiz E. (2008) Effect of carbon nanofiber-matrix adhesion on polymer nanocomposite properties—part II. *J. Nanomater.*, Article ID 310126, 8 pages.
  - Laoutid F., Bonnaud L., Alexandre M., Lopez-Cuesta J.-M., Dubois Ph. (2009) New prospects in flame retardant polymer materials: From fundamentals to nanocomposites. *Materials Science and Engineering R: Reports*, 63(3), 100-125.

## References

---

- Lee S.K., Bai B.C., In J. S., Lee Y.S. (2010) Flame retardant epoxy complex produced by addition of montmorillonite and carbon nanotube. *J. of Ind. And Eng. Chem*, 16, 891- 895.
- Levchik S.V., Camino G., Luda M.P., Costa L., Costes B., Henry Y., Muller G., Morel E. (1995) Mechanistic study of thermal behaviour and combustion behaviour of epoxy resins. II. TGDDM/DDS system. *Polym. Deg. Stab.*, 48, 359-370.
- Li C., Thostenson ET., Chou T-W. (2008) Sensors and actuators based on carbon nanotubes and their composites: A review. *Compos Sci Technol*, 68(6), 1227-1249.
- Li C., Thostenson ET., Chou T-W. (2007) Dominant role of tunneling resistance in the electrical conductivity of carbon nanotube-based composites. *Appl. Phys. Lett.*, 91(22), 223114.
- Li G., Wang L., Ni H., Pittman Jr C. U.( 2002) *J. Inorg. Organmet. Chem.*, 11, 123.
- Li L., Yu Y., Wu Q., Zhan G., Li S. (2009) Effect of chemical structure on the water sorption of amine-cured epoxy resins. *Corrosion Science*, 51(12), 3000-3006.
- Lichtenhan J.D. and J.W. Gilman. Pre ceramic additives as fire retardants for plastics. US 6,362,279 B2, issued March 26, 2002.
- Lincoln Vogel F and R. Popowich (1976) Changes of electrical resistivity of graphite fibers with nitration Petroleum Derived Carbons (ACS Symposium Series) vol 21 ed M L Deviney and T M O'Grady (Washington, DC: ACS Publications) chapter 28 pp 411–7.
- Liu W., Hoa SV., Pugh M. (2005) Fracture toughness and water uptake of high-performance epoxy /nanoclay nanocomposites . *Composites Science and Technology*; 65(15-16), 2364 - 2373.
- Liu Y-L. et al. (1997) Synthesis, thermal properties, and flame retardancy of phosphorus containing polyimides. *Journal of Applied Polymer Science*, 63(7), 875–882.
- Lu S.Y. and I. Hamerton (2002) Recent developments in the chemistry of halogen-free flame retardant polymers. *Prog. Polym. Sci.*, 27(8),1661-1712.
- Lu W., Weng J., Wu D., Wu C., Chen G. (2006) Epoxy Resin/Graphite Electrically Conductive Nanosheet Nanocomposite. *Materials and Manufacturing Processes*, 21(2), 167-171.
- Lucchese M M. et al (2009). Quantifying ion-induced defects and Raman relaxation length in grapheme. *Carbon*, 48(5), 1592-1597.

- 
- Ma P.C., Kim J.K., Tang B.Z. (2007) Effects of silane functionalization on the properties of carbon nanotube/epoxy nanocomposites. *Com. Sci. Tech.*, 67, 2965-2972.
  - Maas TAMM. (1978) Optimalization of processing conditions for thermosetting polymers by determination of the degree of curing with a differential scanning calorimeter. *Polym. Eng. Sci.*, 18(1), 29–32.
  - Martin CA., Sandler JKW., Windle AH., Schwarz MK., Bauhofer W., Schulte K., Shaffer MSP. (2005) Electric field-induced aligned multi-wall carbon nanotube networks in epoxy composites. *Polymer*, 46(3), 877–886.
  - Martone A., Faiella G., Antonucci V., Giordano M., Zarrelli M. (2011) The effect of the aspect ratio of carbon nanotubes on their effective reinforcement modulus in an epoxy matrix. *Compos. Sci. Technol.*, 71(8), 1117-1123.
  - Maxwell ID. and RA. Pethrich (1983) Dielectric studies of water in epoxy resins. *Journal of Applied Polymer Science*, 28(7), 2363-2379.
  - McAllister M. J. et al. (2007) Single Sheet Functionalized Graphene by Oxidation and Thermal Expansion of Graphite. *Chem. Mater.*, 19(18), 4396-4404.
  - McCreery R. L. (2008) Advanced Carbon Electrode Materials for Molecular Electrochemistry. *Chem. Rev.*, 108(7), 2646–2687.
  - McLachlan DS., Chiteme C., Park C., Wise KE., Lowther SE. et al. (2005) AC and DC Percolative Conductivity of Single Wall Carbon Nanotube Polymer Composites. *Journal of Polymer Science Part B: Polymer Physics*, 43(22), 3273–3287.
  - Mdarhri A., Carmona F., Brosseau C., Delhaes P. (2008) Direct current electrical and microwave properties of polymer-multiwalled carbon nanotubes composites. *J. Appl. Phys.*, 103(5), 054303(1)-054303(9).
  - Miller S. G., Heimann P. J., Barlow J. P., Allred R. E. Physical Properties Of Exfoliated Graphite Nanocomposites By Variation Of Graphite Surface Functionality. *Proc. 52nd Int SAMPE Symp. and Exhib.*, Baltimore, MD, June 3-7, 2007
  - Moisala A., Li Q., Kinloch IA., Windle AH. (2006) Thermal and electrical conductivity of single- and multi-walled carbon nanotube-epoxy composites. *Composites Science and Technology*, 66(10), 1285–1288
  - Moniruzzaman M. and KI. Winey (2006) Polymer nanocomposites containing carbon nanotubes. *Macromolecules*, 39(16), 5194–5205.

## References

---

- Montalvao D., Maia NMM., Ribeiro AMR. (2006) A review of vibration-based structural health monitoring with special emphasis on composite materials. *The Shock and Vibration Digest*, 38(4), 295-324.
- Murphy EJ. and SO. Morgan (1939) The Dielectric Properties of Insulating Materials, III Alternating and Direct Current Conductivity. *Bell System Technical Journal*, 18, 502-537.
- Nigrawal A. and N. Chand. (2010) Electrical and Thermal Investigations on Exfoliated Graphite filled Epoxy Gradient Composites. *Malaysian Polymer Journal*, 5(2), 130-139.
- Nobile M R. (2011) Rheology of polymer-carbon nanotube composite melts Chap. 15 428-481 in “Polymer-carbon nanotube composites. Preparation, properties and application”, Edited by Tony McNally and Petra Pötschke P., Woodhead Publishing, Cambridge (UK).
- Nobile M.R., Fierro A., Rosolia S., Guadagno L., Raimondo M. Viscoelastic Properties of CNT/Epoxy-Amine Resins for Structural Applications. *NanotechITALY 2013 – 6TH edition Key Enabling Technologies for Responsible Innovation Proc.*, 27th – 29th November 2013, Venice, Italy.
- Nobile M. R., Simon G. P., Valentino O., Morcom M. (2007) Rheological and Structure Investigation of Melt Mixed Multi-Walled Carbon Nanotube/PE Composites. *Macromol. Symp.*, 247(1), 78–87.
- Nobile M. R., “Carbon nanotube polymer composites” in *Wiley Encyclopedia of Composites*, 2nd Edition, editors: L. Nicolais and A. Borzacchiello, Publisher John Wiley & Sons, 2012, pp. 1-20.
- Pal G. and H. Macskasy. *Plastics: Their behavior in fires (Studies in Polymer Science)*, Publisher: Elsevier Science Ltd (July 1991), New York.
- Panwar V., Kang B., Park J.O., Park S., Mehra R M. (2009) Study of Dielectric Properties of styrene-acrylonitrile graphite sheets composites in low and high frequency region. *European Polymer Journal*, 45(6), 1777-1784.
- Pappalardo L T. (1974) DSC Evaluation of B-Stage Epoxy-Glass Prepregs for Multilayer Boards. *Soc. Plast. Eng. Tech. Papers.*, 20, 13–16.
- Pereira V.M., Castro Neto A.H., Liang H.Y. Mahadevan L. (2010) Geometry, mechanics and electronics of singular structures and wrinkles in graphene. *Phys. Rev. Lett.*, 105(15), 156603 [4 pages].
- Pötschke P., Fornes T D., Paul D R. (2002) Rheological behavior of multiwalled carbon nanotube/polycarbonate composites. *Polymer*, 43(11), 3247-3255.

- 
- Prolongo S G., Meliton B G., Del Rosario G. and Ureña A. (2012) Simultaneous dispersion and alignment of carbon nanotubes in epoxy resin through chronoamperometry. *Carbon*, 50(15), 5489-5497.
  - Rahatekar S.S., Koziol K.K.K., Butler S.A., Elliot J A., Shaffer M.S.P., Mackley M.R., Windle A.H. (2006) Optical microstructure and viscosity enhancement for an epoxy resin matrix containing multiwall carbon nanotubes. *J Rheol*, 50(5), 599-610
  - Rahatekar S.S., Zammarano M., Matko S., Koziol K.K., Windle A.H., Nyden M., Kashiwagi T., Gilman J.W. (2010) Effect of carbon nanotubes and montmorillonite on the flammability of epoxy composites. *Polym, Deg. Stab.*, 95, 870-879.
  - Raimondo M., Guadagno L., Bonnaud L., Murariu O., Dubois Ph. Effect of Incorporation of POSS Compounds on Thermal and Fire Resistance of Aeronautic Resins. ICEAF III 3rd International Conference of Engineering Against Failure. 26-28 June, 2013 - Kos island, Greece, Patras Spiros Pantelakis Vol.III, Pag.542-550 ISBN:9789608810433.
  - Raimondo M., Chirico S., Guadagno L., Longo P., Mariconda A., Bonnaud L., Murariu O., Dubois Ph., Dumas L. Fire properties of TGMDA resins for aeronautic applications. 3rd EASN Association International Workshop on AeroStructures Proc. 9th- 11th October 2013, Milan, Italy (ISSN 2309-7213).
  - Ratna D. (2005) Epoxy composites: Impact resistance and flame retardancy. *Rapra Review Reports (Report 185)* 16(5), 23-28, ISSN: 0889-3144.
  - Rose N., LeBras M., Delobel R., Costes B., Henry Y. (1993) Thermal oxidative degradation of an epoxy resin. *Polym. Deg. Stab.*, 42,307-316.
  - Sandler JKW., Kirk JE., Kinloch IA., Shaffer MSP., Windle AH. (2003) Ultra-low electrical percolation threshold in carbon-nanotube-epoxy composites. *Polymer*; 44(19), 5893–5899.
  - Sanjana Z. N. and R. N. Sampson. (1981) Measuring the degree of cure of multilayer circuit boards. *Insul Circuits*, 27,87–92.
  - Sarti GC. (1979) Solvent Osmotic Stresses and the prediction of case II transport kinetics. *Polymer*, 20(7), 827-832.
  - Sarti GC. and A. Apicella (1980) Non-equilibrium glassy properties and their relevance in case II transport kinetics. *Polymer*, 21(9), 1031-1036.
  - Sengupta R., Bhattacharya M., Bandyopadhyay S., Bhowmick A. K. (2011) A review on the mechanical and electrical properties of graphite and modified graphite reinforced polymer composites. *Progress in Polymer Science*, 36(5), 638–670.

## References

---

- Shen J., Huang W., Wu L., Hu Y., Ye M. (2007) Thermo-physical properties of epoxy nanocomposites reinforced with amino-functionalized multi-walled carbon nanotubes. *Composites: Part A*, 38, 1331-1336.
- Sheppard Jr. NF. and SD. Senturia. (1986) Chemical interpretation of the relaxed permittivity during epoxy resin cure. *Polym. Eng. Sci.*, 26(5), 354–357.
- SpecialChem4Polymers - FR Home page - Flame Retardants Center <http://www.specialchem4polymers.com/tc/flame-retardants/?id=9303>
- Spinelli G., Giustiniani A., Lamberti P., Tucci V., Zamboni W. (2012) Numerical Study of Electrical Behaviour in Carbon Nanotube Composites. *Int. J. Appl. Electrom.*, 39(1-4), 21-27.
- Spitalsky Z., Krontiras CA., Georga SN., Galiotis C. (2009) Effect of oxidation treatment of multiwalled carbon nanotubes on the mechanical and electrical properties of their epoxy composites. *Composites Part A: Applied Science and Manufacturing*, 40(6-7), 778-783.
- Spitalsky Z., Tasis D., Papagelis K., Galiotis C. (2010) Carbon nanotube–polymer composites: chemistry, processing, mechanical and electrical properties. *Prog. Polym. Sci.*, 35(3), 357-401.
- Stankovich S. et al (2007) Synthesis of graphene-based nanosheets via chemical reduction of exfoliated graphite oxide. *Carbon*, 45(7), 1558–1565.
- Staudenmaier, “Verfahren zur Darstellung der Graphitslure”, *Berichte der Deutschen Chemischen Gesellschaft*, 1898, 31, 1481-1487.
- Sun L., Gibson RF., Gordaninejad F., Suhr J. (2009) Energy absorption capability of nanocomposites: a review. *Compos Sci Technol*, 69(14), 2392-2409.
- Tao K., Yang S., Grunlan J.C., Kim Y.S, Dang B., Deng Y., Thomas R.L., Wilson B.L, Wei X. (2006) Effects of Carbon Nanotube Fillers on the Curing Processes of Epoxy Resin-Based Composites. *J. Appl. Polym. Sci.*, 102(6), 5248-5254.
- Thomas NL. and AH. Windle. (1980) A deformation Model for case II Diffusion. *Polymer*, 21(6), 613-619.
- Thostenson E T., Ren Z., Chou T-W (2001) Advances in the science and technology of carbon nanotubes and their composites: a review. *Compos Sci Technol*, 61(13), 1899-1912.
- Tkac A. and I. Špilda (1981) Radical processes in polymer burning and its retardation. II. An ESR study of flame retardation of polypropylene. *Journal of Polymer Science: Polymer Chemistry Edition*, 19(6), 1495-1508.

- 
- Toldy A. (2007). PHD Thesis: Synthesis and applications of reactive organophosphorus flame retardants. Supervisor: Prof. Marosi György.
  - Toldy A., Anna P., Csontos I., Szabo A., Marosi G. (2007) Intrinsically flame retardant epoxy resin – Fire performance and background – Part I. *Polym. Deg.Stab.*, 92, 2223-2230.
  - Toldy A., Szabo A., Novak C., Madarasz J., Toth A., Marosi G. (2008) Intrinsically flame retardant epoxy resin – Fire performance and background – Part II. *Polym. Deg.Stab.*, 93, 2007-2013.
  - Troitzsch J., *International plastics flammability handbook : principles, regulations, testing and approval 2nd ed.*, published 1990 by Hanser in Munich.
  - Uchida T., Anderson D P., Minus M L., Kumar S. (2006) Morphology and modulus of vapor grown carbon nano fibers. *J. Mater. Sci.*, 41(18), 5851-5856.
  - Varley R.J., Liu W., Simon G.P. (2006) Investigation of the reaction mechanism of different epoxy resins using a phosphorous-based hardener. *J. Appl. Polym. Sci.*, 99(6), 3288-3299.
  - Wang Q. and G. Chen (2012) Effect of nanofillers on the dielectric properties of epoxy nanocomposites. *Adv Mater Res*, 1(1), 93-107.
  - Wang X, Song L, Yang H, Xing W, Kandola B, Hu Y (2012). Simultaneous reduction and surface functionalization of graphene oxide with POSS for reducing fire hazards in epoxy composites. *J. Mater. Chem.*, 22, 22037-22043.
  - Weil E.D. and S. Levchik (2004) A review of current Flame Retardant Systems for Epoxy Resins. *J. Fire Sci.*, 22(1), 25-40.
  - Williams. James R. White Paper: “Flame Retardant Label Materials”, May 24, 2010
  - Xie XL., Mai YW., Zhou XP. (2005) Dispersion and alignment of carbon nanotubes in polymer matrix: a review. *Materials Science and Engineering: R: Reports*; 49(4), 89–112.
  - Ye L., Lu Y., Su Z., Meng G. (2005) Functionalized composite structures for new generation airframes: a review. *Compos Sci Technol*, 65(6), 1436-1446.
  - Yu H., Liu J., Wen X., Jiang Z., Wang Y., Wang L., Zheng J., Fu S., Tang T. (2011) Charing polymer wrapped carbon nanotubes for simultaneously improving the flame retardancy and mechanical properties of epoxy resin. *Polymer* , 52, 4891-4898.

## References

---

- Zhang W., Li X., Yang R. (2011) Pyrolysis and fire behaviour of epoxy resin composites based on a phosphorous-containing polyhedral oligomeric silsesquioxane (DOPO-POSS). *Polym. Deg. Stab.*, 96, 1821-1832.
- Zhang W., Li X., Fan H., Yang R. (2012) Study on mechanism of phosphorus-silicon synergistic flame retardancy on epoxy resins. *Polym. Deg. Stab.*, 97, 2241-2248.
- Zhang W., Li X., Jiang Y., Yang R. (2013) Investigations of epoxy flame retarded by phenyl silsesquioxanes of cage and ladder structures. *Polym. Deg. Stab.*, 98, 246-254.
- Zheng W., Wong S-C., Sue H-J. (2002) Transport behavior of PMMA/expanded graphite nanocomposites. *Polymer*, 43(25),6767-6773.
- Zhou Y., Pervin F., Jeelani S. (2007) Effect vapor grown carbon nanofiber on thermal and mechanical properties of epoxy. *J. Mater. Sci.*, 42(17), 7544-7553.
- Zhuang H. Synthesis and characterization of aryl phosphine oxide containing thermoplastic polyimides and thermosetting polyimides with controlled reactivity. Ph.D. Thesis, Virginia Polytechnic Institute And State University, 1998
- Zou Y., Tong L., Steven GP. (2000) Vibration-based model dependent damage identification and health monitoring for composite structures – a review. *J Sound Vib*, 230(2), 357-378.